Investigating the ability of RIG-I agonists to provide protection in mouse and ferret models of respiratory virus infection

Lara Sonja Ute Schwab

from Nördlingen, Germany

ORCID ID:

0000-0003-1344-0569

Submitted in total fulfilment of the requirements of the joint degree of

Doctor of Philosophy (PhD)

of the Medical Faculty

The Rheinische Friedrich-Wilhelms-Universität Bonn

and

The Department of Microbiology and Immunology

The University of Melbourne

Bonn/Melbourne, 2022

Performed and approved by the Medical Faculty of the Rheinischen Friedrich-Wilhelms-Universität Bonn and The University of Melbourne

1. Supervisor: Prof. Gunther Hartmann

2. Supervisor: Prof. Patrick Reading

Date of submission: 03.09.2021
Date of the oral examination: 16.02.2022

Institute of Clinical Chemistry and Clinical Pharmacology, Bonn,
Director: Prof. Gunther Hartmann

Table of content

Abbreviations

3pRNA	5′-triphosphorylated RNA
µg	microgram
µL	microlitre
µm	micrometre
°C	degree Celsius

A

AM	alveolar macrophage
APC	antigen-presenting cell
ASC	apoptosis-associated speck-like protein containing a CARD
ATCC	American Type Culture Collection
ATP	adenosine triphosphate
AUC	area under curve

B

BAL	bronchoalveolar lavage
BSE	bundle signaling element

C

C-terminal	carboxy-terminal
CARD	caspase activation and recruitment domains
Cas9	CRISPR-associated protein 9
CBA	cytometric bead array
CDC	Centers for Disease Control
CDV	canine distemper virus
cDNA	complementary deoxyribonucleic acid
CHIKV	chikungunya virus
CLR	C-type lectin receptor
cOVA	cytoplasmic OVA
CPE	cytopathic effect
CRISPR	clustered regularly interspaced short palindromic repeats
cRNA	complementary ribonucleic acid
CSFV	classical swine fever virus
CTD	carboxy-terminal domain
ctrl	control
CXCL10	C-X-C motif chemokine 10

D

DAMP	danger-associated molecular pattern
DC	dendritic cell
DENV	dengue virus
DMI	Department of Microbiology and Immunology
DNA	deoxyribonucleic acid
DOX	doxycycline
dpi	day post infection

dsRNA	double-stranded ribonucleic acid

E

E.coli	*Escherichia coli*
EDTA	ethylenediamine tetraacetic acid
EGFR	epidermal growth factor
EIAV	equine infectious anemia virus
EJC	exon junction complex
ELISA	Enzyme-Linked Immunosorbent Assay

F

F	fusion protein
FAM3	family with sequence similarity 3
FCS	foetal calf serum
FDA	Food and Drug Administration
FITC	fluorescein isothiocyanate

G

G	glycoprotein
GAPDH	glyceraldehyde 3-phosphate dehydrogenase
GBP	guanylate binding protein
GE	gene end
GFP	green fluorescent protein
GPP	Genetic Perturbation Platform
GS	gene start

H

HA	hemagglutinin
HBS	HEPES buffered saline
HBV	hepatitis B virus
HCV	hepatitis C virus
HEK	human embryonic kidney cell
Hep-2	human epithelial type 2
HIV-1	human immunodeficiency virus 1
HMPV	human metapneumovirus
HPAI	highly pathogenic avian influenza
hpi	hours post infection
hr(s)	hour(s)
hRSV	human respiratory syncytial virus
HSV-1	herpes simplex virus 1

I

i.n.	intranasal
i.v.	intravenous
IAV	influenza A virus
IBV	influenza B virus
ICAM	intercellular adhesion molecule
IFIT	interferon-induced proteins with tetratricopeptide repeats

IFITM	interferon-induced transmembrane
IFN	interferon
IFNAR	interferon-α/β receptor
IKK	IκB kinase
IL	interleukin
IRF	interferon regulatory factor
ISG	interferon-stimulated gene
ISRE	interferon-stimulated response element

J

JAK	Janus kinase

K

kB	kilo base
KO	knockout

L

L	large polymerase protein
LB	Luria-Bertani
LGP2	laboratory of genetics and physiology 2
LRT	lower respiratory tract

M

M	matrix protein
MAVS	mitochondrial antiviral signaling protein
MDA5	melanoma differentiation-associated gene 5
MDCK	Madin-Darby canine kidney
MEF	mouse embryonic fibroblast
MHC	major histocompatibility complex
min	minute
mL	millilitre
MOI	multiplicity of infection
mRNA	messenger ribonucleic acid
ms	millisecond
Mx	myxovirus resistance/ myxoma resistance
MyD88	myeloid differentiation factor 88

N

N	nucleoprotein
N-terminal	amino-terminal
NA	neuraminidase
NAI	neuraminidase inhibitor
NC	nucleocapsid
NDV	Newcastle disease virus
NEP	nuclear export protein
NET	neutrophil extracellular trap
NF-κB	nuclear factor 'kappa-light-chain-enhancer' of activated B-cells
NK cell	natural killer cell

NLR	NOD-like receptor
NMD	nonsense-mediated decay
NOD	nucleotide-binding oligomerisation domain
NP	nucleoprotein
ns	not significant
NS	non-structural protein

O

OAS-1	2'-5'-oligoadenylate synthetase 1
ORF	open reading frame
OVA	ovalbumin

P

P	phosphoprotein
PA	polymerase acid
PAMP	pathogen-associated molecular pattern
PB1	polymerase basic protein 1
PB2	polymerase basic protein 2
PBMC	peripheral blood mononuclear cell
PBS	phosphate buffered saline
PCR	polymerase chain reaction
pDCs	plasmacytoid dendritic cell
PEI	polyethylenimine
PFA	paraformaldehyde
PFU	plaque-forming units
pg	picogram
PIV	parainfluenza virus
Pol II	polymerase II
post-F	postfusion form of RSV F
pre-F	prefusion form of RSV F
PRR	pattern recognition receptor

Q

qRT-PCR	quantitative polymerase chain reaction

R

RdRp	RNA-dependent RNA polymerase
RIG-I	retinoic-acid-inducible gene I
RLR	RIG-I-like receptor
RNA	ribonucleic acid
rpm	revolutions per minute
RSV	respiratory syncytial virus
RT	room temperature
RV	rhinovirus

S

SA	sialic acid
SARS-CoV-2	severe acute respiratory syndrome coronavirus 2

SBI	secondary bacterial infection
SD	standard deviation
SEM	standard error of the mean
SeV	Sendai virus
SH	small hydrophobic protein
shRNA	short hairpin ribonucleic acid
SIV	simian immunodeficiency virus
SNP	single nucleotide polymorphism
SOCS	suppressor of cytokine signaling
ssRNA	single-stranded RNA
STAT	signal transducer and activator of transcription

T

TANK	TRAF associated NF-κB activator
TBK1	TANK-binding kinase 1
$TCID_{50}$	50 % tissue culture infectious dose
TLR	Toll-like receptor
TMD	transmembrane domain
TMPRSS2	transmembrane protease serine subtype 2
TNF(R)	tumour necrosis factor (receptor)
TRADD	TNFR-associated death domain
TRAF	TNF receptor-associated factor
TRIF	TIR-domain-containing adaptor inducing IFN-β
TYK2	tyrosine kinase 2

U

UoM	University of Melbourne
URT	upper respiratory tract
UTR	untranslated region

V

vol	volume
vRNA	viral ribonucleic acid
vRNP	viral ribonucleoprotein
VS	Virospot
VSV	vesicular stomatitis virus

W

WHO	World Health Organisation
WHO CCRRI	WHO Collaborating Centre for Reference and Research on Influenza
WHV	woodchuck hepatitis virus
WT	wild-type
wt	weight

List of tables

List of figures

Abstract

Respiratory infections caused by influenza A virus (IAV) or respiratory syncytial virus (RSV) lead to substantial morbidity and mortality. Treatment options are limited and there is urgent need for the development of efficient therapeutic and prophylactic treatments. Pattern recognition receptors (PRRs) such as the cytoplasmic helicase retinoic-acid-inducible gene I (RIG-I) are part of the innate immune system. RIG-I can be activated by recognition of viral nucleic acids, leading to downstream activation of interferon-stimulated genes (ISGs) and restriction of viral replication. We have used synthetic RNA oligonucleotides to stimulate RIG-I to inhibit replication of respiratory viruses using *in vitro* and *in vivo* models of infection.

Our *in vitro* approaches used airway cell lines from humans, mice and ferrets and investigated the effects of RIG-I agonist pre-treatment on subsequent infection with either IAV or RSV. Prophylactic RIG-I agonist treatment induced multiple ISGs and inhibited infection and growth of respiratory viruses in cell lines from each of the different species.

In vivo, we utilised mouse and ferret models to study the antiviral potential of RIG-I agonists against IAV and RSV. In mice, we compared animals which do or do not express a functional Mx1 protein and found that a single prophylactic treatment with RIG-I agonist via the intravenous route resulted in ISG induction in the lungs and this correlated with reduced IAV replication. Of interest, these effects were particularly potent and long-lasting in mice expressing a functional Mx1 confirming an important role of Mx1 for RIG-I agonist-induced protection against IAV. In a mouse model of RSV, we found that a single prophylactic treatment with RIG-I agonist resulted in reduced replication of virus in the lung, as observed using bioluminescence imaging of luciferase-labelled RSV as well as plaque assay for infectious virus. Thus, our studies in mouse models indicate that a single pre-treatment with RIG-I agonists resulted in potent inhibition of two very different respiratory viruses.

In ferrets, after establishing assays to monitor ISG induction in the blood and in airway tissues, we confirmed that a single intravenous injection of RIG-I agonist induced ISG induction in both peripheral blood mononuclear cells (PBMCs) and the lungs. Moreover, a single treatment prior to infection also resulted in reduced replication of both IAV and RSV in ferret lungs, although this treatment had only negligible effects on virus replication in the nasal tissues. A single treatment to animals with an established IAV infection also resulted in reduced virus titres in the lungs, suggesting its potential as a therapeutic antiviral agent.

Myxoma (Mx) proteins are ISGs with potent antiviral effects against IAV. While human and mouse Mx proteins have been studied in detail, ferret Mx proteins have not been characterised. Therefore, we generated different experimental approaches to assess the induction of three endogenous ferret Mx (two splice variants of Mx1 as well as Mx2) in a ferret cell line, as well as *in vitro* overexpression systems to assess the cellular localisation and antiviral functions of each ferret Mx. Our findings indicate that each ferret Mx localises to the cytoplasm and that particular proteins exhibit antiviral functions against IAV, but not RSV. However, further studies are required to clearly define the antiviral activity of ferret Mx, since our preliminary results indicate that ferret Mx proteins display different antiviral activity following overexpression in human or in ferret cells.

Together, studies described in this thesis demonstrate the potential of RIG-I agonists as antiviral treatments against diverse respiratory viruses both *in vitro* and *in vivo* and represent an important step towards the development of novel antiviral treatments in humans.

Declaration

This is to certify that,

(i) the thesis comprises only my original work towards the PhD except where indicated in the preface;

(ii) due acknowledgement has been made in the text to all other material used;

(iii) the thesis is less than 100,000 word limit in length, exclusive of tables, maps, bibliographies and appendices as approved by the Research Higher Degrees Committee.

Lara Schwab

Preface

The work presented in this thesis was partly conducted at The University of Melbourne, in the laboratory of Prof. Andrew Brooks, under the supervision of Prof. Patrick Reading, Associate Prof. Aeron Hurt and Prof. Andrew Brooks and partly conducted at The Rheinische Friedrich-Wilhelms-Universität Bonn, in the laboratory of Prof. Gunther Hartmann under the supervision of Prof. Gunther Hartmann. Lara Schwab was supported by the Melbourne Research Scholarship (Stipend and Fee offset).

My contribution to experiments in each of the Chapters was as follows:

• Chapter 3: 90 %

- Infection of mice and tissue/sample collection from infected mice were partly performed by Prof. Patrick Reading (The University of Melbourne, Melbourne, Australia).
- Plaque assays and CBAs were partly performed by Dr. Fernando Javier Villalón Letelier (The University of Melbourne, Melbourne, Australia).

• Chapter 4: 90 %

- Infection of mice, tissue/sample collection and plaque assays from infected mice were partly performed by Prof. Patrick Reading and Dr. Rubaiyea Farrukee (The University of Melbourne, Melbourne, Australia).

• Chapter 5: 75 %

- 293T cells were generated and infected by Dr. Rubaiyea Farrukee and James Barnes (WHO CCRRI , Melbourne, Australia).
- 3’-RNA- sequencing was performed by Dr. André Heimbach (Universität Bonn, Bonn, Germany) and data analysis was performed by Dr. Anshupa Sahu, Dr. Farhad Shakeri and Andreas Buness (all Universität Bonn, Bonn, Germany).

I acknowledge these important contributions to the experiments presented in this thesis.

Acknowledgement

This thesis would not have been possible without the support of many people.

First, I would like to thank my Melbourne supervisors, Prof. Patrick Reading, A/Prof. Aeron Hurt and Prof. Andrew Brooks. Pat, thank you so much for giving me the opportunity to do this joint PhD. I think both of us did sometimes not know where this journey would end but you were a constant support, always encouraging me in all situations, both personal and work-related, and you helped me so much to become the person and scientist I am today. You are the best mentor I could have asked for and I am very grateful to have done this PhD under your supervision.

Also thanks to Aeron and Andrew for their constant support, their precious time and valuable advices during all the meetings we had together.

Then I would like to thank my Bonn supervisor, Prof. Gunther Hartmann. Thank you for joining me in this joint PhD program and for supporting me, despite of me being at the other side of the world for most of my PhD. This project would not have been possible without your support and I am very grateful to have received all the support from you whenever I needed.

I would like to thank my PhD committee Prof. Katherine Kedzierska, Dr. Brendon Chua and A/Prof. Linda Wakim for all their valuable advices, their support and their encouragement throughout our meetings.

Next, I would like to thank my “non-official” supervisor, Sarah Londrigan. You were a constant source of help, always asking how I was and you were always taking care of me, both inside as well as outside of the lab. Thank you.

Thanks also to my Bonn-based “non-official” supervisors, Thomas Zillinger and Christoph Coch for supporting me and for all your help to bring this project to work. Whenever I was desperately in needed for oligos, you always did your best to help me out and to support me with all the issues coming along.

Then I would like to thank my Melbourne-based lab, all past and present members of the Brooks and Reading lab. You are an amazing bunch of people

and I highly enjoyed working with you, being part of your group was very inspiring and motivational! Every one of you made me feel welcome from the very first day. Thank you for all the lab meetings we had together, all Christmas parties, Christmas-in-July parties and not to forget the Monday Morning teas and birthday celebrations. I wish I could have told you this in person during my oration but I still hope that we will see each other soon again. I miss you guys a lot!

To my special lab buddies from “Team flu” Fernando, Melkamu, Tina: I am glad that we were together on this journey of a PhD where we were sharing all ups and downs, we spent so much time together and always supported each other during the long hours in the lab, all the lunch breaks and all the get-togethers outside of the lab. Thanks also to the other “Team flu” members Harry, Svenja and Ruby for being great colleagues and for making my time so enjoyable.

To the former lab members, Ron, Shinta and Sedi: thank you for all the time we spent together, all the fun karaoke nights, the hotpots and game nights. I am so glad that we met and I value our friendship a lot.

Thanks also to all lab members of the Hartmann and Bartok group in Bonn for being a lovely bunch of people and for always being supportive. Due to COVID-19 restrictions this year was so different from how I was hoping it to be but I still hope that one day we can celebrate Karneval together!

Then I would like to thank all members of the IRTG2168 program, especially Marie Greyer, Lucie Delforge and Sandra Rathmann for doing a fantastic job on running this program and for always supporting the students.

Last, I would like to thank my friends back home and my family, Mama, Papa, Patrick, Björn and Till. I know that it was sometimes not easy for you to understand the decisions I made but you never questioned anything I did and always supported me. You always believed in me, often more than I did in myself, and only because of your trust and love I managed to be where I am today.

1 Chapter: Literature Review

1.1 Introduction

Respiratory viruses are the most frequent causative agents of human disease worldwide and lead to high morbidity and mortality, especially in children (Weston et al., 2019). The most common viruses associated with respiratory disease include rhinovirus, influenza virus, respiratory syncytial virus, human metapneumovirus, parainfluenza virus, adenoviruses and coronavirus (Boncristiani et al., 2009). Infections of the upper respiratory tract (URT) are generally mild and self-limiting, whereas infections of the lower respiratory tract (LRT) have the potential to result in more severe and sometimes life-threatening disease. Studies described in this thesis will focus on influenza viruses, belonging to the family *Orthomyxoviridae*, and respiratory syncytial virus, a member of the *Pneumoviridae* family.

1.1.1 Influenza virus

1.1.1.1 General features

Influenza viruses are among the most common causes of human respiratory infections and are of particular concern as they can be associated with high morbidity and mortality. Infections of the URT generally result in mild symptoms such as fever, sore throat and nasal discharge whereas infections of the LRT can be much more severe, resulting in complications, including pneumonia, which is often associated with secondary bacterial infections (Krammer et al., 2018).

Influenza viruses are enveloped, negative-sense single-stranded RNA (ssRNA) viruses with a segmented genome that belong to the family *Orthomyxoviridae.* They can be classified into four types (A, B, C and D) based on the genetic and antigenic properties of their internal proteins. While influenza D virus primarily infects animals such as swine and cattle, influenza A, B and C viruses readily infect humans (Paules et al., 2017). Influenza C infections are generally mild, although they have been associated with influenza-like illness and hospitalisation, especially in children (Matsuzaki et al., 2006). Influenza A and B

viruses (IAV and IBV, respectively) are responsible for annual seasonal influenza epidemics whereas only IAVs have been associated with global pandemics. IAVs are the focus of studies described in this thesis and have therefore been discussed in detail below.

The IAV genome is comprised of 8 single-stranded RNA segments with a total genome size of ~13.5 kB that can encode up to 17 proteins (Lee, Nara et al., 2017; Li et al., 2021). Gene segments are named according to the first protein that they were reported to encode, namely hemagglutinin (HA), neuraminidase (NA), polymerase basic protein (PB)2, nucleoprotein (NP), polymerase basic protein (PB)1, matrix (M), nonstructural protein (NS), and polymerase acidic protein (PA) (Krammer et al., 2018).

Viral particles are composed of a viral envelope, associated M proteins and the viral ribonucleoproteins (vRNPs) (**Figure 1.1**). The envelope is a host-derived lipid bilayer which incorporates three viral transmembrane proteins, namely HA, NA and M2 (Bouvier et al., 2008). The HA glycoprotein is the most abundant transmembrane protein and is responsible for recognition of sialylated receptors on the surface of host cells as well as fusion of the viral and endosomal membranes to facilitate infectious entry. The NA glycoprotein exhibits enzymatic activity, acting to cleave sialic acid residues to facilitate release of newly-synthesised virions from the surface of infected cells and to aid in virus motility in the presence of sialic acid-rich mucins in the airways (Wang, Hao et al., 2019). The viral M2 protein, the least abundant of the transmembrane proteins, acts as a pH-dependent ion channel through the viral envelope into the core of the virus and plays a critical role in acidification and subsequent uncoating of virions in the endosomal compartment. Beneath the viral envelope, a layer of M1 protein forms a stable matrix which associates with the viral NP to stabilise the vRNPs in the core of the virions (Rossman et al., 2011). Each segment of viral genomic RNA is associated with viral NP and the polymerase proteins to form a vRNP complex (Nayak et al., 2009). The viral RNA is tightly wrapped around multiple copies of NP and, due to conserved nucleotides at the 5′ and 3′ termini in the viral genome, complementary regions bind and lead to the formation of characteristic

“panhandle” structures (Lee, Nara et al., 2017). The polymerase proteins PB1, PB2 and PA associate together at the end of each vRNP to form the RNA-dependent RNA polymerase complex. Additionally, non-structural proteins such as nuclear export protein (NEP), NS1, PB1-F2, PB1-N40, PA-X, PA-N155 and PA-N182 are encoded by the viral genome and display diverse functions, including suppression of host cell-intrinsic immunity and enhancement of viral replication and pathogenesis (Hale et al., 2008; Vasin et al., 2014; Hu et al., 2018).

The viral surface HA and NA glycoproteins are the most variable proteins expressed by IAV and are the basis by which IAV are classified into different subtypes. To date, 9 antigenically distinct NA (N1-9) and 16 HA (H1-16) subtypes have been identified in wild aquatic birds, which are considered the natural reservoir of many IAV (Fouchier et al., 2005). Two additional HA (H17 and H18) and NA (N10 and N11) subtypes have also been identified in bats (Tong et al., 2013). Of note, IBVs are not divided into subtypes but instead are classified into two lineages, namely B/Victoria and B/Yamagata, based on genetic and antigenic differences in the viral HA (Caini et al., 2019).

The viral HA and, to a lesser extent the NA, are the main targets of neutralizing antibodies generated following infection or vaccination. However, IAV undergo two modes of antigenic variation which contribute to their ability to persist in the human population, even in the presence of pre-existing immunity (Webster et al., 1992). These two modes of antigenic variation, known as antigenic drift and antigenic shift, are possible largely due to the lack of proof-reading ability in the viral polymerase complex and the segmented nature of the viral genome (Kim et al., 2018). Antigenic drift describes the constant evolution and gradual accumulation of mutations in the genome of viruses that have been circulating in humans for an extended time. Mutations occur in all viral genes due to the low fidelity of the viral RNA polymerase and mutations in the HA and NA genes can lead to amino acid substitutions in key antigenic sites, resulting in the generation of variants which can evade antibody-mediated immunity elicited following vaccination or previous infection (Krammer et al., 2018). This gradual process

explains the occurrence of seasonal influenza epidemics, which are generally observed in winter months in temperate climates. As a result, the World Health Organisation (WHO) meets regularly to assess the genetic and antigenic characteristics of the most recently circulating IAV and IBV to determine the need to update the composition of current influenza vaccines.

Antigenic shift describes the second major mechanism responsible for antigenic variation in human IAV. Antigenic shift can result in the emergence of a novel IAV in humans which expresses a HA and/or NA that is immunologically distinct to those of recently circulating IAV. As the population has little or no pre-existing humoral immunity to the emerging virus this can lead to the global spread of the virus, resulting in a pandemic (Paules et al., 2017). Antigenic drift is unique to IAV and has been proposed to occur by at least two mechanisms. The first is by classical reassortment, which is considered to be the primary mechanism responsible for the majority of human pandemics. Due to the segmented nature of the viral genome, infection of the same host by two different viruses can result in the exchange of viral gene segments, resulting in the generation of a new subtype. Of note, IAV have been isolated from many different species, including humans, pigs, horses and other mammals, as well as domestic and wild birds, highlighting the potential for co-infections to occur in nature (Olsen et al., 2006). The second mechanism that could introduce a new IAV subtype into humans is the direct transmission of an avian or mammalian virus to humans, followed by adaptation to the new host. For example, it has been proposed that the Spanish influenza H1N1 pandemic in 1918 resulted from direct transmission of an avian virus into the human population (Belshe, 2005; Anhlan et al., 2011). More recently, a number of avian IAV, including highly pathogenic avian influenza (HPAI) H5N1, as well as H7N9 and H9N2, amongst others, have been associated with human infections. Although disease associated with HPAI H5N1 is often very severe in humans, there is currently little evidence of effective human-to-human transmission (Beigel et al., 2005; Paules et al., 2017).

Despite the many different HA and NA subtypes that exist in nature, only H1N1, H2N2 and H3N2 subtypes have been associated with sustained

human-to-human transmission resulting in occasional pandemics and more regular seasonal epidemics. Four influenza pandemics occured in the human population in the last century, namely the devastating “Spanish flu” (H1N1) pandemic in 1918/1919, followed by the “Asian flu” (H2N2) in 1957/1958, the “Hong Kong flu” (H3N2) in 1968/1969 and the reappearance of H1N1 in 1977 (Saunders-Hastings et al., 2016). Since then, the most recent influenza pandemic “swine flu” (H1N1pdm09) occurred in 2009/2010 (Kilbourne, 2006; Morens et al., 2018). Today, the H3N2 and H1N1pdm09 subtypes continue to co-circulate, along with the two lineages of IBV (B/Victoria-like and B/Yamagata-like) and it is these viruses that are currently associated with seasonal influenza epidemics (Belshe, 2010).

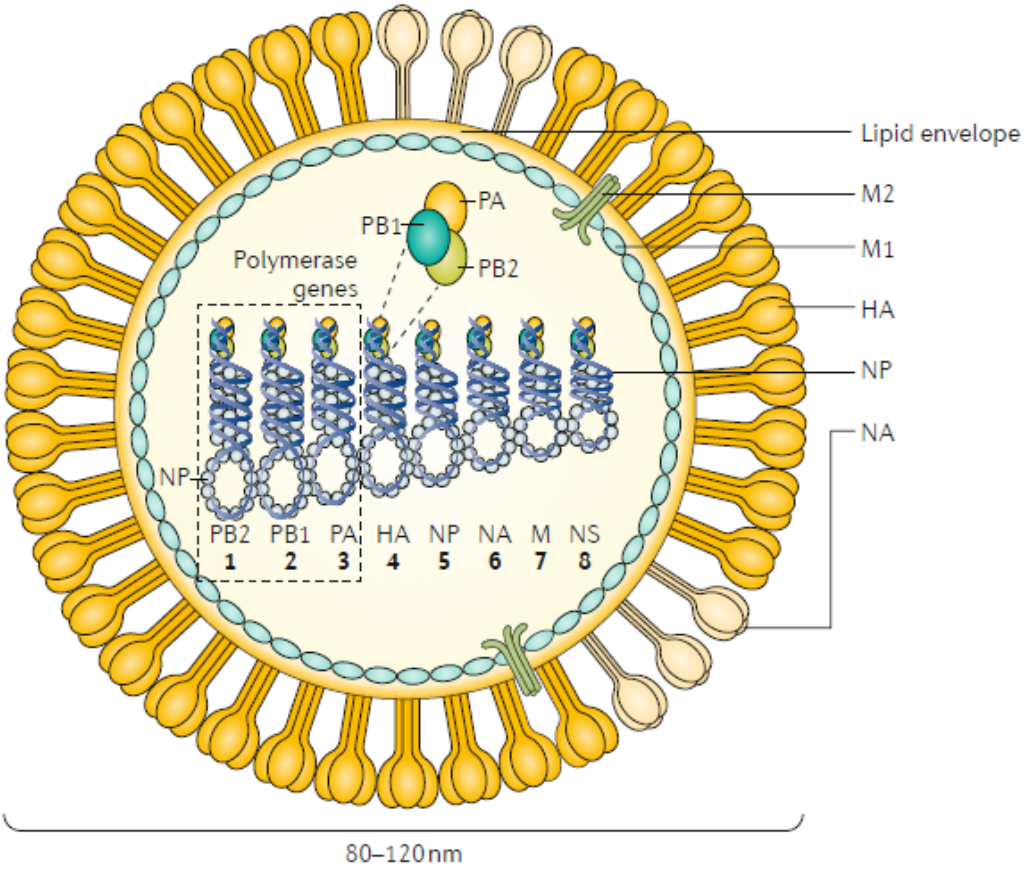

Figure 1.1: Schematic representation of an IAV virion. Virus particles consist of a lipid envelope in which the transmembrane proteins hemagglutinin HA, NA and M2 are embedded. A thin layer of M1 sits beneath the lipid envelope. The viral genome is comprised of 8 segments of single-stranded viral RNA, which are wrapped around the viral NP to form “panhandle” structures. These structures associate with the RNA-dependent RNA polymerase complex (comprising the viral PB1, PB2 and PA proteins), to form viral ribonucleoproteins vRNPs. Figure from (Krammer et al., 2018).

1.1.1.1 Viral replication

In humans, airway epithelial cells represent the primary targets of IAV infection, although immune cells in the respiratory tract, including airway macrophages and DCs, are also susceptible to infection (Short et al., 2012). Infection is initiated by attachment of the viral HA glycoprotein to glycoconjugate receptors on host cells which express terminal sialic-acid (SA) residues (Gamblin et al., 2010). Terminal SAs can be linked to the underlying glycoconjugates in either an α2,6- or an α2,3-dependent manner. Importantly, α2,6 linkages are preferentially bound from human IAV while receptors with α2,3 linkages are preferred by avian IAV (Connor et al., 1994). This preference coincides with the distribution of SA residues at the site of virus infection in different species, with α2,6-linked SA predominantly expressed throughout the human airways whereas α2,3-linked SA is expressed throughout the avian gastrointestinal tract (Skehel et al., 2000). As both linkages are expressed throughout the airways of swine, these animals have been proposed to act as a "mixing vessel" for virus reassortment and therefore the generation of novel viruses with pandemic potential (Ma et al., 2008). In general terms, HA preference for α2,3-linked SA therefore represents an important barrier limiting the introduction of avian viruses into the human population (Byrd-Leotis et al., 2017).

Following attachment of the viral HA to cell-surface SA, infectious entry of virions into host cells occurs via receptor-mediated endocytosis (**Figure 1.2**). Binding of IAV to SA receptors alone is not sufficient to mediate viral entry however to date the specific cell-surface proteins that act as entry receptors for IAV on epithelial cells are not well defined (Maginnis, 2018). In terms of immune cells, a number of C-type lectin receptors (CLRs) have been shown to function as bonafide entry receptors for IAV infection (Londrigan et al., 2012). After receptor binding, viral internalisation and uptake into endosomal compartments is generally mediated by clathrin- or calveolae-dependent endocytosis although virus entry by micropinocytosis has also been described (Grove et al., 2011). Internalised virions then traffic to endosomes where the viral M2 ion channel protein forms pH-gated proton channels in the viral envelope, leading to acidification of the viral

core (Manzoor et al., 2017). The viral HA consists of two subunits, HA_1 and HA_2, and the low pH of the endocytic vesicles trigger an irreversible conformational change in the HA to expose the fusion peptide at the N-terminus of HA_2. While the fusion peptide anchors to the endosomal membrane, the C-terminal transmembrane domain (TMD) anchors in the viral membrane. The HA_2 then folds back to bring the viral and endosomal membranes into close proximity, resulting in membrane fusion (Dou et al., 2018). Additionally, the low endosomal pH facilitates dissociation of the vRNPs from M1, allowing for their entry into the cytosol. Nuclear localisation signals within the NP, PA, PB1 and PB2 proteins then facilitate migration of vRNP complexes to the nucleus where they are imported through nuclear pores for the commencement of viral genomic replication (Boulo et al., 2007).

Within the nucleus, the negative-sense genomic RNA is transcribed into positive-sense complementary (c)RNA, which then serves as template for the transcription of viral (v)RNA. Moreover, the genomic RNA is also transcribed into messenger (m)RNA for protein production. Translation of viral mRNA into proteins is dependent on the activity of the cellular RNA polymerase II (Pol II). However, as recognition by Pol II requires a 5´cap modification and polyadenylation signal and these structures are not expressed on influenza virus mRNA, the virus has evolved a strategy to “steal” 5´ caps from host pre-mRNAs known as “cap-snatching” (Fodor, 2013). As a result of cap-snatching, viral mRNAs are then equipped with the necessary signals to facilitate export to the cytoplasm for subsequent protein translation (Dou et al., 2018). To further amplify viral RNA synthesis, the viral polymerase proteins (PB1, PB2 and PA) and the NP are then shuffled back into the nucleus whereas the viral membrane proteins (HA, NA and M2) traffic to the plasma membrane. In the nucleus, newly-synthesised vRNA complexes associate with M1 and nuclear export protein (NEP) which then facilitate their export out of the nucleus before they are transported to the plasma membrane and incorporated into nascent virus particles (Boulo et al., 2007). Newly-formed virions acquire a lipid bilayer containing the HA, NA and M2 viral proteins as they bud from the apical membrane of polarised host cells (Rossman et al., 2011). The enzymatic activity

of the viral NA facilitates virus budding and release by cleaving SA residues from viral glycoproteins to prevent virus aggregation as well as from cell-surface glycoproteins and glycolipids to promote virus release (McAuley et al., 2019).

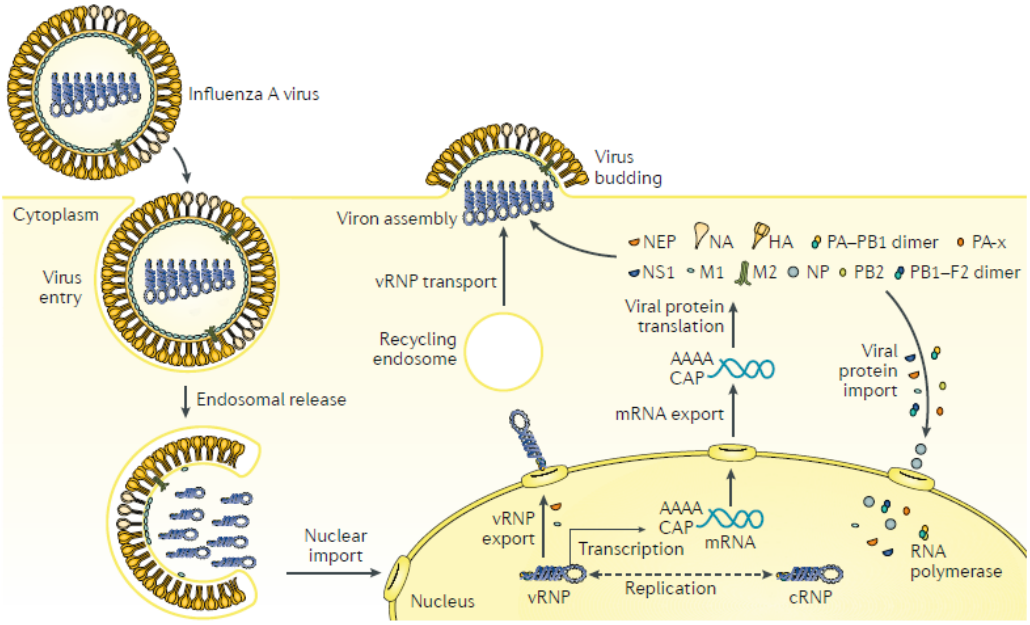

Figure 1.2: IAV replication cycle. Virions enter host cells by receptor-mediated endocytosis and are processed in endosomal compartments, where fusion of viral and endosomal membranes results in release of the vRNP into the host cytoplasm. vRNPs are then transported into the nuclear compartment, where the negative-sense genomic vRNA is transcribed in positive-sense cRNA which forms positive-sense complementary RNP intermediates. Viral mRNA is transcribed from vRNA, translated into proteins in the cytoplasm and then particular viral proteins are transported back into the nucleus to promote the generation of additional vRNPs. The viral transmembrane proteins (HA, NA, M2) are transported to the plasma membrane where new virions assemble with vRNPs. Newly-formed virions then bud from the surface of infected cells with the enzymatic activity of the viral NA acting to prevent aggregation and to promote virus release. Figure from (Krammer et al., 2018).

1.1.1.2 Influenza antivirals

There are a limited number of licensed antiviral drugs available for the treatment of influenza infections. To date, four antiviral drugs are approved by the Centers for Disease Control (CDC): three neuraminidase inhibitors (NAI), namely oseltamivir phosphate (Tamiflu®), zanamivir (Relenza®) and peramivir (Rapivab®), as well as the polymerase inhibitor baloxavir marboxil (Xofluza®) (CDC, 2021). NAIs act by blocking the enzymatic activity of the viral NA and thereby inhibiting virus release from infected cells (Davidson, 2018). NAI treatment has been shown to effectively reduce the duration of clinical symptoms in several meta-analyses however NAIs generally have to be administered within 48 hours (hrs) after symptom onset to be effective and to reduce viral shedding (Fielding et al., 2014; Jefferson et al., 2014).

Importantly, viruses with amino acid substitutions in the viral NA that reduce their sensitivity to oseltamivir and other NAIs have been reported. In 2007-2009 seasonal H1N1 with a H274Y substitution in the viral NA associated with reduced sensitivity to oseltamivir emerged and rapidly spread to become the dominant H1N1 circulating globally (Hurt et al., 2009). The emergence of the novel A(H1N1)pdm09 ‘swine flu’ virus in 2009 coincided with reduced circulation and ultimately disappearance of seasonal H1N1, however this incident emphasised the need to closely monitor currently circulating viruses for mutations that might be associated with resistance to current antiviral treatments for influenza (Dawood et al., 2009; McKimm-Breschkin, 2013).

Baloxavir marboxil is a small molecule inhibitor of the viral PA protein that blocks viral replication by inhibiting the cap-dependent endonuclease activity of PA (Shirley, 2020). Several phase 2 and 3 clinical trials have shown that baloxavir was superior to both placebo and oseltamivir treatment during influenza infections and that baloxavir treatment within the first 48 hrs of symptom onset reduced time to alleviation of symptoms to a similar extent as oseltamivir (Hayden et al., 2018). Interestingly, baloxavir treatment appears to be more effective against IBV than against IAV (Zaraket et al., 2021). However, viruses with some resistance against baloxavir have already been reported, with mutations resulting

in the I38T substitution in the viral PA being the most common described to date (Gubareva et al., 2019). Historically, adamantane derivates targeting the M2 ion channel of IAV have also been used but are no longer recommended due to their lack of activity against IBV and the widespread incidence of the S31N substitution in almost all circulating IAV, which is associated with adamantane resistance (van der Vries et al., 2013; Hurt, 2014).

Without doubt, vaccines represent the best prophylactic agents currently available to limit the impact of influenza infections, however studies indicate that they confer only limited protection. Vaccine effectiveness can be impacted by patient-specific factors, such as age, comorbidities or previous influenza exposure (Radin et al., 2016), but also by the continual accumulation of additional mutations within the HA and NA as a result of antigenic drift (Wang, Y. et al., 2018). Reformulation and adjustment of vaccine composition is therefore necessary every year. Moreover, while vaccines provide protection against circulating seasonal viruses, there is always a delay of several months to formulate a new vaccine following the emergence of novel pandemic viruses in the human population.

1.1.2 Respiratory syncytial virus

1.1.2.1 General features

Respiratory syncytial virus (RSV) is a major cause for respiratory tract infection, particularly in infants and young children. Severe infections are marked by the development of lower respiratory tract infections leading to bronchiolitis, especially in children, the elderly and immunocompromised (Nam et al., 2019). RSV is one of the three major causes of death during post-neonatal lower respiratory infections, along with *Streptococcus pneumonia* and *Haemophilus influenza* (Nair et al., 2010; Lozano et al., 2012). By the age of 2, almost all children have been infected with RSV, although reinfections are common

throughout adult life and these are mainly present as mild URT infections (Nam et al., 2019).

RSV belongs to the family of *Pneumoviridae* and is an enveloped virus with non-segmented, negative-sense ssRNA genome of 15.2 kb (**Figure 1.3**) (Ascough et al., 2018). The ssRNA genome consists of 10 genes which are arranged in sequential order, coding for two non-structural (NS) and nine structural proteins (Schildgen et al., 2011). The two NS proteins (NS1 and NS2) inhibit apoptosis and cellular type I interferon (IFN) responses by targeting aspects of both IFN induction and IFN-induced signaling (Spann et al., 2005; Bitko et al., 2007). The remaining viral proteins, including the M proteins, are structural proteins. Notably, the M gene contains two overlapping open reading frames (ORFs) which encode for the M2-1 and M2-2 proteins, which exhibit distinct functions (Alison et al., 1999). In general, M proteins are non-glycosylated proteins lining the inner leaflet of the viral envelope which interact with cytoplasmic domains of the fusion (F) protein (Battles et al., 2019). M2-1 is a nucleocapsid-associated transcription factor and binds to RNA and phosphoprotein (P) to enhance transcription efficiency, whereas the M2-2 polypeptide is associated with genome replication and regulates the switch between the viral RNA transcription and replication (Hu et al., 2020). Additional structural proteins such as nucleoprotein (N), the large polymerase (L) and P are associated with the nucleocapsid. The RNA genome is coated with the viral N protein to form the nucleocapsid (NC), which serves as the template for RNA synthesis by the viral RNA-dependent RNA polymerase (Bakker et al., 2013). P protein interacts with N and serves as a polymerase cofactor and it also interacts with L protein, which is important for gene transcription (Cifuentes-Muñoz et al., 2019). The three remaining structural proteins are transmembrane glycoproteins embedded in the viral envelope. The small hydrophobic (SH) protein is a viroporin which forms hydrophilic pores in the host cell membrane while the attachment glycoprotein (G) mediates viral attachment to host cell receptors. The viral F protein facilitates both virus-to-cell and cell-to-cell fusion (Ascough et al., 2018).

Based on divergent antigenic reactivity of the G glycoprotein, RSV can be classified into A and B subtypes which are further divided into 13 RSV A and 20 RSV B genotypes (Pangesti et al., 2018). The transmembrane F and G glycoproteins are the main targets of humoral immune response and the G glycoproteins show significant variation between subtypes whereas the F protein is more highly conserved, making F protein a more attractive candidate for RSV vaccine development (Vekemans et al., 2019).

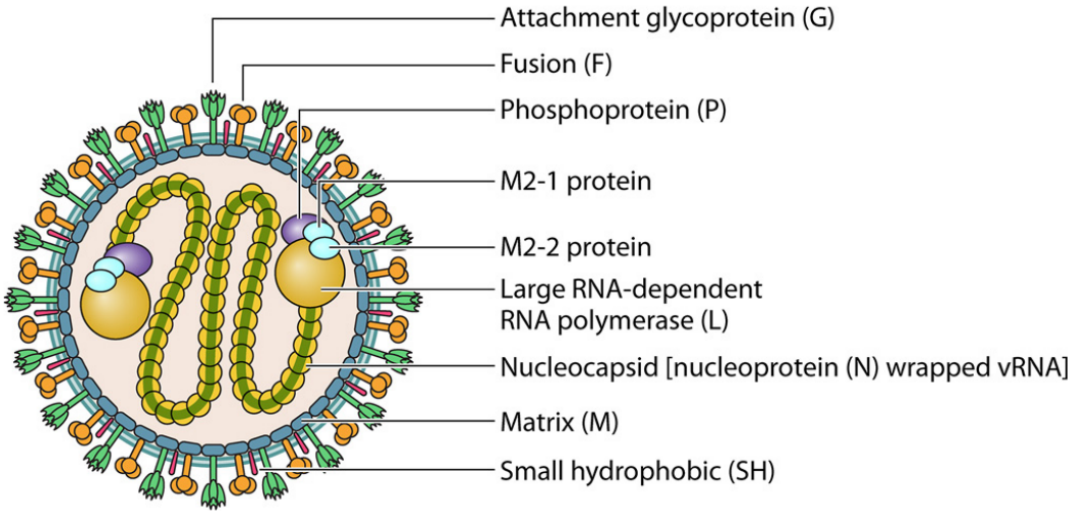

Figure 1.3: Schematic representation of a RSV virion. Virus particles consist of a lipid envelope in which the attachment glycoprotein (G), as well as the fusion (F) and small hydrophobic (SH) proteins are embedded. Matrix (M) protein lines the inner lipid envelope. The viral genome is comprised of non-segmented ssRNA, which is wrapped around nucleoprotein (N). The ribonucleoprotein complex is associated with the vRNA and consists of the large RNA-dependent RNA-polymerase (L), phosphoprotein (P) and M2-1 and M2-2 proteins. Figure from (Céspedes et al., 2016).

1.1.2.2 Viral replication

RSV infection is initiated by attachment of the viral G glycoprotein to host cells (**Figure 1.4**). Airway epithelial cells are the primary targets of human RSV infection but immune cells such as alveolar macrophages (AMs) and DCs are also susceptible (Sarmiento et al., 2002; Guerrero-Plata et al., 2006; Johnson et al., 2011). Several host factors, including glycosaminoglycans, CX_3CR1, intercellular adhesion molecule (ICAM)-1, epidermal growth factor receptor (EGFR) and nucleolin have been implicated as attachment factors and/or receptors for glycoprotein G (Battles et al., 2019). The F protein can also mediate attachment, although to a lesser extent than the G glycoprotein (Techaarpornkul et al., 2001). Following attachment, viral entry is then facilitated by fusion of the virion with the host cell membrane, a process which is mainly mediated by the F glycoprotein.

RSV F protein is a type I viral fusion glycoprotein expressed on the surface of the virion which is synthesised as precursor F0 protein. Three F0 monomers assemble into a trimer and undergo activation by furin-like host proteases in the Golgi of host cells, generating the F1 and F2 subunits (González-Reyes et al., 2001). Trimers of F1 and F2 form the metastable prefusion structures (pre-F) which are expressed on the virion surface. Upon binding of the virion to the target cell, pre-F is triggered and structural rearrangements in F result in formation of an unstable pre-hairpin intermediate. This intermediate forces viral and host cell membranes into close proximity, such that membranes fuse and the stable post-fusion form (post-F) is formed (Mejias et al., 2017; Battles et al., 2019). While it is widely accepted that conformational changes in RSV F can result in direct fusion with the plasma membrane, there is also evidence to indicate that RSV infection of certain cell types, including airway epithelial cells, can occur via micropinocytosis and/or clathrin-mediated endocytosis (Kolokoltsov et al., 2007; Krzyzaniak et al., 2013). Irrespective of the route of entry, viral genomic RNA is then released into the cytoplasm for subsequent transcription and genomic replication.

RSV replication occurs exclusively in specialised cytosolic organelles known as “inclusion bodies” (Norrby et al., 1970). Inclusion bodies contain the viral replication complex (consisting of polymerase L, P and M2-1 proteins), as well as the genomic RNA which is bound to the viral N protein (Munday et al., 2015). The viral polymerase transcribes the genome sequentially from 3’ to 5’, generating a gradient of expression with highest levels of viral mRNA close to the 3’ end (Dickens et al., 1984). Each viral gene possesses its own promotor called the gene start (GS), as well as a transcription ending sequence at the gene end (GE). Viral mRNAs are then 5’-capped, polyadenylated at the 3’ end and transported to host cell ribosome complexes for translation into viral proteins. The RSV F, G and SH glycoproteins undergo processing through the endoplasmic reticulum (ER) and Golgi and are then transported to the apical plasma membrane. After mRNA transcription, the viral polymerase switches to transcribe positive-sense antigenomes which are a necessary intermediate for the production of the negative-sense genomic RNA (Fearns et al., 2000). For transcription of antigenomes, the viral polymerase operates in a “read-through” mode where the GS and GE of each gene are not recognised, a process likely mediated by the M2-2 protein (Hu et al., 2020). Antigenomes are then transcribed into negative-sensed RNA genomes and wrapped to N proteins.

Viral assembly and budding of RSV are not particularly well understood. Assembly of nascent virions occurs at the plasma membrane in a process which appears to be mediated by the F and M proteins. One model suggests that the cytoplasmic tails of F proteins in the plasma membrane act to recruit M proteins and that this, in turn, induces the movement of viral components to the budding site in an actin-dependent manner (Battles et al., 2019). RSV budding occurs independently of the ESCRT machinery, which is the most well-defined budding mechanism for enveloped RNA viruses (Utley et al., 2008). Apical recycling systems, including the apical recycling endosome (ARE), have been implicated in directional budding of RSV from polarised epithelial cells (Utley et al., 2008). For RSV, virus spread is also mediated via fusion of infected cells to neighbouring cells via a process dependent on both the viral F protein and RhoA, a cellular small GTPase protein. Fusion of RSV-infected cells results in the formation of

large syncytia, which is a characteristic feature of RSV infections in mammalian cell culture (Pastey et al., 1999; Collins et al., 2008).

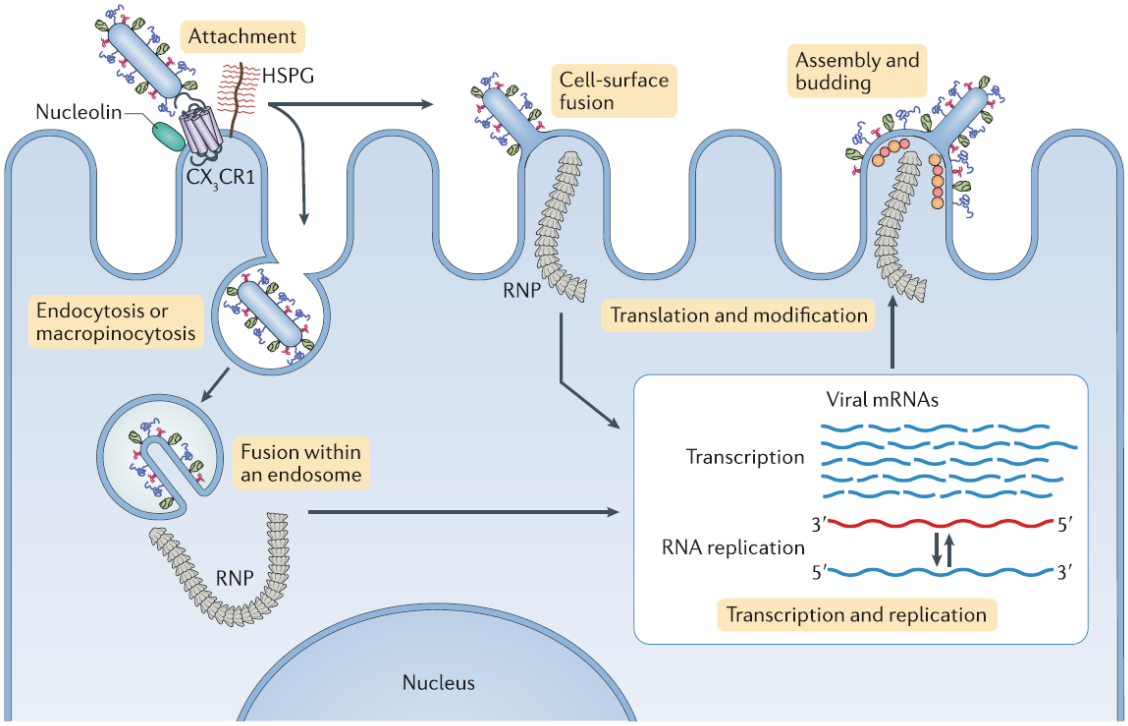

Figure 1.4: RSV replication cycle. Virions attach to the host cell by interactions between the viral attachment G glycoprotein and appropriate attachment/entry receptors on the cell surface. Viral particles enter cells following direct fusion at the plasma membrane or by internalisation via endocytosis and/or micropinocytosis prior to subsequent fusion. The viral F protein undergoes conformational changes to induce fusion and subsequent release of vRNP into the cytoplasm. Viral replication and transcription occur in viral inclusion bodies in the cytoplasm. Viral mRNAs are transcribed by the viral polymerase complex. Unsegmented, negative-sense vRNA is also transcribed into an antigenome which serves as template for the generation of new vRNA. Viral spread is mediated via F protein-dependent formation of syncytia, allowing for direct fusion to neighbouring cells, or by budding of new virions from the apical membrane. Figure from (Battles et al., 2019).

1.1.2.3 RSV antivirals

Despite extensive research, there are no licenced vaccines available for RSV, no curative therapies and only two FDA-approved antiviral drugs suitable for prevention or treatment of serious respiratory tract infections caused by RSV. Supportive care with fluid and oxygen management remain the mainstay approaches to treat RSV infections.

Historically, the lack of RSV vaccine development can be attributed to a disastrous vaccine failure in the 1960s, where a clinical trial involving a formalin-inactivated RSV vaccine in children led to enhanced disease following subsequent natural infection of vaccinees with RSV (Acosta et al., 2016). Hospitalisation in vaccinated participants occurred at higher incidence than in the control group and the trial was associated with two fatalities (Kim et al., 1969). The enhanced RSV disease in vaccinated individuals correlated with nonprotective antibody responses and the development of a pathogenic Th2 memory response characterised by an influx of eosinophils into the lungs after RSV infection (Kim et al., 1969). While this deterred research into RSV vaccine candidates for many years, passive immune prophylaxis using monoclonal antibodies such as palivizumab (Synagis®) has represented an alternative and effective prophylactic that has been used for many years (Hu et al., 2010). Palivizumab is a humanised monoclonal antibody, comprising 95 % human and 5 % murine amino acid sequences and is directed against a conserved epitope of the RSV F protein. Binding of palivizumab to F protein prevents viral fusion and shows activity against both RSV A and B (Scott et al., 1999). However, the high costs associated with this treatment have limited widespread use and it is generally only recommended for high-risk infants (Homaira et al., 2014).

The only FDA-approved antiviral therapeutic against RSV is aerosolised ribavirin, a guanosine-nucleoside analogue that mimics purines such as inosine and adenosine and therefore inhibits viral RNA synthesis. Ribavirin was developed in the 1970s and has been shown to have antiviral properties against a range of DNA and RNA viruses (Fernandez et al., 1986). Ribavirin is currently used for

treatment of RSV and, in combination with IFN-α, for treatment of HCV (Olchanski et al., 2018). Other strategies currently in development to treat RSV infections include the use of recombinant antibodies or nanobodies to RSV proteins, fusion inhibitors to block fusion of the virus with host cells, NP inhibitors to impede viral replication, and nucleoside analogues and non-nucleoside inhibitors, amongst others (Behzadi et al., 2019; Karron, 2021). Of note, in the last 10 years, advances in the structural biology of the RSV F protein have resulted in intense interest in the development of an array of different RSV vaccine candidates, including particle based, live-attenuated, vector based and subunit vaccine candidates (Mazur et al., 2018). Recently, several vaccine candidates in clinical trials for infants and children as well as for elderly adults have shown promising results both in terms of vaccine immunogenicity and safety, highlighting the renewed interest in developing strategies to lessen the impact of this global health problem (Shan et al., 2021).

1.1.3 Immunity to respiratory virus infections

The immune system plays a critical role in controlling replication of different respiratory viruses, promoting virus clearance and establishing resistance to re-infection. The immune system is typically divided into innate and adaptive immunity, although these distinctions are not mutually exclusive. Adaptive immunity provides a pathogen-specific, fine-tuned immunological response which requires specific and highly regulated interactions between antigen-presenting cells (APCs) and T and B lymphocytes (Bonilla et al., 2010). In the early stages of infection, innate immune responses represent the first line of defence, limiting virus replication and spread prior to the expansion of antigen-specific adaptive immune responses. Pre-existing and rapidly induced innate immune mechanisms include soluble pattern recognition receptors (PRRs) of the galectin, defensin and C-type lectin families present in serum and respiratory fluids (Ganz, 2003; Rabinovich et al., 2009; Brown et al., 2018). Other components of humoral innate

immunity include proteins of the complement system which can opsonise or lyse virions or virus-infected cells (Bonilla et al., 2010).

The cellular component of innate immunity involves cells of the myeloid lineage which act as professional APCs, including DCs, monocytes and macrophages. DCs patrol the skin and mucosal surfaces, sampling and internalising both self and non-self proteins via phagocytosis or endocytosis before presenting peptide antigens on their surface via major histocompatibility complex (MHC) class II molecules. This process of antigen presentation ultimately results in the activation of T cell responses to provide cell-mediated immunity against invading pathogens, including viruses (Aristizábal, 2013). Monocytes and macrophages can also function as APC and play key roles in releasing cytokines and chemokines to modulate adaptive and innate responses (Silva, 2010). Thus DCs, monocytes and macrophages play an important role in bridging innate and adaptive immune response. Innate lymphoid cells such as natural killer (NK) cells are rapidly induced and activated following viral infections, producing proinflammatory and cytotoxic proteins such as perforin and granzymes to kill virus-infected cells (Vivier et al., 2008). Neutrophils are also rapidly recruited to sites of viral and other infections, where they limit virus infection by releasing chemokines and cytokines, triggering degranulation or generating neutrophil extracellular traps (NETs) (Johansson et al., 2021).

Effector cells of innate immunity have direct antiviral and/or immunoregulatory functions themselves, as well as promoting recruitment and activation of a range of additional cells. Type I IFNs are a key family of cytokines produced after viral infection which can also regulate aspects of adaptive immunity. For example, type I IFN induces maturation of DCs by increasing expression of costimulatory and MHC class I molecules. Additionally, type I IFNs mediate induction of antigen-specific $CD8^+$ T cells and chemokines which recruit lymphocytes and monocytes (Kawai et al., 2006).

Thus, the early inflammatory responses mediated by the innate immune system act to limit virus infection and spread in the first few days of infection, prior to the development and expansion of antigen-specific T cell and B cell responses to

promote virus clearance. In addition to limiting early infection, innate immunity is also key to regulating aspects of adaptive immunity.

1.1.4 Pattern recognition receptors and detection of IAV and RSV

As mentioned above, macrophages, DCs and epithelial cells lining the respiratory tract represent the primary targets of respiratory virus infection (Kreijtz et al., 2011). These cells express a variety of evolutionarily conserved, germline-encoded PRRs, which detect conserved pathogen-associated molecules or molecular structures, known as pathogen-associated molecular patterns (PAMPs) (Akira et al., 2006). Of the PRRs, Toll-like receptors (TLRs), RIG-I like receptors (RLRs) and NOD-like receptors (NLRs) have been particularly well characterised. TLRs are type I transmembrane receptors that sense a broad variety of pathogens, including bacteria, fungi, viruses and parasites. Depending on their localisation, particular TLR can detect extracellular pathogens at the cell surface or internalised pathogens within endosomal compartments. In general terms, cell-surface TLRs sense microbial membranes or cell wall components while endosomal TLRs sense nucleic acids (Fitzgerald et al., 2020). The expression of TLRs is often restricted to immune cells such as macrophages, neutrophils, DCs, B cells and specific T cell subsets. In contrast, RLRs are broadly expressed in different cell types throughout the body (Hartmann, 2017). RLRs sense viral pathogens by recognizing so called “non-self RNA” that represent nucleic-acid structures not usually present within mammalian cells (i.e. viral genomes or replication intermediates) to induce a broad antiviral signaling response, as discussed below. The relative contribution of particular PRRs to the detection of IAV and RSV is not completely clear, although both viruses have been demonstrated to interact with specific TLRs, NLRs and RLRs.

The TLR family comprises 10 members (TLR1-TLR10) in human and 12 (TLR1-TLR9, TLR11-TLR13) in mouse. TLR either localise to cell surface (TLR1, TLR2, TLR4-TLR6 and TLR10) or to intracellular compartments (TLR3, TLR7-TLR9 and TLR11-TLR13) such as the endosome, lysosome or

endolysosome (Kawasaki et al., 2014). Most TLRs utilise a MyD88-dependent signaling pathway. Upon activation of TLRs, MyD88 recruits IRAK1, which in turn activates TRAF6. This is followed by IκB kinase (IKK)-mediated phosphorylation and degradation of I kappa B (IκB)α, resulting in nuclear translocation of NF-κB and expression of inflammatory cytokines and chemokines. TLR3 utilises a MyD88-independent signaling cascade which consists of recruitment of TRIF, activation of TBK1 and RIPK1 and subsequent phosphorylation of IRF3 (Nie et al., 2018). TLR4 activates both MyD88-dependent and TRIF-dependent pathways (Yamamoto et al., 2003).

TLR3, TLR4, TLR7, TLR8, TLR9 and TLR10 can all be activated following IAV infection either by sensing double-stranded (ds) RNA (TLR3 and TLR10), ssRNA (TLR7, TLR8, TLR9) or danger-associated molecular patterns (DAMPs) such as cellular proteins HMGB1 or SAP130 released from infected cells (TLR4) (Malik et al., 2020). A number of TLRs, namely TLR2, TLR3, TLR4, TLR6, TLR7, TLR8 and TLR9 have all been implicated in antiviral responses to RSV infections (Samy et al., 2015; Ascough et al., 2018).

The NLR family comprises 22 cytosolically expressed proteins. Based on N-terminal effector domains, NLRs are divided into four subfamilies, namely NLRA, NLRB, NLRC and NLRP. Biology of NLRs is extremely complex and studies suggest that the function of NLRs goes beyond the function of PRRs as they have been implicated in autophagy, apoptosis, modification of signal transduction and gene transcription, as well as reproductive biology (Fritz et al., 2015). Many pathogens can activate NLR with NLRP3 being the best studied member which is activated by many microbes, including several RNA viruses such as IAV, RSV, and Sendai virus (SeV), as well as DNA viruses such as poxviruses and adenoviruses (Jacobs et al., 2012). NLRP3 recruits apoptosis-associated speck-like protein (ASC) and caspase-1 to form the inflammasome – a multimeric protein platform that plays an important role during viral infections, including IAV and RSV, by regulating the release of inflammatory cytokines IL-1β and IL-18 (Allen et al., 2009; Segovia et al., 2012; Triantafilou et al., 2013).

The RLR family comprises three members: retinoic acid-inducible gene I (RIG-I), melanoma differentiation-associated gene 5 (MDA5) and laboratory of genetics and physiology 2 (LGP2) (Yoneyama et al., 2005). RLRs are generally regarded as cytoplasmic RNA sensors although a nuclear form of RIG-I was recently described (Liu et al., 2018). All RLR possess a central helicase domain and a carboxy-terminal domain (CTD). RIG-I and MDA5 additionally possess two amino- terminal caspase activation and recruitment domains (CARDs) which are essential for downstream signaling.

RIG-I represents the key sensor of IAV and RSV infections in mammalian cells. As this thesis focuses on RIG-I and its role during RNA virus infections, RIG-I is discussed in more detail in subsequent sections of the literature review. In terms of IAV, the viral genome forms a panhandle structure due to self-complementarity between the 5' and 3' ends of the viral gene segments and this acts as potent activator of RIG-I (Rehwinkel et al., 2010; Liu et al., 2015). Short aberrant RNAs generated as a by-product of viral replication have also been implicated in RIG-I activation, indicating that RIG-I has the potential to sense ligands associated with both incoming and replicating IAV (Te Velthuis et al., 2018; Liu et al., 2019). Recently, a nuclear-resident form of RIG-I was described and this was shown to bind to vRNPs in the nucleus, which is the location of IAV replication (Liu et al., 2018). The role of MDA5 during IAV infection is less well defined. For example, studies have reported that MDA5 does (Xing et al., 2011; Benitez et al., 2015) and does not (Kato et al., 2006; Guo et al., 2007) contribute to cellular responses following IAV infection. In general, the function of RLRs and ISGs can be studied in a variety of ways including overexpression or siRNA screens. While overexpression screens identify a loss of virus replication when critical genes are overexpressed, siRNA screens show enhanced virus replication resulting from loss of function of antiviral factors. While most of the studies characterised the function of MDA5 by using siRNA strategies *in vitro*, Benitez *et al.* generated an IAV-based library of viruses encoding a unique mouse-specific siRNA capable of silencing a single virus-induced host transcript which was then subsequently administered to mice and selective pressure was used to identify out those host factors that restore replication of the attenuated virus. While *in vitro* systems

represent valuable and useful tools to assess single protein functions, especially the effects of interaction of molecules from different cell compartments are not expressed and subsequently lead to misinterpretation of results. Thus, the *in vivo* screening approach represents a more physiological and probably more relevant model, which makes a contribution of MDA5 sensing following IAV infection likely but probably secondary to that of RIG-I.

RIG-I has also been identified as an innate sensor of RSV, although the exact viral structures recognised by RIG-I are yet to be resolved (Xing et al., 2011). The specific roles of RIG-I versus MDA5 during RSV infection are also not clearly defined. Initial studies in mouse fibroblasts suggested that MDA5 was dispensable while RIG-I was essential for signaling following RSV infection (Loo et al., 2008). However, subsequent studies suggest that MDA5 may play a complementary role to RIG-I during RSV infection by preventing the early degradation of transcription factor IRF3 and therefore sustaining IRF3-dependent antiviral gene expression (Grandvaux et al., 2014).

LGP2 is an additional RLR that lacks the amino-terminal CARDs required for initiating the activation of IRF3 and IFN transcription. Studies have proposed LGP2 can mediate both antiviral and proviral functions during different virus infections and suggested that its function might be dependent on both cell type and/or nature of the particular virus (Rodriguez et al., 2014). In regard to IAV infection, LGP2 has been reported to downregulate IFN production during infection by seasonal IAV that activate IRF3 and IFN transcription (Malur et al., 2012), however its role during RSV infections has yet to be reported.

1.1.4.1 RIG-I and RIG-I signaling

RIG-I is a DExD/H box helicase that was first described in 2004 as an essential receptor to detect viral dsRNA and to induce downstream signaling upon viral infection (Yoneyama et al., 2004). Until recently it was thought to be exclusively expressed in the cytoplasm, however Liu *et al*. recently demonstrated that RIG-I was also expressed in the nucleus (Liu et al., 2018). RIG-I contains three

functionally distinct domains; a helicase domain, as well as a C-terminal and a N-terminal domain (Yoneyama et al., 2004). The helicase core that comprises of two helicase domains, Hel1 and Hel2, is framed on one side by the N-terminus, consisting of two repeating CARDs and on the other side by the CTD. RIG-I mediated signaling requires the adaptor protein MAVS (also called IPS-1, Cardiff or VISA) which interacts with the CARDs of RIG-I to promote recruitment of downstream signaling molecules and, ultimately, to the transcriptional activation of IFN and proinflammatory cytokine genes (Seth et al., 2005). The CTD of RIG-I is involved in the recognition of viral RNA and binding to dsRNA induces a conformational change that exposes the N-terminus of the CARDs. The helicase core serves as an active site for ATP binding and hydrolysis and also contains a RNA binding site (Yoneyama et al., 2007). Despite similar structures, RIG-I and MDA5 generally play non-redundant roles in the detection of different viruses. For example, MDA5 is essential for sensing picornavirus infection whereas RIG-I acts as the primary sensor for a range of other RNA virus infections including SeV, Newcastle disease virus (NDV), vesicular stomatitis virus (VSV) and Japanese encephalitis virus (Kato et al., 2006; Loo et al., 2008; Goutagny et al., 2010; Weber-Gerlach et al., 2016). For IAV and RSV, as discussed above, RIG-I appears to act as the primary sensor of virus infection but there is evidence to suggest that MDA5 might play a complementary role in antiviral immunity (Grandvaux et al., 2014; Sun et al., 2017).

RIG-I binding to viral RNA occurs via binding of the CTD to the 5’ triphosphate end of the RNA as well as recognition by the helicase domain. RIG-I recognises short dsRNA regions with blunt ended 5’-triphosphate or 5’-diphosphate moieties, which are often at the end of (+) ssRNA viruses (Schlee et al., 2009; Goubau et al., 2014). Furthermore, the presence of an unmethylated 5’-terminal nucleotide at the 2’-O position is important for RIG-I activation as the presence of N1-2’O-methylated RNA results in steric hindrance and inhibition of recognition by RIG-I (Schuberth-Wagner et al., 2015). While RIG-I recognises short dsRNA species, MDA5 detects long (>1kb) dsRNA (Kato et al., 2008). For (-) ssRNA viruses which generally do not form dsRNA during infection, RIG-I-mediated detection can still occur due to the formation of short double-stranded structures

by highly complementary 5'- and 3'-sequences. The formation of such "panhandle" structures triggers binding and subsequently activation of RIG-I (Schlee et al., 2009; Goubau et al., 2014; Liu et al., 2015). Interestingly, expression of these panhandle moieties serves as a tool to distinguish self from non-self RNA, as these secondary structures are typical of viral, but not mammalian, RNA (Gack, 2014).

In uninfected cells, RIG-I exists in a conformation where the critical signaling CARDs are masked and kept in an autoinhibited state which sterically cannot induce downstream signaling to MAVS (**Figure 1.5**) (Kowalinski et al., 2011). In this inactive state, RIG-I is phosphorylated at several residues within the CARD and the CTDs (Chan et al., 2015). Following binding of vRNA to the CTD and the helicase domains during viral infection, ATP-dependent conformational changes are induced and the CARD are released from the autoinhibited state to form a 2-CARD tetramer structure which serves a signaling platform (Kowalinski et al., 2011). These conformational changes are accompanied by a number of additional posttranslational modifications, including polyubiquitination and dephosphorylation of the RIG-I protein (Saito et al., 2007).

E3 ubiquitin ligases such as TRIM25, Riplet, TRIM4 and MEX3C facilitate Lys63-(K63)-linked polyubiquitination at the CTD and CARDs. While the specific roles of each of the E3 ubiquitin ligases are not yet completely understood, recent studies suggest that Riplet is indispensable for RIG-I activation while others, such as TRIM25, are dispensable and may exhibit redundant functions (Okamoto et al., 2017; Okude et al., 2020). Although the function of TRIM25 on RIG-I activation are reported to be redundant and dispensable, evidence is emerging that TRIM25 possesses other antiviral properties independent on its regulation of RIG-I. Meyerson *et al.* reported that TRIM25 possesses anti-influenza activity in the nucleus and current studies from Choudhury *et al.* confirmed the destabilising activity of TRIM25 on IAV mRNA and a subsequent antiviral function independent of RIG-I (Meyerson et al., 2017; Choudhury et al., 2021).

In addition to polyubiquitination, CARDs are also dephosphorylated by the phosphoprotein phosphatases 1 (PP1)-α and PP1-γ (Wies et al., 2013). Acetylation and SUMOylation, as well as involvement of other regulatory proteins, have also been reported to modulate RIG-I activation (Liu, Yiliu et al., 2017).

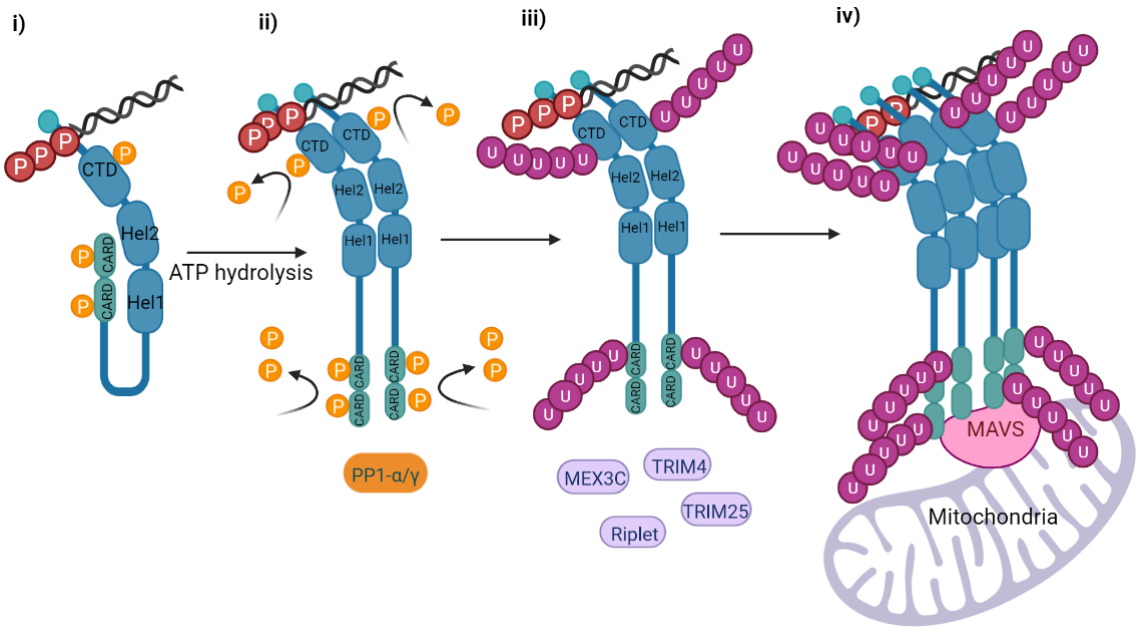

Figure 1.5: Activation of RIG-I. **i)** In uninfected cells, RIG-I is in an inactive state and the CARDs and CTDs are phosphorylated. **ii)** Following binding of dsRNA to the CTD and subsequent ATP hydrolysis, RIG-I is dephosphorylated by PP1-α and PP1-γ, resulting in a conformational change and dimerisation. **iii)** Several ubiquitin ligases (MEX3C, Riplet, TRIM4, TRIM25) then mediate Lys63-linked ubiquitination of the CTDs and CARDs. **iv)** After formation of oligomers, RIG-I then translocates to MAVS which is located at the mitochondrial membrane before interactions between MAVS and the CARDs induce downstream signaling. Adapted from (Brisse et al., 2019), generated in BioRender.

Release of the RIG-I CARD from its auto-inhibitory state allows for the formation of filamentous oligomers of RIG-I and facilitates interactions between CARD and the downstream adaptor protein MAVS, a key determinant for the antiviral signaling cascade. MAVS localises to the outer mitochondrial membrane and interacts with several kinases and proteins such as TRAF3, TRAF6 TNFR associated death domain (TRADD) and TRAF-associated NF-κB activator (TANK1), resulting in the generation of a large multimeric protein complex called the “MAVS signalosome” (Dutta et al., 2020). The MAVS signalosome then activates the IKK complex (IKKα, IKKβ and NEMO) and TBK1 kinases, which phosphorylate and activate the transcription factors IRF3/7 and also mediate NF-κB activation by phosphorylation and degradation of the inhibitory subunit IκBα (Seth et al., 2005). Translocation of NF-κB to the nucleus results in the expression of a variety of chemokines and cytokines which are generally pro-inflammatory in nature (e.g. IL-1, IL-6 and TNF-α) (Liu, Ting et al., 2017). Dimerisation of phosphorylated IRF3/7 also results in translocation to the nucleus and subsequent transcription of genes encoding type I (IFN-α/β) and type III (IFN- λ) IFNs (**Figure 1.6**).

1.1.4.2 Pathways to regulate RIG-I antiviral signaling

Activation of RLR signaling and the corresponding induction of inflammatory and antiviral pathways must be tightly controlled to prevent aberrant activation and the induction of a “cytokine storm”, a phenomenon where over-active immune responses can weaken the host and enhance disease pathogenesis. Virus-infected cells regulate RIG-I activation by negative regulatory feedback loops. For example, a splice variant of RIG-I (RIG-I SV), carrying a short deletion within the CARD, is induced upon viral infection. As truncated RIG-I SV loses interaction with TRIM25, CARD ubiquitination and the downstream signaling cascades are interrupted. Thus, RIG-I SV serves as an ‘off-switch’ for its own signal pathway (Gack et al., 2008). Furthermore, a splice variant of MAVS, called MAVS1a, has been shown to bind to RIG-I and inhibit its interaction with full-length MAVS (Lad et al., 2008). Interestingly, MAVS mRNA is bicistronic and translation results in

expression of a truncated MAVS protein, named “miniMAVS” which has also been reported to dampen IFN induction (Brubaker et al., 2014). Cellular levels of RIG-I protein are also negatively regulated by the IFN-inducible LGP2 and ISG15 proteins. While the role of LGP2 during viral infection is still unclear, studies indicate that it can interfere with recognition of dsRNA by RIG-I (Moresco et al., 2010). ISG15 also regulates levels of RIG-I protein but does so through ISGylation, and reduced levels of RIG-I as a result of this modification lead to reduced antiviral signaling by RIG-I (Yoneyama et al., 2005; Saito et al., 2007; Kim et al., 2008).

Besides the cell-specific RIG-I regulation, viral pathogens have evolved different mechanisms to escape detection by RIG-I. For example, it has been speculated that replication of *Orthomyxoviruses* takes place within the nucleus in order to minimise detection by cytoplasmic RIG-I (Weber et al., 2015). Experimental studies have also demonstrated that the IAV NS1 protein can antagonise RIG-I and interact at different steps within the RIG-I signaling cascade. NS1 can inhibit RIG-I sensing by interacting with RIG-I itself (Pichlmair et al., 2006). The activation and translocation of downstream transcription factors as IRF3 and NF-κB are also hampered by NS1 (Talon et al., 2000; Wang et al., 2000). Moreover, NS1 inhibits the ubiquitin ligases Riplet and TRIM25 to interrupt ubiquitination and subsequently activation of RIG-I (Gack et al., 2009; Rajsbaum et al., 2012). Inhibition of RIG-I activation and signaling is a feature of the IAV NS1 and not the NS2 protein (Zhao et al., 2017). IAV proteins PB1 and PB2 can also antagonise RIG-I activation by direct binding and inhibition of MAVS and the viral HA has also been shown to interact with IFN receptors and promote IFNAR1 degradation (Varga et al., 2011; Xia et al., 2015). Recently it was shown that IAV infection was also associated with ubiquitination and degradation of Janus kinase (JAK)1 and that this correlated with increased expression of suppressor of cytokine signaling (SOCS)1. Moreover, the authors then confirmed that SOCS1 mediated JAK1 ubiquitination and SOCS1-dependent degradation during IAV infection (Du et al., 2020).

RSV has also established different mechanisms to circumvent cell-intrinsic immune responses. Many of these act to supress IFN-α, IFN-β and IFN-λ expression and are mediated predominantly by the RSV NS1 and/or NS2 proteins (Spann et al., 2004). For example, NS1 can bind to the adaptor protein MAVS (Boyapalle et al., 2012) while NS2 binds to the CARD of RIG-I (Ling et al., 2009) and either binding event results in decreased RIG-I – MAVS interactions. A recent study suggests that binding of NS2 to the inactive conformation of RIG-I prevents ubiquitination of RIG-I and subsequent downstream signaling (Pei et al., 2021). NS1 and NS2 have also shown to perturb the JAK-STAT signaling pathway and to induce degradation of STAT2, resulting in reduced IFN responsiveness (Lo et al., 2005).

Taken together, both IAV and RSV have developed multiple pathways to suppress the induction of type I and III IFNs, a process which is mainly mediated by the NS1 of IAV and by the NS1 and NS2 proteins of RSV.

1.1.4.3 Secretion and signaling by type I and type III IFNs

Type I IFN proteins that are translated and secreted from cells can then bind in an autocrine or paracrine manner to cell surface receptors comprised of two transmembrane subunits, IFNAR1 and IFNAR2, that are expressed on most nucleated cells (Schreiber, 2017). Binding of IFN-α/β to its corresponding receptor results in receptor dimerisation, bringing the receptor-associated JAK proteins in close proximity to induce further signaling. Activated JAK1 and tyrosine kinase 2 (TYK2) phosphorylate tyrosine residues at the intracellular receptor subunit and this serves as the binding site for signal transducer and activator of transcription (STAT) proteins (Stark et al., 2012). In a second phosphorylation step, STAT1 and STAT2 are phosphorylated by JAK proteins, resulting in their dimerisation and translocation to the nucleus, where they form either dimeric STAT complexes or heterotrimeric STAT-IRF9 complexes (Durbin et al., 2013). These complexes induce gene expression by binding to IFN-stimulated response elements (ISREs), resulting in the transcription of hundreds

of IFN-stimulated genes (ISGs) which contribute to the induction of an ‘antiviral state’ in virus-infected cells or in uninfected neighbouring cells (Schoggins et al., 2011a). Induction of type I IFNs and the subsequent induction of ISGs is summarised in (**Figure 1.6**).

In addition to type I IFNs, RIG-I activation also stimulates production of type III IFNs, also known as IFN-λ (Kotenko et al., 2003). Type III IFNs (IFN-λ1, 2 & 3) were discovered as interleukin (IL)-29, 28a & 28b and share many similar functions with type I IFNs (Kotenko et al., 2003). IFN-λ4 was discovered later and most closely resembles IFN-λ3, although the amino acid identity between the two is only approximately 30 % (O'Brien et al., 2014). RIG-I-mediated induction of IFN-λ and IFN-α/β occur via similar pathways however the IFN-λ receptor (comprised of IFNLR1 and IL-10Rβ) is predominantly expressed by epithelial cells (Hemann et al., 2017; Lee, S. et al., 2017) and there does not appear to be cross-reactivity between type I and III IFNs and their corresponding receptors (Durbin et al., 2013). Given this more restricted receptor expression, antiviral immunity associated with IFN-λ has been particularly well studied during epithelial cell infections. For example, following selective administration of IAV to the upper airways, mice lacking functional IFN-λ receptors showed enhanced virus dissemination to the lungs, shed more infectious virus from their nostrils and transmitted virus much more efficiently to naïve contacts when compared to wild type mice or mice lacking functional type I IFN receptors (Klinkhammer et al., 2018). Similar to IFN-α/β, IFN-λ signaling also includes activation of the JAK/STAT pathway and the subsequent induction of hundreds of ISGs (**Figure 1.6**).

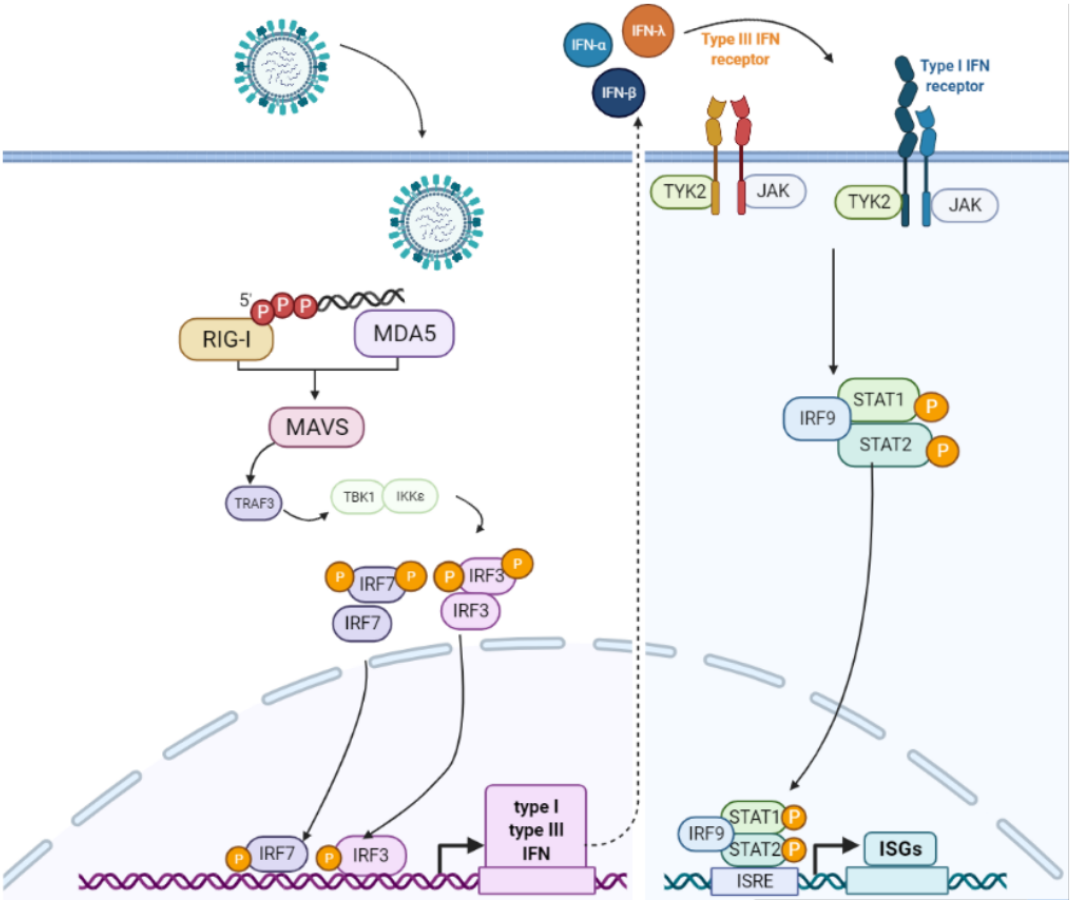

Figure 1.6: Induction of type I and type III IFN-dependent ISG expression following RLR activation. Viral infection is sensed by the cytosolic PRRs RIG-I and/or MDA5, resulting in activation of intracellular signaling cascades and subsequent phosphorylation and dimerisation of transcription factors IRF3 and IRF7, resulting in their translocation into the nucleus to induce transcription of type I (IFN-α and IFN-β) and type III (IFN-λ) IFNs. Following secretion, type I and type III IFNs bind to their corresponding cell-surface receptors in an autocrine or paracrine manner. This, in turn, activates the JAK/STAT pathway and induces subsequent transcription of ISGs. Figure generated in BioRender.

1.1.4.4 Interferon-stimulated genes (ISGs)

Functional IFN-α/β and IFN-λ signaling induces expression of hundreds to thousands of ISGs with the particular number determined by a number of factors, including the particular cell and/or tissue involved (Diamond et al., 2013). A number of ISG proteins have been characterised as antiviral proteins or 'host cell restriction factors' and some, such as the IFN-induced transmembrane (IFITM) proteins, IFN-Induced Proteins with Tetratricopeptide Repeats (IFIT) proteins and the 2′–5′-oligoadenylate synthetase (OAS)/RNase L system have been particularly well studied. However, of the many ISGs induced in host cells in response to viral infection, the antiviral function of relatively few have been characterised in detail (Sadler et al., 2008). Overall, the antiviral functions of ISG proteins have been particularly well-characterised against viruses such as human immunodeficiency virus (HIV)-1 (Colomer-Lluch et al., 2018) and IAV (Villalón-Letelier et al., 2017), while less is known regarding their activity against a range of other viruses, including RSV.

In general terms, ISG proteins characterised to date have been shown to impact different stages of the virus replication cycle. For example, ISG proteins have been reported to inhibit viral entry and/or fusion, while others target subsequent steps during virus replication including transcription, translation or viral protein synthesis. Moreover, a number of different ISG proteins have been reported to interfere with the late stages of viral replication, including virus budding and release (Villalon-Letelier et al., 2017; Farrukee et al., 2020). A number of ISG proteins with reported antiviral activity against IAV and/or RSV are discussed below, highlighting examples of those that restrict virus entry, replication or virus release.

1.1.4.5 Restriction of virus entry by IFITM proteins

Human IFITM-family proteins have been reported to inhibit the early stages of IAV and RSV infections (Brass et al., 2009; Zhang, W. et al., 2015b). IFITM proteins differ in regard to their cellular distribution with IFITM1 expressed

predominantly at the plasma membrane whereas IFITM2 and IFITM3 tend to localise to endosomal/lysosomal compartments. Despite their different cellular locations, the general consensus is that IFITM proteins act to inhibit fusion between viral and cellular membranes thereby restricting the virus from entering the cytoplasm (Diamond et al., 2013). For IAV, IFITM2 and particularly IFITM3 have been implicated in blocking endosomal fusion and therefore infectious virus entry (Brass et al., 2009; Feeley et al., 2011; Kummer et al., 2019). Of interest, IFITM1, IFITM2, and IFITM3 have been implicated in interfering with RSV entry and therefore inhibiting subsequent replication steps (Zhang, W. et al., 2015a). IFITM1 localises to the plasma membrane and has been shown to inhibit a range of viruses that infect cells directly at this site, including RSV (Smith et al., 2019).

1.1.4.6 ISG proteins that inhibit aspects of virus replication

IFIT proteins (IFIT-1/2/3) can be induced through IFN-dependent and -independent pathways and possess multiple functions against invading viruses. First, they bind to the eukaryotic initiation factor 3 (eIF3) translation initiation complex, therefore inhibiting protein translation. Also, IFIT proteins have evolved to detect non-self RNAs, including viral RNAs. mRNA from higher eukaryotes is usually capped and 2′-O-methylated at the 5′ guanosine end (also called the N-7-methylguanoside cap), whereas many viral RNAs express an uncapped 5’-ppp moiety sequestered by a 2′-O-unmethylated 5′ guanosine end and these structures are readily detected by IFIT proteins, resulting in inhibition of viral mRNA translation (Vladimer et al., 2014). Silencing of IFIT proteins has been reported to enhance IAV replication (Pichlmair et al., 2011) and a recent study by Drori *et al.* showed that silencing of IFIT1-3 resulted in enhanced RSV replication while in contrast overexpression of IFIT1-3 resulted in reduced RSV replication (Drori et al., 2020).

ISG15 is an ubiquitin-like IFN-inducible protein that elicits diverse and pathogen-specific functions. ISG15-induced conjugation to target proteins (ISGylation), as well as unconjugated ISG15 have been associated with antiviral activity, however

the exact mechanisms are poorly understood (Perng et al., 2018). ISGylation of viral proteins affects stability and function and can disrupt their interaction with host pathways required for viral replication. Extracellular, unconjugated ISG15 has been reported to function as cytokine which promotes activation of different immune cell subsets, including NK cells, DCs, T cells and macrophages (Perng et al., 2018). *In vivo*, ISG15 $^{-/-}$ mice showed increased susceptibility to IAV infection and *in vitro* knockout or knockdown of ISG15 in human cells was used to confirm its antiviral activity against RSV (Lenschow et al., 2007; Morales et al., 2015; González-Sanz et al., 2016).

The OAS are a family of ISGs which bind dsRNA associated with the replication of a broad range of viruses, including IAV and RSV (Behera et al., 2002; Li et al., 2016). Upon activation of OAS, 2'-5'-oligomers of adenosine are formed which act as second messengers on the latent ribonuclease (RNase L), triggering its dimerisation and activation. RNase L is a ribonuclease which degrades cellular and viral RNA, resulting in the degradation of viral RNA and inducing apoptosis of virus-infected cells (Hartmann, 2017; Schwartz et al., 2019).

1.1.4.7 Inhibition of late stages of infection by ISG proteins

Of the ISG proteins reported to inhibit late stages in virus replication, tetherin has been reported to be active against IAV (Gnirß et al., 2015) and RSV (Berry et al., 2018), as well as against other enveloped viruses such as HIV-1, Ebola virus, Herpes simplex virus (HSV)-1 and Lassa virus (Farrukee et al., 2020). Tetherin inhibits viral replication by preventing virus budding from the plasma membrane and by inducing an antiviral state in cells adjacent to infection via unique inflammatory signaling mechanisms.

1.1.5 Mx proteins

1.1.5.1 General features

Mx (myxovirus resistance) proteins are dynamin-like GTPases that are probably the best-studied ISGs induced in response to IAV infection (Haller et al., 2020). Although most intensively studied in regard to inhibition of IAV, there is increasing evidence that particular Mx proteins can restrict viruses from a number of different genera (Haller et al., 2015). *Mx* genes tend to be highly conserved across different species with one to seven *Mx* genes expressed in almost all vertebrates (Verhelst et al., 2013). Most mammals, including humans and mice, express two *Mx* genes. Human MxA is a cytoplasmic protein whereas MxB localises to the nucleus. Mouse Mx1 is an ortholog of human MxA that is expressed in the nucleus whereas mouse Mx2, a paralog of mouse Mx1 rather than an ortholog of human MxB, is expressed in the cytoplasm (Busnadiego et al., 2014). **Table 1.1** provides examples of viruses inhibited by different human and mouse Mx proteins, while a more comprehensive summary can be found in (Verhelst et al., 2013).

Mx proteins consist of a N-terminal GTPase (G) domain, a middle domain (MD) and a C-terminal GTPase effector domain (GED) (**Figure 1.7**). A stalk domain, consisting of the MD and GED, is separated from the G domain by a bundle signaling element (BSE). The BSE forwards the conformational changes induced by GTP hydrolysis in the G domain to the stalk of the Mx protein (Rennie et al., 2014). The crystal structure of human MxA, but not human MxB, mouse Mx1 or mouse Mx2, has been resolved (Gao et al., 2011). In the stalk domain, a 40 amino acid long loop named L4 (residues 533 to 572) is critical for viral target recognition of MxA (von der Malsburg et al., 2011; Mitchell et al., 2012). Of note, Mx proteins which are expressed in the nuclear compartment express a nuclear localisation signal (NLS) which is located at the N-terminus for human MxB (Melén et al., 1996) or at the C-terminus for mouse Mx1 (Noteborn et al., 1987; Zürcher et al., 1992c) and which is critical for protein localisation. Human MxB elicits antiviral activity against HIV-1 (Goujon et al., 2013; Kane et al., 2013) and HSV-1 (Crameri et al., 2018; Schilling et al., 2018) whereas mouse Mx1 is active against IAV and

VSV, and a limited number of additional viruses (Pavlovic et al., 1992; Dittmann et al., 2008; Sehgal et al., 2020). Steiner *et al.* showed that MxB expressed in distinct nuclear domains instead of the perinuclear region still mediated anti-HIV-1 activity and that a chimeric MxA-MxB protein (containing the N-terminal amino acids of MxA in place of the N-terminal amino acids of MxB) actually acquired anti-IAV activity (Steiner et al., 2020). In mouse Mx1, single amino acid substitution in its NLS resulted in redistribution to the cytoplasm and loss of antiviral activity against IAV and VSV (Zürcher et al., 1992c).

Upon activation, MxA oligomerises into multimeric filamentous or ring-like structures by virtue of its stalk domain (Kochs et al., 2002; Gao et al., 2011). Mutational analyses have shown that antiviral activity of MxA depends on GTP binding and hydrolysis, an intact BSE and intact oligomerisation via the stalk, while for MxB the N-terminus was important for antiviral activity as only the long 78 kDa form with an intact N-terminal NLS-like sequence was found to be antiviral against HIV-1 (Haller et al., 2015). Of interest, Mx expression is only induced by type I and III IFNs and not by virus infection itself, making Mx proteins excellent markers for studies investigating IFN induction (Fasciano et al., 2005; Holzinger et al., 2007).

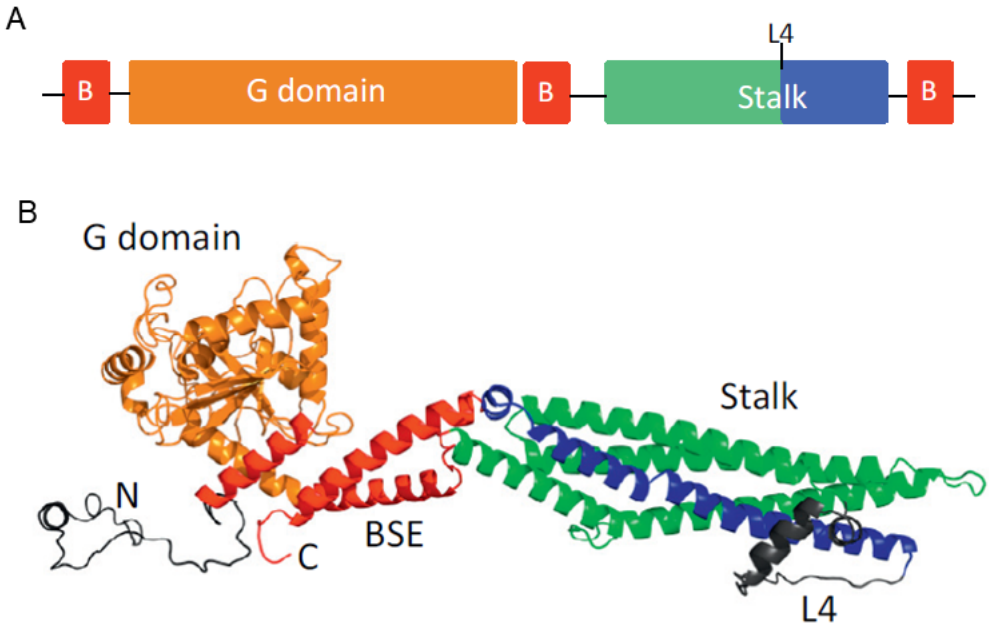

Figure 1.7: Structure of human MxA protein. **A)** Individual domains of human MxA. The BSE is labeled 'B' and is colored in red, the G domain is coloured in orange, the stalk domain consists of the middle domain in green and the GTPase effector domain in blue. **B)** Crystalized structure of human MxA (72 kDa). Figure adapted from (Haller et al., 2015), structure isolated by (Gao et al., 2011).

1.1.5.2 Antiviral activity of human and mouse Mx1 proteins

The exact mechanisms by which human and mouse Mx proteins mediate their antiviral activities are still not fully understood. Given that the antiviral activities of Mx proteins are often linked to their cellular localisation, nuclear Mx proteins often restrict viruses such as IAV that replicate within the nucleus, whereas cytoplasmic Mx proteins often inhibit viruses such as VSV that replicate exclusively in the cytoplasm. However, exceptions do exist. For example, cytoplasmic human MxA restricts a diverse range of viruses including *Orthomyxoviridae* which replicate in the nucleus, as well as *Bunyaviridae, Rhabdoviridae, Paramyxoviridae* and *Hepadnaviridae,* amongst others, which, except for *Hepadnaviridae*, replicate exclusively in the cytoplasm (Haller et al., 2015; Hu et al., 2015; Dietzgen et al., 2017; Fearns et al., 2017; Ferron et al., 2017). Nuclear expression of human MxB also correlates with its ability to inhibit retroviruses (Goujon et al., 2013; Kane et al., 2013; Liu et al., 2013) and herpesviruses (Crameri et al., 2018; Schilling et al., 2018) which replicate in the nucleus. Mouse Mx1 is also expressed in the nucleus and its antiviral activity appears to be quite specific for *Orthomyxoviridae.* Of interest, a recent study suggested that under certain conditions, mouse Mx1 can also form cytoplasmic intermediate filaments and condensates and that these are associated with inhibition of VSV, a member of the *Rhabdoviridae* (Sehgal et al., 2020). Cytoplasmic mouse Mx2 does not inhibit IAV but is reported to be active against a small number of viruses that replicate in the cytoplasm such as VSV and Hantaan virus (Zürcher et al., 1992b; Jin et al., 2001).

The exact mechanisms by which Mx proteins inhibit different viruses are still under investigation and most current knowledge relates to inhibition of IAV by different Mx proteins. For example, human MxA retains IAV nucleocapsids in the cytoplasm, preventing their nuclear import and thereby blocking early steps in the viral replication cycle (Xiao et al., 2013; Haller et al., 2020). In contrast, mouse Mx1 inhibits primary transcription and is reported to interact with the ribonucleoprotein complex, disrupting interactions between the viral NP and PB2 (Pavlovic et al., 1992; Verhelst et al., 2012). A recent study identified human MxB as a potent inhibitor of different herpesviruses which blocked the uncoating of

viral DNA from the incoming viral capsid, thereby inhibiting infection at a stage prior to genomic replication (Crameri et al., 2018; Schilling et al., 2018).

In some but not all instances, the cellular localisation of Mx proteins is a key determinant of antiviral activity. For example, human MxA engineered to express an artificial NLS was detected in the nucleus and retained antiviral activity against IAV, whereas mutations in mouse Mx1 resulting in its redistribution to the cytoplasm abolished its antiviral activity against IAV (Zürcher et al., 1992a; Zürcher et al., 1992c).

Table 1.1: Localisation and antiviral function of human and mouse Mx proteins.

Protein	Localisation	Virus	Virus family	Reference
Human MxA	cytoplasmic	IAV (H7N7, H3N2, H1N1, H5N1)	*Orthomyxoviridae*	(Pavlovic et al., 1990) (Pavlovic et al., 1992) (Dittmann et al., 2008) (Xiao et al., 2013)
		Hantaan virus La Crosse virus Rift Valley fever virus Sandfly fever virus	*Bunyaviridae*	(Frese et al., 1996)
		VSV	*Rhabdoviridae*	(Pavlovic et al., 1990)
		Measles virus	*Paramyxoviridae*	(Schnorr et al., 1993)
		Hepatitis B virus	*Hepadnaviridae*	(Li et al., 2012)

		Hepatitis C virus	*Flaviviridae*	(Wang, H. et al., 2018)
Human MxB	nuclear pore	HIV-1	*Retroviridae*	(Goujon et al., 2013) (Kane et al., 2013)
		HSV	*Herpesviridae*	(Crameri et al., 2018) (Schilling et al., 2018)
Mouse Mx1	nuclear	IAV (H1N1, H5N1, H7N7)	*Orthomyxoviridae*	(Lindenmann et al., 1963) (Krug et al., 1985) (Haller et al., 1995) (Salomon et al., 2007) (Tumpey et al., 2007) (Dittmann et al., 2008) (Zimmermann et al., 2011) (Deeg et al., 2017)
		Thogovirus, Dhori virus, Batken virus		(Thimme et al., 1995) (Frese et al., 1997)

		classical swine fever virus (CSFV)	*Flaviviridae*	(Chen et al., 2020)
	cytoplasmic	VSV	*Rhabdoviridae*	(Sehgal et al., 2020)
Mouse Mx2	cytoplasmic	VSV	*Rhabdoviridae*	(Zürcher et al., 1992b)
		Hantaan virus	*Bunyaviridae*	(Jin et al., 2001)

1.1.5.3 Antiviral activities of Mx proteins from different species

While human and mouse Mx proteins have been well studied, Mx proteins from other species have also been reported to mediate antiviral activity. Mx proteins are widely conserved and expression has been confirmed in rats, chickens, cows, pigs, horses, hamsters, sheep, frogs and various fish species (Verhelst et al., 2013). Antiviral activity of Mx proteins against IAV has been described, amongst others, for rat (Arnheiter et al., 1988), horse (Fatima et al., 2019) and pig Mx proteins (Palm et al., 2010). For some animals, such as duck and chicken, conflicting reports exist with some studies reporting that Mx proteins do (Ko et al., 2002) or do not (Bazzigher et al., 1993; Bernasconi et al., 1995; Benfield et al., 2008) inhibit IAV. In *Odontoceti cetaceans* (toothed whales, including dolphins and orcas), the antiviral function of Mx proteins is completely lost and it has been speculated that in evolution, an unknown virus may have manipulated Mx function to promote infection, thereby driving the loss of a functional *Mx* over time (Braun et al., 2015).

The Mx2 protein from different species has been defined as a restriction factor against retroviruses and lentiviruses. Equine Mx2 was identified to possess antiviral activity against equine infectious anemia virus (EIAV) (Ji et al., 2018; Meier et al., 2018). Interestingly, while equine Mx2 inhibits other primate

lentiviruses such HIV-1, HIV-2 or simian immunodeficiency viruses (SIVs), human MxB does not restrict EIAV (Meier et al., 2018).

1.1.5.4 Mx proteins in mice – establishing the importance of mouse Mx1 *in vivo*

The *in vivo* roles of Mx proteins and, in particular Mx1, have been particularly well studied during IAV infection of mice. Lindenmann first reported the A2G strain of laboratory mice to be resistant to lethal IAV infection and demonstrated the need to use much higher inoculum doses to induce mortality when compared to other laboratory mouse strains (Lindenmann, 1962). Soon after, Lindenmann determined that this trait was inherited by a single dominant allele named *Mx* (Lindenmann, 1964).

Subsequent studies revealed that common laboratory strains of mice were highly susceptible to infection with mouse-adapted IAV due to deletions or nonsense mutations within the *Mx1* locus and therefore premature termination of Mx1 protein translation (Staeheli et al., 1988), while the resistance of A2G mice was inherited as a dominant autosomal trait and was dependent on the *Mx1* gene (Staeheli et al., 1988). The mouse Mx2 protein is also non-functional in most laboratory mouse strains due to an insertional mutation and subsequent frameshift mutation (Jin et al., 1999). It is unclear why most laboratory mouse strains lack functional *Mx1* genes. The loss of the *Mx* loci may be a classical founder effect as most laboratory strains are derived from a relatively small pool of ancestors (Guénet et al., 2003). The absence of positive selection for a functional *Mx* locus or an unknown selective advantage for a non-functional *Mx* locus in laboratory mice represent alternate possibilities.

With an understanding of the prevalence of the disrupted *Mx* locus in most strains of laboratory mice, Mx1-congenic and MxA-transgenic mice were generated to investigate the antiviral activity of functional Mx proteins *in vivo*. Compared to control mice, transgenic mice expressing functional Mx1 under the control of ISRE (interferon signaling response element) showed reduced susceptibility following infection with the neurotropic IAV strain A/NWS/33 (H1N1) (Arnheiter et

al., 1990). More recently, BALB/c.A2G-*Mx1* mice exhibited remarkable resistance to infection with pandemic 1918 H1N1 or HPAI H5N1 viruses, with very modest signs of infection observed compared to standard BALB/c mice which rapidly succumbed to disease (Tumpey et al., 2007). Compared to control animals, a transgenic mouse line with IFN-inducible expression of human MxA (hMx-tg) also showed reduced titres of virus in the lungs, as well as reduced morbidity and mortality following infection with HPAI H5N1, H7N7 and H7N9 viruses (Deeg et al., 2017). Interestingly, the hMx-tg mice showed only moderate resistance to seasonal IAV of human origin such A/PR/8/1934 (H1N1), A/WSN/1933 (H1N1) or A/Hong Kong/8/68 (H3N2). It is well established that circulating human IAV strains show reduced sensitivity to human MxA and this has been mapped to a 'escape signature' associated with three amino acid substitutions (100I/V, 283P, and 313Y) in the viral NP (Mänz et al., 2013; Götz et al., 2016). Avian IAV are generally highly sensitive to restriction by human MxA and bear a distinct NP sequence. Consistent with this, the three amino acid substitutions, namely R100V, L283P, and F313Y, into the viral NP resulted in enhanced resistance against MxA *in vitro* and in hMx-tg mice (Mänz et al., 2013; Götz et al., 2016; Deeg et al., 2017). Importantly, avian IAV which acquire mutations in NP associated with the 'escape signature' generally show a significant loss in viral fitness and this has been proposed as a factor that might underly the frequent failure of avian viruses to emerge and spread in humans (Haller et al., 2020). Thus, MxA might represent an important barrier limiting zoonotic transmission of avian IAV in humans.

Quite recently, MxA has also been identified to act as an inflammasome sensor in respiratory epithelial cells (Lee et al., 2019). MxA was reported to recognise the viral NP and interact with ASC to trigger ASC oligomerisation, inflammasome formation and IL-1β secretion. While the implications of this finding are still unclear it highlights that human MxA has evolved multiple and diverse strategies to restrict IAV infection.

1.1.6 Development of pan-antivirals for respiratory virus infections

Emerging viral infections are a major global public health issue. In particular, some emerging and re-emerging RNA viruses (e.g. influenza viruses, hantaviruses, Ebola virus, Nipah virus and coronaviruses, amongst others) continue to represent a threat to human health. Genetic variation as a result of mutation (due to lack of proof-reading abilities of the viral RNA polymerase), recombination and reassortment, as well as environmental factors, including the increasing human population and urbanisation, create an increased opportunity for viral emergence and spread (Nichol et al., 2000). While a major focus of antiviral development involves targeting specific viral proteins and/or unique steps in the replication cycle of different viruses, these approaches tend to be virus specific, time consuming and are associated with the risk of selecting for virus variants with enhanced resistance to the antiviral compound. As discussed earlier, in the winter of 2007-2008, an oseltamivir-resistant seasonal H1N1 virus with a H274Y substitution in the viral NA emerged and rapidly spread to become the dominant circulating virus (Dharan et al., 2009; Meijer et al., 2009), highlighting the importance of monitoring currently circulating IAV for the emergence of NAI-resistant strains.

A number of emerging viruses are enveloped viruses that express a class I fusion protein, which consists of a surface subunit (SfS) and a transmembrane subunit (TmS). Class I fusion proteins are conserved among viruses from the same genus but also among some viruses from different genera, therefore representing a promising target for the development of pan-antivirals (Vigant et al., 2015). Other antivirals such as ribavirin and favipiravir also exhibit antiviral activity against a diverse range of viruses. These nucleoside analogues target viral DNA or RNA polymerases and act to inhibit viral replication both *in vivo* and *in vitro*. Ribavirin inhibits RNA-dependent RNA polymerases (RdRp) from different viruses, including SARS-CoV-2 (Wang, Manli et al., 2020). Ribavirin is the main antiviral used during haemorrhagic fever with renal syndrome as a result of Hantaan virus infection (Mayor et al., 2021) and has also been used to treat Lassa fever virus (McCormick et al., 1986) and RSV infections (Fernandez et al., 1986). Favipiravir

acts as a substrate for the viral RdRp and can inhibit diverse RNA viruses including IAV and RSV (Furuta et al., 2002), Ebola virus (Oestereich et al., 2014) and others (Daikoku et al., 2018). Both ribavirin and favipiravir inhibit viral RNA synthesis during IAV infection, albeit by different mechanisms. Ribavirin causes GTP depletion, while favipiravir is used as an alternative nucleoside substrate by the viral polymerase (Vanderlinden et al., 2016). Both ribavirin and favipiravir are currently being assessed for their effectiveness as a treatment against SARS-CoV-2 (clinical trial NCT04828564).

The development of broad-spectrum antivirals for effective treatment of respiratory virus infections is challenging for a number of reasons. As mentioned above, each virus exhibits unique features which presents problems when trying to target a ligand or mechanism common to diverse viruses. Certain viruses, such as IAV, also show high rates of mutation and the potential for reassortment, which have created issues for the generation of effective vaccines and antivirals, due to selection of variants which are no longer targeted effectively. The use of the nucleoside analogues, especially ribavirin has been associated with significant side effects, such as severe anaemia, from prolonged use (Gonzalez-Casas et al., 2009). Clearly, there are a number of significant challenges when considering development of antivirals with broad activity and minimal side effects to treat diverse respiratory viruses.

1.1.6.1 Targeting RLRs to develop pan-antivirals

An alternative approach to generating specific antivirals that target the virus itself is to focus on stimulation of effective host immunity. Activation of RLRs such as RIG-I results in induction of an antiviral state and triggers both innate and adaptive immune mechanisms. To date, several pan-antivirals targeting RIG-I have been developed. Based on their chemical structure, RIG-I agonists can be classified as nucleotide-based, RNA-based or small compound-based compounds (Yong et al., 2018). The nucleotide-based antiviral SB9200 possesses dual action as it can activate both RIG-I and NOD2 and daily oral

treatment of woodchucks chronically infected with woodchuck hepatitis virus (WHV), a *hepadnavirus* closely related to human HBV, led to significant reductions in viral load (Korolowicz et al., 2016). The efficacy of SB9200 in combination with the nucleotide analogue tenofovir (Kaneko et al., 2019) on patients with chronic HBV infection was recently assessed in a phase 2 clinical trial, however results outcomes are not currently available (NCT03434353).

RNA-based compounds represent the largest group of RIG-I agonists with several already developed and tested. All are based around a structure incorporating 5' tri-phosphorylated or di-phosphorylated short dsRNA as the ligand for RIG-I recognition. Particular RNA-based RIG-I agonists have been shown to inhibit IAV, HCV, VSV, vaccinia virus, DENV, HIV-1 and CHIKV in different cell culture models *in vitro* (Ranjan et al., 2010; Goulet et al., 2013; Olagnier et al., 2014; Chiang et al., 2015) and to display antiviral activity against IAV (Coch et al., 2017) and SARS-CoV-2 (Mao et al., 2021; Marx et al., 2021) in mouse models of infection. A number of small molecular compounds that can activate RLR signaling have also been identified by high-throughput screening. Isoflavone-like compounds or hydroxyquinolines are activators of IRF3 and have been reported to display antiviral activity against different RNA viruses, including viruses from the *Orthomoyxoviridae, Flaviviridae* and *Paramyxoviridae* families (Bedard et al., 2012; Pattabhi et al., 2015).

1.1.7 Animal models to study IAV and RSV infections

After assessment in an *in vitro* cell culture model, the use of small animal models is a critical step in the preclinical development of novel antiviral treatments and vaccines against respiratory virus infections. A diverse array of animals has been used to study human IAV and/or RSV infections, including mice, guinea pigs, hamsters, ferrets, pigs, swine and non-human primates. Mice, ferrets, pigs, and chickens have been the main animal models used to study human IAV infections. As studies described in this thesis utilise mouse and ferret models to study IAV and RSV infections, these are discussed in more detail below. Of the other

models, pigs are susceptible to experimental infection by both human and avian IAV due to expression of both α2,3 and α2,6 SA linkages in the trachea of these animals, however the size of these animals and their husbandry requirements are problematic for large scale studies. Chickens are especially useful to study avian IAV although less suitable to study human IAVs due to the lack of α2,6 SA, amongst other issues (Margine et al., 2014; Hemmink et al., 2018).

For RSV, non-human primates, cotton rats, mice, and lambs have been the main animal models used to study infection and immunity. Apart from chimpanzees, these animals (including ferrets) are considered semi-permissive for human RSV replication and even large inoculation doses result in little or no clinical signs of disease (Taylor, 2017). Overall, neonatal lambs have proven especially useful as model for RSV infections in the young while cotton rats are preferred over inbred mouse strains as they tend to be much more permissive to infection (Taylor, 2017).

1.1.7.1 Mice as small animal models for IAV and RSV infections

Mice (*Mus musculus*) are the most common and widely used small animal model for basic and translational research associated with IAV and RSV infections. Many important insights regarding IAV pathogenicity and immunity have been obtained from mouse models, largely through the use of knockout and/or transgenic animals. Particular advantages of working in mouse models include low costs for animal purchase and housing, easy handling, minimal variability between inbred littermates, profound knowledge of the biology of mice and the availability of a diverse array of mouse-specific reagents (Rodriguez et al., 2017).

However, mouse models are also associated with a number of distinct disadvantages. Unlike inbred mouse strains, human are genetically diverse and show particular infection histories with various pathogens, therefore caution must be exercised with relating studies in mice to infection in humans. Moreover, mice are not naturally susceptible to IAV infection and human IAV must generally be adapted to mice by sequential lung-to-lung passage to promote efficient virus

replication in the airways. IAV generally do not transmit well among co-housed animals and while weight loss can be used to monitor disease, mice do not cough, sneeze or develop fever following IAV infections (Margine et al., 2014). In regard to RSV, BALB/c mice are the preferred mouse strain for infection (Openshaw, 2013). Like most animal models for RSV, mice are only semi-permissive and large inoculation doses are required to induce infection. It is well established that aged mice older than 15 weeks are more susceptible to RSV infection than neonatal mice, which contrasts human infections where infants show greatest risk of severe disease following RSV infection (Openshaw, 2013). Also, while mice show modest but distinct weight loss upon infection, weight loss is not generally a feature of RSV infection in children.

As IAV and RSV to do not transmit effectively between co-housed mice, animals tend to be experimentally infected under anaesthesia via the intranasal route using volumes of 25-50 µL, resulting in inoculation of the upper and lower airways. Mouse-adapted IAV strains, such as A/PR8/34 (H1N1) tend to be highly virulent for mice and infections are associated with high lung virus titres (Tate et al., 2011). For some strains, application of a small inoculum volume to the nostrils is associated with local replication, before viruses ‘travel’ from the URT to replicate in the lungs (Edenborough et al., 2016).

1.1.7.2 Ferrets as small animal models for IAV and RSV infections

Studies performed in the 1930s were the first to describe infection of ferrets with human IAV (Shope, 1934). Today, ferrets are widely considered to be the ‘gold standard’ small animal model to study the pathogenesis and transmission of human IAV. A number of factors highlight the utility of ferrets to study human IAV infections (Oh et al., 2016). First, ferrets can be infected with a wide range of human IAV strains without prior adaption and infected animals show similar clinical signs to humans, including fever, sneezing and coughing. Second, ferrets show a lung physiology that is quite similar to that of humans, including a similar distribution of SA receptors, with predominant expression of α2,6-linked SA in the

upper and lower airways (Jayaraman et al., 2012). Moreover, unlike inbred strains of mice, ferrets are genetically outbred and therefore studies in this model are more likely to reflect the diversity in the human population.

Despite significant advantages compared to studying IAV infections in mice, a number of important drawbacks must be considered. For example, the limited availability of antibodies and other immunological reagents presents challenges for flow cytometry and immunohistochemistry approaches to accurately characterise immune responses to infection, although significant advances have been made in these areas. A range of qRT-PCR are now routinely used to assess mRNA induction in ferrets, including for diverse chemokines, cytokines and other immune effectors, including in lung tissue and cells obtained following bronchoalveolar lavage of infected animals (Carolan et al., 2014; Carolan et al., 2015; Chan et al., 2017). There are now also a number of ELISpot assays (Carolan et al., 2015; DiPiazza et al., 2018) as well as antibodies either specific for ferret proteins or raised to proteins from other species but with validated cross-reactivity for ferrets that have been described (Wong et al., 2019).

Ferrets have been used to study infections caused by different subtypes of human IAV (both seasonal and pandemic), a range of HPAI and low pathogenicity avian influenza (LPAI) and human IBV (Belser et al., 2020). In addition to their utility in studying influenza infections, ferrets have also been shown to support infection and replication of other respiratory viruses namely human RSV (Coates et al., 1962; Carolan et al., 2015; Stittelaar et al., 2016) and human metapneumovirus (MacPhail et al., 2004). In terms of RSV, intranasal infection of ferrets resulted in virus replication in the upper and lower airways, as well as induction of a range of chemokines and cytokines in the airways (Chan et al., 2017). In this study, RSV A2 and Long strains also showed some evidence of transmission from infected donors to naïve recipient animals.

Ferrets can be experimentally infected with IAV or other respiratory viruses via intranasal and intratracheal inoculation, with the latter delivering the virus inoculum directly to the lower airways. In addition, transmission to naïve models has been well studied using a number of different approaches. For example, in

direct contact transmission a serological naïve ferret is co-housed with an experimentally infected animal, leading to transmission of virus from the infected to the uninfected animal. In some ways, this model simulates a ‘natural’ contact infection, however the exact time of infection and the inoculum dose received by the naïve recipient will vary between animals. In contrast, experimental infections allow both the timing and the inoculation dose and volume to be defined. Aerosol transmission is also becoming increasing common to study IAV infections in ferrets. For aerosol transmission, an experimentally infected donor is housed in a cage next to another cage containing a naïve ferret. In this instance, the cages are separated by a mesh to prevent direct contact between the animals but do allow droplet transmission between cages (Belser et al., 2011; Belser et al., 2020).

1.2 Aims of this thesis

Activation of RIG-I receptors via synthetic RIG-I agonists represents a promising prophylactic and therapeutic strategy for the treatment of respiratory virus infections. Previous studies from our group and by others have used synthetic RIG-I agonists for prophylactic or therapeutic treatments against a number of different viruses, including IAV. While most studies have described the antiviral activities of RIG-I agonists using *in vitro* approaches, a number have described their ability to limit virus infection *in vivo* using mouse models of infection. Of particular interest, Prof. Gunther Hartmann and Dr. Christoph Coch demonstrated that intravenous treatment of mice expressing a functional Mx1 with RIG-I agonist led to potent protection against lethal IAV infection (Coch et al., 2017). In fact, after prophylactic treatment, mice showed no clinical signs of disease following subsequent challenge with IAV. The prophylactic effect was also long-lasting, as treatment with RIG-I agonist 7 days prior to IAV challenge was still sufficient to prevent morbidity and mortality. Besides its prophylactic effectiveness, the RIG-I agonist was also effective when used therapeutically to treat mice already infected with IAV.

Studies described in this thesis build upon these observations using *in vitro* approaches to investigate the effectiveness of RIG-I agonists against IAV and RSV infections using airway cell lines derived from mice, ferrets and humans. Moreover, we also investigate the effectiveness of RIG-I agonist treatment in protecting mice from subsequent challenge with either IAV or RSV, with a focus on understanding the importance of mouse Mx1 for potent and long-lasting RIG-I-mediated protection against IAV. Finally, we investigate the utility of RIG-I agonists as antivirals against IAV and RSV using ferret models of infection.

Overall, this thesis aims to define the effectiveness of synthetic RIG-I agonists against IAV and RSV infections in different mammalian species. The specific aims of this thesis are:

1. To evaluate the function of RIG-I agonists using different *in vitro* and *in vivo* models of IAV infection.

2. To determine if RIG-I agonists inhibit RSV replication in human, mouse and ferret cells, as well as in mice and ferrets infected with RSV.
3. To characterise ferret Mx proteins and to assess their contribution to RIG-I agonist-induced protection against IAV and RSV.

2 Chapter: Materials and Methods

2.1 Cell lines

Human lung epithelial (**A549**) cells (American Type Culture Collection (ATCC) CCL-185), human epithelial type 2 (**HEp-2**) cells (ATCC CCL-23), ferret lung cells (**FRL**, a kind gift from Dr Tuck-Weng Kok, The University of Adelaide, Adelaide, Australia), (HEK)**293T** (ATCC CRL-3216) and (HEK)**293FT** (Thermo Fisher Scientific) cells were maintained and passaged in DMEM (Gibco) containing 10 % (vol/vol) fetal calf serum (FCS) (Sigma-Aldrich) and supplemented with 2 mM L-glutamine (Gibco), 1 mM sodium pyruvate (Gibco), 100 U/mL penicillin and 100 µg/mL of streptomycin (Gibco). Mouse lung epithelial (**LA-4**) cells (ATCC CCL-196) were cultured in Ham's F-12K (Kaighn's)-Medium (Gibco), supplemented with 10 % (vol/vol) FCS and additives as described above. Madin-Darby canine kidney (**MDCK**) cells (ATCC CCL-34) were maintained and passaged in RPMI 1640 medium (Gibco) supplemented with 10 % (vol/vol) FCS, 2 mM L-glutamine, 100 Units/mL of penicillin, 100 µg/mL of streptomycin and 1 mM sodium pyruvate.

All cells were cultured at 37°C under humidified conditions with 5 % (vol/vol) CO_2. For culturing and seeding, cells were detached by incubation with 0.05 % trypsin EDTA (ethylenediamine tetraacetic acid, Gibco) at 37°C followed by resuspension in growth media containing 10 % FCS to inactivate the enzyme. All cell lines were routinely tested for mycoplasma using the MycoAlert mycoplasma detection kit (Lonza).

2.2 Viruses

2.2.1 Influenza A viruses (IAV)

Influenza A virus (IAV) strains used in this study were A/Perth/265/2009 (H1N1pdm09), A/Puerto Rico/8/1934 (PR8, H1N1), NS1-deficient PR8 (PR8 ΔNS1) and A/HKx31 (HKx31, H3N2), a high-yielding reassortant of A/Aichi/2/68

(H3N2) with PR8 bearing the H3N2 surface glycoproteins. PR8 ΔNS1 was obtained from Dr. Anja Wieland, University of Bonn, Bonn, Germany and the remaining viruses were obtained from the Department of Microbiology and Immunology, The University of Melbourne (DMI UoM), Melbourne, Australia or from the WHO Collaborating Centre for Reference and Research on Influenza (WHO CCRRI), Melbourne, Australia). Viruses were generally propagated in the allantoic cavity of 10-day embryonated chicken eggs following standard procedures (Brauer et al., 2015) and titres of infectious virus were determined on MDCK cells by standard plaque assay and expressed as plaque-forming units (PFU) per mL (Xue, J. et al., 2016). However, stocks of A/Perth/265/2009 (H1N1pdm09) were propagated in MDCK cells following standard procedures (Szretter et al., 2006) and virus titres determined on MDCK cells by 50 % tissue culture infectious dose ($TCID_{50}$) assay and expressed as $TCID_{50}$/mL (Mifsud et al., 2020).

2.2.2 Respiratory syncytial viruses (RSV)

RSV strains used for this study were RSV A2 from DMI UoM and RSV Long (VR-26, purchased from ATCC and obtained from the WHO CCRRI). Stocks of rHRSV-Luc expressing Firefly luciferase or rHRSV-Cherry expressing mCherry (both recombinant viruses derived from RSV Long) were obtained from Prof. Jean-François Eléouët (Unité de Virologie et Immunologie Moleculaires (UR892), INRA, Jouy-en-Josas F78352, France). To generate RSV stocks, HEp-2 cells cultured to 90 % confluence were inoculated with RSV Long, RSV A2, rHRSV-Luc or rHRSV-Cherry at a multiplicity of infection (MOI) of 0.05 in serum-free media for 2 hrs, then cultured at 37°C in DMEM containing 2 % (vol/vol) FCS and supplemented with 2 mM L-glutamine, 1mM sodium pyruvate, 100 Units/mL of penicillin and 100 µg/mL of streptomycin until syncytium formation was observed in >50 % of cells, generally at days 3-5 post-inoculation. Flasks were then snap-frozen at -80°C, thawed rapidly at 37°C, and then cells and supernatant were collected and vortexed for 3 min. After pelleting cell debris (2000 x g for

3 min), clarified supernatants were snap-frozen in a bath of dry ice with 80 % (vol/vol) ethanol in water and aliquots were stored at -80°C. Titres of infectious virus were quantified on HEp-2 cells by standard plaque assay or by Virospot (VS) assay as described (Chan et al., 2017).

2.3 Primers

Table 2.1: Primers used for quantitative RT-PCR

name	**sequence (5' to 3')**	**species**
muRIG-I (F)	GAG AGT CAC GGG ACC CAC T	mouse
muRIG-I (R)	CGG TCT TAG CAT CTC CAA CG	mouse
muISG15 (F)	GGAACGAAAGGGGCCACAGCA	mouse
muISG15 (R)	CCTCCATGGGCCTTCCCTCG	mouse
muIFIT1 (F)	CTGAGATGTCACTTCACATGGAA	mouse
muIFTI1 (R)	GTGCATCCCCAATGGGTTCT	mouse
muMx1 (F)	TGTACCCCAGCAAAACATCA	mouse
muMx1 (R)	TTGGAAGCGCTAAAGTGGAA	mouse
muGAPDH (F)	CCAGGTTGTCTCCTGCGACTT	mouse
muGAPDH (R)	CCTGTTGCTGTAGCCGTATTCA	mouse
huIFITM1 (F)	AGCATTCGCCTACTCCGTGAAG	human
huIFITM1 (R)	CACAGAGCCGAATACCAGTAACAG	human
huGAPDH (F)	TGAAGGTCGGAGTCAACGG	human
huGAPDH (R)	GGCAACAATATCCACTTTACCAGAG	human
feCCL5 (F)	GCTGCTTTGCCTACATTTCC	ferret
feCCL5 (R)	CCCATTTCTTCTGTGGGTTG	ferret
feGAPDH (F)	AACATCATCCCTGCTTCCACTGGT	ferret
feGAPDH (R)	TGTTGAAGTCGCAGGAGACAACCT	ferret
feMx1_1 (F)	GGGCTCTAATATTCCCTGTGGT	ferret
feMx1_1 (R)	CGCACCTTCTCCTCATAGTGG	ferret
feMx1_2 (F)	ATCCAGACATGGAGCCTGAG	ferret
feMx1_2 (R)	AGGGAGTCGATGAGGTCGAT	ferret

feMx2 (F)	AAGTGGCTCAGAACCTCACG	ferret
feMx2 (R)	GTCAGTCTTTCCGCCAGACA	ferret

Table 2.2: Oligonucleotides used for generation of pLKO.1 plasmids

name	**sequence (5' to 3')**	**species**
shRNA muRIG-I 1 (F)	CCGGCAAGCATTCAGAGACTATATCCTCGA GGATATAGTCTCTGAATGCTTGTTTTTG	mouse
shRNA muRIG-I 1 (R)	AATTCAAAAACAAGCATTCAGAGACTATATC CTCGAGGATATAGTCTCTGAATGCTTG	mouse
shRNA muRIG-I 2 (F)	CCGGCGGACTTCGAACACGTTTAAACTCGA GTTTAAACGTGTTCGAAGTCCGTTTTTG	mouse
shRNA muRIG-I 2 (R)	AATTCAAAAACGGACTTCGAACACGTTTAAA CTCGAGTTTAAACGTGTTCGAAGTCCG	mouse
shRNA feRIG-I 1 (F)	CCGGAGCGTTTACAACCAGAATTTACTCGA GTAAATTCTGGTTGTAAACGCTTTTTTG	ferret
shRNA feRIG-I 1 (R)	AATTCAAAAAAGCGTTTACAACCAGAATTTA CTCGAGTAAATTCTGGTTGTAAACGCT	ferret
shRNA feRIG-I 2 (F)	CCGGATCCATATTCTCCGATTATTTCTCGAG AAATAATCGGAGAATATGGATTTTTTG	ferret
shRNA feRIG-I 2 (R)	AATTCAAAAAATCCATATTCTCCGATTATTTC TCGAGAAATAATCGGAGAATATGGAT	ferret

Table 2.3: General primers used for sequencing

name	**sequence (5' to 3')**	**function**
pTRE-tight seq	GTCGCCCTTATTCGACTCTA	sequencing pTRE-tight (forward)
M13 seq	ACTGGCCGTCGTTTTACA	sequencing pTRE-tight (reverse)

FgH1tUTG seq	CAGACATACAAACTAAAGAAT	sequencing pFUV1mCherry (forward)
Ubiquitin-P seq	CGCCCTTCGTCTGACGTGGCA	sequencing pFUV1mCherry (reverse)
GB (F)	AGGCGATTAAGTTGGGTAAC	generic geneblock primer (forward)
GB (R)	CGTATGTTGTGTGGAATTGTGAG	generic geneblock primer (reverse)
U6 (F)	CAAGGCTGTTAGAGAGATAAT TGGA	sequencing pLKO.1
Mx1 FRL (F)	GACTTGCCGATAAGGCAGAGA	amplification Mx1 in FRL
Mx1 FRL 700 (R)	CAGACCAAGCAGCTCATCAG	amplification and sequencing Mx1 in FRL

2.4 Antibodies

Table 2.4: Antibodies to detect virus-infected cells by flow cytometry

Antibody	**Conjugate**	**Clone**	**Company**
Anti-IAV NP	FITC	D67J	Abcam
Anti-RSV NP	FITC	130-12H	Merck
Anti-RSV F	-	133-1H	Merck
Goat anti-mouse IgG	FITC	-	Sigma-Aldrich

Table 2.5: Antibodies used to detect immune cell populations by flow cytometry

Antibody	**Conjugate**	**Clone**	**Company**
Anti-CD3	PerCP-Cy5.5	145-2C11	BioLegend
Anti-CD4	AF700	GK1.5	BioLegend
Anti-CD8	PE-Cy7	53-6.7	BioLegend
Anti-CD45.2	Pacific blue	104	BioLegend
Anti-Ly6G	PE	1A8	BD Pharmingen
Anti-CD11b	BV605	M1/70	BioLegend
Anti-CD11c	BV785	N418	BioLegend
Anti-Siglec-F	PE CF594	E50-2440	BD Horizon
Anti-MHC-II	AF700	M5/114.15.2	BioLegend
Anti-CD24	PE-Cy7	M1/69	BioLegend
Anti-CD64	APC	X54-5/7.1	BioLegend
Anti-NK1.1	BV605	PK136	BioLegend
Anti-CD16/CD32	-	93	BioLegend

2.5 Infection assays

2.5.1 Detection of virus-infected cells *in vitro* by flow cytometry

Mammalian cells were infected with IAV or RSV following established protocols (Boukhvalova et al., 2010; Meischel et al., 2021). Briefly, cells were seeded one day prior to infection to allow for 70-80 % confluency following overnight culture. Cells counts were performed immediately prior to infection and used to determine the appropriate MOI, which was then added to the cells in serum-free medium for 1 hr at 37°C. After removal of virus inoculum, cells were washed twice and incubated in serum-free media for different amounts of time, as indicated in particular experiments. Following incubation, cells were detached by trypsinisation and stained with the fixable viability dye eFluor780 (eBioscience). For detection of RSV-infected cells, a number of different staining methods were applied before subsequent analysis by flow cytometry. For cells of murine origin (LA-4 cells or primary murine fibroblasts), cells were fixed in 4 % (vol/vol)

paraformaldehyde (PFA) in water, permeabilised with 0.5 % (vol/vol) Triton-X 100(Sigma-Aldrich) in phosphate-buffered saline (PBS) and stained in PBS containing 0.25 % (vol/vol) Triton-X 100, 1 % FCS and 1mM EDTA using a fluorescein isothiocyanate (FITC)-conjugated monoclonal antibody (mAb) specific for RSV NP (130-12H, Merck). Other mammalian cells were stained with mAb specific for RSV F protein (133-1H, Merck), followed by staining with FITC-conjugated goat anti-mouse IgG (AP127F, Merck) and fixation in 4 % (vol/vol) PFA in water. Following infection with rHRSV-Cherry, cells were fixed in 2 % (vol/vol) PFA without further staining. IAV-infected cells were detected by fixation of cells in 4 % (vol/vol) PFA in water, followed by permeabilisation in 0.5 % (vol/vol) Triton-X 100 in PBS and staining with a FITC-conjugated mAb specific for IAV nucleoprotein (D67J, Thermo Fisher Scientific) diluted in PBS containing 0.25 % (vol/vol) Triton-X 100, 1 % (vol/vol) FCS and 1mM EDTA. Data acquisitions were performed on BD LSR Fortessa, BD Canto II (both BD Bioscience) or Attune NxT (Thermo Fisher Scientific) flow cytometers.

2.5.2 *In vitro* virus release assays

Virus amplification and release was determined following *in vitro* infection of mammalian cells with IAV or RSV. Cells counts were performed immediately prior to infection. Cells monolayers were then inoculated with a low MOI of virus (as described above) for 1 hr at 37°C, washed twice and cultured at 37°C in serum-free media. For IAV, cells were incubated in the presence of 0.5 µg/mL TPCK-treated trypsin (Worthington Biochemical) to facilitate cleavage of viral HA_0 and therefore multiple cycles of virus replication however this was not required for growth of RSV. Supernatants from IAV-infected cells were harvested at the indicated time points, clarified by centrifugation (2000 x g for 3 min) and stored at -80°C prior to titration by plaque assay or VS assay, as described below. For RSV, whole tissue culture plates were snap-frozen in a bath of dry ice and 80 % (vol/vol) ethanol in water and stored at -80°C. Plates were then thawed rapidly, cells and supernatants were collected, vortexed for 3 min and cell debris

was pelleted by centrifugation (2000 x g, 3 min). Virus titres in clarified supernatants were determined by plaque assay or VS assay, as described below.

2.5.3 Virospot assays for IAV and RSV

Titres of infectious IAV or RSV were determined by VS assay on MDCK or HEp2 cells, respectively (Chan et al., 2017; van Baalen et al., 2017). Briefly, cells were seeded into 96-well tissue culture plates and cultured overnight. Cells were washed in serum-free media and incubated with 10-fold dilutions of clarified samples prepared in serum-free media. After 1-2 hr at 37^{o}C, cell monolayers were overlayed with 100 µL of overlay media (equal volumes of 6.4 % (wt/vol) carboxymethylcellulose sodium salt (CMC)(Sigma-Aldrich) and 2x MEM media (Sigma-Aldrich)). To allow multiple cycles of IAV replication, the overlay for IAV samples were supplemented with 4 µg/mL TPCK-treated trypsin. IAV- or RSV-infected cells were incubated at 37^{o}C for 24 hrs or 48 hrs, respectively, before the overlay was removed and cell monolayers were fixed at 4^{o}C in cold 80 % (vol/vol) acetone in water. For staining, plates were incubated with 200 µL/well blocking solution (5 % (wt/vol) skim milk in PBS containing 0.05 % (vol/vol) Tween 20 (Sigma-Aldrich)) for >30 min and washed in PBS containing 0.05 % (vol/vol) Tween 20. IAV-infected cells were detected using mAb MP3.10g2.1C7 which is specific for the NP of IAV (provided by WHO CCRRI) followed by staining with rabbit anti-mouse IgG conjugated to horseradish peroxidase (Agilent Dako). RSV-infected cells were detected using a chimeric monoclonal antibody based on the heavy and light chain variable regions of motavizumab (provided by WHO CCRRI), followed by staining with goat anti-human IgG (H+L) horseradish peroxidase (Merck Millipore). For colour development and visualisation of virus-infected cells, plates were incubated for 10 min with KPL TrueBlue Peroxidase substrate (SeraCare Life sciences). The reaction was stopped by the addition of water, before plates were washed in water, air dried and then scanned using a CTL-Immunospot S6 Macro analyzer with CTL Switchboard 2.6.0 (x86). Spots

(10-150/well) were counted manually using ImageJ Cell Counter software. Titres of infectious virus were expressed as VS/mL of original sample.

2.5.4 Plaque assay for IAV

Titres of infectious IAV were determined by standard plaque assay on MDCK cells as described (Xue, Jia et al., 2016). Briefly, MDCK cells seeded into 6-well tissue cultures plates were cultured overnight, washed and inoculated with 10-fold dilutions of clarified samples prepared in serum-free media. After incubation for 45 min at 37ºC, cells monolayers were overlayed with 3 mL of equal volumes of 1.8 % (wt/vol) type I low EEO agarose (Sigma-Aldrich) and 2x L15 media (Sigma-Aldrich), supplemented with 0.056 % (wt/vol) $NaHCO_3$ (Sigma-Aldrich), 100 Units/mL of penicillin, 100 µg/mL streptomycin and 2 µg/mL TPCK-treated trypsin. Cells were incubated for 3-4 days at 37ºC. Plaques were counted and used to determine infectious virus titres, expressed as PFU/mL of original sample.

2.5.5 $TCID_{50}$ assay for IAV

Titres of infectious IAV in nasal wash and respiratory tissues samples from ferrets were determined by standard $TCID_{50}$ assay on MDCKs as described (Oh et al., 2015). Briefly, 96-well plates containing confluent monolayers of MDCK cells were prepared and inoculated with 10-fold dilutions of triplicate samples diluted in serum-free media, supplemented with 4 µg/mL of TPCK-treated trypsin. After 2 hrs at 37ºC, the inoculum was removed and cell monolayers were washed in PBS and then cultured in serum-free media supplemented with 4 µg/mL of TPCK-treated trypsin. Cells were incubated for 4 days at 37ºC until morphological changes of cell monolayer and cytopathic effects were confirmed. To determine $TCID_{50}$ titres, 25 µL of cell supernatant were removed and incubated for 30 min at room temperature (RT) with 25 µL of 1 % turkey red blood cells in 96-well-U-bottom plates to identify wells containing hemagglutination activity.

Titres of $TCID_{50}$ were calculated using the method of Reed and Muench (Reed et al., 1938) and titres are expressed as $TCID_{50}$/mL of original sample.

2.5.6 Plaque assay for RSV

Titres of infectious RSV were determined by standard plaque assay on HEp-2 cells as described (Chan et al., 2017). Briefly, HEp-2 cells seeded into 12-well tissue cultures plates were cultured overnight, washed and inoculated with 10-fold dilutions of clarified samples prepared in serum-free media. After incubation for 2 hrs at 37°C, inoculum was removed and cell monolayers were overlayed with 3 mL of DMEM plus additives, supplemented with 0.3 % (wt/vol) agarose (Sigma-Aldrich) and 2 % (vol/vol) FCS and then incubated for a further 7 days at 37°C. After incubation, cell monolayers were fixed in 1 % (vol/vol) formalin (Sigma-Aldrich) in water and stained with 0.05 % (wt/vol) neutral red (Sigma-Aldrich) in water. Plaques were counted and used to calculate infectious virus titres, expressed as PFU/mL of original sample.

2.6 3’-RNA Sequencing

FRL cells were transfected with 3pRNA, ctrl RNA or treated with recombinant ferret IFN-α as described (**section 2.8.1**). RNA was isolated at indicated time points, prepared with a QuantSeq 3´-mRNA Library Prep Kit (Lexogen) and sequenced on a NovaSeq 6000 (Illumina). Reads were trimmed and STAR aligned to an available ferret genome (GenBank: AEYP00000000.1).

2.7 Molecular cloning

To study the function of particular proteins, especially their role during RIG-I agonist-mediated protection, several cell lines with loss or overexpression of particular proteins were generated during this thesis. **Figure 2.1** gives an overview of different experimental approaches used to generate cell lines expressing Mx proteins or cell lines with knockdown of RIG-I.

2.7.1 Generation of Mx overexpressing cells

2.7.1.1 Cloning of ferret Mx1.1, ferret Mx1.2, ferret Mx2, human MxA for doxycycline-inducible overexpression systems

Genes encoding ferret Mx1.1, ferret Mx1.2, ferret Mx2 and human MxA were cloned into TRE-tight and pFUV1mCherry plasmids for generation of lentiviral vectors and the generation of stable cell lines with doxycycline (DOX)-inducible expression.

Coding sequences of ferret Mx (Mx1 splice variant 1 (feMx1.1), Mx1 splice variant 2 (feMx1.2) and feMx2) and human MxA (huMxA) proteins were obtained from NCBI databases. Geneblocks containing the coding sequences of feMx1.1, feMx1.2, feMx2 and huMxA were synthesised (GeneArt Gene Synthesis, Thermo Fisher Scientific) and designed to express a N-terminal FLAG tag sequence and N- and C-terminal restriction sites for BamHI/EcoRI, as well as generic geneblock amplification sequences. Geneblocks of the individual Mx proteins were amplified using the High-fidelity DNA polymerase (New England Biolabs, NEB) according to manufacturer's instructions. Amplified geneblocks were digested with BamHI and EcoRI (NEB) and ligated into BamHI and EcoRI-digested pTRE-tight plasmids using the T4 DNA ligase (Promega), following manufacturer's instructions. Positive clones were confirmed by sequencing (AGRF, Peter MacCallum Cancer Center, Melbourne, Australia). pTRE-tight is a response plasmid for the tetracyclin-regulated expression of genes of interest (Tet-On system) containing a Tet response element with seven direct repeats of the tet

operator sequence (tetO). This allows DOX-inducible expression of Mx proteins. In the next step, the TRE response element and genes of interest were released from the pTRE-tight plasmid by digestion with PacI enzyme (NEB) followed by gel purification (Wizard SV Clean-Up System, Promega) and ligated into the PacI enzyme-digested pFUV1mCherry lentivirus transfer plasmid using the T4 DNA ligase. pFUV1mCherry plasmids constitutively express mCherry under an ubiquitin promotor which allows for enrichment of transduced cells by cell sorting for mCherry-positive cells. Sequencing was used to confirm expression of genes of interest in the relevant plasmids (AGRF). Note that pTRE-tight and pFUV1mCherry plasmids were a kind gift from Prof. Marco Herold (Walter and Eliza Hall Institute of Medical Research, Melbourne, Australia).

2.7.1.2 Generation of stable cell lines with DOX-inducible overexpression of Mx proteins

To generate stable cell lines with DOX-inducible overexpression of FLAG-tagged Mx proteins, cell lines were transduced with different lentivirus stocks, followed by cell sorting to enrich for transduced mCherry-positive cells.

For the generation of lentiviral particles, 293T cells were seeded into 12-well tissue culture plates and incubated overnight to reach 80 % confluency. Cells were transiently transfected using Lipofectamine 2000 (Thermo Fisher Scientific) and pMDL, pRSV-REV, pMD2.G and a pFUV1mCherry plasmid at a ratio of 2:1:1.2:4 for a total of 1 µg plasmid per transfection reaction. The lentiviral packaging plasmids pMDL, pRSV-REV, pMD2.G were also a kind gift from Prof. Marco Herold (Walter and Eliza Hall Institute of Medical Research, Melbourne, Australia). At 6-8 hrs after transfection, media was changed to DMEM with 10 % (vol/vol) FCS and supplements. Cell supernatants containing lentiviral particles were then harvested 48 hrs post transfection and filtered through a 0.22 µm filter to remove residual cell debris. Filtered lentiviral particles were supplemented with 8 µg/mL polybrene (Sigma-Aldrich) to enhance transduction efficiency. For transduction, FRL and A549 cells were seeded one day prior into 6-well tissue culture plates to achieve 70-80 % confluency after overnight incubation. Cells

were transduced by spinoculation at 1800 rpm for 1 hr at 32°C and incubated overnight at 37°C. At 24 hrs post-transduction, virus inoculum was removed and replenished with media containing 10 % (vol/vol) FCS and supplements. After an additional 48 hrs, cells were stained with fixable viability dye eFluor 780, filtered through a falcon tube with a 35 µm cell strainer cap (BD Bioscience) and sorted for viable mCherry-positive cells. Sorting was performed using a BD FACSAria III Cell Sorter (BD Biosciences). Enriched mCherry-positive cells were cultured and expanded in media containing 10 % (vol/vol) FCS and supplements at 37°C in 5 % (vol/vol) CO_2.

After enrichment for mCherry-positive cells, intracellular expression of FLAG-tagged proteins was then determined. For this, cells were detached, stained with fixable viability dye eFluor 780 for 15 min on ice, washed in FACS buffer (PBS supplemented with 1 % (vol/vol) FCS and 1 mM EDTA) and fixed in 2 % (vol/vol) PFA in water. Cells were then permeabilised in PBS containing 0.5 % (vol/vol) Triton X-100 for 10 min at RT and stained with anti-FLAG-allophycocyanin (APC) mAb (Clone L5, Biolegend) in permeabilisation buffer (PBS supplemented with 2 % (vol/vol) FCS, 0.25 % (vol/vol) Triton X-100 and 1 mM EDTA). Viable FLAG-positive cells were detected by flow cytometry using a BD Canto II (BD Bioscience). A similar strategy was used to generate cell lines with DOX-inducible expression of a cytoplasmic version of hen egg ovalbumin (cOVA) lacking the sequence for cell-surface trafficking (Boyle et al., 1997) and the N-terminal FLAG tag, to generate cell lines expressing an irrelevant control protein.

2.7.1.3 DOX-induction of stably transduced cell lines

For the induction of the TET-inducible expression system, cells were seeded in 24-well plates and cultured overnight. The next day, media was supplemented with 1 µg/mL of DOX (Sigma- Aldrich) and cells were incubated for an additional 24 hrs at 37°C.

2.7.2 Cloning of ferret and mouse RIG-I into shRNA pLKO.1 plasmids for generation of RIG-I knockdown cells

2.7.2.1 Generation of pLKO.1 plasmids

A shRNA-mediated gene silencing method was used to generate RIG-I-deficient LA-4 and FRL cells. While CRISPR/Cas-9-mediated gene editing techniques result in knockout of the gene of interest, RNAi-mediated knockdowns can markedly reduce, but not abolish, expression of the target gene. However, CRISPR/Cas9-mediated knockouts are only functional if all alleles in target cells are mutated. Due to the unstable karyotype of LA-4 cells, ranging from 38 to 256 chromosomes (ATCC, 2021), it was not possible to generate LA-4 cell knockouts.

The Genetic Perturbation Platform (GPP) was used to identify optimal 21-mer target sites for murine and ferret RIG-I transcripts. While the transcript of murine RIG-I (Gene ID 230073) was listed in the GPP Web Portal database (Broad Institute, 2021), the GPP design tool was used to create shRNA sequences targeting ferret RIG-I. Forward oligonucleotides (5’ CCGG—21bp sense—CTCGAG—21bp antisense—TTTTTG 3’) and reverse oligonucleotides (5’ AATTCAAAAA—21bp sense—CTCGAG—21bp antisense 3’) were generated following the GPP Web Portal guidelines.

Forward and reverse oligonucleotides were diluted in NEBuffer 2 (NEB) to a final concentration of 2 µM. To allow annealing of the oligonucleotides, samples were incubated for 4 min at 95°C, followed by slow cooling to RT. The pLKO.1-TRC cloning vector was digested with EcoRI and AgeI (both NEB), followed by agarose gel purification (Moffat et al., 2006). Annealed oligonucleotides were ligated into digested pLKO.1 TRC-cloning vector using NEB T4 DNA ligase following the manufacturer’s protocol. The ligation was used for bacterial transformation into chemocompetent *Escherichia coli* (*E. coli*) Stbl3 cells. Bacteria were grown on Luria-Bertani (LB) agar plates (100 µg/mL ampicillin), colonies were isolated and sequences confirmed by Sanger Sequencing (Microsynth, Göttingen, Germany). A non-hairpin control plasmid (pLKO.1 ctrl 1)

was included in the assays. These plasmids were used to generate lentiviral particles for transduction of the relevant mammalian cells.

2.7.2.2 Generation of lentiviral particles by calcium-phosphate precipitation

293FT cells were seeded in 10 cm tissue culture plates to reach 70 % confluency 6 hrs prior to transfection. The VSV-G envelope expressing pMD2.G plasmid, the psPAX2 packaging plasmid and the pLKO.1 plasmids with inserts of interest (each 15 µg, 10 µg and 10 µg, respectively) were diluted in 500 µL of water and vortexed. Next, 500 µL of 2x HEPES Buffered Saline (HBS) at pH 7.1 was added, followed by dropwise addition of 50 µL of calcium chloride ($CaCl_2$ at 2.5 M) with constant, gentle vortexing and incubated for 20 min at RT to allow the generation of calcium-phosphate-DNA co-precipitates. 293FT media was replenished and the calcium-phosphate solution was added dropwise onto the cells. After 12 hrs incubation at 37°C, cells were washed in PBS and cultured in fresh media. After an additional 24-30 hrs, lentivirus particles were harvested, filtered through a 0.22 µm filter, supplemented with polybrene (8 µg/mL) and inoculated onto LA-4 or FRL cells at 70-80 % confluency by spin transduction (800 x g for 60 min at 32°C). After 24-36 hrs in culture, media was replaced and then, 3 days after spinoculation, was replaced again but with media supplemented with puromycin (InvivoGen) at 2 µg/mL for FRL cells and 5 µg/mL for LA-4 cells to allow for selection of lentivirus-transduced cells. Fresh media supplemented with puromycin was added every 3 days until all untransduced control cells were dead.

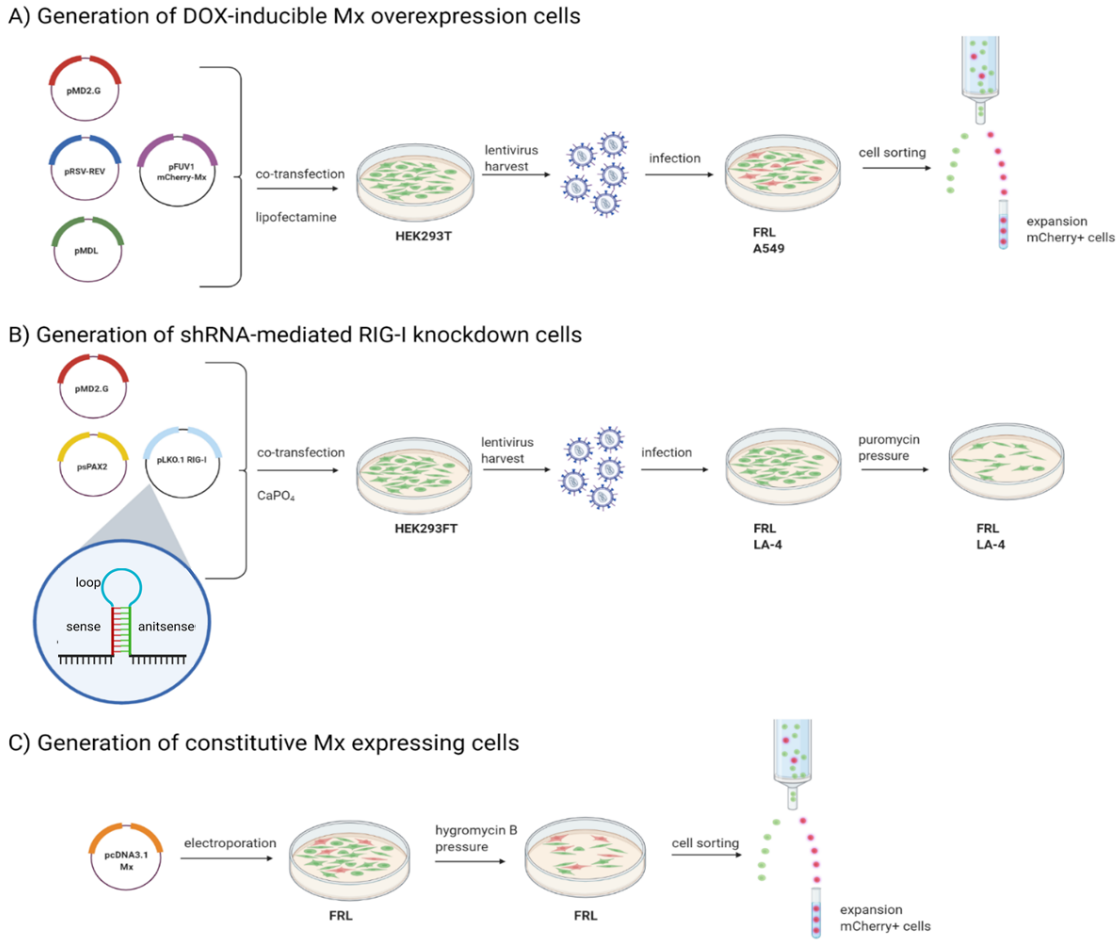

Figure 2.1: Overview of cell lines generated.**A)** Cells with DOX-inducible overexpression of Mx protein of interest were generated by preparation of lentiviruses in 293T cells, transduction of target cells and enrichment of mCherry+ cells. **B)** shRNA-mediated RIG-I knockdown cells were generated by preparation of lentiviruses in 293FT cells, followed by selection in the presence of puromycin. **C)** Cells with constitutive expression of Mx proteins were generated by electroporation of target cells and selection in the presence of hygromycin B, followed by cell sorting to enrich for mCherry+ cells. Figure generated in BioRender.

2.7.3 Generation of stable FRL cell lines with constitutive expression of Mx proteins

Genes encoding ferret Mx1.1, ferret Mx1.2, ferret Mx2, human MxA, human MxB, mouse Mx1 or mouse Mx2 containing a N-terminal FLAG tag (peptide sequence DYKDDDK) were cloned into pcDNA3.1-mCherry expression plasmids which were generated and kindly provided by Ms Clare Oates and Dr. Rubaiyea Farrukee (both DMI UoM). cOVA lacking a N-terminal FLAG tag was also cloned into the same vector to generate a cell line expressing an irrelevant cytoplasmic protein. FRL cells were then electroporated with these plasmids using the Neon transfection system (Thermo Fisher Scientific) with 2 pulses of 1230 volt for 30 milliseconds (ms). Cells were cultured at 37°C for 2 days, then media was replaced with fresh media supplemented with 100 µg/mL hygromycin B (InvivoGen). Fresh media supplemented with hygromycin B was added every 3 days until all unelectroporated control cells were dead. Following hygromycin B selection, mCherry-positive FRL cells were enriched using a BD Aria III cell sorter. Cells were then expanded and cell-sorting was repeated to further enrich the mCherry-positive population. In addition to generating FRL cells with stable constitutive Mx protein expression, similar approaches were applied to generate lines of 293T cells expressing ferret Mx1.1, ferret Mx1.2, ferret Mx2, human MxA, human MxB, mouse Mx1 and mouse Mx2, as well as a cOVA control cell line (generated by Dr. Rubaiyea Farrukee (DMI UoM) and Mr James Barnes (WHO CCRRI)).

2.7.4 Bacterial transformation

At various steps in the cloning process, ligation reactions or plasmids were used to transform competent DH5-α or Stbl3 *E.coli*. For each transformation, 50 µL competent cells were incubated with 1-2.5 µL of plasmid or ligation product and incubated for 30 min on ice followed by a heat shock at 42°C for 90 sec. Cells were then incubated an additional 3 min on ice, before 950 µL of LB broth was added followed by incubation at 37°C with shaking (180 rpm) for 1 hr. Cells were

plated on LB agar plates containing appropriate antibiotic (100 µg/mL of ampicillin for pTRE-tight, pFUVmCherry or pLKO.1 plasmids) and incubated overnight at 37°C. Single colonies were then isolated, inoculated into 2-10 mL LB media containing antibiotic and cultivated at 37°C with shaking (180 rpm) overnight. Plasmid DNA was isolated using the AccuPrep Plasmid Mini Extraction kit (Bioneer) or PureLink Quick Plasmid Miniprep kit (Thermo Fisher Scientific) following the manufacturer's instructions. After isolation, plasmid concentrations were determined using a NanoDrop spectrophotometer (Thermo Fisher Scientific).

2.8 RIG-I agonists

5′-triphosphorylated RNAs (3pRNAs) were used as RIG-I agonists. 3pRNAs were generated at the Institute of Clinical Chemistry and Clinical Pharmacology at the University of Bonn as described elsewhere (Goldeck et al., 2014; Coch et al., 2017).

2.8.1 Transfection of RIG-I agonists

Cells were seeded one day prior to transfection to reach 70-80 % confluency after overnight culture. Cells were then transfected with 200 ng/mL 3pRNA or control (ctrl) RNA using cationic lipid-based Lipofectamine 2000 following the manufacturer's instructions. Briefly, oligonucleotides and Lipofectamine 2000 dilutions were prepared in OptiMEM (Gibco), incubated for 5 min, mixed and incubated for an additional 20 min at RT. The liposome mixture was then added dropwise to the cells to allow uptake via the endocytic pathway. For indicated experiments, reverse transfections were performed. Here, cells were plated into cell culture dishes and transfected at the same time. The liposome mixture was generated as described before. Cell densities were adjusted so that 70 % confluency was reached when cells were seeded.

2.9 Murine IFN-α ELISA

An enzyme linked immunosorbent assay (ELISA) was used to determine IFN-α levels in supernatants from LA-4 cells. For this ELISA, 96-well high binding, half-area plates (Corning) were coated overnight at 4°C with a rat anti-mouse IFN-α mAb (RMMA-1, PBL Assay Science) diluted in coating buffer (0.2 M sodium phosphate; pH 6.5). After incubation, plates were washed in wash buffer (PBS with 0.05 % (vol/vol) Tween 20), and blocked for 2 hrs at RT with 10 % (vol/vol) FCS in PBS. Plates were washed 3 times before addition of cell culture supernatants (diluted 1:5 in media). A 2-fold dilution series of a recombinant mouse IFN-α (PBL Assay Science) standard was also prepared in media. Samples and standards were incubated overnight at 4°C, washed 3 times and then incubated for 3 hrs with a rabbit polyclonal anti-mouse IFN-α antibody (PBL Assay Science) diluted in PBS containing 10 % (vol/vol) FCS. Plates were washed 7 times, incubated with a mouse anti-rabbit horseradish peroxidase (Santa Cruz Biotechnology) for 2 hrs in the dark, then washed again and incubated with TMB Substrate (BD OptEIA, BD Bioscience). After colour development, the reaction was stopped by the addition of 2N H_2SO_4 and absorbance at 450/570 nm was measured on a Cytation 3 microplate reader (Bio Tek). Cytokine concentrations were calculated by interpolating from the standard curve using GraphPad Prism.

2.10 Microscopy

Fluorescence microscopy was used to examine the cellular localisation of Mx proteins. For these studies, black 96-well plate with a flat and clear bottom (PerkinElmer) was coated for 2 hrs at 37°C with 15 µg/mL (wt/vol) poly L-ornithine (Sigma-Aldrich) in water, washed 3 times with PBS and coated with 0.1 % (wt/vol) gelatin from pork skin (Sigma-Aldrich) in water overnight at 4°C. Next, A549 cells were reverse transfected with pcDNA3.1-mCherry vectors expressing ferret Mx1.1, Mx1.2, Mx2, human MxA and human MxB using Lipofectamine 2000

(Thermo Fisher Scientific) transfection reagent following the manufacturer's instructions. Cells were incubated for 30 hrs at 37°C and fixed in 4 % (vol/vol) PFA in water for 10 min at RT. Cells were then washed in PBS and permeabilised in 0.1 % (vol/vol) Triton-X 100 in PBS for 10 min at RT and washed in PBS. Next, cells were blocked for 30 min at 37°C in 5 % (wt/vol) BSA and 0.1 % (vol/vol) Triton-X 100 in PBS, followed by incubation with a mouse anti-FLAG M2 mAb (clone M2, Sigma-Aldrich) for 2 hrs at RT in 3 % (wt/vol) BSA and 0.1 % (vol/vol) Triton-X 100 in PBS. Cells were washed in PBS and incubated with a polyclonal FITC-conjugated goat anti-mouse IgG (H+L) antibody (R37120, Thermo Fisher Scientific) for 1.5 hrs at RT in 3 % (wt/vol) BSA and 0.1 % (vol/vol) Triton-X 100 in PBS. Next, cells were washed in PBS, incubated with DAPI (Invitrogen) diluted 1:1000 in PBS for 20 min at RT, washed again and stored in the dark at 4°C prior to analysis on a DMi8 microscope with THUNDER Imager (Leica).

2.11 Gene expression analysis by quantitative real time RT-PCR

Since work in this study was conducted on two institutions, two different cycler and RT-qPCR reagents were used, however results were consistent indicating no effect on reliability of results.

Method performed at The University of Melbourne, The Peter Doherty Institute for Infection and Immunity: Cells were harvested in RLT buffer (Qiagen) supplemented with β-mercaptoethanol, for subsequent total RNA isolation using a RNeasy Mini Kit or a RNeasy Mini Plus Kit (Qiagen) according to manufacturer's instructions. To exclude DNA contamination, an on-column RNase-free DNase digestion (Qiagen) was performed. RNA purity and quantity were determined by nanodrop (Thermo Fisher Scientific). RNA was reverse transcribed into cDNA using the Omniscript RT Kit (Qiagen) and used for subsequent real-time PCR reactions. A SYBR-green based Sensifast Lo-ROX SYBR Green (Bioline) reaction was performed on the ABI7500 Real Time PCR System (Applied Biosystems) to determine expression of genes of interest. Species-specific primers were used to determine expression of particular genes in human, mouse

of ferret cells or tissues (**Table 1.1)**. For some experiments, ISG15 and IFIT1 expression in samples of murine origin (either tissues or LA-4 cells) were determined by using RT^2 qPCR Primers (ISG15: PPM05488A-200, IFIT1: PPM05530E-200, both Qiagen). The thermocycling condition in Melbourne consisted of 1 cycle of 45°C for 10 min and 95°C for 2 min and 45 cycles of 95°C for 5 seconds, 60°C for 30 seconds using the 7500 Fast real-time system (Applied Biosystems), following the manufacturer's recommendation. Gene expression was normalised to expression of the housekeeping gene GAPDH and graphed as fold change to untreated controls using $\Delta\Delta C_T$ method (Livak et al., 2001).

Method performed at The University of Bonn, Institute of Clinical Chemistry and Clinical Pharmacology: Cells harvested in RLT buffer were mixed 1:1 with 70 % (vol/vol) ethanol in water and this was applied to a Zymo Research Spin III column (Zymo Research) and centrifuged for 1 min at 10.000 rpm. After washing the column with RW1 (Qiagen buffer), an on-column RNase-free DNase digestion (Thermo Fisher Scientific) was performed. The column was then washed twice in Zymo wash buffer (Zymo Research) and RNA was eluted in RNase-free water. RNA was reverse transcribed into cDNA using the RevertAid Reverse Transcriptase (Thermo Fisher Scientific) and used for subsequent real-time PCR reactions. A SYBR-green based EvaGreen (Biobudget) reaction was performed on a QuantStudio6 (Thermo Fisher Scientific). The thermocycling condition in Bonn was as followed: 15 min of 95°C, 40 cycles of 15 seconds at 95°C, 20 seconds at 60°C and 20 seconds at 60°C following the manufacturer's recommendation. Gene expression was normalised to expression of the housekeeping gene GAPDH and graphed as fold change to untreated controls using $\Delta\Delta C_T$ method (Livak et al., 2001).

2.12 Mouse studies

2.12.1 Generation of primary murine fibroblasts

Primary murine lung fibroblasts were isolated from dissociated lung tissue as described (Edelman et al., 2018). Briefly, 6-12 week old mice were killed in accordance with the Animal Experimentation and Ethics guidelines at The University of Melbourne. The lungs were perfused by injecting PBS into the right ventricle before lung tissue was isolated, cut into small pieces and digested with 0.5 mL collagenase per lung (1 mg/mL, Sigma-Aldrich) for 45 min at 37^{o}C. After passing through a 5 mL syringe to dissociate aggregates, cells were pelleted, washed in Hank's buffered salt solution (Media Preparation Unit, DMI UoM) and then digested with 0.25 % trypsin-EDTA (Media Preparation Unit, DMI UoM) for 15 min at 37^{o}C. After passing through a syringe, cells were filtered through a 70 µm cell strainer and washed with DMEM containing 10 % (vol/vol) FCS supplemented with 2 mM L-glutamine, 1mM sodium pyruvate, 100 Units/mL of penicillin and 100 µg/mL of streptomycin. Cells were pelleted and resuspended in DMEM supplemented with 10 % (vol/vol) FCS and additives and seeded into tissue culture flasks. Primary lung fibroblasts were passaged upon confluency and were stable for up to 10 passages *in vitro*.

2.12.2 Virus infection

Mice were bred and maintained in specific pathogen-free conditions at the Bioresources Facility at The Peter Doherty Institute for Infection and Immunity, Melbourne, Australia. All research complied with the Animal Experimentation Ethics guidelines and policies at the University of Melbourne and were in accordance with the NHMRC Australian code for the care and use of animals for scientific purposes (the Code). Mice were anesthetised by isoflurane inhalation and infected via the intranasal (i.n.) route with virus (as indicated) and infectious dose (as indicated) in 50 µL of PBS. Mice were monitored daily for body weights and signs of disease.

2.12.3 RIG-I agonist administration

3pRNA or ctrl RNA was formulated using *in vivo*-jetPEI transfection reagent (Polyplus-transfection) in 5 % (vol/vol) glucose solution according to manufacturer's recommendations. The N/P ratio (number of nitrogen (N) residues in the *in vivo*-jetPEI per phosphate (P) residue) of RNA was 8. Mice received 12.5 µg of 3pRNA or ctrl RNA via an intravenous (i.v.) injection into the tail vein in a total volume of 200 µL.

2.12.4 Bioluminescent imaging

Mice were intranasally infected with 10^5 infectious particles (as determined by VS assay) of rHRSV-Luc in 50 µL of PBS. Replication of rHRSV-Luc was visualised by bioluminescence after infection. Briefly, mice were weighed and received an intraperitoneal (i.p.) injection of 200 µL per 20 gram body weight of PBS containing 15 mg/mL VivoGlo™ Luciferin (Promega). Mice were rested for 5 min to allow for VivoGlo™ Luciferin distribution throughout the animal, then anaesthetised by isoflurane inhalation and bioluminescence signals were measured using a Lumina XRMS Series III In Vivo Imaging System (IVIS, Perkin Elmer). Living Image software (version 4.0, Caliper Life Sciences) was used to measure the luciferase activities. Bioluminescence images were acquired for 1 min with f/stop =1 and binning= 8.

2.12.5 Tissue collection and processing

Mice were killed and respiratory tissues such as lung and nasal turbinates were collected at indicated time points. Tissue samples were homogenised in PBS using a Polytron PT 2100 homogeniser (Kinematica AG), debris was removed by centrifugation (3000 rpm, 10 min, 4^{o}C) and clarified supernatants were stored at -80^{o}C. Titres of infectious IAV and RSV in clarified tissue homogenates from IAV-

or RSV- infected mice were determined by standard plaque assay on MDCK or HEp-2 cells (**sections 2.5.4 and 2.5.6**).

In some experiments, lung and nasal turbinates were removed, cut into smaller pieces and submerged in RNALater (Ambion, Life Technologies) overnight before extraction of total RNA using RNeasy Plus Mini spin columns (Qiagen) for subsequent use in qRT-PCR (**section 2.11**).

In some experiments, bronchoalveolar lavage (BAL) fluid was also obtained at the time points indicated. For BAL, a flexible catheter was inserted into the proximal trachea and the lung was flushed 3 times with 1 mL of PBS. Immune cell populations within the BAL were determined via flow cytometry (**section 2.12.6**), while the cell-free BAL fluid was analysed for the presence of cytokines and chemokines using cytokine bead array (**section 2.12.7**).

2.12.6 Detection of immune cell population within BAL

Cells were isolated from BAL fluid by centrifugation (1800 rpm, 5 min, 4^{o}C) and incubated for 5 min in 1 mL Red Blood Cell Lysing Buffer Hybri-Max (Sigma-Aldrich). Cells were then washed in DMEM, resuspended in PBS containing 1 % (vol/vol) FCS and incubated for 15 min on ice with an anti-CD16/CD32 mAb to block Fc receptors on different immune cell populations. Cells were stained with a fixable viability dye eFluor 780, followed by staining with fluorescent-conjugated antibodies to different immune cell markers namely: NK1.1 (PK136), CD3 (145-2C11), CD8 (53-6.7), CD4 (RM4-5), CD45.2 (104), Ly6G (1A8), MHC II (M5/114.15.2), CD11c (N418), CD11b (M1/70), Siglec-F (E50-2440), CD24 (M1/69) or CD64 (X54-5/7.1) all obtained from BD or BioLegend. Data acquisition was performed on a BD LSR Fortessa flow cytometer to allow for identification of distinct immune cell population as follows: neutrophils (Ly6G^{+}, CD11b^{+}), eosinophils (Siglec-F^{+}, CD11b^{+}, CD64^{-}), NK cells (NK1.1^{+}, CD3^{-}), alveolar macrophages (CD64^{+}, Siglec-F^{+}, CD11c^{+}), pan-macrophages (CD64^{+}, Siglec-F^{-}, CD11b^{+}), pan-dendritic cells (pan-DC, CD64^{-}, CD11c^{+}, MHC II^{+}, CD24^{+}), CD4^{+} T cells (CD3^{+}, CD4^{+}) and CD8^{+} T cells (CD3^{+}, CD8^{+}).

2.12.7 Detection of inflammatory mediators in cell-free BAL

Levels of cytokines and chemokines such as IFN-α, IFN-β, IFN-γ, IL-1β, IL-6, IL-10, IL-12, CCL2, CCL5, CXCL1, CXCL10, TNF-α and GM-CSF were determined in cell-free BAL fluid by using the cytometry bead array (CBA) LEGENDplex Mouse Anti-Virus Response Panel (BioLegend) following manufacturer's instructions. Data acquisition was performed on a BD Canto II. The LEGENDplexTM Data Analysis Software was used to determine analyte concentrations.

2.13 Ferret studies

Adult outbred ferrets (600-1500 gram) were housed in the Bioresources Facility at the Peter Doherty Institute for Infection and Immunity, Melbourne, Australia. All research complied with the Animal Experimentation Ethics guidelines and policies at The University of Melbourne and were in accordance with the NHMRC Australian code of practice for the care and use of animals for scientific purposes.

2.13.1 RIG-I agonist administration

3pRNA or ctrl RNA was formulated using *in vivo*-jetPEI transfection reagent in 5 % (vol/vol) glucose solution following manufacturer's recommendations. The N/P ratio was 8 as for mouse studies. Administration of 3pRNA or ctrl RNA to ferrets was via the i.n. or i.v. route, as indicated. Prior to treatment, the body weight of all animals was recorded to allow for comparable dosing of animals. For i.v. administration, ferrets received 0.3 mg/kg 3pRNA or ctrl RNA into the cephalic vein in a total volume of 1000 µL 5 % (vol/vol) glucose solution. Injections were performed under reversible anaesthesia by intramuscular injection of ketamine (10 mg/kg, Troy Laboratories), midazolam (0.5 mg/kg, Troy Laboratories) and medetomidine (0.02 mg/kg, Troy Laboratories) mixture, which was then antagonised by atipamezole (0.01 mg/kg, Troy Laboratories).

For i.n. administration, ferrets received 0.3 mg/kg 3pRNA or ctrl RNA in 500 µL of 5 % (vol/vol) glucose solution. Intranasal administrations were performed under non-reversible anaesthesia (25 mg/kg ketamine and 5 mg/kg ilium Xylazil in a 1:1 (vol/vol) mixture; Troy Laboratories).

2.13.2 Virus infection

2.13.2.1 IAV infection via contact transmission

Prior to the commencement of experiments, hemagglutination inhibition assays were used to confirm all animals to be seronegative against IAV strain A/Perth/265/2009 ((H1N1)pdm09). Donor ferrets were anaesthetised (25 mg/kg ketamine and 5 mg/kg ilium Xylazilin a 1:1 (vol/vol) mixture) and inoculated by dropwise i.n. delivery of 500 µL PBS containing 10^5 $TCID_{50}$ of A/Perth/265/2009. After 24 hrs, naïve recipient ferrets were exposed to donor ferrets. After 48 hrs co-housing, donor animals were removed and recipients were kept for the times indicated in each experiment. Each day after infection, ferrets were monitored for body weight and temperature measurements were also performed using implanted temperature transponders fitted to identification chips (LifeChip Bio-Thermo, Digivet). The proportion of weight change was calculated relative to body weight at the first day of the experiment.

2.13.2.2 Experimental RSV infection

For experimental infection of ferrets with RSV Long, animals were anaesthetised (12.5 mg/kg ketamine and 2.5 mg/kg ilium Xylazil in a 1:1 (vol/vol) mixture) and inoculated by dropwise delivery of 500 µL PBS containing $5x10^5$ VS of RSV. Each day after infection, body weight and temperature were recorded as described above. The proportion of weight change was calculated relative to the weight on the day of RSV challenge.

2.13.2.3 Anaesthesia and sedation

Depending on the downstream procedure, ferrets were treated with different anaesthesia and sedatives. For collection of nasal wash samples, ferrets were lightly anaesthetised with 5 mg/kg ilium Xylazil. For i.n. infection and i.n. drug administration, ferrets were sedated with using equal volumes of 25 mg/kg ketamine and 5 mg/kg ilium Xylazil. For i.v. drug administration, reversible anaesthesia consisting of of equal volumes ketamine (10 mg/kg), midazolam (0.5 mg/kg) and medetomidine (0.02 mg/kg) were injected and reversed by intramuscular injection with 0.01 mg/kg atipamezole. For euthanasia, ferrets were anesthetised using a mixture of ketamine and xylazine following pentobarbitone sodium (≥1000 mg/kg, Lethabarb Troy Laboratories) injection.

2.13.3 PBMC isolation

Ferret peripheral blood was collected at indicated time points into heparinised tubes via jugular vein puncture. Whole blood was diluted 1:1 in RPMI, mixed thoroughly and overlaid onto Ficoll-Paque Plus (GE Healthcare) in a 1:1 ratio (i.e. 2 mL blood per 2 mL RPMI per 2 mL Ficoll-Paque Plus), followed by centrifugation at 850 x g for 20 min (no brake). Peripheral blood mononuclear cells (PBMCs) were isolated from the interface, washed in PBS and incubated for 5 min in Red Blood Cell Lysing Buffer Hybri-Max to lyse erythrocytes. Samples were then washed in PBS, resuspended in RLT buffer supplemented with β-mercaptoethanol and total RNA was extracted using RNeasy Plus Mini spin columns. cDNA synthesis and qRT-PCR reactions were performed as described above (**section 2.11**).

2.13.4 Nasal wash collection

From 24 hrs after first exposure to donor animals, recipient ferrets received daily nasal washes. Ferrets were lightly sedated (5 mg/kg ilium Xylazil) and then 1 mL

of PBS was flushed through the nostril and the expelled liquid was collected. Nasal wash samples from IAV-infected animals were stored at -80°C prior to determination of viral titre by $TCID_{50}$ assay. Nasal wash samples from RSV-infected animals were snap-frozen in a bath of dry ice and 80 % (vol/vol) ethanol in water and stored at -80°C prior to determination of viral titre by VS assay.

2.13.5 Tissue collection

At experimental endpoints, ferrets were anesthetised with ketamine and xylazine prior to intracardiac injection of sodium pentobarbitone before removal of nasal tissues and lungs. From IAV-infected animals, individual lung lobes were stored at -80°C while lobes from RSV-infected animals were snap-frozen in dry ice/80 % (vol/vol) ethanol in water baths. To prepare samples for detection of infectious virus, lung lobes were thawed on ice and homogenised in 5 mL of DMEM in gentleMACS M tubes (Miltenyi Biotec) using a gentleMACS dissociator (Miltenyi Biotec). Nasal tissue was disrupted using a Polytron PT 2500E (Thermo Fisher Scientific). Homogenised lung and nasal tissue samples were clarified twice by centrifugation (3000 rpm, 10 min, 4°C). Titres of infectious IAV or RSV were determined by $TCID_{50}$ assay or plaque assay, respectively, as described (**sections 2.5.5 and 2.5.6**).

For the isolation of total RNA from ferret tissue, individual lung lobes and nasal tissues were stored in 5 mL RNALater at 4°C overnight. Tissue was then removed from the stabilizing agent and stored at -80°C. Lung and nasal tissues were homogenised as described above and RNA extraction was performed using the RNeasy Maxi kit (Qiagen). Briefly, tissue was homogenised in RLT buffer containing β-mercaptoethanol. Lung tissues were homogenised in gentleMACS M tubes using a gentleMACS dissociator and nasal tissue were homogenised using a Polytron PT 2500E. Samples were clarified twice by centrifugation (3000 rpm, 10 min, 4°C), mixed with 70 % (vol/vol) ethanol in water in a 1:1 ratio and transferred onto a RNeasy Maxi column, followed by a centrifugation for 5 min at 1800 rpm. The column was washed once with wash buffer RW1, twice

with RPE buffer and centrifuged again to dry the column. To isolate the RNA, 800 µL of RNase-free water was applied to the column, incubated for 1 min at RT and then centrifuged for 3 min at 1800 rpm. The flow-through (containing RNA) was collected and purity determined by spectrophotometry (A_{260}/A_{280}) using a Nanodrop. RNA samples were stored at -80°C prior to cDNA synthesis and qRT-PCR (**section 2.11**).

2.14 Data analysis

Flow cytometry data was analysed using FlowJo software for Windows, version 10 (Becton, Dickinson and Company). Fluorescence microscopy images were analysed using ImageJ software (Schneider et al., 2012). Graphs and statistical analysis (as indicated in the figure legends) were performed using GraphPad Prism version 9.2.0 (GraphPad software). For cloning procedures, ApE (A plasmid Editor) version 2.0.61 was used.

3 Chapter: Evaluation of RIG-I agonists as antiviral in different models of IAV infection

3.1 Introduction

Influenza viruses are a major threat to global health and seasonal influenza infections are associated with 3-5 million annual cases and 290,000 to 650,000 fatalities worldwide (Iuliano et al., 2018). Moreover, emerging IAV also have the potential to cause devastating global pandemics in an immunologically naïve population. Conventional antiviral therapies against IAV tend to target specific viral components, such as NAIs, M2 ion channel blockers (adamantanes) and inhibitors of the PA protein (baloxavir). These antivirals inhibit distinct steps in the viral replication cycle, namely virus release from infected cells (NAI), virus uncoating in endosomes (adamantanes) or genomic replication (baloxavir) (Krammer et al., 2018). Particularly alarming in this context are H1N1 variants that had acquired mutations associated with resistance to oseltamivir, the most commonly used NAI, which emerged in 2009 and rapidly spread to become the dominant population globally, highlighting the importance of monitoring currently circulating IAV for acquisition of resistance to NAI (Dharan et al., 2009; Meijer et al., 2009). A number of mutations associated with baloxavir resistance were also reported to emerge in phase 2 and 3 clinical trials (Takashita, 2021). While vaccination is important in limiting the impact of influenza infections, current vaccines have suboptimal effectiveness against seasonal viruses across all age groups, and particularly in the elderly (Osterholm et al., 2012; Kim et al., 2018). Moreover, as influenza viruses continually undergo antigenic variation, vaccine composition must be regularly evaluated and updated to provide protection against the most recent circulating strains. In the face of circulating seasonal IAV and the continuing threat of emerging pandemic IAV, new antiviral treatment strategies are urgently required.

The innate immune system acts as first line of defence against invading pathogens. Viral nucleic acids can be recognised by endosomal or intracellular PRRs, such as TLRs and RLRs (Kell et al., 2015). While endosomal TLRs are mainly expressed by immune cells, cytosolic RLRs are abundant in most somatic cells (Loo et al., 2011). RIG-I activation triggers a signaling cascade that activates transcription factors IRF3, IRF7 and NF-κB which ultimately induce transcription

of type I and type III IFNs. Secreted IFNs bind to their cognate receptors (IFNARs and IL10R2/IFNLR1 for type I IFN and type III IFN, respectively) in an autocrine and/or paracrine manner to induce expression of hundreds of ISGs (Schoggins et al., 2011b). Expression of ISG proteins is associated with induction of an 'antiviral state' within virus-infected cells, as well as in uninfected neighbouring cells acting to limit virus replication and spread within the host.

A number of studies have used synthetic RNA agonists to elicit broad-spectrum antiviral responses prior to and/or after viral infection. Optimal RIG-I activation is mediated by short (<300 bp) dsRNA ligands with blunt ends that bear a 5'-triphosphate or di-phosphate (Schlee et al., 2009; Schmidt et al., 2009; Goubau et al., 2014). From *in vitro* studies it is well established that treatment of human cells with RIG-I agonists results in induction of ISGs and that this correlates with inhibition of infection by viruses such as VSV, dengue virus (DENV), Vaccinia virus, HIV-1, hepatitis C virus (HCV), chikungunya virus (CHIKV) and IAV (Chakravarthy et al., 2010; Ranjan et al., 2010; Goulet et al., 2013; Olagnier et al., 2014; Chiang et al., 2015). While *in vitro* studies have demonstrated that RIG-I agonist treatment of human lung epithelial A549 (Chakravarthy et al., 2010; Ranjan et al., 2010; Goulet et al., 2013; Chiang et al., 2015) and monocyte-derived dendritic cells (Chiang et al., 2015) induced anti-IAV activity, it is not clear if RIG-I agonist treatment inhibits IAV infection and growth in cells from other mammalian species, such as mice and ferrets, which represent the most widely used animal models to study human IAV infections.

Numerous studies have used mouse models to demonstrate the prophylactic and/or therapeutic effects of RIG-I agonists against IAV *in vivo* (Ranjan et al., 2010; Lin et al., 2012; Goulet et al., 2013; Chiang et al., 2015; Coch et al., 2017). In general terms, prophylactic treatment of mice with RIG-I agonists can provide protection against IAV infection, resulting in improved survival and reduced titres of virus in the lungs (Goulet et al., 2013; Chiang et al., 2015). Goulet *et al*. demonstrated that the combination of prophylactic (day -1 and day 0) and therapeutic treatments (day 1) of C57BL/6 mice with RIG-I agonist (delivered by the i.v. route) was more effective in reducing lung virus titres than a single

prophylactic or therapeutic treatment alone. In the absence of infection, RIG-I agonist treatment was associated with rapid induction of IFN-α/β mRNA in the lungs and serum, peaking at 6 hrs post-treatment, as well as increased recruitment of neutrophils, macrophages and DCs to the lungs at 6 or 24 hrs post-treatment (Goulet et al., 2013). More recently, Coch *et al.* showed that pre-treatment of Mx1-positive B6.A2G-*Mx1* mice with RIG-I agonist up to 7 days prior to lethal challenge with IAV resulted in reduced weight loss and increased survival, while a therapeutic treatment 18 hrs after lethal IAV infection also resulted in increased survival, as well as reduced disease score and weight loss (Coch et al., 2017). While RIG-I agonist treatment of mice has the potential to mediate potent and long-lasting protection against IAV, the mechanisms underlying this protection are not fully understood. Moreover, to our knowledge, the anti-IAV activity of RIG-I agonist treatment has not been examined in ferrets, the gold standard small animal model to study human IAV infections.

Herein, we demonstrate that RIG-I agonist treatment resulted in specific and potent induction of antiviral ISG expression in mouse, human and ferret airway cell lines. Moreover, ISG induction following RIG-I agonist treatment correlated with reduced levels of IAV infection and growth in cell lines from each of the three species. Using inbred mice which do or do not express a functional Mx1 protein, we demonstrate the importance of a functional Mx1 to induce potent and long-lasting RIG-I agonist-mediated protection against IAV. Finally, we demonstrate that a single prophylactic treatment of ferrets with RIG-I agonist induces potent upregulation of ISGs in PBMCs, as well as in lung tissue. Prophylactic RIG-I treatment also resulted in a significant reduction in viral titres in the lungs of IAV-infected ferrets. Together, these data provide important insights regarding the use of RIG-I agonists as next-generation antiviral drugs against IAV infections.

3.2 Results

3.2.1 RIG-I agonist treatment induces ISG expression and inhibits IAV infection and growth in human, murine and ferret airway cell lines

Previous studies using human A549 airway epithelial cells demonstrated that RIG-I agonists are potent inhibitors of IAV (Chakravarthy et al., 2010; Ranjan et al., 2010; Goulet et al., 2013; Chiang et al., 2015). However, their ability to limit IAV infection in cells from other mammalian species, including mice and ferrets, is less clear. Therefore, human A549, mouse LA-4 and ferret FRL cells were treated with RIG-I agonist (3pRNA) and ISG induction was assessed 24 hrs later. Note that cells were also treated with a synthetic control RNA (ctrl RNA) which does not activate RIG-I, or with the appropriate species-specific IFN-α to promote ISG induction. As seen in **Figure 3.1 A**, 3pRNA or IFN-α treatment induced potent upregulation of IFITM1, ISG15 and Mx1 in human, mouse and ferret cells, whereas ctrl RNA treatment did not.

To determine if prophylactic treatment with RIG-I agonist was protective against IAV infection, A549, LA-4 and FRL cells were transfected with 3pRNA or ctrl RNA (200 ng/mL), or incubated with species-specific IFN-α, cultured for 24 hrs and then inoculated with IAV strain HKx31 at the indicated MOI for 1 hr at 37°C. After washing, cells were incubated an additional 8 hrs, permeabilised and stained for intracellular expression of IAV NP. Flow cytometry was then used to determine the percentage of virus-infected cells. Prophylactic treatment with 3pRNA or IFN-α resulted in significant reductions in the percent of IAV-infected cells compared to ctrl-treated cells (**Figure 3.1 B**). To assess the impact on virus growth (i.e. productive IAV replication and release from infected cells), cells treated with 3pRNA or ctrl RNA were infected 24 hrs later with IAV at a low MOI (MOI = 0.01) in the presence of exogenous trypsin to allow for multi-cycle virus replication. Supernatants were recovered at indicated time points and titres of infectious virus were determined by standard VS assay (van Baalen et al., 2017). Pre-treatment of human, mouse or ferret cells with 3pRNA completely abolished

virus release compared to ctrl-treated cells which supported high virus titres at 24-48 hrs post-infection (hpi) (**Figure 3.1 C**).

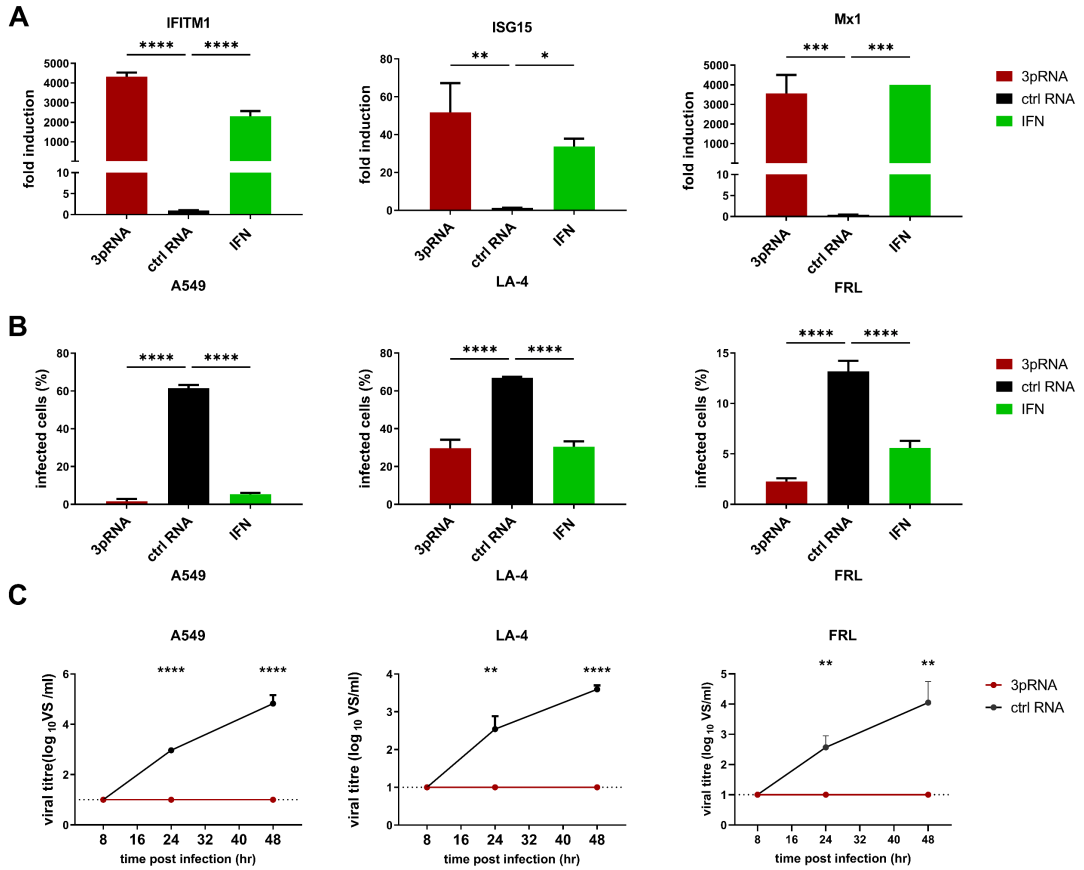

Figure 3.1: Treatment of human, mouse or ferret airway cell lines with RIG-I agonist induces ISG expression and inhibits IAV infection and replication. A549, LA-4 and FRL cells were transfected with RIG-I agonist (3pRNA, 200 ng/mL) or control RNA (ctrl RNA, 200 ng/mL), or incubated with human (10^4 units/mL), mouse (10^4 units/mL) or ferret (50 ng/mL) IFN-α. **A)** After 24 hrs, total RNA was isolated and the expression of ISGs was assessed by qRT-PCR. Expression is normalised to GAPDH and expressed as fold induction relative to untreated cells. **B)** After 24 hrs, cells were inoculated for 1 hr at 37°C with IAV (strain HKx31, H3N2) at MOI of 5 (A549), 10 (LA-4) or 1 (FRL). Cells were incubated an additional 7 hrs and then fixed and stained for intracellular expression of the viral NP. Cells were analysed by flow cytometry. **C)** After 24 hrs, cells were inoculated for 1 hr with HKx31 (MOI = 0.01), washed and incubated at 37°C in the presence of exogenous trypsin (0.5 mg/mL). After 8 hrs, 24 hrs and 48 hrs, cell culture supernatants were harvested and titres of infectious virus were determined in clarified supernatants using a VS assay on MDCK cells. All data show the mean (± SD) from triplicate samples and are representative of 2 or more independent experiments. A one-way ANOVA with Bonferroni's multiple comparison test was used in A) and B) and a Student's unpaired *t*-test was used in C) to compare 3pRNA or IFN-α to ctrl RNA treatment. * = p<0.05; ** = p<0.01; *** = p<0.001; **** = p<0.0001.

3.2.2 RIG-I agonist treatment induces ISG expression in primary mouse lung fibroblasts

Several groups have demonstrated that RIG-I agonists act as antiviral agents against IAV both *in vivo* and *in vitro* (Chakravarthy et al., 2010; Ranjan et al., 2010; Lin et al., 2012; Goulet et al., 2013; Chiang et al., 2015; Coch et al., 2017). However, only Coch *et al.* used mice expressing a functional Mx1 protein and these studies reported particularly potent and long-lasting RIG-I agonist-mediated protection *in vivo*. As Mx1 is an ISG and a potent inhibitor of IAV, we first aimed to compare 3pRNA-mediated ISG induction and protection against IAV using primary lung fibroblast generated from mice which do (B6.A2G-*Mx1*), and do not (B6-WT) express a functional Mx1 protein (Lindenmann, 1962).

First, mouse lung fibroblasts were assessed for ISG induction 24 hrs after treatment with 3pRNA, ctrl RNA or recombinant IFN-α. Both 3pRNA and IFN-α induced upregulation of IFIT1, ISG15 and Mx1 in B6-WT fibroblasts, whereas very little ISG induction was detected using B6.A2G-*Mx1* cells (**Figure 3.2 A**). In this instance, expression was determined using the $2^{-\Delta\Delta Ct}$ method which determines the fold change in ISG of interest after test conditions relative to control (unstimulated) conditions, which is then normalised to the housekeeping gene GAPDH, as for **Figure 3.1 A** (Livak et al., 2001). However, it was clear from the raw data that Ct values for all ISGs were markedly lower in untreated samples from B6.A2G-*Mx1* compared to B6-WT cells (data not shown). Therefore, we focused on comparison of untreated samples from each mouse strain (i.e. the constitutive expression) by calculating the relative expression, defined as the difference in Ct values of each ISG relative to GAPDH ($2^{-\Delta Ct}$) (Livak et al., 2001). Using this analysis, we confirmed that the constitutive expression of each ISG was significantly higher in B6.A2G-*Mx1* cells compared to B6-WT cells (**Figure 3.2 B**). Next, we determined the relative expression for B6-WT and B6.A2G-*Mx1* cells after 3pRNA, ctrl RNA or IFN-α treatment. In cells from both B6-WT and B6.A2G-*Mx1* mice, the highest relative expression of each ISG was observed following 3pRNA treatment (**Figure 3.2 C**). While relative expression after 3pRNA were similar for IFIT1 in B6-WT and B6.A2G-*Mx1* cells, ISG15 values were higher

in B6-WT cells and Mx1 values were higher in B6.A2G-*Mx1* cells. Together, these data indicate that the increased constitutive expression of ISGs in unstimulated B6.A2G-*Mx1* cells likely contributes to the relatively modest increase observed after 3pRNA treatment when analysed using the $2^{-\Delta\Delta Ct}$ method.

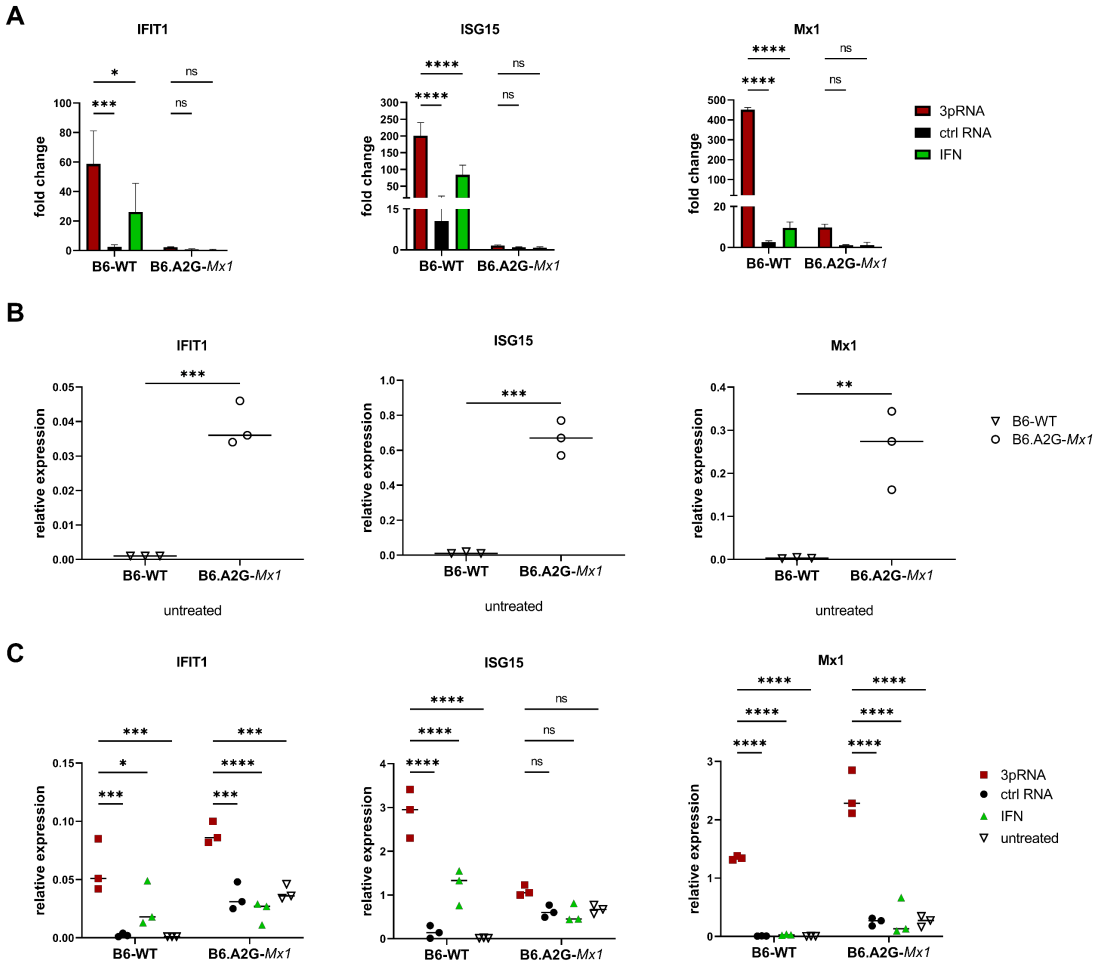

Figure 3.2: RIG-I agonist-mediated ISG induction in B6.A2G-*Mx1* and B6-WT primary fibroblasts. Cultures of primary lung fibroblasts were transfected with RIG-I agonist (3pRNA, 200 ng/mL) or control RNA (ctrl RNA, 200 ng/mL), or treated with IFN-α (10^4 units/mL). After 24 hrs, total RNA was isolated and the expression of IFIT1, ISG15 or Mx1 was assessed by qRT-PCR. **A)** Expression was normalised to GAPDH and is shown as fold induction relative to untreated cells. **B)** ISG expression relative to GAPDH was determined in untreated cells by calculating $2^{-\Delta Ct}$ values. **C)** ISG expression relative to GAPDH was determined in 3pRNA- (red squared), ctrl RNA- (black circles) or IFN-α-treated cells (green triangles) or in untreated samples (open triangles). Data represent the mean (± SD) for A) or the median for B) and C) from triplicate samples and are representative of 2 experiments, using fibroblasts sourced from different animals in each experiment. A two-way ANOVA with Bonferroni's multiple comparison test was performed to compare 3pRNA to other conditions in A) and C). An unpaired Student's *t*-test was performed in B) to compare B6-WT to B6.A2G-*Mx1* cells. * = p<0.05; ** = p<0.01; *** = p<0.001; **** = p<0.0001; ns = not significant.

3.2.3 A functional Mx1 is required for potent and long-lasting RIG-I agonist-mediated protection against IAV in primary mouse fibroblasts

Next, primary lung fibroblasts from B6-WT and B6.A2G-*Mx1* mice were treated with 3pRNA or ctrl RNA and then assessed for susceptibility to IAV infection and growth. Given that 3pRNA treatment of B6.A2G-*Mx1* mice was associated with potent and long-lasting protection against IAV challenge (Coch et al., 2017), B6-WT or B6.A2G-*Mx1* fibroblasts transfected with 3pRNA or ctrl RNA were then infected with IAV either 1 day or 5 days later. Flow cytometry was used to determine the percentage of IAV-infected cells at 8 hpi. As seen in **Figure 3.3 A**, 3pRNA treatment 1 day prior to infection significantly reduced the percentage of IAV-infected cells in both B6-WT and B6.A2G-*Mx1* fibroblasts**.** Notably, 3pRNA-mediated inhibition was more potent in B6.A2G-*Mx1* cells. Even 5 days after 3pRNA treatment, IAV infection was potently inhibited in B6.A2G-*Mx1* cells but the inhibitory effect seen at day 1 post-3pRNA treatment was lost in B6-WT cells (**Figure 3.3 A**). When considering infection of ctrl RNA-treated cells, IAV infection of B6-WT cells increased between cells infected at 1 versus 5 days post-treatment whereas infection of B6.A2G-*Mx1* cells was reduced between cells infected at 1 versus 5 days post-treatment. While the reasons behind different infection levels of ctrl RNA-treated cells 'aged' in cell culture for 1 versus 5 days are not known, it is very clear that 3pRNA-mediated inhibition of IAV infection is maintained for 5 days in B6.A2G-*Mx1*, but not B6-WT cells.

To determine if long-term protection correlated with enhanced ISG expression, levels of ISG15, Mx1 and IFIT1 in B6-WT and B6.A2G-*Mx1* fibroblasts were determined either 1 or 5 days after 3pRNA or ctrl RNA treatment (**Figure 3.3 B**). Using the $2^{-\Delta\Delta Ct}$ method, 3pRNA-induced ISG expression in B6-WT and, to lesser extent, in B6.A2G-*Mx1* fibroblasts at day 1 post-treatment, similar to results reported in **Figure 3.2 A**. Again, B6.A2G-*Mx1* fibroblasts showed higher constitutive ISG expression in unstimulated conditions compared to B6-WT cells when $2^{-\Delta Ct}$ ratios were examined (data not shown). Of interest, 5 days after 3pRNA-treatment levels of ISG15, Mx1 or IFIT1 were not significantly higher than ctrl-treated cells for either B6-WT or B6.A2G-*Mx1* fibroblasts. Together, these

data highlight the importance of a functional Mx1 protein for RIG-I agonists to mediate potent and long-lasting protection against IAV infection in primary lung fibroblasts *in vitro*. However, while B6.A2G-*Mx1* fibroblasts showed higher constitutive ISG expression, we did not find a direct correlation between long-lasting protection against IAV infection in B6.A2G-*Mx1* fibroblasts and maintenance of 3pRNA-induced upregulation of the ISGs examined.

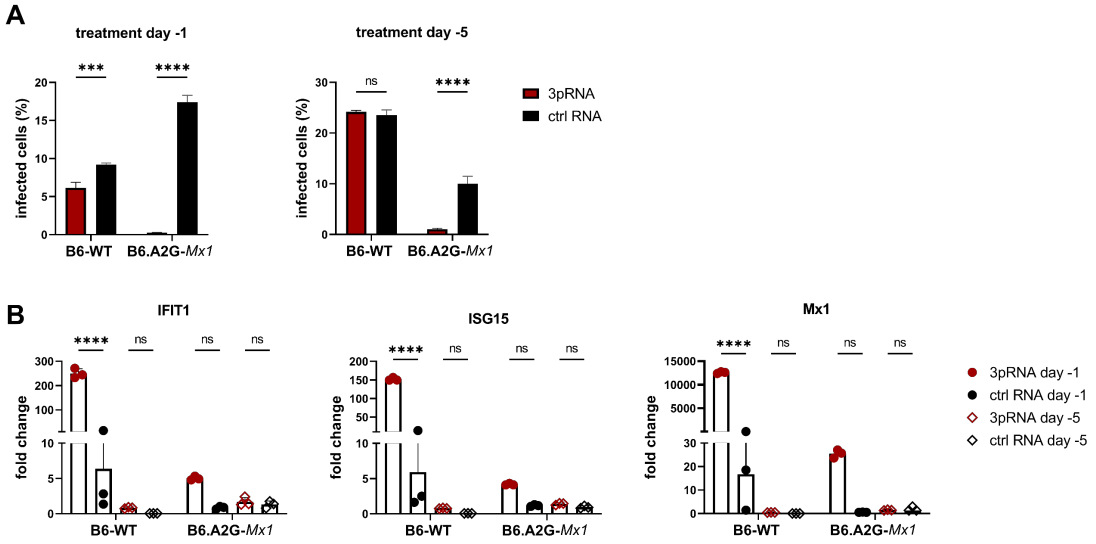

Figure 3.3: Treatment of primary lung fibroblasts from B6-WT or B6.A2G-*Mx1* mice with RIG-I agonists inhibits IAV and induces Mx1-dependent long-term protection. Cells were transfected with RIG-I agonist (3pRNA, 200 ng/mL) or control RNA (ctrl RNA, 200 ng/mL). **A)** At 1 or 5 days after treatment cells were infected with HKx31 (MOI = 10), then fixed and stained for intracellular expression of the IAV NP at 8 hpi. Cells were analysed by flow cytometry. **B)** RNA was harvested either 1 (filled symbols) or 5 days (open symbols) after 3pRNA (red symbols) or ctrl RNA (black symbols) treatment. Expression of Mx1, ISG15 and IFIT1 was assessed by qRT-PCR. Expression was normalised to GAPDH and expressed as fold induction relative to untreated cells. Data represent the mean (± SD) from triplicate samples and are representative of 2 independent experiments. A two-way ANOVA with Bonferroni's multiple comparison test was performed to compare 3pRNA and ctrl RNA treatment. *** = $p<0.001$; **** = $p<0.0001$; ns = not significant.

3.2.4 Intravenous injection of RIG-I agonist induces ISG expression in the lungs of B6-WT and B6.A2G-*Mx1* mice

Given that *in vitro* treatment of mouse cells and cell lines with RIG-I agonist induced upregulation of ISGs and protection against IAV infection and growth, we next investigated if a single i.v. injection of 3pRNA induced ISG upregulation in the lungs of naïve mice. For these studies, B6-WT and B6.A2G-*Mx1* mice received a single i.v. injection with 3pRNA or ctrl RNA and, 1 or 5 days later, animals were euthanised, lungs were removed and RNA isolation was performed. RNA isolated from untreated animals was also included in the analyses.

As for primary lung fibroblasts, qRT-PCR data for ISG15 and Mx1 was first analysed using the $2^{-\Delta\Delta Ct}$ method to determine the fold change in each ISG after test conditions relative to unstimulated conditions, which was then normalised to GAPDH. These analyses demonstrated that ISG15 and Mx1 were potently induced in the lungs of B6-WT and B6.A2G-*Mx1* mice 1 day after 3pRNA treatment (**Figure 3.4 A**). Although induction was variable between animals, levels were significantly higher after 3pRNA treatment compared to ctrl RNA treatment. At day 5 post-treatment, ISG levels were no longer significantly increased after 3pRNA treatment in either mouse strain, although we did observe a trend for upregulated expression of ISG15 and Mx1 in lungs from B6.A2G-*Mx1* mice.

When examining Ct values for ISG expression in the lungs from untreated mice, it was noted that Ct values for ISG15 were very similar between B6-WT and B6.A2G-*Mx1* mice whereas Ct values for Mx1 were markedly lower in lungs from B6.A2G-*Mx1* mice compared to B6-WT mice (data not shown). Analysis of the relative expression of ISG compared to GAPDH using the $2^{-\Delta Ct}$ method confirmed significantly increased expression of Mx1, but not ISG15, in B6.A2G-*Mx1* lungs (**Figure 3.4 B**). We also determined the relative expression 1 and 5 days after i.v. injection with 3pRNA or ctrl RNA. In both B6-WT and B6.A2G-*Mx1* mice, the highest relative expression of each ISG was observed following 3pRNA treatment (**Figure 3.4 C**). While relative expression after 3pRNA were similar for ISG15 in B6-WT and B6.A2G-*Mx1* mice, Mx1 values were higher in B6.A2G-*Mx1* mice.

These findings are consistent with relative expression patterns in primary lung fibroblasts from B6-WT and B6.A2G-*Mx1* mice following 3pRNA treatment *in vitro* (**Figure 3.2**).

Together, these data indicate that a single i.v. treatment with RIG-I agonist induces ISG expression in the lung tissue of both B6-WT and B6.A2G-*Mx1* mice but that this induction is short-lived and does not remain significantly upregulated day 5 post-treatment in either mouse strain. Of note, our *in vivo* studies confirm increased constitutive expression of Mx1 in lungs of B6.A2G-*Mx1* compared to B6-WT mice.

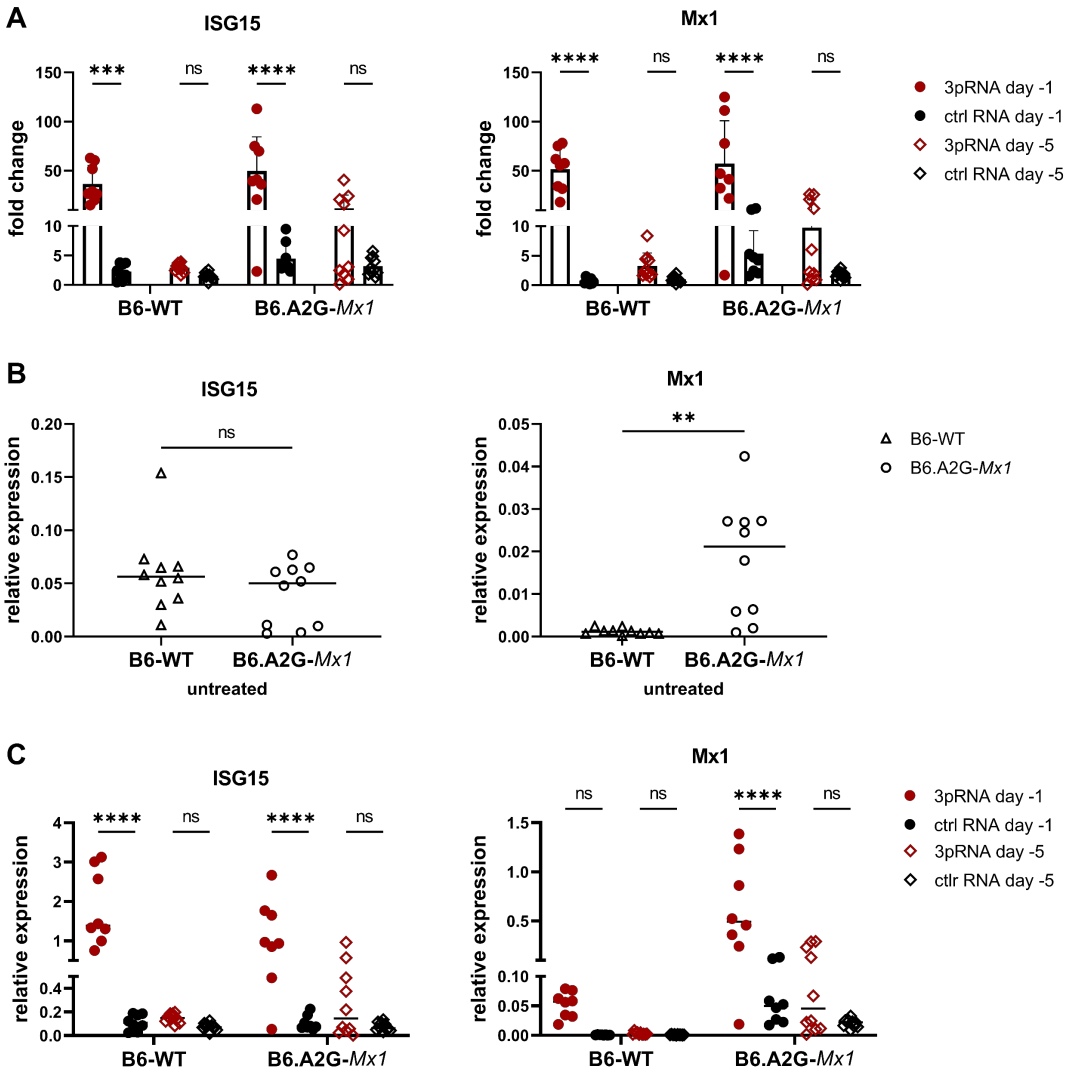

Figure 3.4: Intravenous RIG-I agonist treatment of B6.A2G-*Mx1* and B6-WT mice results in ISG induction in lung tissue. Mice received a single i.v. injection with 12.5 µg RIG-I agonist (3pRNA) or control (ctrl) RNA and, 1 or 5 days later, lung tissue was collected, total RNA was isolated and ISG expression determined by qRT-PCR. Lung tissue from untreated B6.A2G-*Mx1* and B6-WT mice was also collected for RNA isolation. **A)** ISG expression 1 (filled symbols) or 5 days (open symbols) after 3pRNA (red symbols) or ctrl RNA (black symbols) treatment was normalised to GAPDH and expressed as fold induction relative to untreated. **B)** Relative ISG expression compared to housekeeping gene expression was determined in untreated samples by calculating $2^{-\Delta Ct}$ values. **C)** Relative ISG expression 1 (filled symbols) or 5 days (open symbols) after 3pRNA (red symbols) or ctrl RNA (black symbols) treatment compared to GAPDH expression was determined by calculating $2^{-\Delta Ct}$ values. Data represent the mean (± SD) for A) or the median for B) and C). Data are pooled from 2 independent experiments (n= 8-10 mice/group). A two-way ANOVA with Bonferroni's multiple comparison test was performed to compare ISG induction between lungs from 3pRNA or ctrl

RNA-treated mice in A) and C) and a Student's *t*-test was performed to compare B6.A2G-*Mx1* and B6-WT mice in B). ** = p<0.01; *** = p<0.001; **** = p<0.0001; ns = not significant.

3.2.5 Immune cell recruitment and cytokine and chemokine release in the lung after i.v. treatment of B6-WT and B6.A2G-*Mx1* mice with 3pRNA

To gain insight as to how i.v. 3pRNA treatment modifies the airways prior to IAV infection, we assessed the inflammatory environment in the lungs of B6-WT and B6.A2G-*Mx1* mice 24 hrs after i.v. injection with 3pRNA or ctrl RNA. BALs were performed and immune cell infiltrates characterised by flow cytometry. We did not record significant differences in the number of total immune ($CD45^+$) cells, or in numbers of neutrophils ($CD11b^+$, $Ly6G^+$), eosinophils ($CD11b^+$, $Siglec\text{-}F^+$, $CD11c^-$, $CD64^-$), NK cells ($CD3^-$, $NK1.1^+$), alveolar macrophages ($CD11b^+$, $Siglec\text{-}F^+$, $CD11c^+$, $CD64^+$) and pan-macrophages ($CD11b^+$, $Siglec\text{-}F^-$, $CD64^+$), or in $CD4^+CD3^+$ or $CD8^+CD3^+$ T lymphocytes in BAL from 3pRNA or ctrl RNA treated animals in either mouse strain (data not shown).

Next, we used a multiplex CBA assay to determine levels of inflammatory cytokines and chemokines in cell-free BAL fluid of naïve mice and of mice 24 hrs after treatment with 3pRNA or ctrl RNA. Analysis of individual mediators indicated that 3pRNA treatment resulted in significant upregulation of CXCL10 relative to naïve mice or ctrl RNA-treated mice (**Figure 3.5**). While there was a trend for enhanced CXCL10 induction by 3pRNA in B6-WT mice compared to B6.A2G-*Mx1* mice, this was not significant. Other inflammatory mediators tested that were below detection limit and/or not significantly upregulated after 3pRNA treatment were IFN-γ, CXCL1, TNF-α, CCL2, IL-12 p70, CCL5, IL-1β, GM-CSF, IL-10, IFN-β, IFN-α and IL-6 (data not shown). Of note, this analysis was done in the BAL at 24 hrs post-treatment and future analysis could also aim to detect inflammatory mediators at earlier time points in the blood.

Overall, we noted no significant differences between B6-WT and B6.A2G-*Mx1* mice in any of the inflammatory mediators tested. Our data confirm that 3pRNA

treatment is associated with upregulated levels of CXCL10 at 24 hrs post-treatment in both B6-WT and B6.A2G-*Mx1* mice.

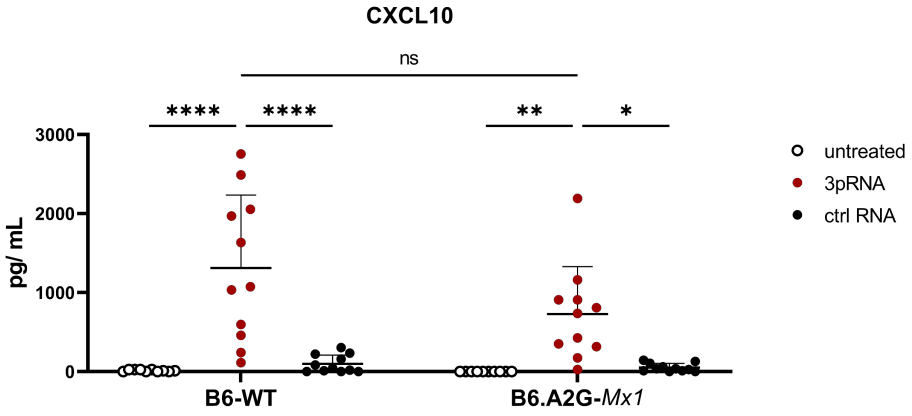

Figure 3.5: CXCL10 induction in BAL of B6-WT and B6.A2G-*Mx1* mice after RIG-I agonist treatment. B6-WT and B6.A2G-*Mx1* mice received a single i.v. injection of 12.5 µg RIG-I agonist (3pRNA) or control RNA (ctrl RNA) and, 24 hrs later, BAL was collected and analysed for cytokine and chemokine expression by CBA assay. BAL from untreated mice was included for comparison. Data show CXCL10 levels (mean ± SD) and are pooled from three independent experiments (n = 10-11 mice/group). A two-way ANOVA with Bonferroni's multiple comparison test was performed to compare CXCL10 levels after 3pRNA to ctrl RNA treatment, or to untreated samples. * = $p<0.05$; ** = $p<0.01$; **** = $p<0.0001$; ns = not significant.

3.2.6 A single prophylactic treatment of B6.A2G-*Mx1* but not B6-WT mice with 3pRNA results in potent inhibition of IAV HKx31 infection

Previous studies reported potent and long-lasting 3pRNA-mediated protection against IAV using B6.A2G-*Mx1* mice (Coch et al., 2017). Moreover, our *in vitro* studies comparing B6-WT versus B6.A2G-*Mx1* cells indicate that a functional Mx1 protein is the key determinant of both the potency and the duration of 3pRNA-mediated protection against IAV. Therefore, we next aimed to compare the ability of 3pRNA treatment to provide protection against IAV infection using B6-WT versus B6.A2G-*Mx1* mice.

B6-WT and B6.A2G-*Mx1* mice received a single i.v. injection with 12.5 µg of 3pRNA or ctrl RNA and, 24 hrs later, were infected by the i.n. route with 10^4 PFU of the mouse-adapted HKx31 strain of IAV in 50 µL of PBS. First, weight loss was assessed over 10 days. As seen in **Figure 3.6 A**, infection of ctrl RNA-treated B6-WT mice resulted in marked weight loss over time whereas mice pre-treated with 3pRNA showed more modest weight loss. In contrast, IAV infection of B6.A2G-*Mx1* mice did not result in weight loss, irrespective of 3pRNA or ctrl RNA treatment. Thus, while analysis of body weight indicated that 3pRNA pre-treatment provided some protection against IAV in B6-WT mice, B6.A2G-*Mx1* mice were markedly more resistant to HKx31 infection.

In a second experiment, mice were euthanised at day 5 post-infection to analyse virus titres in the upper (nasal tissues) and lower (lungs) respiratory tract. As seen in **Figure 3.6 B**, 3pRNA pre-treatment of B6-WT mice resulted in a modest, but significant reduction in virus titres in the lung, but not in the nasal tissues. In contrast, 3pRNA treatment resulted in a potent and significant reduction in virus titres in both the nasal tissues and the lungs of B6.A2G-*Mx1* mice. When comparing ctrl RNA-treated B6-WT versus B6.A2G-*Mx1* mice, titres in nose and lung were reduced by ~2-logs (100-fold) compared to B6-WT mice, confirming the increased resistance of B6.A2G-*Mx1* mice to IAV infection. When analysing the BAL of B6-WT and B6.A2G-*Mx1* mice we found increased cell numbers of $CD45^+$ cells, alveolar macrophages, $CD4^+CD3^+$ and $CD8^+CD3^+$ T lymphocytes in 3pRNA and ctrl RNA-treated B6-WT mice compared to B6.A2G-*Mx1* mice,

however due to large variations between animals this increase was not significant (data not shown).

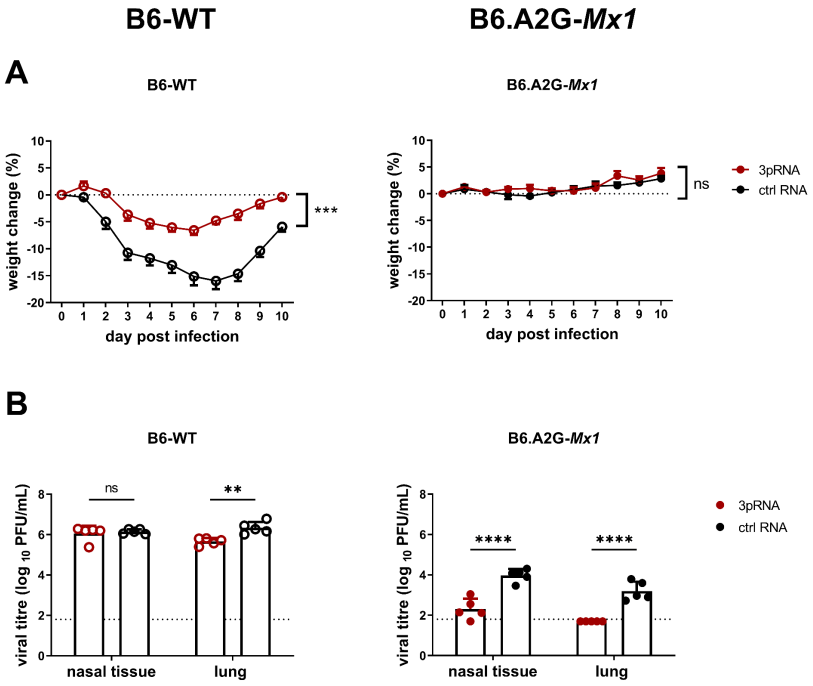

Figure 3.6: Effect of a single intravenous treatment of B6-WT and B6.A2G-*Mx1* mice with RIG-I agonist on subsequent challenge with IAV strain HKx31. B6-WT and B6.A2G-*Mx1* mice received a single i.v. injection of 12.5 µg RIG-I agonist (3pRNA) or control RNA (ctrl RNA) and, 24 hrs later, were infected by the i.n. route with 10^4 PFU of HKx31 (H3N2) in 50 µL of PBS. **A)** Mice were monitored daily and body weight was recorded. Data show the mean percent (± SEM) of weight change over time determined relative to original body weight (n = 5/group). **B)** At 5 dpi, nasal tissue and lungs were harvested, homogenised and virus titres in clarified homogenates were determined by plaque assay on MDCK cells (n = 4-5/group). Results are expressed as mean (± SD) and the dashed line represents the limit of detection for the plaque assay. Samples below the detection limit (<1.8 $\log_{10}$PFU/mL), were assigned values of 1.7 $\log_{10}$PFU/mL for statistical analysis. Data are representatives of two independent experiments. A two-way ANOVA with Bonferroni's multiple comparison test was performed to compare virus titres after 3pRNA or ctrl RNA treatment and a Student's *t*-test was performed to compare weight loss after 3pRNA or ctrl RNA treatment. ** = p<0.01; *** = p<0.001; **** = p<0.0001; ns = not significant.

3.2.7 A single prophylactic treatment with 3pRNA induces long-term protection from lethal PR8 infection in B6.A2G-*Mx1* but not in B6-WT mice

To determine if a single pre-treatment of 3pRNA provided long-lasting protection against subsequent IAV challenge, B6.A2G-*Mx1* and B6-WT mice were treated at 1 and 5 days prior to challenge with 10^2 PFU (B6-WT) or 10^6 PFU (B6.A2G-*Mx1*) of the mouse virulent PR8 strain of IAV. Given the marked

resistance of B6.A2G-*Mx1* observed following challenge with an equivalent dose of HKx31, we used a more virulent virus in both mouse strains and adjusted the inoculum dose to be higher for B6.A2G-*Mx1* animals, with the aim of achieving more comparable weight loss between B6-WT and B6.A2G-*Mx1* animals. As seen in **Figure 3.7**, 3pRNA treatment of B6-WT mice at day -1, but not -5, relative to PR8 challenge (10^2 PFU) resulted in less pronounced weight loss (**Figure 3.7 A, left panel**) and improved survival rates (**Figure 3.7 B, left panel**). All B6-WT mice which received 3pRNA treatment at day -1 survived whereas only 20 % (1/5) of those receiving ctrl RNA survived at 10 dpi. Most B6-WT mice challenged 5 days after treatment did not survive at 10 dpi, with survival numbers low following either 3pRNA (1/5) or ctrl RNA (2/5) treatment.

Following infection with a high dose (10^6 PFU) of PR8, ctrl RNA-treated B6.A2G-*Mx1* mice lost up to 15-20 % of their original body weight (**Figure 3.7 A, right panel**). Moreover, some ctrl RNA-treated animals from both -1 and -5 day treatment groups were euthanised due to excessive weight loss (3/5 and 4/5 for -1 and -5 day treatments, respectively) (**Figure 3.7 B, right panel**). In contrast, B6.A2G-*Mx1* mice treated with 3pRNA at day -1 or -5 relative to PR8 infection showed negligible weight loss (**Figure 3.7 A, right panel**) and all mice (5/5) survived to 10 dpi (**Figure 3.7 B, right panel**).

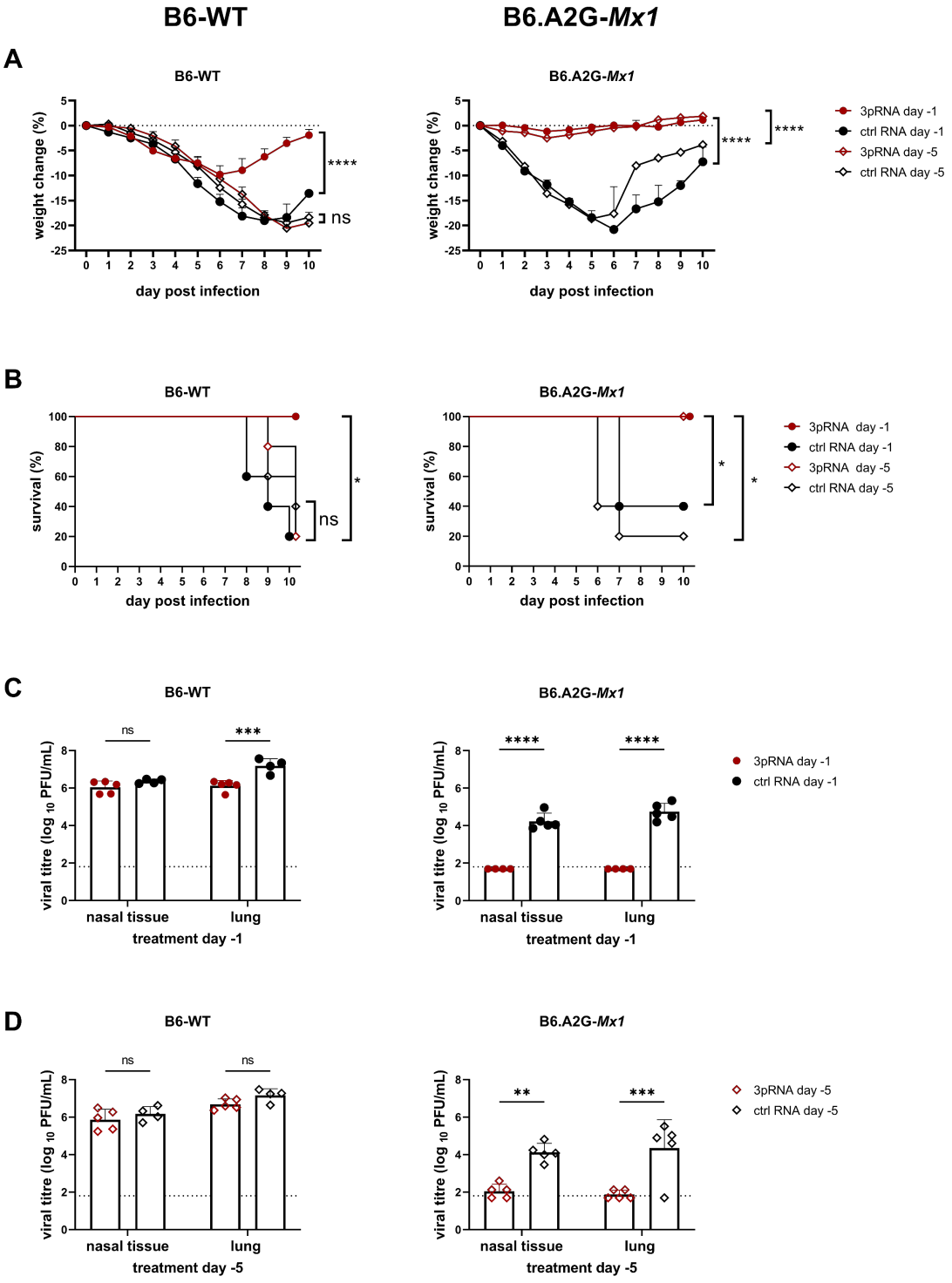

Figure 3.7: A single intravenous treatment with RIG-I agonist results in potent and long-term protection of B6.A2G-*Mx1* mice from subsequent challenge with PR8. B6-WT and B6.A2G-*Mx1* mice received a single i.v. injection of 12.5 µg RIG-I agonist (3pRNA) or control RNA (ctrl RNA) either 1 or 5 days prior to i.n. infection with 10^2 PFU (B6-WT) or 10^6 PFU (B6.A2G-*Mx1*) of IAV strain PR8 (H1N1) in 50 µL of PBS. **A)** Mice were monitored daily and any mice that

had lost > 20 % of their original body weight were euthanised. Data shows the mean percent (± SEM) of weight change over time determined relative to original body weight. Data from 1 experiment (n = 5/group). **B)** Kaplan-Meier 10-day survival analysis. **C)** and **D)** At 5 dpi, nasal tissues and lungs were harvested, homogenised and virus titres in clarified homogenates were determined by plaque assay on MDCK cells. Data are expressed as mean ± SD (n = 4 - 5/group). Data are representative of 2 independent experiments. The dashed line represents the limit of detection. Samples below the detection limit (<1.8 log_{10}PFU/mL) were assigned a value of 1.7 log_{10}PFU/mL for statistical analysis. In A), C) and D) a two-way ANOVA with Bonferroni's multiple comparison test was performed to compare weight loss and viral titres after 3pRNA or ctrl RNA treatment. In B) a log-rank Mantel-Cox test was performed to compare survival rates after 3pRNA or ctrl RNA treatment. * = p<0.05; ** = p<0.01; *** = p<0.001; **** = p<0.0001; ns = not significant.

In a second experiment, mice pre-treated with 3pRNA or ctrl RNA at day -1 or -5 relative to PR8 challenge were culled at 5 dpi to determine virus titres in the respiratory tract. Consistent with data using HKx31 (**Figure 3.6**), 3pRNA treatment of B6-WT mice at day -1 relative to challenge resulted in a significant reduction in virus titres in the lungs, but not the nasal tissues (**Figure 3.7 C, left panel**), although this protective effect was lost when pre-treatment occurred 5 days prior to challenge (**Figure 3.7 D, left panel**). In contrast, 3pRNA treatment at day -1 (**Figure 3.7 C, right panel**) or -5 (**Figure 3.7 D, right panel**) prior to challenge resulted in significantly reduced virus titres in both nasal tissue and lungs from B6.A2G-*Mx1* mice. In fact, infectious virus could not be detected in lung and nasal tissue of B6.A2G-*Mx1* mice when treated with 3pRNA at day -1 and only very low titres were detected in mice treated with 3pRNA at day -5 relative to PR8 infection. Together, these data indicate that RIG-I agonists mediate inhibition of IAV *in vivo* and that a functional Mx1 protein is required for induction of a potent and long-lasting protection.

3.2.8 Intranasal administration of 3pRNA prior to and after IAV infection of ferrets results in a modest reduction in viral shedding from the upper airways

Ferrets are considered the gold standard animal model to study IAV infections as they are an outbred population, their respiratory physiology shows similarities to that of humans, they can be infected with human viruses without the need for prior adaptation and infected animals can show clinical signs of disease similar to that of humans (Oh et al., 2016). Moreover, our *in vitro* studies demonstrated that 3pRNA, but not ctrl RNA, treatment of FRL airway cells induced potent upregulation of different ISGs and this correlated with inhibition of IAV infection and replication (**Figure 3.1**).

To our knowledge, the antiviral effectiveness of 3pRNA treatment against IAV in ferrets has not been reported. There were notable differences in experimental design between our studies in mice and in ferrets. First, we extrapolated the functional dose of 3pRNA required for IAV protection in mice such that ferrets received a weight-dependent dose of RIG-I agonist or ctrl RNA (Nair et al., 2016). Second, we aimed to assess the effectiveness of both intranasal (i.n.) and intravenous (i.v.) 3pRNA inoculation, given that i.n. represents a less invasive route that should also deliver 3pRNA locally to sites of IAV replication (i.e. the upper and lower airways). Third, we used a transmission model of influenza infection based on natural infection of household contacts to determine if 3pRNA treatment of ferrets could impact IAV transmission and also replication in the upper airways of infected animals. In this model, donor ferrets experimentally infected with IAV are co-housed with naïve recipient ferrets for 48 hrs (Oh et al., 2014). Studies in our group have confirmed that using IAV strain A/Perth/265/2009 (H1N1pdm09) in this experimental design generally results in 100 % transmission of IAV to recipient ferrets after co-housing for 48 hrs (Mifsud et al., 2020). In this design, our aim was to treat recipient ferrets with 3pRNA to determine impacts of virus transmission and growth.

In our first experiment, naïve recipient animals received one dose of 3pRNA (0.3 mg/kg, n = 4/group) via the i.n. route in a volume of 500 µL (i) 24 hrs prior to

exposure to donor animals experimentally infected 1 day prior with 10^5 $TCID_{50}$ of A/Perth/265/2009 (H1N1pdm09) or (ii) 24 hrs prior to exposure to infected donor animals, with a second dose 72 hrs later (i.e. at the completion of co-housing with donor ferrets). Due to limited animal numbers, the only ctrl RNA-treated animal group was one that received two doses. Recipient animals were then assessed daily for weight and temperature and daily nasal wash samples were collected until day 10 after the commencement of co-housing. The experimental overview of this ferret study is shown in **Figure 3.8 A**.

Following co-housing with infected donors, ctrl RNA-treated animals showed a modest peak in temperature at day 4 (~39.5^{o}C compared to ~38^{o}C at day 0) which was significantly higher (p = 0.026) than animals which received two doses of 3pRNA (**Figure 3.8 B, left panel**). Ctrl RNA-treated animals showed some weight loss over time (~8 % relative to day 0), whereas animals which received one or two doses of 3pRNA showed weight gain or modest weight loss (<5 %), respectively (**Figure 3.8 B, right panel**). Note that weight loss over time between ctrl RNA-treated animals and 3pRNA-treated animals receiving one dose was significantly different (p <0.0001).

Next, we determined titres of infectious virus in nasal wash samples from recipient animals. Infectious virus was detected in nasal wash samples from all recipient animals at 2 or more time points, confirming transmission to all naïve recipient animals (**Figure 3.8 C**). Area under the curve (AUC) analysis of virus titres was performed to determine the impact of 3pRNA treatment on virus shedding over time. Comparing AUC for 3pRNA- versus ctrl RNA-treated animals, no significant differences were observed (Kruskal-Wallis H test, p = 0.0997 for 1 dose 3pRNA: 9.941 ± 1.735 SD, p = 0.0620 for 2 doses 3pRNA: 9.628 ± 1.876 SD, 2 doses ctrl RNA: 14.81 ± 1.323 SD). However, it did appear that 3pRNA-treated animals showed different characteristics in their viral shedding compared to ctrl RNA-treated animals, particularly at days 2-3 post co-housing. Comparison of viral titres on individual days between the different groups indicated that 3pRNA significantly reduced viral titres at day 2 post co-housing (**Figure 3.8 D**) (1 dose 3pRNA p = 0.0415, 2 doses 3pRNA p =0.0098)

and the 2 dose 3pRNA regimen also reduced viral titres in day 3 samples compared to ctrl RNA-treated animals (p = 0.0296). On day 5 post co-housing, viral titres after 1 dose of 3pRNA were also reduced (p = 0.022), whereas viral titres after 2 doses of 3pRNA were even increased at day 6 (p = 0.023). Virus titres were not significantly different between 3pRNA and ctrl RNA-treated animals on any other dpi (data not shown). Together, these data indicate that neither prophylactic (1 dose) nor prophylactic and therapeutic (2 doses) intranasal treatment of ferrets with RIG-I agonist prevented IAV transmission and treatment resulted in only a modest reduction in viral shedding from the upper respiratory tract.

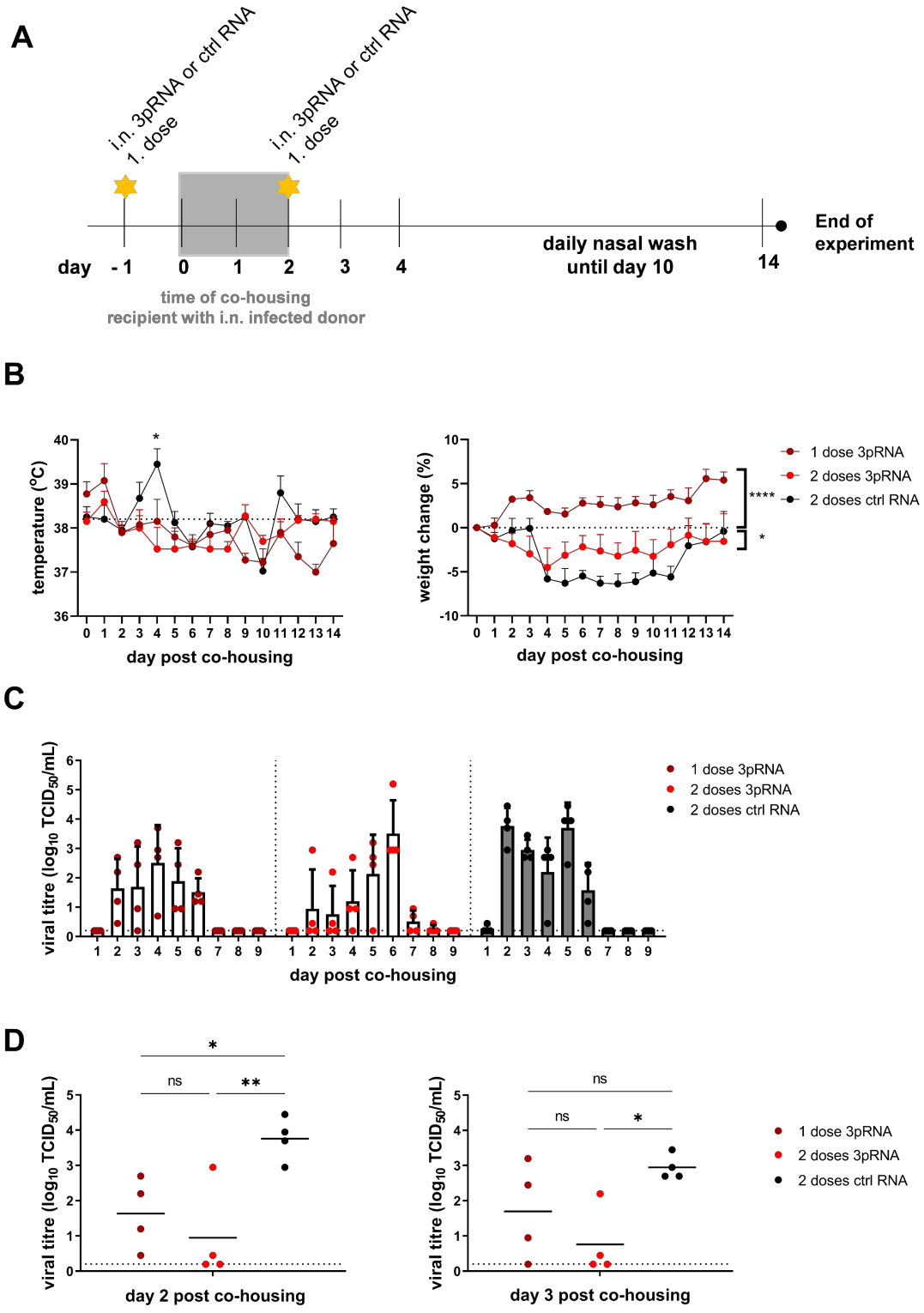

Figure 3.8: Intranasal treatment of ferrets with 3pRNA prior to and after co-housing with IAV-infected donor animals results in a modest reduction in early viral shedding. **A)** Recipient animals (n = 4/group) received either one dose of

3pRNA (0.3 mg/kg) 24 hrs prior to co-housing or two doses of 3pRNA or ctrl RNA (0.3 mg/kg) 24 hrs prior to and 48 hrs after commencement of co-housing. 3pRNA or ctrl RNA were formulated in 500 µL. For co-housing, donor animals were experimentally infected via the i.n. route with 10^5 $TCID_{50}$ of A/Perth/265/2009 (H1N1pdm09) in 500 µL and, 24 hrs later, co-housed with naïve recipients. After 48 hrs, donor animals were removed and recipients were kept for an additional 14 days. **B)** Animals were assessed daily for temperature and body weight. Data show the mean percent (± SEM) of temperature or weight change over time relative to the original body weight of each animal. **C)** Titres of infectious IAV in nasal washes (days 1-9 post co-housing) from recipient animals were determined by $TCID_{50}$ assay. **D)** Titres of infectious IAV in nasal washes from recipient animals on days 2 or 3 after the completion of co-housing. Dashed line represents limit of detection. Circles represent individual animals. Data in B) represent mean (± SEM), C) represent mean (± SD), D) represent mean. In B), a one-way ANOVA with Bonferroni's correction was performed to compare day-to-day differences in temperature after 3pRNA versus control RNA treatment and a two-way ANOVA with Bonferroni's correction was performed to compare weight change after 3pRNA versus ctrl RNA treatment. In D), a one-way ANOVA with Bonferroni's correction was performed to 3pRNA versus control RNA treatment. * = $p<0.05$; ** = $p<0.01$; **** = $p<0.0001$; ns = not significant.

3.2.9 Intravenous treatment of ferrets with 3pRNA after experimental IAV infection results in reduced virus replication in the lung

Intranasal administration of 3pRNA reduced viral shedding in nasal washes, however this effect was modest but significant on days 2 and 3 post co-housing (**Figure 3.8**). Intravenous RIG-I agonist treatment elicited potent and long-lasting protection from subsequent IAV infection in B6.A2G-*Mx1* mice. Therefore, we next assessed the ability of intravenous delivery of 3pRNA to impact subsequent IAV infection of ferrets, making use of donor ferrets that were used to infect naïve recipient animals in experiments described above. Therefore, donor ferrets were experimentally infected via the i.n. route with 10^5 $TCID_{50}$ of A/Perth/265/2009 (H1N1pdm09) and, 3 days later received a single i.v. injection of 3pRNA or ctrl RNA (0.3 mg/kg, n = 3-4/group) (**Figure 3.9 A**). After an additional 2 days (i.e. 2 days post-treatment, 5 dpi), animals were euthanised and titres of infectious virus were determined.

As seen in **Figure 3.9 B**, 3pRNA treatment did not reduce titres of infectious virus in nasal tissues (p = 0.2311, 3pRNA: 4.532 ± 0.144 SD, ctrl RNA: 4.261 ± 0.315 SD), but did result in significant reductions in virus titres recovered from the lung (**Figure 3.9 C**, lung 1: p = 0.0127, 3pRNA: 0.449 ± 0.306 SD, lung 2: p = 0.0091, 3pRNA 0.349 ± 0.335 SD, lung 3: p =0.0075, 3pRNA: 0.299 ± 0.137 SD, compared to ctrl RNA: 2.299 ± 1.499 SD). Note that virus titres were determined in individual lung lobes from each animal and data are presented as titres in lung lobes from individual 3pRNA-treated animals compared to titres in lobes from all ctrl RNA-treated animals. Together, these data provide evidence that i.v. 3pRNA treatment of ferrets mediates potent inhibition of IAV growth in the lungs.

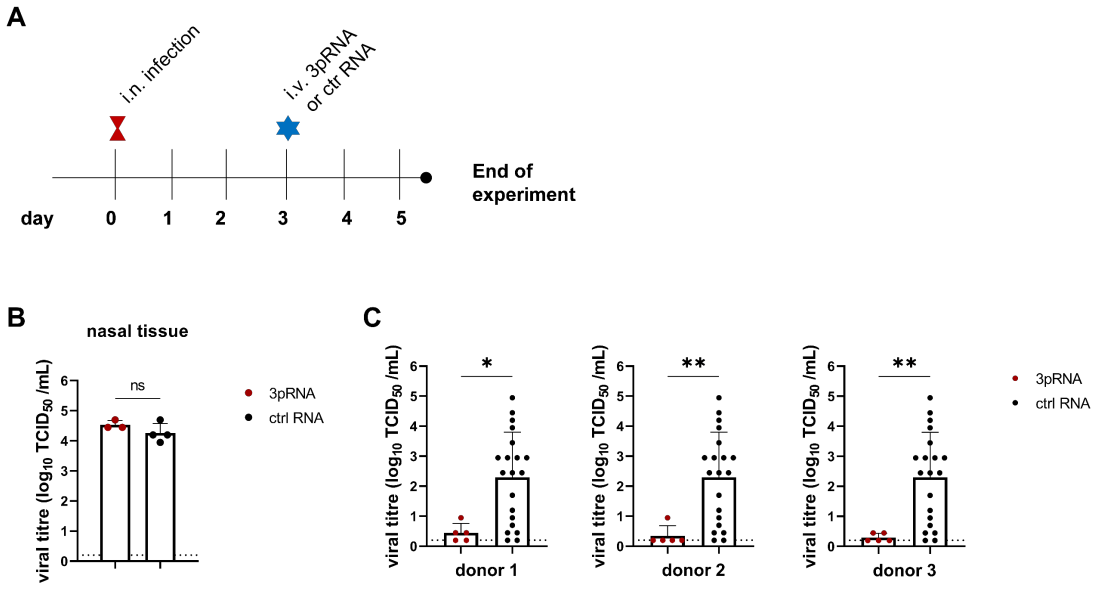

Figure 3.9: A single intravenous injection of IAV-infected donor ferrets with 3pRNA results in reduced virus replication in the lung, but not in the nose. **A)** Donor animals were infected via the i.n. route with 10^5 $TCID_{50}$ of A/Perth/265/2009 (H1N1pdm09) in 500 µL. At 3 dpi, animals received an i.v. injection of 3pRNA or ctrl RNA (0.3 mg/kg). At 5 dpi (i.e. 2 days after treatment), ferrets were euthanised, and **B)** nasal tissue and **C)** lungs were collected, homogenised in PBS and virus titres in clarified homogenates were determined by $TCID_{50}$ assay. Symbols represent in B) individual animals, or in C) single lung lobes, and bars represent the mean (± SD) viral titre. Data in C) show virus titres in individual lung lobes (5 per animal) from each 3pRNA-treated animal (n = 3/group) compared to a pool of lung lobes from all ctrl RNA-treated animals (n = 4/group). The dashed line represents the limit of detection. Samples below the detection limit (<0.2 $log_{10}TCID_{50}$/mL) were assigned values of 0.1 $log_{10}TCID_{50}$/mL for statistical analysis. An unpaired Student's *t*-test was performed to compare the viral load in respiratory tissue after 3pRNA or ctrl RNA treatment. * = $p<0.05$; ** = $p<0.01$; ns = not significant.

3.2.10 *Ex vivo* stimulation of ferret PBMCs with 3pRNA induces ISGs, but not other inflammatory cytokines

As we planned towards further studies to investigate the effects of i.v. 3pRNA treatment on ISG induction and protection from IAV infection in ferrets, we first considered approaches to assess systemic ISG induction in ferrets. As a first step, we aimed to isolate ferret PBMCs from naïve animals, stimulate with 3pRNA *in vitro* and determine the spectrum of ferret chemokines, cytokines and ISGs induced 6 hrs later. Using this approach, 3pRNA treatment did not result in induction of IL-2, IL-4, IL-6, IL-20, IL-12p40 or TNF-α, while IFN-α and IFN-γ showed modest upregulation compared to ctrl RNA-treated PBMCs (**Figure 3.10**). In contrast, the ISGs Mx1, OAS1 and ISG15 were all strongly upregulated in 3pRNA- compared to ctrl RNA-treated PBMCs. Note that statistical analyses were not performed on this preliminary experiment as each sample represents only 2 data points. Despite this, the results indicated that Mx1, OAS1 and ISG15 represent appropriate ISGs to assess in future studies the systemic ISG induction following i.v. 3pRNA treatment in ferrets.

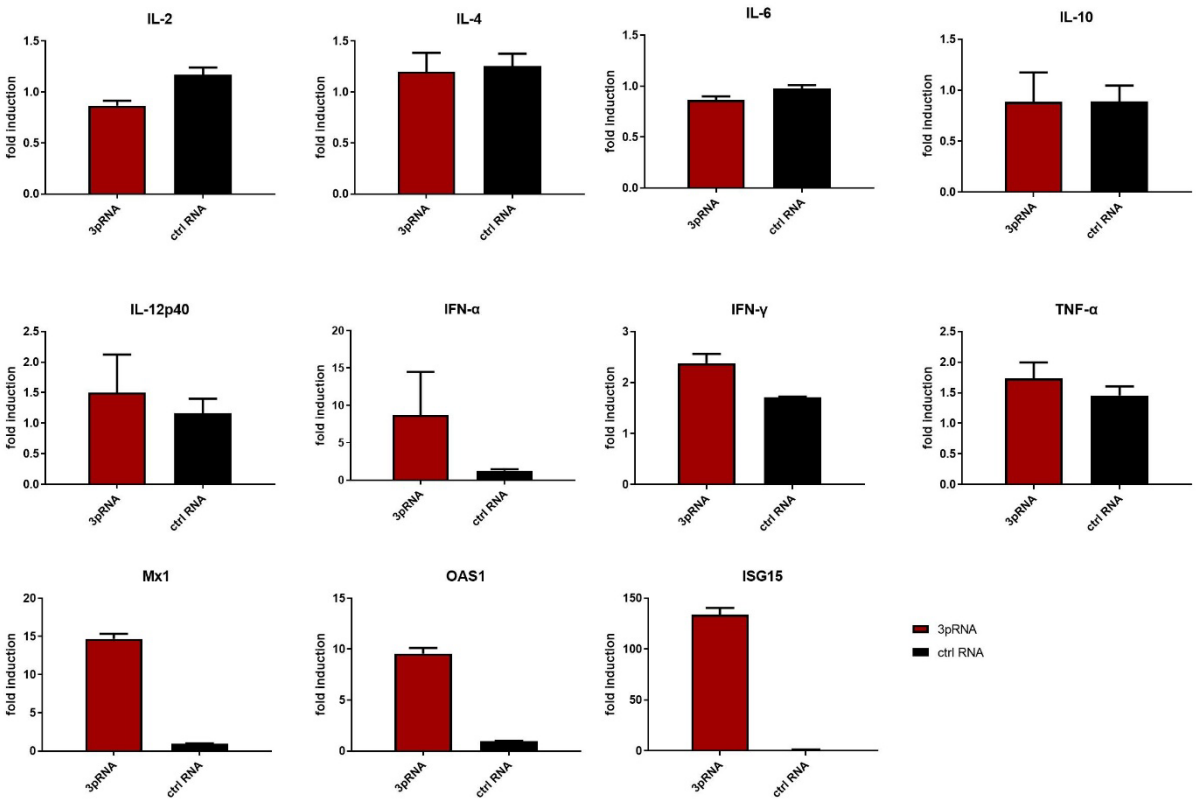

Figure 3.10: *Ex vivo* stimulation of ferret PBMC with 3pRNA induces ISG expression. PBMCs isolated from a naïve ferret were seeded at 10^6 cells/well in 96-well tissue culture plates and transfected with 3pRNA or ctrl RNA (0.5 µg/mL) and incubated at 37°C. Total RNA isolated 6 hrs later was used to determine expression of ferret cytokines, chemokines and ISGs by qRT-PCR. Results were normalised to GAPDH and expressed as fold induction relative to untreated cells. Data represent the mean ± SD (n = 2). Note that statistical analyses were not performed due to the limited number of data points.

3.2.11 Intravenous administration of 3pRNA induces ISG expression in PBMC and lung tissue of ferrets

Next, we assessed if i.v. 3pRNA administration resulted in systemic (i.e. in PBMCs) and/or local (i.e in lungs and/or nasal tissues) ISG induction in ferrets. Ferrets received a single i.v. injection of 3pRNA or ctrl RNA (0.3 mg/kg) and, 24 hrs later, animals were euthanised and individual lung lobes, nasal cavities and whole blood were collected. Respiratory tissues were processed directly for RNA isolation while PBMCs were isolated from whole blood by Ficoll gradient separation before subsequent RNA isolation. Of note, PBMCs were also isolated from each animal prior to 3pRNA/ctrl RNA injection to obtain baseline levels of ISG expression for each animal. As seen in **Figure 3.11 B** (**left panel**), we detected robust and significant upregulation of Mx1 in PBMCs following i.v. injection of ferrets with 3pRNA, but not ctrl RNA (p = 0.03). Similar trends were observed for ISG15 (**middle panel**) and OAS1 (**right panel**), although these were not significant. As baseline ISG levels could not be determined in respiratory tissues, expression of Mx1, ISG15 and OAS1 in 3pRNA-treated ferrets were compared to animals treated with ctrl RNA. In these analyses, we compared corresponding lung lobes from different animals to account for any potential bias in 3pRNA delivery to particular sites in the lung following i.v. administration. Compared to ctrl RNA-treated animals, 3pRNA treatment resulted in potent and significant Mx1 induction (5-12 fold) in all lung lobes (**Figure 3.11 C, left panel**) whereas induction of ISG15 and OAS1 was more variable, but significantly enhanced in 2/5 and 3/5 lobes, respectively (**Figure 3.11 C, middle and right panels**). No significant differences in ISG expression (Mx1, OAS1 and ISG15) were detected in nasal cavities from animals treated with RIG-I agonist compared to those treated with ctrl RNA (**Figure 3.11 A**). Together, these data demonstrate that i.v. administration of RIG-I agonist results in induction of ISGs in PBMC and in lung tissue 24 hrs later. Of note, induction was significant at both sites when assessing Mx1 expression.

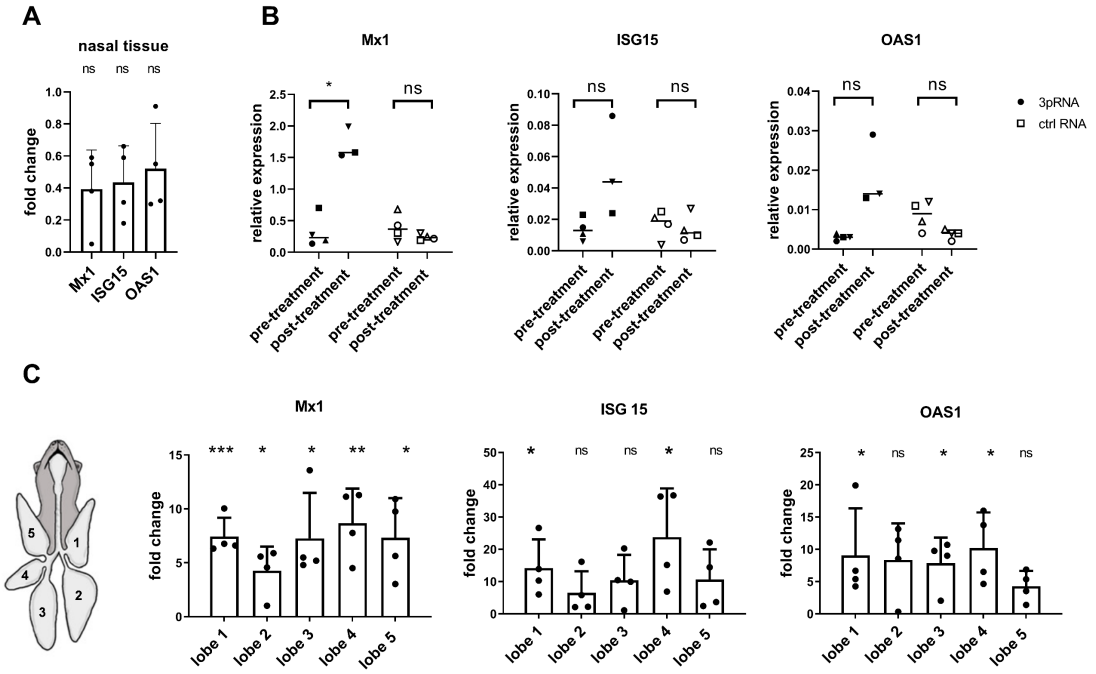

Figure 3.11: A single intravenous 3pRNA treatment of ferrets results in systemic upregulation of ISGs, as well as upregulation of ISGs in the lung. Ferrets received a single i.v. injection with 3pRNA or ctrl RNA (0.3 mg/kg). After 24 hrs, blood (for PBMC isolation) and respiratory tissues were collected for RNA isolation and then examined for expression of Mx1, ISG15 and OAS1 by qRT-PCR. **A)** ISG expression in nasal tissue. Data show the fold change in ISG expression, defined as the expression level in 3pRNA-treated animals compared to ctrl RNA-treated animals. **B)** ISG expression in PBMCs collected prior to i.v. injection (pre-treatment) compared to levels 24 hrs after 3pRNA or ctrl RNA injection (post-treatment). Levels of each ISG are expressed relative to GAPDH and each circle represents a single animal. **C)** ISG expression in individual lung lobes. Data show the fold change in ISG expression, defined as the expression level in 3pRNA-treated animals compared to ctrl RNA-treated animals. Each circle represents a single animal. Image in C) adapted from (Chan et al., 2017). The horizontal line in B) represents the median value, bars shown in C) represent the mean ± SD (n = 4 animals/group). In A) and C) an unpaired Student's *t*-test was performed to compare 3pRNA-treated compared to ctrl-RNA-treated animals of individual lung lobes or nasal tissue and in B) a paired Student's *t*-test was performed to compare expression before (pre-) and after (post-) treatment. * = $p<0.05$; ** = $p<0.01$; *** = $p<0.001$; ns = not significant.

3.2.12 A single intravenous injection of ferrets with 3pRNA at 24 hrs prior to IAV infection results in reduced virus replication in the lung

We used the transmission model of influenza infection to confirm if 3pRNA treatment of ferrets could impact IAV replication in the upper airways and/or the lungs. Therefore, naive recipient ferrets received a single, i.v. injection of 3pRNA or ctrl RNA (0.3 mg/kg, n = 4/group) and, 24 hrs later were co-housed for 48 hrs with donor animals that had been experimentally infected with 10^5 $TCID_{50}$ of A/Perth/265/2009 (H1N1pdm09) (**Figure 3.12 A**). Recipient animals were then assessed daily for weight and temperature, and daily nasal wash samples were collected. 5 days after commencement of co-housing (6 days after 3pRNA treatment), recipient animals were euthanised for collection of lung and nasal tissues. Notably, in a repeat experiment we also collected PBMCs from recipient animals immediately before and 24 hrs after 3pRNA/ctrl RNA injection to determine ISG expression.

3pRNA- and ctrl RNA-treated ferrets showed slight weight loss over time (a maximum of 5-10 % relative to day 0 body weight) and a modest peak in temperature at day 4 post exposure (~38^{o}C compared to ~37^{o}C at day 0), however, no significant differences were recorded between groups (data not shown). In one of two independent experiments, we also collected PBMCs prior to and 24 hrs after 3pRNA/ctrl RNA injection (recipients (R) 5-8, marked with # **Figure 3.12 B**), noting that these samples were obtained before exposure to IAV-infected donor animals. As seen in **Figure 3.12 B**, 3pRNA treatment resulted in upregulated ISG expression and this was significant for Mx1 (p = 0.0138) and OAS1 (p = 0.0365), confirming previous results (**Figure 3.11**). ISG15 expression showed a trend for increased expression in response to 3pRNA, however this was not significant (p = 0.1171). Note that large variations in relative ISG expression levels were observed, with one 3pRNA-treated animal showing negligible upregulation of ISG15 and OAS1 compared to ctrl RNA-treated animals.

Next, we determined titres of infectious virus in nasal wash samples from recipient animals. Infectious virus was detected in nasal wash samples at one or

more days of sampling (**Figure 3.12 C**) and/or in nasal cavity samples collected at day 5 post exposure (**Figure 3.12 D**) from all 3pRNA- and ctrl RNA-treated animals, indicating that treatment did not prevent transmission of virus from donors to naïve recipients. Moreover, AUC analysis comparing viral titres in nasal wash samples from 3pRNA- and ctrl RNA-treated animals across all days indicated significant reductions in viral loads after 3pRNA treatment (p = 0.003, 3pRNA: 8.062 ± 2.687 SD, ctrl RNA: 10.31, ± 2.259 SD, pooled from 2 experiments). Titres of infectious virus were detected in the nasal cavity of 7/8 3pRNA-treated animals euthanised 5 days after commencement of co-housing and these were not significantly different to those from ctrl RNA-treated animals (**Figure 3.12 D**, p = 0.3549, 3pRNA: 3.543 ± 2.129 SD, ctrl RNA: 4.449 ± 1.626 SD).

Finally, we determined virus titres in individual lung lobes from 3pRNA- and ctrl RNA- treated animals euthanised 5 days after commencement of co-housing. Across two independent experiments, 3pRNA treatment resulted in significantly reduced titres of infectious virus recovered from the lungs in 6/8 animals (**Figure 3.12 E and F**). Infectious virus was detected in 1 or more lung lobes from all 8 animals treated with ctrl RNA (28/38 lung lobes across the two experiments, noting that an error resulted in 2 lung lobes not collected for analysis). For 3pRNA-treated ferrets, no virus was detected in any lung lobes of 2/8 animals (R5 # and R7 #) and low titres (<1 $\log_{10}TCID_{50}$/mL) were recovered from 1/5 (R1), 3/5 (R3), 2/5 (R4) and 3/5 (R8 #) 3pRNA-treated animals. However, virus was recovered from 4/5 and 5/5 lung lobes from 3pRNA-treated animals R2 and R6 # and the titres recovered were not significantly different to those from ctrl RNA-treated groups. Of interest, when ISG induction in PBMCs was assessed we noted that high virus titres in R6 # correlated with the lowest induction of Mx1, ISG15 and OAS1 (**Figure 3.12 B,** black upright triangle “post-treatment”). Together, these data indicate that a single prophylactic i.v. treatment of ferrets with 3pRNA can induce systemic ISGs and reduce titres of infectious virus in the lungs of IAV-infected ferrets.

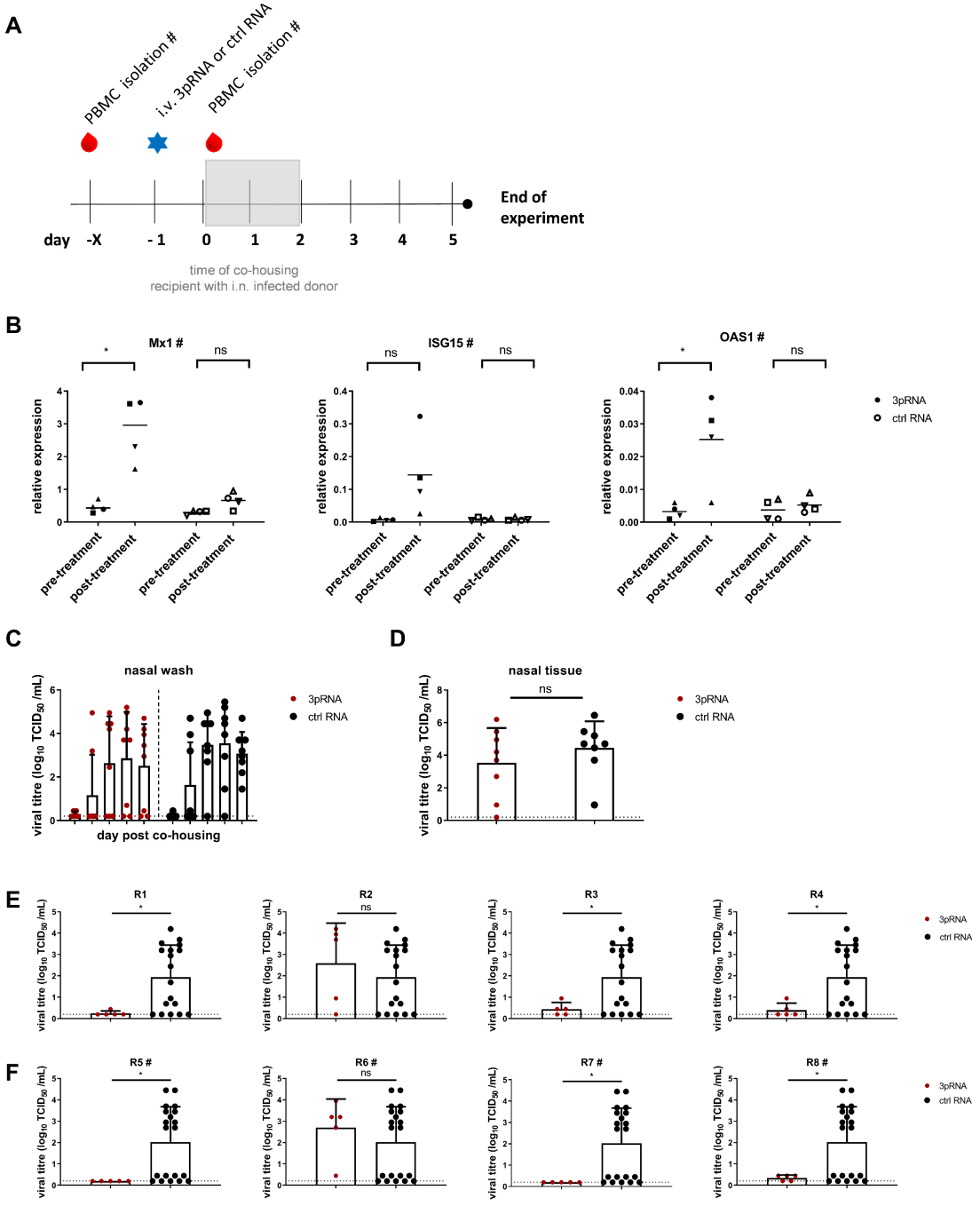

Figure 3.12: A single intravenous 3pRNA injection of ferrets at 24 hrs prior to co-housing with IAV-infected donor animals results in reduced virus replication in the lung, but not the nasal tissues. **A)** Recipient animals (n = 4/group) received a single intravenous injection of 3pRNA or ctrl RNA (0.3 mg/kg) 24 hrs prior to co-housing with IAV-infected donor animals. For co-housing, donor animals were experimentally infected via the i.n. route with 10^5 $TCID_{50}$ of A/Perth/265/2009 (H1N1pdm09) in 500 µL and, 24 hrs later, these animals were co-housed with naïve recipients. After 48 hrs, donor animals are removed and recipients are kept for an additional 3 days. Nasal wash samples were collected daily and animals

were euthanised at day 5 post-exposure for collection of nasal tissues and lung lobes. **B)** Whole blood was collected and PBMCs were isolated several (-X) days prior to (pre-treatment) and 24 hrs after (post-treatment) i.v. injection with 3pRNA or ctrl RNA. qRT-PCR was used to determine ISG levels, which are expressed relative to GAPDH. Each symbol represents a single animal and data are from a single experiment. **C)** and **D)** Titres of infectious virus in nasal washes (days 1 – 5 post co-housing) and nasal tissues (day 5 post co-housing) from 3pRNA- or ctrl RNA-treated animals. Data are pooled from 2 independent experiments. Circles represent individual animals. **E)** and **F)** Titres of infectious virus in lung tissue from 3pRNA-treated recipient animals (R1 - 4 and R5 - 8 from independent experiments) compared to ctrl RNA-treated recipients. Each symbol represents individual lung lobes (5 per animal) from each 3pRNA-treated animal compared to a pool of lung lobes from the corresponding 4 ctrl RNA-treated animals in each experiment. Bars represent the mean (± SD) viral titre in lung lobes. The dashed line represents the limit of detection. Samples below the detection limit (<0.2 $log_{10}TCID_{50}$/mL) were assigned values of 0.1 $log_{10}TCID_{50}$/mL for statistical analysis. Data in B) represent the median, data in C)- F) represent the mean ± SD. A paired Student's *t*-test was performed in B) to compare ISG levels before and after 3pRNA or ctrl RNA treatment. In C)- F) a two-tailed Mann-Whitney U test was performed to compare viral loads in nasal wash samples or respiratory tissue after 3pRNA or ctrl RNA treatment over time. * = $p<0.05$; ns = not significant.

3.3 Discussion

RIG-I agonists are antiviral agents which induce innate immune signaling via type I and type III IFN pathways and show potential as antiviral agents against a variety of RNA and DNA viruses (Yong et al., 2018). In the present study we explored the function of synthetic RIG-I agonists as antiviral treatments for IAV infections *in vitro* and *in vivo*. We showed that 3pRNA treatment of airway cells from humans (A549), mice (LA-4) and ferrets (FRL) induced ISG expression and this correlated with significantly reduced IAV infection (measured by flow cytometry), as well as viral replication and release from infected cells (**Figure 3.1**). IFN-α treatment of cells from different species also induced ISG levels and inhibited viral infection, consistent with the reported function of 3pRNA as a potent stimulator of the type I IFN pathway (Yoneyama et al., 2004). Host cells encode numerous intracellular proteins, including ISG proteins induced by IFNs, that can target different steps in the IAV replication cycle including virus entry, replication and/or exit (Villalón-Letelier et al., 2017). In our studies it is likely that RIG-I agonist treatment induces multiple ISG proteins to effectively inhibit IAV infection and virus growth. While others have reported that pre-treatment of A549 cells with 3pRNA mediates protection from subsequent IAV challenge (Chakravarthy et al., 2010; Lin et al., 2012; Goulet et al., 2013; Chiang et al., 2015), including with adamantane- and oseltamivir-resistant avian H5N1 (Ranjan et al., 2010), to our knowledge our studies are the first to confirm that RIG-I agonist pre-treatment also induces ISGs and inhibits IAV infection and growth in mouse cells, including primary lung fibroblasts, as well as in airway cells of ferret origin.

To date, most *in vivo* studies evaluating the antiviral function of RIG-I agonists against IAV have been performed using laboratory mouse strains such as C57BL/6 and BALB/c which do not express a functional Mx1 protein, an ISG protein which is known to mediate potent anti-IAV activity (Verhelst et al., 2013). In general terms, these studies have reported that prophylactic, i.v. administration of RIG-I agonists can protect mice from subsequent challenge with different IAV, including H5N1 (Lin et al., 2012; Goulet et al., 2013; Chiang et al., 2015), however protection was generally quite modest when assessed at 24 hrs and the duration

of its effects were not reported. In contrast, one study from Coch *et al*. used B6.A2G-*Mx1* mice to demonstrate potent and long-lasting protection from IAV following treatment with 3pRNA (Coch et al., 2017). To investigate these discrepancies further, we performed a direct comparison of the effects of 3pRNA pre-treatment on subsequent IAV infection in mice that do (B6.A2G-*Mx1*) or do not (B6-WT) express a functional Mx1.

First, we used primary mouse fibroblasts to demonstrate potent upregulation of ISGs in response to 3pRNA treatment in B6-WT, but not B6.A2G-*Mx1* cells using the $2^{-\Delta\Delta Ct}$ method (**Figure 3.2 A**). However, subsequent analysis using the $2^{-\Delta Ct}$ method (i.e. to examine ISG expression relative to GAPDH housekeeping gene) indicated that constitutive ISG expression was markedly elevated in B6.A2G-*Mx1* cells and this likely contributes to the modest increase in ISGs following 3pRNA treatment when analysed using the $2^{-\Delta\Delta Ct}$ method (**Figure 3.2 B and C**). Next, we examined if 3pRNA treatment of fibroblasts from B6.A2G-*Mx1* and B6-WT mice could provide long-term protection from IAV infection. While 3pRNA treatment one day prior to IAV infection protected both B6.A2G-*Mx1* and B6-WT cells, potent protection was only maintained five days after treatment using B6.A2G-*Mx1* cells (**Figure 3.3 A**). After one day, 3pRNA strongly induced ISG expression in B6-WT cells and, to a lesser extent in B6.A2G-*Mx1* cells (**Figure 3.3 B**), with the latter result likely due to the high constitutive expression of at least some ISGs in B6.A2G-*Mx1* cells. After five days, ISG expression in 3pRNA-treated cells from either mouse strain had returned to baseline levels. Given that RIG-I receptor signaling must be tightly controlled to promote antiviral defence whilst not inducing exaggerated inflammatory responses (Rehwinkel et al., 2020), it is not surprising that Mx1 mRNA levels were not elevated at day 5 post-treatment. However, it is possible that Mx1 protein expression remains elevated and relatively stable in B6.A2G-*Mx1* fibroblasts, such that it is able to mediate potent anti-IAV activity for many days after induction by 3pRNA treatment. Unfortunately, attempts to quantitate Mx1 expression in cell lysates by western blot were not successful. While protein turnover will be determined by the characteristics of both the cell type and the protein of interest, it is interesting to note that unpublished studies

from our laboratory using LA-4 cells with doxycycline-induced expression of Mx1 showed that protein levels were not markedly reduced at 72 hrs after removal of doxycycline. In contrast, inducible expression of the ISGs IFITM1, IFITM2 and IFITM3 had returned to background levels 48 hrs after removal of doxycycline (personal communication, Prof. Patrick Reading, The University of Melbourne). These examples demonstrate that protein turnover is dependent on the particular protein evaluated, however, given the relatively slow turnover of Mx1 in LA-4 cells, protein stability could be similar in primary fibroblasts and explain the RIG-I agonist-induced long-lasting protection from IAV infection.

Next, we assessed RIG-I agonist mediated protection *in vivo*, first using a mouse model of infection. When we assessed the lung environment 24 hrs after naïve mice received a single i.v. dose of 3pRNA, we did not detect significant differences in inflammatory cells recruited to the airways of B6.A2G-*Mx1* and B6-WT mice. Furthermore, CXCL10 was the only inflammatory mediator induced to significant levels in cell-free BAL fluids following 3pRNA, but levels were not significantly different between B6.A2G-*Mx1* and B6-WT mice (**Figure 3.5**). Moreover, ISG induction in lung tissue following 3pRNA treatment of naïve mice showed similar patterns to our *in vitro* data using primary lung fibroblasts in that (i) Mx1 showed higher levels of constitutive expression in tissues from B6.A2G-*Mx1* mice, (ii) ISGs (particularly Mx1) were induced in the lungs one day after 3pRNA treatment, but had largely returned to baseline levels five days after treatment for both mouse strains (**Figure 3.4**).

A direct comparison of 3pRNA pre-treatment on subsequent IAV infection of B6.A2G-*Mx1* and B6-WT mice one day later confirmed that while treatment was protective in both mouse strains (as assessed by IAV-induced weight loss and virus replication in the airways at day 5 post-infection), it was particularly potent in mice expressing a functional Mx1 protein (**Figure 3.6 and Figure 3.7**). Data obtained using ctrl RNA-treated animals also confirmed B6.A2G-*Mx1* mice to be intrinsically less susceptible to IAV infection as evidenced by negligible weight loss and reduced virus titres 5 dpi following infection with an equivalent virus dose (**Figure 3.6**). These latter findings are consistent with numerous studies that have

reported the resistance of mice expressing functional Mx1 to IAV infection, including by H5N1 and pandemic IAV (Haller et al., 1981; Tumpey et al., 2007; Song et al., 2013). The novelty in our findings lies in a direct comparison of the effectiveness of 3pRNA pre-treatment against subsequent IAV infection in mice that do and do not express a functional Mx1.

In subsequent studies using different doses of the mouse-adapted PR8 (adjusted to induce similar weight loss in the two mouse strains), we confirmed that 3pRNA pre-treatment either 1 or 5 days prior to PR8 challenge in B6.A2G-*Mx1* mice resulted in potent protection as shown by less severe weight loss and increased survival (**Figure 3.7**), and this correlated with reduced virus titres in the lungs and nose of infected animals. In contrast, B6-WT mice were only protected when 3pRNA treatment occurred 1 day before infection, resulting in increased survival and reduced virus titres in the lungs, although no differences in viral titres were noted in the nasal tissues. Overall, our findings regarding the effects of 3pRNA treatment of B6.A2G-*Mx1* and B6-WT mice are consistent with our *in vitro* studies using primary fibroblasts, confirming the importance of a functional Mx1 protein for potent and long-term protection to subsequent IAV challenge. As we detected no major differences in inflammatory cells and mediators in BAL from the two mouse strains following 3pRNA treatment, we propose that the functional Mx1 is the primary mediator of potent and long-term protection against IAV. This is likely due to its direct antiviral effects against IAV, where the functional Mx1 is known to potently inhibit IAV replication, likely by disrupting interactions between components of the viral RNA polymerase to block transcription (Huang et al., 1992; Pavlovic et al., 1992; Verhelst et al., 2012). Its higher constitutive mRNA expression in B6.A2G-*Mx1* mice can be further boosted by 3pRNA treatment (**Figure 3.4 C**) and this likely results in increased expression of the functional protein. It is interesting to note that we observed enhanced constitutive expression of other ISGs in primary fibroblasts (IFIT1, ISG15) from B6.A2G-*Mx1* mice although this trend in mouse lung was not observed, however ISG15 was the only ISG examined. It is intriguing to speculate that expression of a functional Mx1 might also modulate expression of other ISGs. Further studies examining Mx1 expression in a range of different tissues from B6.A2G-*Mx1* mice will be

necessary to assess if Mx1 mRNA levels are constitutively enhanced in other organs than the lung and if constitutive higher levels of a broader panel of ISGs or IFNs could be responsible for enhanced protection from viral infection.

To date, no published studies have evaluated the antiviral potential of RIG-I agonists in ferrets. We used a natural transmission model where naïve recipient ferrets are co-housed for 2 days with H1N1pdm09-infected donor ferrets to examine the impact of 3pRNA treatment of recipient animals (either via i.n. or i.v. routes) on virus transmission and replication in the airways as well as virus replication in 3pRNA-treated donor animals. We also established assays to examine ISG induction in response to 3pRNA treatment in PBMCs and in lung and nasal tissues. Irrespective of treatment route or regimen for recipient animals, we detected infectious virus in nasal wash samples from recipient ferrets across all experiments, indicating that 3pRNA treatment does not limit onward transmission of IAV from donor to recipients under any of the conditions examined. When examining the effect of i.n. 3pRNA treatment, we did not detect an overall reduction in viral titres in nasal wash samples over time although in a day-to-day comparison we did observe a significant reduction in viral titres at days 2 and 3 in one or both groups receiving i.n. 3pRNA (**Figure 3.8 D**). Thus, intranasal 3pRNA treatment of recipient ferrets did not prevent their ability to acquire IAV infection from donor animals (i.e. transmission) and had a modest, but significant effect in reducing virus shedding from recipient animals at early time points after treatment. It is tempting to speculate that 3pRNA treatment had minimal effect on viral shedding as viral load in nasal tissue was not affected by the treatment. In ferret studies, people have shown that reduced viral load in nasal tissue does (Toots et al., 2019) and does not (Marriott et al., 2014) correlate with reduced viral shedding. Toots *et al.* showed that IAV-infected ferrets therapeutically treated with a ribonucleoside analogue showed reduced viral shedding compared to control animals and this correlated with significantly reduced viral titres in the nasal tissue (Toots et al., 2019). Marriot *et al.* compared antiviral effectiveness of oseltamivir treatment in ferrets challenged with high or low dose of H1N1pdm09 A/California/04/2009 and they showed that oseltamivir treatment reduced viral shedding but not viral RNA load in nasal turbinates

(Marriott et al., 2014). However, they did detect reduced viral RNA load in trachea and lung tissue. One important ferret transmission study by Richard *et al.* showed that virus expelled from the upper respiratory tract rather than from trachea or lower airways is the site of generation of airborne IAVs, thus viral replication in the upper rather than in the lower respiratory tract is responsible for viral transmission (Richard et al., 2020). This would be in line with our finding that, while 3pRNA treatment efficiently reduces viral titres in the lung, minimal effects on viral shedding were observed and this indicates that the viral load in the nasal tissue but not the lung compartment affects viral shedding.

Other studies to date have examined the impact of i.n. administration of IFN-α on IAV infection in ferrets. For example, Kugel *et al.* reported that prophylactic IFN-α reduced virus titres in the upper airways and in nasal wash samples from ferrets infected with H1N1 A/USSR/90/77 and repeated treatments substantially increased the protective effect (Kugel et al., 2009). However, while prophylactic i.n. IFN-α also reduced viral shedding from the upper airways at days 1 and 3 after A/Vietnam/1203/2004 (H5N1) infection it did not increase survival, leading the authors to propose that this treatment is more effective against seasonal viruses that primarily replicate in the upper respiratory tract and not against viruses that disseminate to the lung. The administration volume (300 µL) may also be key here and a larger volume or an aerosolised administration might be more effective in promoting delivery to the lung. Similar considerations are also relevant if we were to pursue i.n. administration of 3pRNA in ferrets further. Of interest, some studies in mice have reported that administration of liquids by the i.n. route can exacerbate IAV infections, which has important implications for drug delivery. In the 1940s, Taylor reported that i.n. instillation of different fluids (e.g. distilled water or saline) into an IAV-infected mouse increased virus titres in the lungs as well as mortality (Taylor, 1941). This was confirmed in a more recent study which showed that i.n. treatment of IAV-infected mice with saline during A/Victoria/3/75 (H3N2) infection enhanced weight loss and mortality and promoted lung pathology (Smee et al., 2012). In studies not presented in this thesis, we also assessed the impact of a smaller i.n. inoculum of 3pRNA (50 µL compared to 500 µL in **Figure 3.8**) delivered on multiple days to recipient animals

(days -1, 1, 3, 5 and 7 relative to co-housing with infected donors) but did not observe a significant reduction in virus titres in nasal wash samples over time (data not shown).

Intravenous (i.v.) administration of RIG-I agonists has been widely used to assess their effectiveness against IAV in mice, including in studies described in this thesis. Given that i.n. administration of 3pRNA afforded little protection against subsequent IAV infection in our first ferret study, we next assessed the effectiveness of i.v. RIG-I agonist administration. In a preliminary experiment, experimentally infected donor animals received i.v. 3pRNA at day 3 post-infection, resulting in significantly reduced viral titres in the lungs, but not in the nose, at day 5 post-infection (**Figure 3.9**). Given these encouraging results, we focused on developing assays to examine ISG induction in response to i.v. 3pRNA in PBMCs and in lungs and nasal tissues. These studies confirmed that 24 hrs after i.v. 3pRNA treatment ISGs (particularly Mx1) were upregulated in PBMCs and lungs, but not in nasal tissue (**Figure 3.11**). In the final experiments in this chapter, recipient ferrets were treated via i.v. route with 3pRNA or ctrl RNA 24 hrs prior to exposure to H1N1pdm09-infected donor ferrets (**Figure 3.12 A**). In a first experiment, daily nasal washes were performed before animals were euthanised and analysed at day 6 post-treatment (day 5 after co-housing commenced). In the repeat experiment (marked with "#"), PBMCs were isolated before and after 3pRNA treatment to confirm induction of ISGs, which was significant for Mx1 and OAS1 but not for ISG15 (**Figure 3.12 B**). As for i.n. treatment, i.v. 3pRNA did not block onward transmission of IAV from donor animals to any of the naïve recipient ferrets. However, 3pRNA treatment resulted in significantly reduced virus shedding over time in nasal wash samples (**Figure 3.12 C**), but not in nasal cavities (**Figure 3.12 D**), and lung virus titres were significantly reduced in 6/8 3pRNA-treated animals (**Figure 3.12 E and F**). While we observed strong inhibition of virus growth in the lungs of 6/8 animals, no significant protection was observed in the remaining 2 animals.

Analysis of ISG induction in PBMCs confirmed that virus 'breakthrough' seen in R6 # (i.e. no difference in lung virus titres between this 3pRNA-treated animal

and ctrl RNA-treated animals) correlated with the lowest levels of all three ISGs at 24 hrs post-treatment. Note that PBMCs from animal R2, which showed also no difference in virus titres compared to ctrl RNA-treated lungs, were not collected and not analysed. Thus, it is possible that differences in the effectiveness of i.v. delivery, and hence the initial treatment dose of 3pRNA, might differ between animals. It is also possible that the responses elicited to 3pRNA may wane over time and this would be impacted by the initial dose delivered. It may be that once 3pRNA induced effects fall below a critical threshold the virus replication can 'bounce back' effectively. Considering that virus titres are assessed 6 days after a single i.v. treatment with 3pRNA it is quite remarkable that reduced lung virus titres were recorded in 6/8 animals. It is also important to consider that ferrets are outbred animals and it is possible that ferrets which did not respond to 3pRNA treatment exhibit specific mutations that diminish RIG-I signaling and/or expression of RIG-I-induced antiviral effector proteins. For example, single-nucleotide polymorphisms (SNPs) in *DDX58* and *IFIH1*, the encoding genes for RIG-I and MDA5, respectively, have been described as gain-of-function mutations associated with autoimmune and inflammatory diseases such as Singleton-Merten syndrome and Aicardi-Goutières syndrome (Kasumba et al., 2019). One study described loss-of-function mutations of RIG-I in human, however these mutations were associated with resistance to type I diabetes and to date no studies have described enhanced susceptibility to infection (Shigemoto et al., 2009).

Overall, our studies in mice and ferrets confirm that a single i.v. 3pRNA treatment induces potent protection against subsequent IAV challenge, particularly in terms of reducing virus replication in the lungs.

4 Chapter: Evaluation of RIG-I agonists as antiviral in different models of RSV infection

4.1 Introduction

RSV is one of the most important causes of respiratory disease worldwide, especially for children within their first 2 years of life. RSV is the most frequent causative agent of paediatric bronchiolitis and pneumonia and can result in acute lower respiratory infection (Piedimonte et al., 2014). While reducing the impact of RSV infection of the lower airways is particularly important, treatment options are limited and supportive care remains the mainstay of treatment.

Airway epithelial cells are the primary targets of human RSV infection, but immune cells such as alveolar macrophages (AMs) and DCs are also susceptible to RSV (Sarmiento et al., 2002; Guerrero-Plata et al., 2006; Johnson et al., 2011). As discussed in previous chapters, viral nucleic acids are recognised by intracellular PRRs such as TLRs, RLRs and NLRs (Kell et al., 2015). RSV is detected by several different PRRs although the relative importance of each receptor is still a matter of debate (Marr et al., 2013). RLRs such as RIG-I and MDA5 have both been implicated in recognition of RSV (Liu et al., 2007; Bhoj et al., 2008; Loo et al., 2008; Gitlin et al., 2010; Grandvaux et al., 2014). Viral sensing by RIG-I and/or MDA5 triggers an intracellular signaling cascade to activate transcription factors IRF3, IRF7 and NF-κB, which ultimately induces transcription of type I and type III IFNs. Secreted IFNs induce expression of hundreds of ISGs, resulting in an ‘antiviral state’ in virus-infected and uninfected neighbouring cells (Schoggins et al., 2011b).

In this chapter, we aimed to use synthetic agonists to target the RIG-I signaling pathway *in vitro* in cell lines from humans, mice and ferrets and *in vivo* using mice and ferrets, and to examine the impacts of this treatment on RSV infections. Prophylactic and therapeutic treatments using RIG-I agonists have shown promising results as antiviral agents against a number of viruses, including influenza A viruses (Ranjan et al., 2010; Goulet et al., 2013; Chiang et al., 2015; Coch et al., 2017). However, their effectiveness against other human respiratory viruses such as RSV is not clear. Herein, we use *in vitro* approaches to demonstrate that prophylactic treatment of airway cells from different species (human, mice and ferret) with a RIG-I agonist resulted in reduced susceptibility

to subsequent RSV infection and in decreased virus growth. We also used primary murine fibroblasts to define the importance of transcription factors IRF3/7 and a functional IFNAR for RIG-I-mediated protection against RSV. Furthermore, we assessed the impact of a single prophylactic treatment with RIG-I agonist in mouse and ferret models of human RSV infection. Our findings confirm that a single i.v. injection of RIG-I agonist induced potent protection of the lower, but not the upper respiratory tract, in both mice and ferrets. Together, these *in vitro* and *in vivo* studies extend studies from the previous results chapter to highlight the potential of RIG-I agonists as an effective antiviral prophylactic treatment against additional respiratory viruses, including RSV.

4.2 Results

4.2.1 RIG-I agonist treatment before, but not after, inoculation with RSV inhibits virus infection and growth in A549 cells

Previous studies using human A549 airway epithelial cells demonstrated that RIG-I agonists act as broad-spectrum antiviral agents against a range of viruses, including IAV, chikungunya virus, VSV, DENV, vaccinia virus and HIV-1 (Chakravarthy et al., 2010; Ranjan et al., 2010; Goulet et al., 2013; Olagnier et al., 2014; Chiang et al., 2015; Coch et al., 2017). However, their ability to limit virus infection in cells from other mammalian species, including mice and ferrets, is less clear. Moreover, it is not known if RIG-I agonists are protective against RSV in cells from humans or other species. Therefore, human A549 cells were transfected with 3pRNA or ctrl RNA (200 ng/mL), cultured for 24 hrs and then inoculated with RSV (MOI = 1) for 1 hr at 37^{o}C. After washing, cells were incubated an additional 17 hrs and stained for expression of RSV F protein at the cell surface by flow cytometry. Prophylactic treatment with 3pRNA resulted in a significant reduction in the percent of RSV-infected cells compared to ctrl RNA-treated cells (**Figure 4.1 A**) using two different strains of RSV (Long and A2). To determine if 3pRNA treatment also impacted virus growth, A549 cells treated with 3pRNA or ctrl RNA were infected 24 hrs later with a low inoculum dose

(MOI = 0.01) to allow for multiple cycles of viral replication. As newly-formed RSV virions often remain associated with host cells (Cifuentes-Muñoz et al., 2018), we harvested total virus (i.e. virus in culture supernatant as well as cell-associated virus) by snap-freezing tissue culture plates. After thawing, titres of infectious virus in clarified supernatants were determined by standard VS assay (Chan et al., 2017). As seen in **Figure 4.1 B**, pre-treatment with 3pRNA resulted in significantly reduced virus titres compared to ctrl RNA-treated cells, which supported high virus titres at 24-72 hpi.

To assess the therapeutic potential of RIG-I agonists against RSV infection, A549 cells were inoculated with RSV Long (MOI = 1), then treated with 3pRNA or ctrl RNA (200 ng/mL) either 1 hr or 3 hrs after virus inoculation. Flow cytometry was then performed at 18 hpi to detect cells expressing RSV F protein, as described above. Therapeutic treatment of cells with 3pRNA did not reduce the percentage of infected cells when compared to ctrl RNA-treated cells, irrespective of whether treatment occurred at 1 hr or 3 hrs after virus inoculation (**Figure 4.1 C**). As expected, pre-treatment of A549 cells with RIG-I agonist resulted in a marked reduction in the percent of RSV-infected cells.

To assess if RIG-I agonist has therapeutic potential to prevent RSV spread, A549 cells were inoculated with a low inoculum dose of RSV (MOI = 0.1) and then treated with 3pRNA or ctrl RNA at 24 hrs post-infection. After an additional 17 hrs (i.e. at 41 hpi), cells were harvested and stained for RSV F protein. In this experimental approach, therapeutic 3pRNA treatment did not reduce the percentage of RSV-infected cells compared to ctrl RNA-treated cells (**Figure 4.1 D**), indicating that 3pRNA treatment did not inhibit RSV spread in the culture, at least under the experimental conditions described.

To confirm that the antiviral activity of 3pRNA against RSV was mediated via RIG-I receptor signaling, two clones of RIG-I knockout (KO) A549 cells (a kind gift from Dr. Ann Kristin Bruder, University of Bonn, Bonn, Germany) were treated with 3pRNA or ctrl RNA prior to infection with RSV Long or A2. Flow cytometry confirmed that 3pRNA treatment of A549 RIG-I KO #2 did not reduce the percent of RSV-infected cells at 18 hpi although a modest, but significant reduction in

infected cells was observed using the A2, but not the Long strain of RSV using A549 RIG-I KO #1 (**Figure 4.1 E**). It was surprising to see that despite the RIG-I KO genotype, 3pRNA treatment resulted in a small inhibitory effect in A549 RIG-I KO #1. It is unclear why 3pRNA had some effects in A549 RIG-I KO #1 but not in A549 RIG-I KO #2. In general it is known that during the in vitro synthesis of 3pRNAs other side product such as simulators of TLR signalling could be generated which possess possible stimulatory functions. Despite this discrepancy it is still obvious that the protective effects induced by 3pRNA treatment were clearly diminished in both RIG-I KO clones when compared to WT cells and clearly, 3pRNA treatment of A549 RIG-I KO cells did not result in potent inhibition of RSV growth over time (**Figure 4.1 F**). These experiments confirm the critical role of RIG-I in 3pRNA-mediated protection of A549 cells against subsequent RSV infection.

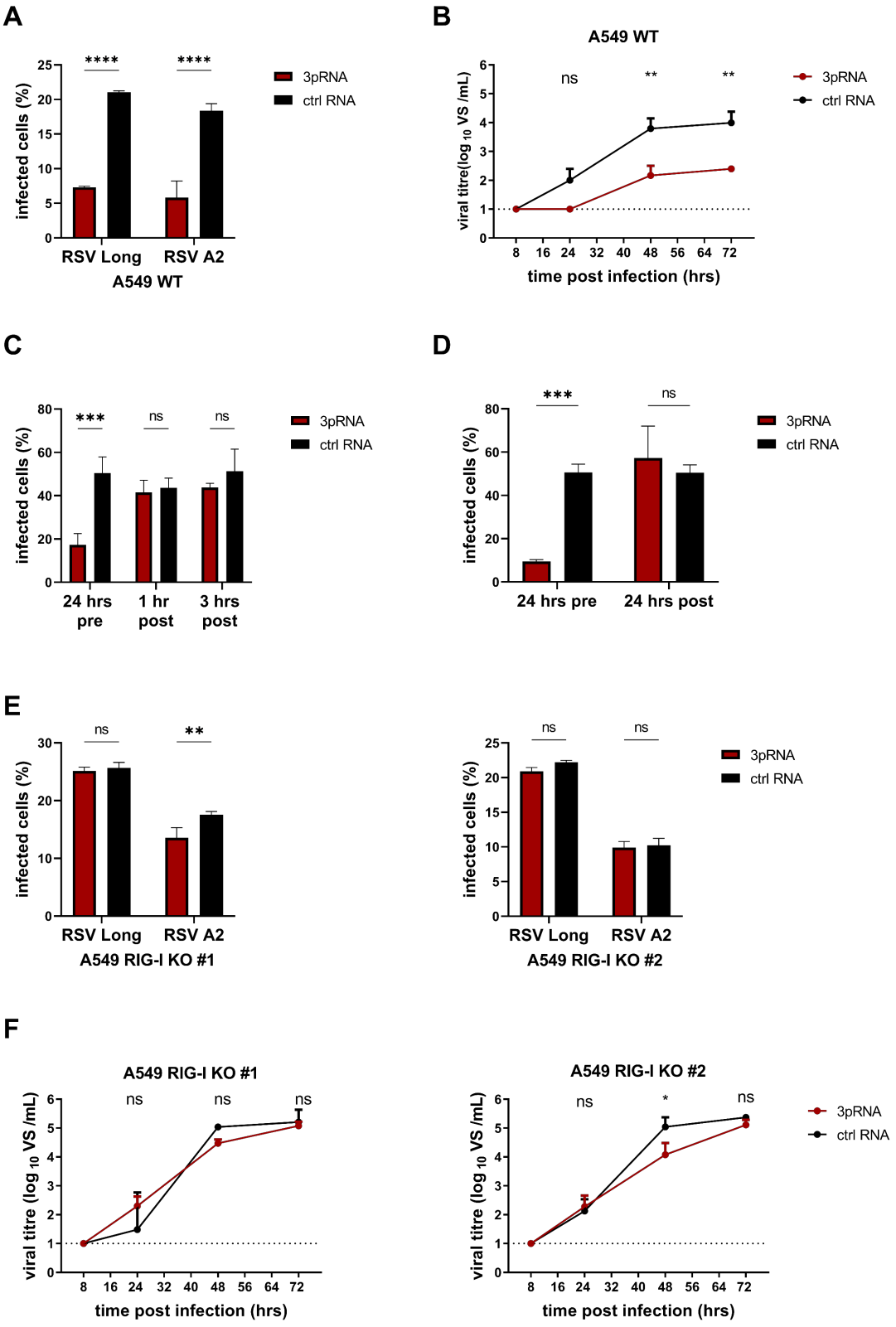
A
infected cells (%)
****
****
3pRNA
ctrl RNA
RSV Long
RSV A2
A549 WT
B
A549 WT
viral titre(log 10 VS /mL)
ns
**
**
3pRNA
ctrl RNA
time post infection (hrs)
C
infected cells (%)
***
ns
ns
3pRNA
ctrl RNA
24 hrs pre
1 hr post
3 hrs post
D
infected cells (%)
***
ns
3pRNA
ctrl RNA
24 hrs pre
24 hrs post
E
infected cells (%)
ns
**
RSV Long
RSV A2
A549 RIG-I KO #1
infected cells (%)
ns
ns
3pRNA
ctrl RNA
RSV Long
RSV A2
A549 RIG-I KO #2
F
A549 RIG-I KO #1
viral titre (log 10 VS /mL)
ns
ns
ns
time post infection (hrs)
A549 RIG-I KO #2
viral titre (log 10 VS /mL)
ns
*
ns
3pRNA
ctrl RNA
time post infection (hrs)

Figure 4.1: Treatment of human airway epithelial A549 cells with RIG-I agonists inhibits RSV infection and replication. A549 cells were transfected with RIG-I agonist (3pRNA, 200 ng/mL) or control RNA (ctrl RNA, 200 ng/mL). **A)** After 24 hrs, A549 WT cells were inoculated for 1 hr at 37°C with RSV Long or RSV A2 (MOI = 1), washed and incubated an additional 17 hrs before cells were fixed and stained for cell surface expression of the viral RSV F protein. Cells were analysed by flow cytometry. **B)** After 24 hrs, A549 WT cells were inoculated for 1 hr with RSV Long (MOI = 0.01), washed and incubated at 37°C. After 8 hrs, 24 hrs, 48 hrs or 72 hrs, tissue culture plates were snap-frozen, then thawed and titres of infectious virus were determined in clarified supernatants using a VS assay on HEp-2 cells. The dashed line represents the limit of detection. **C)** Transfection was performed 24 hrs prior (24 hrs pre) or either 1 hr or 3 hrs after (1 hr post/ 3 hrs post) infection with RSV Long (MOI = 1) as above. Cells were fixed and stained for cell-surface RSV F protein at 18 hpi and analysed by flow cytometry. **D)** Transfection was performed either 24 hrs prior (24 hrs pre) or 24 hrs after (24 hrs post) infection with RSV Long (MOI = 0.1). Cells were fixed and stained for cell-surface RSV F protein at 18 hpi and analysed by flow cytometry. **E)** A549 RIG-I KO cells (clone #1 and clone #2) inoculated with RSV Long (MOI = 1) were fixed and stained for cell-surface surface RSV F protein at 18 hpi and analysed by flow cytometry. **F)** A549 RIG-I KO cells (clone #1 and clone #2) were inoculated with RSV Long (MOI = 0.01) for 1 hr, washed and incubated at 37°C. After 8 hrs, 24 hrs, 48 hrs or 72 hrs, tissue culture plates were snap-frozen, then thawed and titres of infectious virus were determined in clarified supernatants using a VS assay on HEp-2 cells. The dashed line represents the limit of detection. Data from all represent the mean (± SD) from triplicate samples and are representative of 2 independent experiments. An unpaired Student's *t*-test was performed to compare 3pRNA and ctrl RNA treatment for each time point in B) and F). A two-way ANOVA with Bonferroni's correction was performed to compare 3pRNA and ctrl RNA treatment in A), C), D) and E). * = $p<0.05$; ** = $p<0.01$; *** = $p<0.001$; **** = $p<0.0001$; ns = not significant.

4.2.2 RIG-I agonist pre-treatment of mouse LA-4 airway epithelial cells results in RIG-I-dependent inhibition of RSV

Next, we assessed the impact of RIG-I agonist treatment on RSV infection of murine cells. First, a mouse epithelial lung adenoma cell line (LA-4) was transfected with 3pRNA or ctrl RNA (200 ng/mL), followed by RSV infection (MOI = 1) 24 hrs later and the percentage of RSV-infected cells was determined at 18 hpi by flow cytometry. In these studies we used recombinant RSV Long and A2 viruses expressing green-fluorescent protein (GFP), as described in Materials and Methods. Prophylactic treatment with 3pRNA resulted in significant reductions in the proportion of RSV-infected cells for both strains (**Figure 4.2 A**). To determine if prophylactic 3pRNA treatment also inhibited RSV growth, LA-4 wells were treated with 3pRNA or ctrl RNA and then 24 hrs later infected with RSV (MOI = 0.01). After washing, total virus was harvested by snap-freezing tissue culture plates and, after thawing, virus titres in clarified supernatants were determined by VS assay. Pre-treatment of LA-4 cells with 3pRNA completely abolished growth of infectious RSV, whereas ctrl RNA-treated cells supported virus growth at 24-72 hpi (**Figure 4.2 E**).

To gain insight regarding the role of RIG-I agonist-induced type I IFN signaling, LA-4 cells were treated with 3pRNA or ctrl RNA and cell supernatants harvested 24 hrs later were analysed for IFN-α by ELISA. In these studies, 3pRNA but not ctrl RNA treatment resulted in high levels of IFN-α secretion (**Figure 4.2 B**). Next, we attempted to generate RIG-I knockout cells using CRISPR/Cas9, however this approach was unsuccessful. LA-4 cells showed extremely poor survival rates after electroporation with Cas9-plasmids and cell sorting. Further investigation revealed that LA-4 cells are reported to possess an unstable and polyploid karyotype (ATCC, 2021), and possess up to 256 chromosomes and not the 40 chromosomes which is considered to be normal in mice (Hernandez et al., 1999). To successfully generate CRISPR/Cas9 KO cells it would be necessary to disrupt the target sequence in all of the several alleles present in these cells.

As an alternative, we next generated a lentiviral pLKO.1 vector for expression of shRNAs targeting RIG-I mRNA expression. This vector also expresses a

puromycin resistance gene to allow for selection of lentiviral-transduced cells with stable shRNA expression. Two pLKO.1 vectors with distinct targets in RIG-I (RIG-I shRNA 1 and RIG-I shRNA 2) were included in our experiments. LA-4 cells were also transduced with shRNA ctrl, a control vector containing a non-hairpin insert, to generate an appropriate control cell line. Stably transfected cell lines were then generated by culture in the presence of puromycin.

To assess if knockdown and control cell lines induce ISGs upon 3pRNA stimulation, we treated cells with 3pRNA or ctrl RNA and assessed ISG15 expression 6 hrs later by qRT-PCR. Treatment with 3pRNA induced potent upregulation of ISG15 in LA-4 shRNA ctrl cells, however little was induced in the LA-4 RIG-I shRNA 1 and RIG-I shRNA 2 cells, indicating that RIG-I knockdown was successful (**Figure 4.2 C**). For infection experiments, cell lines were then treated with 3pRNA or ctrl RNA prior to infection with RSV Long (MOI = 2) and the percentage of RSV-infected cells was determined by flow cytometry (**Figure 4.2 D**). 3pRNA treatment potently reduced the percentage of RSV-infected LA-4 shRNA ctrl cells, whereas this effect was less pronounced, but still significant in LA-4 RIG-I shRNA 1 cells. However, the other knockdown cell line (LA-4 pLKO.1 shRNA RIG-I 2) showed reduced susceptibility to RSV infection and this was not significantly different following 3pRNA or ctrl RNA treatment (**Figure 4.2 D**). Given differences in the percent of RSV infection between knockdown cell lines, we also determined the fold reduction of RSV-infected cells following 3pRNA treatment in each cell line. Compared to ctrl RNA-treated cells, 3pRNA treatment resulted in a ~5-fold reduction in LA-4 shRNA ctrl control cells, a ~1.5-fold reduction in LA-4 RIG-I shRNA 1 cells and a ~1.7-fold reduction in LA-4 RIG-I shRNA 2 cells. These results indicate that when assessing the effect of 3pRNA pre-treatment on subsequent RSV infection, the impact of shRNA knockdown of RIG-I in LA-4 cells is not as pronounced as following CRISPR/Cas9 knockout in A549 cells. Moreover, our results imply that RIG-I knockdown might be more effective in LA-4 RIG-I shRNA 1 compared to LA-4 RIG-I shRNA 2 cells. Taken together, our results indicate that 3pRNA treatment inhibits RSV infection and growth in LA-4 cells and that RIG-I knockdown reduces the potency of inhibition.

4.2.3 RIG-I agonist pre-treatment of primary mouse lung fibroblast results in IFN-dependent inhibition of RSV

As little is known regarding mechanism of RIG-I agonist-mediated inhibition of RSV, particularly in mice, we isolated and cultured fibroblasts derived from the lungs of mouse strains which differ in their ability to express particular host factors relevant to RNA virus infection. First, we isolated fibroblasts from mice which lacked transcription factors IRF3/7 (IRF3/7$^{-/-}$) or the type I IFN receptor 2 (IFNAR2$^{-/-}$) and compared them to fibroblasts from WT-B6 animals. Cells pre-treated with 3pRNA or ctrl RNA (200 ng/mL) were infected 24 hrs later with RSV Long (MOI = 1) and the percentage of virus-infected cells was determined (**Figure 4.2 F**). Compared to ctrl RNA-treatment, 3pRNA treatment of cells from WT animals resulted in a ~3-fold reduction in the percentage of RSV-infected cells (i.e. from 29.3 ± 10.7 % SD to 10.9 % ± 2.0 SD). Interestingly, ctrl RNA-treated cells from IRF3/7$^{-/-}$ and IFNAR2$^{-/-}$ animals were markedly more susceptible to RSV infection compared to WT cells, highlighting the importance of intact IRF3/7 and IFN signaling pathways against RSV in mouse cells. Moreover, 3pRNA treatment of IFNAR2$^{-/-}$ cells was not associated with reduced RSV infection and 3pRNA-treatment of IRF3/7$^{-/-}$ cells resulted in a modest reduction in RSV infection, however this was not significant (**Figure 4.2 F**). Thus, these data confirm the critical role of type I IFN signaling pathways in RIG-I agonist-mediated protection against RSV in mouse cells.

In Chapter 3 we used fibroblasts from B6.A2G-*Mx1* and B6-WT mice which do, and do not, express functional Mx1 proteins (Haller et al., 2015) to demonstrate that following pre-treatment with 3pRNA, expression of a functional Mx1 protein was required for potent and long-lasting protection against IAV. In contrast, there are no studies to date which report an antiviral function of Mx1 proteins against RSV. To determine if Mx1 might modulate 3pRNA-mediated inhibition of RSV, we pre-treated mouse lung fibroblasts from B6.A2G-*Mx1* and B6-WT mice with 3pRNA or ctrl RNA (200 ng/mL) and, 24 hrs later, infected them with RSV. As seen in **Figure 4.2 G**, 3pRNA treatment resulted in a modest but significant reduction in the percentage of RSV-infected B6-WT cells at 18 hpi. Surprisingly,

fibroblasts from B6.A2G-*Mx1* mice showed higher levels of RSV-infected cells after ctrl RNA treatment and infection levels were potently reduced by 3pRNA treatment (**Figure 4.2 G**). Despite differences in the percent of infected cells between mouse strains following ctrl RNA treatment, it was clear that 3pRNA treatment was particularly potent in inhibiting RSV infection of cells from B6.A2G-*Mx1* mice suggesting that expression of a functional Mx1 protein might exert direct or indirect antiviral effects against RSV in primary mouse fibroblasts.

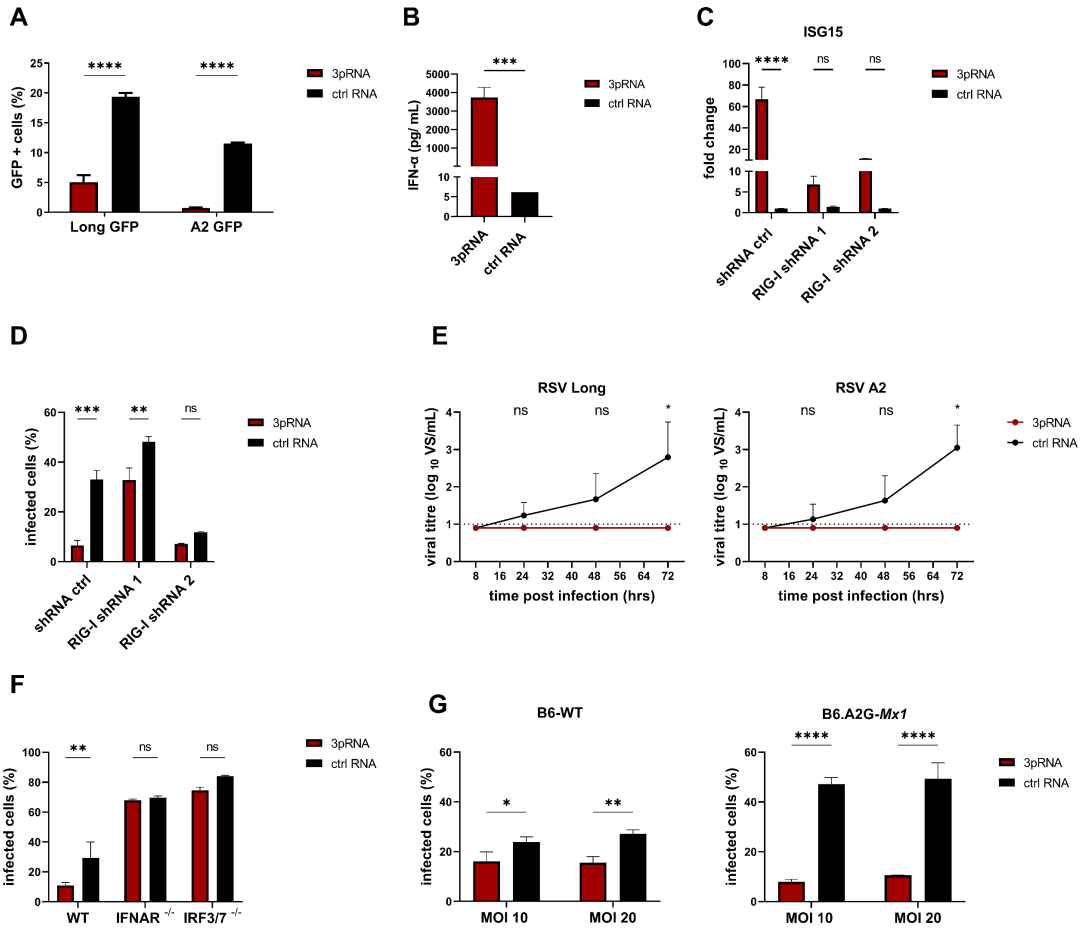

Figure 4.2: Treatment of a mouse airway epithelial (LA-4) cell line or primary mouse lung fibroblasts with RIG-I agonists inhibits RSV infection in an IFN-dependent manner. Cells were transfected with RIG-I agonist (3pRNA, 200 ng/mL) or control RNA (ctrl RNA, 200 ng/mL) and cultured for 24 hrs. **A)** LA-4 cells were then infected with RSV Long-GFP or A2-GFP (MOI = 1), fixed at 18 hpi and analysed by flow cytometry. **B)** LA-4 cell culture supernatants harvested 24 hrs after transfection were assessed for IFN-α by ELISA (pg/mL). **C)** After 6 hrs, total RNA was isolated from LA-4 control (shRNA ctrl) or LA-4 RIG-I knockdown cells (RIG-I shRNA 1 and RIG-I shRNA 2) and the expression of ISG15 was assessed by qRT-PCR. Levels were normalised to GAPDH and expressed relative to untreated cells. **D)** LA-4 control (shRNA ctrl) or LA-4 RIG-I knockdown cells (RIG-I shRNA 1 and RIG-I shRNA 2) were then infected with RSV Long (MOI = 2) and cells were fixed and stained for intracellular expression of the RSV NP at 18 hpi. Cells were analysed by flow cytometry. **E)** LA-4 cells were then infected with RSV Long (MOI = 0.01), washed and incubated at 37°C. At various time points, tissue culture plates were snap-frozen, then thawed and titres of infectious virus were determined in clarified supernatants using a VS on HEp-2 cells. The dashed line represents the limit of detection. Samples below the detection limit (<1 $\log_{10}$ VS/mL) were assigned values of 0.9 $\log_{10}$ VS/mL for statistical analysis. **F)** Primary lung fibroblasts from C57BL/6 (WT),

IRF3/7-deficient (IRF3/7$^{-/-}$) or IFNAR2-deficient (IFNAR2$^{-/-}$) mice were then infected with RSV Long (MOI = 10) and cells were fixed and stained for intracellular expression of the RSV NP at 18 hpi. Cells were analysed by flow cytometry. **G)** Primary lung fibroblasts from B6-WT or B6.A2G-*Mx1* mice were then infected with RSV Long (MOI = 10 or 20, as indicated) and cells were fixed and stained for intracellular expression of the RSV NP at 18 hpi. Cells were analysed by flow cytometry. Data from all represent the mean (± SD) from triplicate samples and are representative of 2 independent experiments except for D), where one experiment was performed. An unpaired Student's *t*-test was performed to compare 3pRNA and ctrl RNA treatment in B) and for each time point in E). A two-way ANOVA with Bonferroni's correction was performed to compare 3pRNA and ctrl RNA treatment in A), C), D), F) and G). * = $p<0.05$; ** = $p<0.01$; *** = $p<0.001$; **** = $p<0.0001$; ns = not significant.

4.2.4 A single prophylactic treatment of mice with 3pRNA results in potent inhibition of RSV replication in the lung

The impact of a single prophylactic treatment of RIG-I agonist on subsequent RSV infection of mice was assessed using a Bioluminescence imaging system. Here, we used an engineered RSV Long virus expressing a Renilla firefly luciferase between its P and M gene (Rameix-Welti et al., 2014). The firefly luciferase enzyme oxidises the D-luciferin substrate in the presence of Mg-ATP and O_2 to oxyluciferin, a process which leads to photon emission (Ji et al., 2020). Using this approach, RSV infection can be detected and quantified over the course of infection without the need to euthanise animals as is normally required to determine virus titres in the respiratory tract. BALB/c mice have been reported to display an increased susceptibility to RSV compared to C57BL/6 mice (Prince et al., 1979). Moreover, BALB/c mice exhibit no pigment in fur or skin and therefore show enhanced sensitivity to bioluminescence detection, as well as reduced nonspecific photon adsorption (Stabenow et al., 2010).

BALB/c mice received a single i.v. injection with 12.5 µg RIG-I agonist (3pRNA) or control RNA (ctrl RNA) and, 24 hrs later, were infected by the i.n. route with 10^5 infectious particles (determined by VS assay) of rHRSV-Luc in 50 µL of PBS. Bioluminescence was then measured at 3 and 5 days post infection (dpi). As seen in **Figure 4.3 A**, bioluminescence was detected in the respiratory tract of all animals from 3pRNA- and ctrl RNA-treated groups at both time points. Luciferase

activity was quantified as average radiance (photons/s/cm^2/sr) and compared between groups for nasal (upper respiratory tract) and lung (lower respiratory tract) regions (**Figure 4.3 B**). Compared to ctrl RNA, 3pRNA treatment did not reduce luciferase activity in the upper respiratory tract at either 3 or 5 dpi. However, luciferase activity in the lungs was significantly reduced after 3pRNA treatment at both 3 and 5 dpi. Mice were euthanised and tissues from the upper and lower respiratory tract were assessed at 5 dpi for titres of infectious RSV. Consistent with bioimaging results, 3pRNA treatment significantly reduced the viral load in the lungs, and not in the nasal tissues (**Figure 4.3 C**). These data indicate that pre-treatment of mice with RIG-I agonist results in potent inhibition of RSV in the lung, but not in the nasal tissue.

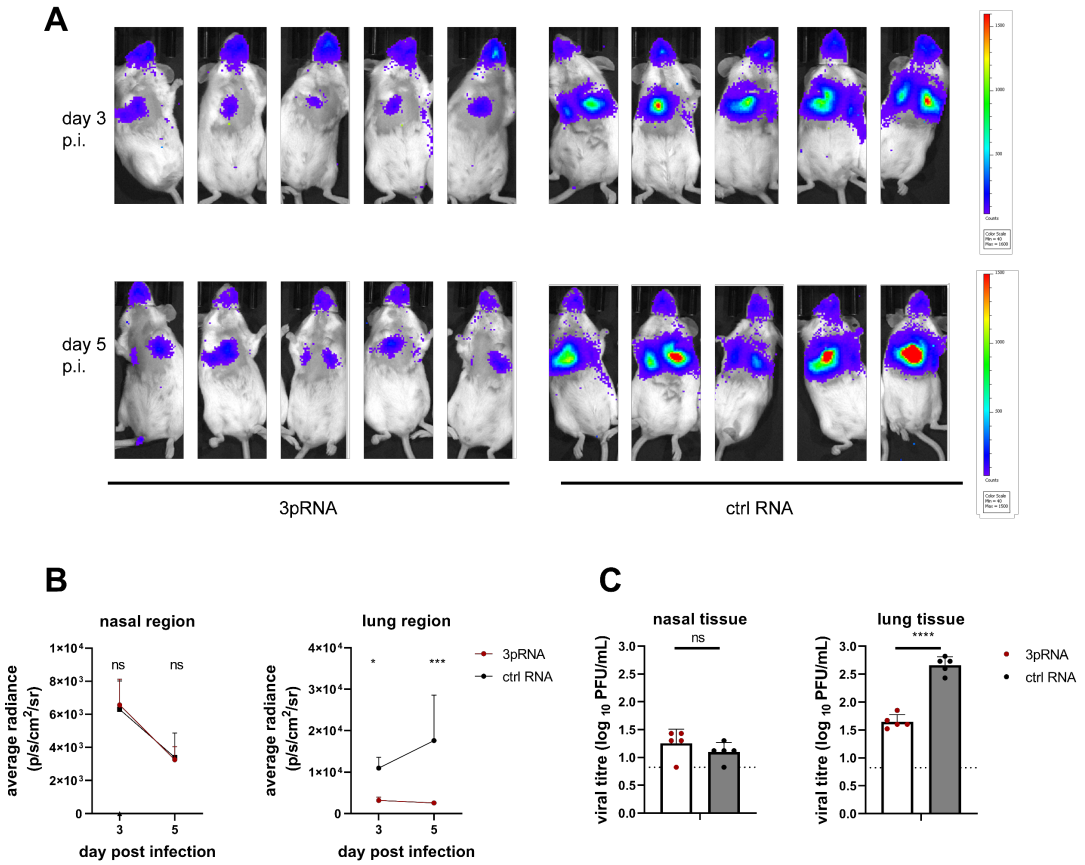

Figure 4.3: A single intravenous treatment of mice with RIG-I agonist results in reduced RSV growth in the lung, but not in the nasal tissues. BALB/c mice received a single i.v. injection with 12.5 µg RIG-I agonist (3pRNA) or control (ctrl) RNA and, 24 hrs later, were infected by the intranasal route with 10^5 infectious particles of rHRSV-Luc in 50 µL PBS. **A)** Bioluminescence was assessed following i.p. injection of 2 mg D-luciferin at 3 and 5 dpi using an IVIS imaging system. **B)** Bioluminescence of nasal and lung regions were quantified and defined as the average radiance per sum of the photons per second from each pixel inside the region of interest/number of pixels (p/s/cm^2/sr). **C)** At 5 dpi, nasal tissues and lungs were harvested, homogenised and virus titres in clarified homogenates were determined by plaque assay on HEp-2 cells. Results are expressed as mean ± SD (n = 5/group). Data are representative of 2 independent experiments. Dashed line represents the limit of detection for the plaque assay. Unpaired Student's *t*-test was performed to compare light emission in B) and viral titres of respiratory tissue in C) after 3pRNA or ctrl RNA treatment. * = $p<0.05$; *** = $p<0.001$; **** = $p<0.0001$; ns = not significant.

4.2.5 RIG-I agonist treatment of ferret airway cells inhibits RSV infection and growth

To assess the impact of RIG-I agonist treatment on a ferret airway cell line (FRL), cells transfected with 200 ng/mL RIG-I agonist (3pRNA) or control RNA (ctrl RNA) were subsequently infected with GFP-labelled RSV Long or A2 viruses, followed by flow cytometry at 18 hpi. As seen in **Figure 4.4 A**, pre-treatment with 3pRNA significantly and potently reduced the percentage of RSV-infected cells. Next, we assessed the impact of 3pRNA on RSV replication and growth in FRL cells. Following pre-treatment with 3pRNA or ctrl RNA, cells were infected 24 hrs later with a low MOI of 0.01 and samples were harvested at various time points by snap-freezing tissue culture plates to determine total virus titres (i.e. cell-associated plus released virus). While both RSV Long and A2 strains were able to replicate and grow in ctr RNA-treated FRL cells at 24-72 hpi, pre-treatment with 3pRNA completely abolished growth of either strain (**Figure 4.4 B**). These findings confirm FRL cells are susceptible to RSV infection and that this is potently inhibited by pre-treatment with 3pRNA.

To confirm the importance of RIG-I signaling for the anti-RSV activity of 3pRNA-treatment in ferret cells, we prepared RIG-I knockdown FRL cell lines. FRL cells were transfected with lentiviral pLKO.1 vectors expressing shRNAs targeting RIG-I mRNA (RIG-I shRNA 1 and RIG-I shRNA 2) or with a control plasmid containing a non-hairpin insert (shRNA ctrl, as used in **Figure 4.2** for mouse cell lines). To assess if knockdown and control cell lines induce ISGs upon 3pRNA stimulation, we treated cells with 3pRNA or ctrl RNA. We also treated cells with recombinant ferret IFN-α to confirm that type I IFN-signaling pathways were still intact in lentivirus transduced cells. qRT-PCR was used to assess ISG expression 6 hrs later.

Treatment with 3pRNA induced potent upregulation of ISG15 in FRL pLKO.1 control cells as expected however little was induced in RIG-I shRNA 1 or RIG-I shRNA 2 cells (**Figure 4.4 C**). Cells treated with ferret IFN-α induced potent ISG15 expression in all ferret cell lines, confirming that shRNA generation did not impact ISG induction following IFNAR stimulation. In human and mouse, CCL5

is induced by RIG-I agonist, but not IFN-α (Ohmori et al., 1997; Imaizumi et al., 2010). Similarly, we found that CCL5 was induced by 3pRNA, but not by ferret IFN-α, in ferret shRNA ctrl cells whereas minimal induction was observed in RIG-I shRNA 1 and RIG-I shRNA 2 cells (**Figure 4.4 C**).

Knockdown and control cell lines were then pre-treated with 3pRNA or ctrl RNA and, 24 hrs later, infected with RSV Long (MOI = 2) and the percentage of RSV-infected cells was determined at 18 hpi. As seen **Figure 4.4 D**, 3pRNA treatment significantly reduced the proportion of RSV-infected cells in FRL pLKO.1 control cells (53.2 ± 0.4 SD % to 7.6 ± 0.5 SD %), however its inhibitory effect was markedly reduced and relatively modest in FRL RIG-I shRNA 2 cells (63.9 ± 0.9 SD % to 55.6 ± 3.7 SD %). Notably, 3pRNA treatment of FRL RIG-I shRNA 1 resulted in a significant reduction in the percent of RSV-infected cells similar to those observed in FRL pLKO.1 control cells (36.6 ± 1.5 SD % to 2.6 ± 1.2 SD %). When repeating infection experiments after several cell passages, we observed increased protection after 3pRNA treatment in FRL RIG-I shRNA 1 and FRL RIG-I shRNA 2 cells (data not shown) which indicated that cells lost the lentiviral shRNA transgene expression during prolonged culture.

Generation of a stable FRL RIG-I KO cell line by CRISPR/Cas9 represents an alternative approach for future studies which may circumvent the issues described using shRNA knockdown.

Overall, these data show that pre-treatment of FRL cells with 3pRNA results in reduction in RSV infection of cells and indicate that this is RIG-I dependent.

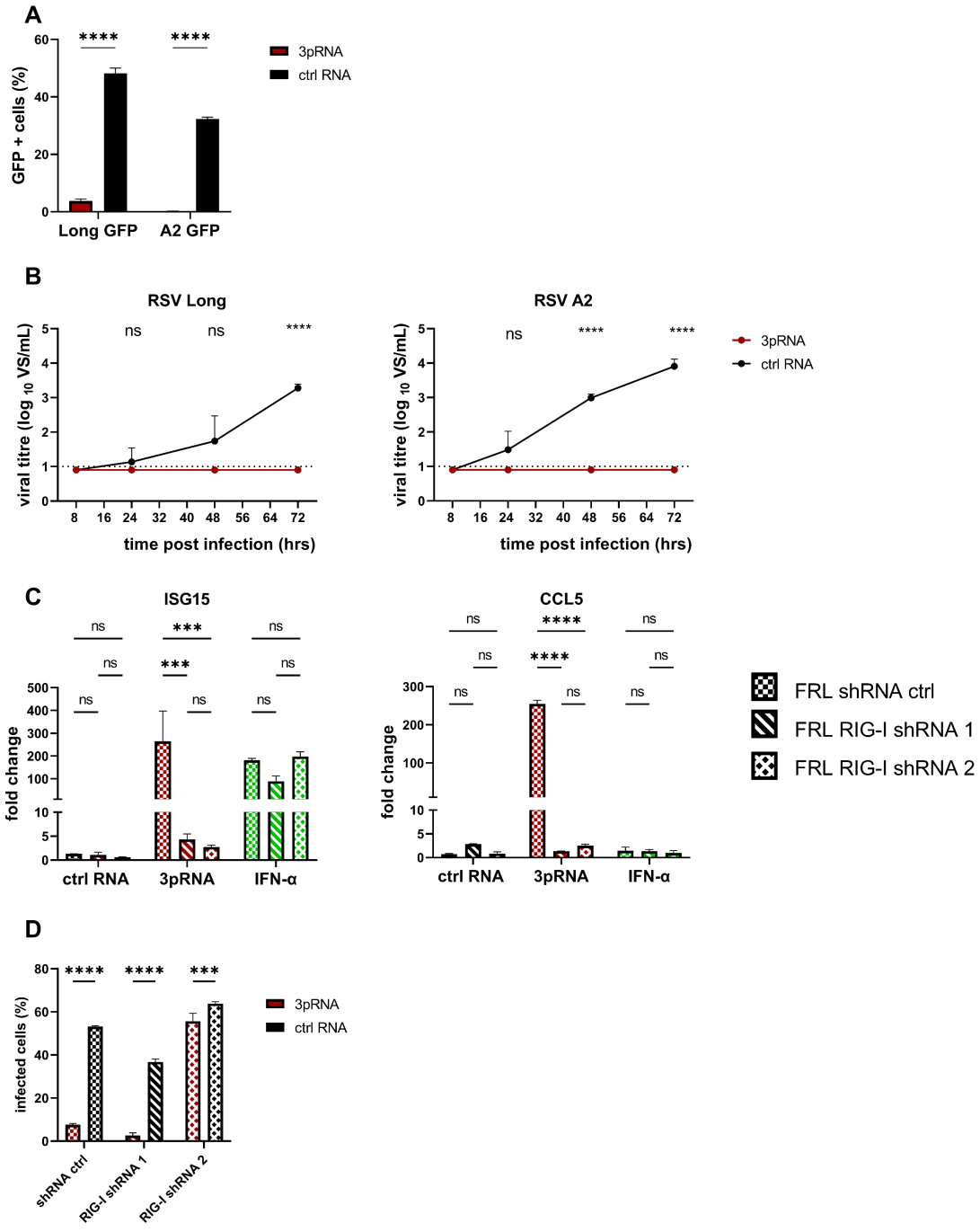

Figure 4.4: A single pre-treatment of a ferret airway cell line (FRL) with RIG-I agonist inhibits RSV infection and replication in a RIG-I-dependent manner. Cells were transfected with RIG-I agonist (3pRNA, 200 ng/mL) or control RNA (ctrl RNA, 200 ng/mL). **A)** After 24 hrs, cells were infected with RSV Long-GFP or A2-GFP (MOI = 1) and GFP-positive cells were analysed by flow cytometry at 18 hpi. **B)** After 24 hrs, cells were infected with RSV Long or A2 (MOI = 0.01), washed and incubated at 37°C. At various time points, tissue culture plates were snap-frozen, then thawed and titres of infectious virus were determined in clarified

supernatants using a VS assay on HEp-2 cells. The dashed line represents the limit of detection. Samples below the detection limit (<1 log_{10} VS/mL) were assigned values of 0.9 log_{10} VS/mL for statistical analysis. **C)** 24 hrs after stimulation of treatment with recombinant ferret IFN-α total RNA was isolated from FRL control (FRL shRNA ctrl) or RIG-I knockdown cells (FRL RIG-I shRNA 1, FRL RIG-I shRNA 2) and the expression of ISG15 and CCL5 was assessed by qRT-PCR. Levels were normalised to GAPDH and expressed relative to untreated cells. **D)** After 24 hrs, FRL control (shRNA ctrl) or RIG-I knockdown cells (RIG-I shRNA 1, RIG-I shRNA 2) were infected with RSV Long (MOI = 2). Cells were fixed and stained for surface expression of the RSV F protein at 18 hpi and analysed by flow cytometry. Data represent the mean (± SD) from triplicate samples and are representative of at least 2 independent experiments, except for C) where one experiment was performed. An unpaired Student's *t*-test was performed to compare 3pRNA and ctrl RNA treatment for each time point in B). A two-way ANOVA with Bonferroni's correction was performed to compare 3pRNA and ctrl RNA treatment in A), C) and D). * = p<0.05; ** = p<0.01; *** = p<0.001; **** = p<0.0001; ns = not significant.

4.2.6 A single prophylactic treatment of ferrets with 3pRNA inhibits RSV replication in the ferret airways

Inbred strains of mice are regarded as semi-permissive to infection with human RSV, requiring high doses of virus inoculum to establish infection and with relatively low virus titres recovered from the lungs (Openshaw, 2013). Recently, ferrets have been used to study human RSV infections and inoculation of ferrets with Long and A2 strains was associated with virus replication in the airways, induction of cytokines and chemokines as well as transmission to naïve animals (Chan et al., 2017). Given that ferrets are outbred, exhibit lung physiology more similar to that of humans and are susceptible to human RSV, we next assessed the *in vivo* effectiveness of a single prophylactic 3pRNA treatment against subsequent RSV infection in ferrets. As studies from our laboratory have indicated that transmission of RSV from experimentally infected donor to naïve recipient animals is not 100 % effective (Chan et al., 2017), we relied on direct experimental infection of ferrets to determine if 3pRNA pre-treatment provides protection against subsequent RSV challenge.

Ferrets received a single, i.v. injection of 3pRNA or ctrl RNA (0.3 mg/kg, n = 4/group) and, 24 hrs later, were inoculated with $5x10^5$ VS of RSV Long in a

volume of 500 µL. Whole blood was collected from each animal prior to, as well as 24 hrs after, 3pRNA or ctrl RNA treatment to allow for isolation of PBMCs such that PBMC RNA could be assessed for ISG induction. Animals were assessed daily for weight and temperature, daily nasal wash samples were collected and at day 3 post-infection, animals were euthanised for collection of lung and nasal tissues. The experimental overview is shown in **Figure 4.5 A**. After isolation of RNA, qRT-PCR confirmed that treatment with 3pRNA resulted in significant upregulation of different ISGs (**Figure 4.5 B**), including Mx1, ISG15 and OAS1, in PBMCs 24 hrs after administration. These results confirm those reported in the previous chapter examining the ability of RIG-I agonist treatment to modulate IAV infection in ferrets. Next, we assessed titres of infectious virus in nasal wash samples, confirming that infectious RSV was detected in samples from all animals at one or more of the sampling time points. To compare the viral load in nasal wash samples from 3pRNA- and ctrl RNA-treated animals, an area under the curve (AUC) analysis was performed across all days sampled (**Figure 4.5 C**). AUC analysis indicated no significant difference in nasal wash samples following 3pRNA treatment (p= 0.2, 3pRNA: 4.794 ± 1.055 SD versus ctrl RNA: 5.903 ± 0.951 SD). Nasal tissue was also removed and homogenised at 3 dpi and virus titres determined. End-point analysis confirmed infectious virus in the nasal cavities of all animals with no significant differences noted between 3pRNA- and ctrl RNA-treated animals (p = 0.87) (**Figure 4.5 D**). Finally, we determined titres of infectious RSV in individual lung lobes from each animal. For 3pRNA-treated ferrets, no virus was detected in any of the lung lobes of 3/4 animals (animals 1-3), while low titres of infectious virus were recovered from 1/5 lung lobes from animal 4 (**Figure 4.5 E**). Virus titres in lung lobes from 3pRNA-treated animals were significantly reduced when compared to pooled titres of all lung lobes from ctrl RNA-treated animals (p = 0.033 for animals 1, 2 and 3) except for animal 4, which had one lung lobe with infectious virus (p = 0.1034). However, in ctrl RNA-treated animals virus was recovered in 13/20 lung lobes, with all ctrl RNA-treated animals showing at least 3/5 lung lobes with detectable virus titres.

Together, these data confirm that intravenous 3pRNA administration induces a systemic ISG response and that this correlates with potent inhibition of RSV replication in the lung, but not in the upper airways.

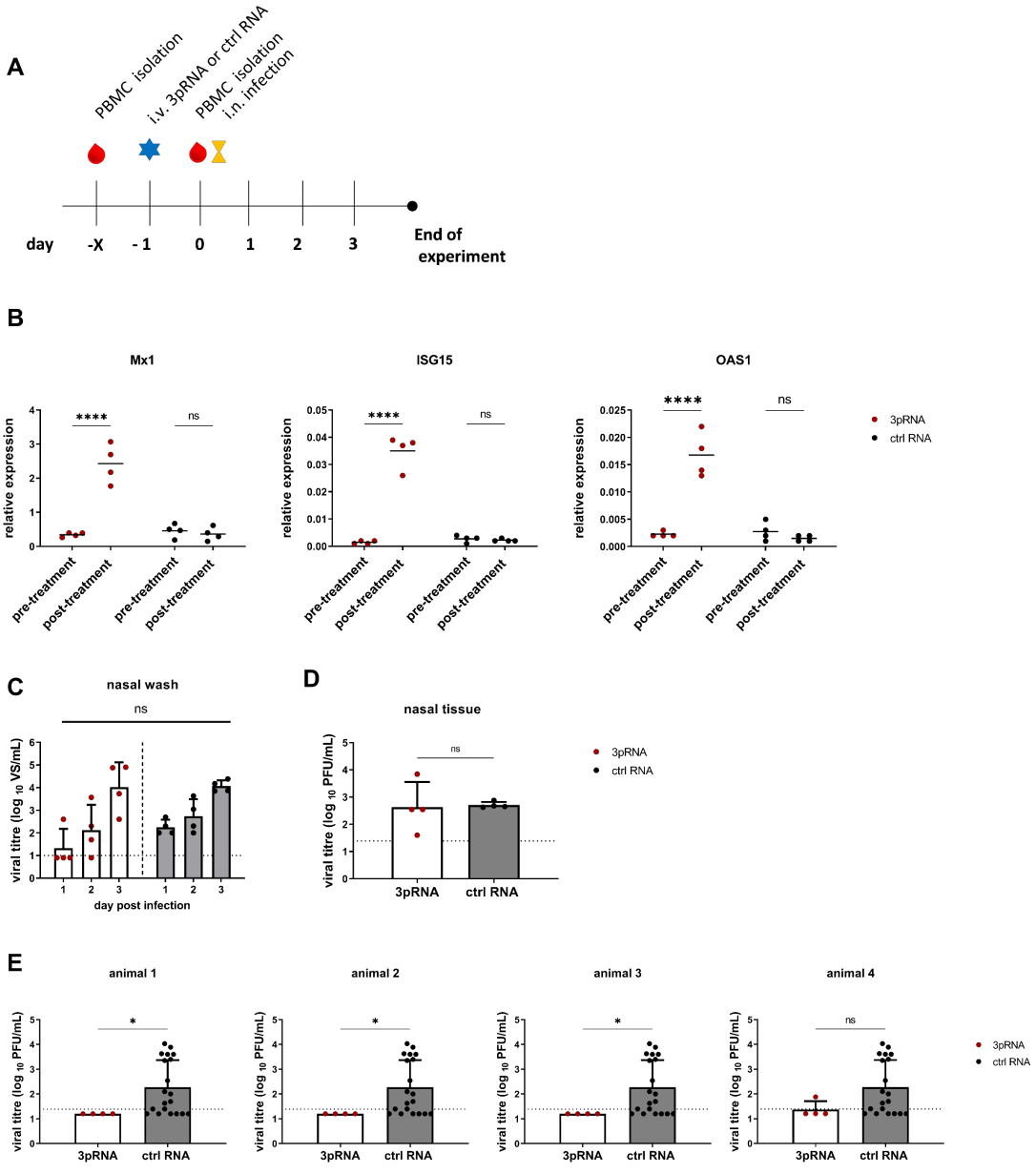

Figure 4.5: A single intravenous injection of ferrets with 3pRNA prior to RSV infection results in systemic ISG induction and reduced virus titres in the lungs. Animals received a single i.v. injection of 3pRNA or ctrl RNA (0.3 mg/kg) 24 hrs prior to inoculation with $5x10^5$ VS of RSV Long in 500 µL. Whole blood was collected and PBMCs isolated several (-X) days prior to (pre-treatment) and 24

hrs after (post-treatment) i.v. injection with 3pRNA or control RNA. **A)** An overview of the experimental approach is shown. **B)** After isolation of RNA from ferret PBMC, qRT-PCR was used to determine Mx1, ISG15 and OAS1 ISG levels, which are expressed relative to GAPDH. Each symbol represents a single animal. **C)** Titres of infectious RSV in nasal washes (1-3 dpi) from 3pRNA- or ctrl RNA-treated animals were determined by VS assay on HEp-2 cells. Circles represent individual animals. **D)** and **E)** At day 3 post infection, ferrets were euthanised and respiratory tissues (lung and nasal tissues) were collected and homogenised in PBS. Viral titres in clarified homogenates were determined by plaque assay on HEp-2 cells. The dashed line represents the limit of detection. Samples below the detection limit (<1.39 log_{10}PFU/mL) were assigned values of 1.2 log_{10}PFU/mL for statistical analysis. Data in B) represent the median. Data in D)-F) represent the mean ± SD. A paired Student´s *t*-test was performed in B) to compare ISGs levels before and after 3pRNA or ctrl RNA treatment. An unpaired Student's *t*-test with non-parametric Mann-Whitney correction was used in C) to compare AUCs and in D) and E) to compare the viral load in respiratory tissue after 3pRNA or ctrl RNA treatment. * = $p<0.05$; **** = $p<0.0001$; ns = not significant.

4.3 Discussion

RSV is a causative agent of respiratory tract infections, especially in young children, and is estimated to cause 3.4 million hospitalisations and 95,000-150,000 deaths globally every year (Stockman et al., 2012; Shi et al., 2017). Treatment options are limited and consist mainly of supportive care. Currently, there is no vaccine and only two FDA-approved antivirals available: aerosolised ribavirin, a guanosine analogue with broad-spectrum antiviral activity (Conrad et al., 1987; Marcelin et al., 2014) and pavilizumab, a humanised monoclonal antibody to the RSV F glycoprotein (Homaira et al., 2014). Both antivirals exhibit clinical benefit, however their use is limited due to a number of factors, including cost. The development of novel prophylactic and/or therapeutic treatment options against RSV is currently an area of intensive research. Strategies include the use of recombinant antibodies or nanobodies to RSV proteins, fusion inhibitors to block fusion of the virus with host cells, nucleoprotein inhibitors to impede viral replication, and nucleoside analogues and non-nucleoside inhibitors, amongst others (Behzadi et al., 2019). Most of these approaches target specific viral components, which is likely to limit their utility

against other viruses and is associated with the risk of drug-resistant variants emerging and spreading. As for IAV, this is of particular relevance to RSV as its viral RNA-dependent polymerase also lacks effective proof-reading capacity (Holland et al., 1982; Steinhauer et al., 1992).

While the current drug discovery landscape is largely focused on designing inhibitors of specific viral components, host-directed therapies targeting intracellular proteins could circumvent issues associated with limited virus specificity or with the risk of antiviral resistance emerging. We and others demonstrate that RIG-I agonists induce a broad spectrum of ISGs (Goulet et al., 2013; Chiang et al., 2015; Linehan et al., 2018), including a number with known antiviral activity in human, mouse and ferret cells. Induction of multiple cellular proteins which can act at one or more stages of the virus replication cycle means that the emergence of 'escape' mutants in highly unlikely. To date, *in vitro* and pre-clinical studies in mice with RIG-I agonists have yielded promising results. RIG-I agonists have been shown to inhibit infection by a range of viruses *in vitro*, including IAV, DENV and HIV-1, amongst others (Chakravarthy et al., 2010; Ranjan et al., 2010; Lin et al., 2012; Goulet et al., 2013; Olagnier et al., 2014; Chiang et al., 2015). While most *in vivo* studies have focused on assessing their effectiveness against IAV in mice (Ranjan et al., 2010; Lin et al., 2012; Goulet et al., 2013; Coch et al., 2017), 3pRNA treatment 24 hrs prior to footpad injection with CHIKV has also reduced viral titres in the serum at 3 dpi as well as footpad swelling over the course of infection (Chiang et al., 2015). Very recently, 3pRNA treatment has been described to possess antiviral function both in prophylactic as well as therapeutic settings against SARS-CoV-2 in a mouse model of infection (Mao et al., 2021; Marx et al., 2021).

Further studies are required to explore the potential of RIG-I agonists as broad-spectrum antivirals, including studies to define their breadth of antiviral activity as well as their effectiveness *in vivo* in different animal models of infection. Our studies showing the protective effects of 3pRNA treatment against IAV and RSV in both mice and ferret models certainly support their potential use as pan-antivirals *in vivo*.

To our knowledge, no studies to date have reported the effectiveness of RIG-I agonists in limiting infection and/or growth of RSV. Hence, in this chapter we investigated if synthetic RIG-I agonists could inhibit RSV infection and growth in different *in vitro* and *in vivo* models. In similar approaches to those described in the previous chapter, we first used airway cells from different mammalian species to demonstrate that prophylactic treatment with 3pRNA led to reduced susceptibility to RSV infection and reduced virus growth in human A549, mouse LA-4 and ferret FRL cells (**Figure 4.1 A and B, Figure 4.2 A and E, Figure 4.4 A and B**, respectively). Similar results were obtained using either Long or A2 strains of RSV. RIG-I agonist pre-treatment of the same cell lines also inhibited infection and growth of IAV (**Figure 3.1**), confirming their ability to limit infection and growth by respiratory viruses of different genera. However, in this chapter, we also utilised knockout and knockdown approaches to address the role of RIG-I itself in the anti-RSV effects of 3pRNA pre-treatment in cells from the different mammalian species. As for IAV, mice and ferrets represent two important small animal models for the study of RSV pathogenesis and immunity. An important advantage of targeting PRRs such as RIG-I is that they are highly conserved in evolution and stimulation by RIG-I agonists results in induction of antiviral IFN pathways which are also highly conserved (Zou et al., 2016). In future studies, it would be of interest to determine if RIG-I agonist treatment also inhibits other human respiratory viruses, such as human metapneumovirus (HMPV), parainfluenza viruses (PIV) and rhinoviruses (RV), to assess their potential as pan antivirals for human respiratory virus disease. Animal models for HMPV include mice and ferrets (MacPhail et al., 2004), while mouse models of RV infection are also established, allowing for *in vivo* effectiveness to be assessed as for IAV and RSV in this thesis.

Other studies have assessed putative antiviral compounds targeting host components for their ability to inhibit RSV in cell culture. For example, Pattabhi *et al.* demonstrated that therapeutic treatment of RSV-infected HeLa cells with KIN1400, an activator for IRF3 signaling, significantly reduced viral release (Pattabhi et al., 2015; Green et al., 2016). Besides inhibition of RSV, the authors also reported inhibition of West Nile virus, DENV, HCV, Ebola virus, IAV, Lassa

virus and Nipah virus. Although the mechanisms underlying KIN1400-induced antiviral activity are not completely clear, it represents an alternative host-directed antiviral approach which also displays broad antiviral activity, at least *in vitro*.

Prophylactic treatment of human nasal epithelial cells with exogenously supplied IFN-λ1 was also associated with reduced RSV release, consistent with findings that type III IFN, not type I IFNs, represent the primary IFN produced by the nasal epithelium during RSV infection (Okabayashi et al., 2011). A particular strength of our *in vitro* studies has been to compare RIG-I agonist treatment in human A549 cells to mouse LA-4 and ferret FRL cells, and this is particularly interesting as mouse and ferrets were the *in vivo* models used to assess effectiveness against RSV. Moreover, stimulation of the RIG-I signaling cascade results in production of both type I and type III IFNs and therefore induces broader protection than either IFN would be likely to achieve alone (Levy et al., 2011).

Studies in Chapter 3 (**Figure 3.1**) demonstrated that 3pRNA treatment induced a potent upregulation of ISGs in human, mouse and ferret airway cell lines and this correlated with protection from IAV infection. As most studies to date have focused on RIG-I-mediated protection in human cell lines, in this chapter we have investigated responses of mouse and ferret cells in more detail. For example, RIG-I agonist treatment results in IFN-α protein secretion from A549 cells (Goulet et al., 2013) and we confirm this to also be true in mouse LA-4 cells (**Figure 4.2 B**) noting that suitable reagents were not available to confirm secretion of IFN-α from ferret cells. We also designed approaches to confirm that 3pRNA-induced protection against RSV was dependent on a functional RIG-I in different species using RIG-I KO cells (human) and RIG-I knockdown cells (ferrets and mice). Our studies demonstrated that 3pRNA-induced protection against RSV was almost completely lost in RIG-I KO human cells (**Figure 4.1 E and F**) and was significantly impacted following knockdown in mouse (**Figure 4.2 D**) and ferret cells (**Figure 4.4 D**). Our studies in ferret cells were particularly informative and we confirmed that RIG-I knockdown did not impact type I IFN signaling as these cells still induced high levels of ISG15 after IFN-α treatment (**Figure 4.4 C**). By comparison, our analyses of RIG-I knockdown in mouse LA-4 cells was less

comprehensive and there was still evidence of RSV inhibition following 3pRNA treatment of RIG-I knockdown cells (**Figure 4.2 D**). In future studies, similar approaches to those described for assessment of RIG-I knockdown in ferret cells would be useful to inform regarding the effectiveness of RIG-I knockdown in mouse LA-4 cells. CRISPR/Cas9 mediated knockout of RIG-I in another mouse cell line (that does not exhibit a polyploid karyotype) or in ferret FRL cells could be pursued to confirm the shRNA knockdown data implicating the importance of RIG-I in 3pRNA-mediated antiviral activity.

RIG-I agonist treatment of human A549 cells after infection with RSV did not reduce the percentage of RSV-infected cells, even if treatment occurred as early as 1 hr after infection (**Figure 4.1 C and D**). In contrast, HeLa cells infected with RSV and treated at 2 hpi with KIN1400, leading to IRF3 activation, showed significant reductions in virus release (Pattabhi et al., 2015; Green et al., 2016). These discrepancies could reflect different assay readouts (i.e. flow cytometry for infected cells versus virus release) or different mechanisms of action between RIG-I agonists and IRF3 activators. Of note, RSV expresses two non-structural proteins (NS1 and NS2) which impact innate immune signaling. NS1 binds directly to MAVS, while NS2 binds to RIG-I and both can therefore disrupt RIG-I-MAVS interactions (Spann et al., 2004; Ling et al., 2009; Boyapalle et al., 2012). The therapeutic applications of RIG-I agonists against RSV could therefore be limited due to the immune evasion functions of NS1 and/or NS2 viral proteins. Several groups have already reported that 3pRNA-treatment on already established infection in cell culture models possessed antiviral effects and inhibited CHIKV, IAV or DENV viral replication (Olagnier et al., 2014; Chiang et al., 2015). We were unable to recapitulate these results using RSV which might be due to the forementioned reasons. In future. It would still be of interest to assess therapeutic effects *in vivo*. Coch *et al.* have shown that 3pRNA treatment of mice with an established IAV infection ameliorated clinical signs of infection and reduced weight loss even when applied 18 hrs after IAV infection (Coch et al., 2017).

These effects may not be evident in a prophylactic setting where 3pRNA pre-treatment can induce RIG-I signaling and subsequent induction of ISGs prior to RSV infection. In future studies, the effects of therapeutic 3pRNA treatment on RSV growth in human, mouse and ferret cells could be investigated further.

We used primary mouse lung fibroblasts to confirm the importance of functional IRF3/7 and IFNAR2 for 3pRNA-mediated protection from subsequent RSV infection (**Figure 4.2 F**). Given that RIG-I signaling depends on IRF3 and IRF7 (Yoneyama et al., 2004; Kawai et al., 2005) the results from IRF3/7$^{-/-}$ mice are not surprising. It was interesting to observe that 3pRNA-mediated protection against RSV was also lost in cells lacking IFNAR2. Given that type I and III IFNs should both be produced following RIG-I stimulation, this finding indicates that only type I IFN production is critical for 3pRNA-mediated protection against RSV, at least in this cell type. Type I and type III IFNs bind to distinct receptors (IFNAR1/IFNAR2 and IFNLR1/IL10R2, respectively) (Kotenko et al., 2003) and while type I IFN receptors are universally expressed, type III IFN receptor expression is primarily restricted to epithelial cells (Mordstein et al., 2010) and expression in human fibroblasts appears to be limited (Apostolou et al., 2016). Although embryonic fibroblasts from chickens and ducks express type III IFN receptors (Zhang, Z. et al., 2015), our results suggest that the primary mouse lung fibroblasts used in our studies do not. This would be consistent with RIG-I agonist-induced protection against RSV being entirely dependent on the presence of a functional IFNAR2.

While Mx1 is directly antiviral for IAV, overexpression studies in LA-4 cells indicate it is not for RSV (personal communication, Melkamu Tessema and Prof. Patrick Reading, The University of Melbourne) and to our knowledge there are no reports to indicate that mouse Mx1 inhibits RSV. However, our studies in mouse fibroblasts confirmed a functional Mx1 was associated with enhanced potency of 3pRNA treatment against RSV (**Figure 4.2 G**). Ctrl RNA-treated B6.A2G-*Mx1* fibroblasts were actually more susceptible to RSV infection than

cells from B6-WT mice, suggesting that the enhanced constitutive ISG expression observed in fibroblasts from B6.A2G-*Mx1* mice (**Figure 3.2**) did not translate to increased resistance to RSV infection. These surprising findings suggest that expression of functional Mx1 might also enhance other aspects of 3pRNA-mediated cell-intrinsic immunity to RSV, at least *in vitro* in primary mouse lung fibroblasts. It is important to note that our RSV studies to date were only performed *in vitro* using primary lung fibroblasts from B6-WT and B6.A2G-*Mx1* mice. Further studies are required to determine if a functional Mx1 contributes to potent and long-lasting inhibition of RSV, as we have reported for IAV both *in vitro* and *in vivo*.

Mx1-deficient BALB/c albino mice and a rHRSV-Luc virus were used to demonstrate that pre-treatment of mice with a single i.v. injection of 3pRNA potently reduced both bioluminescence and virus titres in the lungs (**Figure 4.3 B and C**). Previous studies have assessed the impact of single i.n. treatment with recombinant IFN-α or poly:ICLC 24 hrs prior to RSV A2 infection in mice, reporting significant reductions in both viral lung titres and disease score at 5 dpi (Guerrero-Plata et al., 2005). Of note, the effectiveness of poly:ICLC against RSV was superior to that of recombinant IFN-α, which is interesting given that poly:ICLC is a treatment that is also designed to stimulate PRRs (in this case, TLR3, RIG-I and MDA5) (Sultan et al., 2020). Thus, 3pRNA represents an additional PRR agonist that shows promise as an effective prophylactic antiviral treatment in the mouse model of RSV infection.

A number of studies indicate that ferrets represent another useful small animal model to study aspects of RSV pathogenesis, immunity and transmission (Prince et al., 1976; Stittelaar et al., 2016; Chan et al., 2017). Previous studies in our laboratory confirm that i.n. inoculation of ferrets with A2 or Long strains of RSV resulted in viral replication in the nasal tissue and lung, however, viral transmission from experimentally infected donors to naïve co-housed animals varied from 75 % (A2) to 25 % (Long) (Chan et al., 2017). Given these results, we decided to assess the effects of 3pRNA treatment following direct

experimental infection of ferrets with RSV, instead of the natural-transmission model which was used for IAV studies in ferrets in the previous chapter. Consistent with previous findings, a single i.v. injection of 3pRNA induced robust systemic ISG induction in ferrets after 24 hrs (**Figure 4.5 B**). Despite systemic induction of ISGs, 3pRNA treatment did not reduce shedding of infectious RSV from the upper airways (**Figure 4.5 C**). Thus, it appears unlikely that 3pRNA pre-treatment would reduce the incidence of onward RSV transmission to naïve animals, although this remains to be tested experimentally. End point analysis also confirmed that 3pRNA treatment did not reduce the load of infectious RSV in the nasal cavities at 3 dpi (**Figure 4.5 D**). In contrast, a single injection with 3pRNA did induce potent inhibition of RSV replication in the lungs, with infectious virus detectable in only one lung lobe from one animal (**Figure 4.5 E**). These findings highlight similarities between the impact of 3pRNA treatment on IAV and RSV replication in ferrets. For both viruses, inhibition was potent in the lower respiratory tract but limited in the upper airways. 3pRNA treatment resulted in reduced IAV titres in the lungs of 6/8 animals (**Figure 3.12**), however when comparing IAV and RSV studies in ferrets it is important to note that end point analysis of ferrets occurred 6 days after i.v. 3pRNA treatment in IAV studies (5 days after commencement of co-housing with infected donors) compared to 4 days after treatment in RSV studies (3 days after experimental infection of animals).

A common feature of studies in mice and ferrets using either IAV or RSV is the observation that a single prophylactic treatment with 3pRNA via the i.v. route resulted in protection of the lungs, but little protection of the upper airways. We have demonstrated that i.v. 3pRNA treatment of ferrets induces ISG expression in lung tissue (**Figure 3.11 C**) and in PBMCs, but we know little regarding ISG induction in the nose. As RIG-I receptors are expressed in almost all nucleated cells and the agonist was delivered via the i.v. route, it is possible that increased vascularisation of the lung might result in enhanced delivery of RIG-I agonist (and/or immune cells with upregulated ISG as a result of 3pRNA treatment) compared to the nasal tissues. Future studies could compare ISG induction and immune cell infiltration into the nose versus the lungs, although the limited

availability of ferret-specific antibodies prevents detailed analysis of immune cell infiltration (Wong et al., 2019). Despite these caveats, it is tempting to speculate that repeated RIG-I agonist treatment might still induce some protection in the nose and therefore limit onward virus transmission. As repeated i.n. administration did not impact IAV growth and shedding (**Chapter 3**), it is worth considering if alternate delivery options (e.g. as spray or gel) might increase its effectiveness in general against these respiratory viruses (Garg et al., 2018; Bedford et al., 2020). Effective delivery of 3pRNA to the upper airways using a vehicle that is not easily swallowed or expelled represents an important avenue of research in an effort to enhance its capacity to reduce shedding and therefore transmission of respiratory viruses.

In vitro studies described in this chapter have focused on A2 and Long strains of RSV, while RSV Long was used for *in vivo* studies in mice and ferrets. Both strains were isolated more than 50 years ago and have been used extensively by researchers around the world in published studies. However, it is likely that continued passage has resulted in mutations associated with long-term culture in mammalian cells such that these strains may not be representative of more recent human strains. It is interesting to note that Long and A2 strains show marked differences in their ability to induce IFN-α production with Long inducing approximately five times more IFN-α from human cell lines compared to A2 (Schlender et al., 2005). Thus, while 3pRNA treatment is effective at inhibiting two well-characterised laboratory strains which differ in at least some biological properties, it would be of great value to confirm that RIG-I agonists are also effective against recent clinical isolates of RSV A and B subgroups.

5 Chapter: Understanding the contribution of ferret Mx proteins to RIG-I agonist-mediated protection

5.1 Introduction

Following viral infection, host cells deploy a wide range of mechanisms to limit viral infection and spread. As first line of defence, highly conserved cell-associated PRRs such as RLRs, TLRs or NLRs can detect viruses, triggering a signaling cascade that results in the rapid induction of diverse antiviral effectors. Cell-intrinsic antiviral defences include a range of intracellular proteins with antiviral activity that are regulated independently of IFNs, as well as ISGs (Alandijany, 2019). Collectively, intracellular proteins which mediate antiviral activity against one or more viruses are known as host cell restriction factors. While many restriction factors have been defined for HIV-1 (Colomer-Lluch et al., 2018) and IAV (Villalon-Letelier et al., 2017), relatively few have been defined for other viruses such as paramyxo- and pneumoviruses (Farrukee et al., 2020).

MX dynamin like GTPase (also called “myxoma resistance” and “myxovirus resistance” or “Mx”) family proteins are IFN-inducible dynamin-like large GTPases that have been reported to mediate antiviral activity against particular RNA and DNA viruses. The ability of Mx proteins to act as restriction factors for IAV has been particularly well studied (Haller et al., 2015). *Mx* gene expression is tightly regulated and, in contrast to other ISGs, *Mx* expression is not directly induced by virus infection *per se* but rather by type I and III IFNs (Holzinger et al., 2007; Mordstein et al., 2008), which makes them excellent markers for studies investigating IFN induction.

Mx genes are highly conserved across different species with one to seven *Mx* genes expressed in almost all vertebrates. Most mammals, including humans and mice, express two *Mx* genes (Verhelst et al., 2013). The antiviral activities of Mx proteins are often linked to their cellular localisation, such that nuclear Mx proteins restrict viruses such as IAV that replicate within the nucleus, whereas cytoplasmic Mx proteins often inhibit viruses such as VSV that replicate exclusively in the cytoplasm. However, exceptions do exist. For example, cytoplasmic human MxA restricts a diverse range of viruses including *Orthomyxoviridae* which replicate in the nucleus, as well as *Bunyaviridae, Rhabdoviridae, Paramyxoviridae* and *Hepadnaviridae,* amongst others, which,

with the exception of the *Hepadnaviridae*, exclusively replicate in the cytoplasm (Hu et al., 2015; Dietzgen et al., 2017; Fearns et al., 2017; Ferron et al., 2017). In contrast, mouse Mx1 is expressed in the nucleus and its antiviral activity appears to be quite specific for *Orthomyxoviridae* although a recent study suggests that mouse Mx1 can also form cytoplasmic intermediate filaments and condensates and these are associated with antiviral functions against VSV, a member of the *Rhabdoviridae* (Sehgal et al., 2020). In fact antiviral activity of mouse Mx1 strongly depends on nuclear localisations, as mutations in mouse Mx1 that result in redistribution to the cytoplasm abolish its antiviral activity against IAV (Zürcher et al., 1992c).

The exact mechanisms by which Mx proteins inhibit different viruses are still under investigation but studies to date suggest that human MxA restrains IAV nucleocapsids in the cytoplasm, preventing their nuclear import and thereby blocking early steps in the viral replication cycle (Xiao et al., 2013; Haller et al., 2020). In contrast, mouse Mx1 mediates anti-IAV activity by inhibiting primary transcription and it has been reported to interact with the ribonucleoprotein complex, disrupting interactions between the viral NP and PB2 (Pavlovic et al., 1992; Verhelst et al., 2012). Mice also express a cytoplasmic Mx2 protein which has been reported to mediate antiviral against *Bunyaviridae* and *Rhabdoviridae* (Zürcher et al., 1992b; Jin et al., 2001). In humans, the long isoform of MxB localises to the nuclear envelope and exhibits antiviral activity against *Retroviridae* such as HIV-1 (Goujon et al., 2013; Kane et al., 2013) and is also a pan-herpesvirus restriction factor (Crameri et al., 2018; Schilling et al., 2018). The antiviral activity of MxB against HIV-1 is dependent on its nuclear localisation signal (NLS) as a short isoform lacking the NLS does not mediated antiviral activity (Goujon et al., 2014).

The antiviral roles of human and mouse Mx proteins have been well characterised *in vitro* and the importance of mouse Mx1 has been particularly well studied *in vivo* during IAV infection of mice. As reported in a previous chapter, mice expressing a functional Mx1 were more resistant to IAV infection and much higher inoculum doses were required to induce weight loss and disease compared to

Mx1-deficient mice. This is in line with previous studies demonstrating that Mx1-congenic and MxA-transgenic mice are more resistant to IAV infections (Haller et al., 1981; Tumpey et al., 2007; Deeg et al., 2017). While ferrets are considered to be the gold standard small animal model to study pathogenesis and immunity to human IAV (Oh et al., 2016), little is currently known regarding the characteristics and the antiviral activity of host cell restriction factors in ferrets, including the Mx proteins. Therefore, studies in this chapter aimed to investigate ferret Mx proteins, including their induction in response to RIG-I agonists and other stimuli and their antiviral activity against IAV and RSV.

5.2 Results

5.2.1 Homology between predicted ferret Mx proteins and Mx proteins from other species

In-depth characterisation of the anti-IAV activity of Mx proteins from mice and humans have been performed and Mx proteins from a range of other mammalian species have also been described. However, very little is currently known regarding Mx proteins in ferrets. *Mx* genes are highly conserved in vertebrates with most mammals expressing both Mx1-like and Mx2-like lineages. Previous studies performed whole genome sequencing on an individual female ferret, as well as RNA-seq from 24 samples from male and female ferrets, allowing for annotation of 19,910 protein-coding sequences (Peng et al., 2014). The annotated sequence (NCBI Accession AEYP00000000) includes identification of 3 genes predicted to encode Mx-like proteins, namely ferret Mx1 (with two isoforms, Mx1.1 (NCBI XM_013061287.1) and Mx1.2 (NCBI XM_004762192.2) and ferret Mx2 (NCBI XM_013061286.1). The Mx1.1 mRNA isoform (2,604 base pairs (bp) contains an additional 23 bp at the 5' end, as well as an additional 36 bp from residue 248, which are missing from the Mx1.2 isoform (2,545 bp), resulting in an extra 59 nucleotides that are expressed only in Mx1.1. From these genes, the predicted coding sequence is 2,013 bp for Mx1.1 and 1,977 bp for Mx1.2, corresponding to 670 and 658 amino acid protein sequences, respectively. For ferret Mx2, the gene sequence is 3,973 bp, with a predicted coding sequence of 2,094 bp and a protein of 697 amino acids.

First, we retrieved the confirmed or predicted amino acid sequences encoded by *Mx* genes from different species such as brown bear, cat, chimpanzee, cow, dog, horse, human, mouse, pig and walrus from GenBank genome browser. Protein sequences were aligned by performing a MUSCLE algorithm using the Molecular Evolutionary Genetics Analysis (MEGA X) software (Kumar et al., 2018). It is known that the GTPase domain of Mx proteins contains a number of key Mx protein domains including a tripartite GTP-binding motif (GDXXSGKS, DLPG, TKPD) and a dynamin motif (LPRXXGXXTR) (Verhelst et al., 2013). These motifs

were found in ferret Mx1 and Mx2 proteins and showed 100 % amino acid homology to Mx proteins from all other species examined, emphasising the high conservation of the GTPase domain amongst mammalian species (**Figure 5.1**).

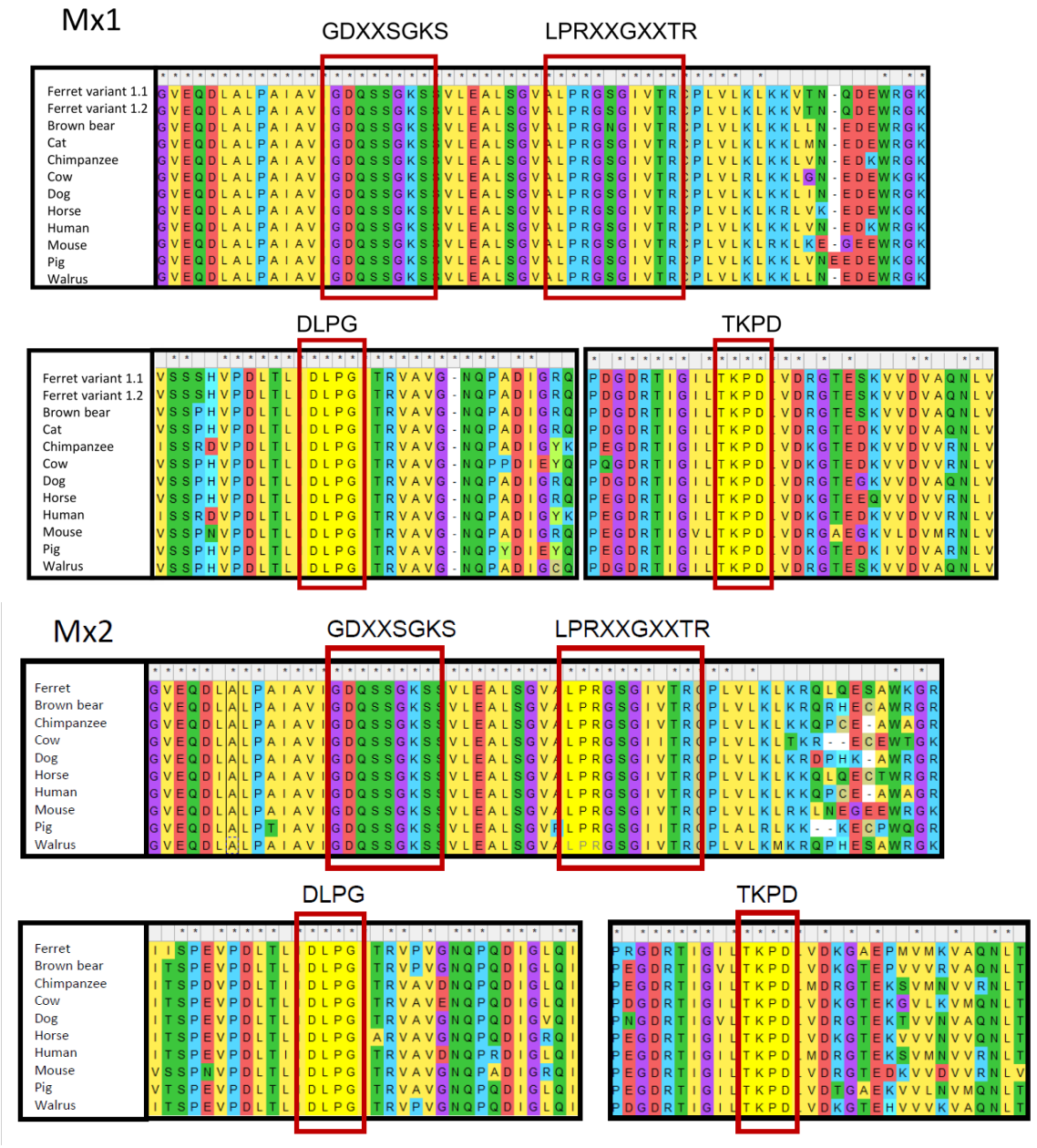

Figure 5.1: Multiple alignments of Mx1 and Mx2 protein from different species reveal conserved amino acid sequences. Predicted amino acid sequences for ferret Mx1 and Mx2 (Mustela putorius furo Mx1 variant 1: XP_012916741.1, variant 2: XP_004762249.1, Mx2: XP_012916740.1), as well as for brown bear (Ursus arctos horribilis Mx1: XP_026356328.1, Mx2: XP_026356450), cat (Felis catus Mx1: XP_023094481.1), chimpanzee (Pan troglodytes Mx1: NP_001266765.1, Mx2 isoform X2: XP_001171751.3), cow (Bos taurus Mx1: NP_776365.1, Mx2: NP_776366.1), dog (Canis lupus familiaris Mx1: NP_001003134.1, Mx2: XP_038299486.1) horse (Equus caballus Mx1: NP_001075961.1, Mx2: XP_005606216.2), human (Homo sapiens Mx1 isoform a: NP_001138397.1, Mx2: NP_002454.1), mouse (Mus musculus Mx1: NP_034976.1, Mx2: Q9WVP9.2), pig (Sus scrofa Mx1: NP_999226.2, Mx2: A7VK00.1) and walrus (Odobenus rosmarus divergens Mx1 isoform

X1: XP_004406610.1, Mx2: XP_004406645.1). Sequences were aligned by performing a MUSCLE algorithm using the Molecular Evolutionary Genetics Analysis (MEGA X) software. Conserved regions in the GTPase domain are marked.

Next, protein homologies were assessed by generating a phylogenetic comparison of predicted protein sequences based on the Maximal Likelihood method (**Figure 5.2 A**) (Jones et al., 1992; Kumar et al., 2018). Mx proteins are separated into two clearly defined clusters, the Mx1 and Mx2 lineages. When comparing ferret Mx1.1 and Mx1.2 with Mx1 proteins from other species, we detected greatest amino acid sequence homology to Mx1 proteins from bear, walrus and dog. Ferret Mx2 also clustered most closely with Mx2 proteins from bear, walrus and dog rather than with Mx2 proteins from humans and mice. Interestingly, mouse Mx1 and Mx2 form a separate small cluster which is located between the Mx1 and Mx2 lineages, with closer proximity to the Mx1 lineage.

We aligned Mx protein sequences from different species, including humans, mice and ferrets, by multiple pairwise alignment using the NCBI protein BLAST (blastp). As shown in **Figure 5.2 B (upper panel)**, ferret Mx1.1 and Mx1.2 proteins show highest sequence homology to brown bear, walrus, cat and dog, confirming their close proximity as shown in the phylogenetic analysis (**Figure 5.2 A**). The amino acid sequence of ferret Mx2 was less closely related to other species using this analysis, however we still observed the greatest homology of ferret Mx2 to Mx2 proteins from walrus, brown bear and dog.

In previous studies, Verhelst *et al*. reported the genomic organisation of the *Mx* locus from different species and found that *Mx* genes are flanked by transmembrane protease serine subtype 2 (*TMPRSS2*) and FAM3 Metabolism Regulating Signalling Molecule B (*FAM3B*) genes (Verhelst et al., 2013). Similar analyses confirmed that the *Mx* locus of ferrets (and most other species included into our analysis), were also flanked by *TMPRSS2* and *FAM3B*, indicating a conserved synteny across different species (**Figure 5.2 C**). Of interest, mouse *Mx* genes show a different gene orientation and arrangement which is likely due to duplication of ancestral *Mx1*-like gene (Haller et al., 2015). Moreover, the *Mx2* locus is not present in cats.

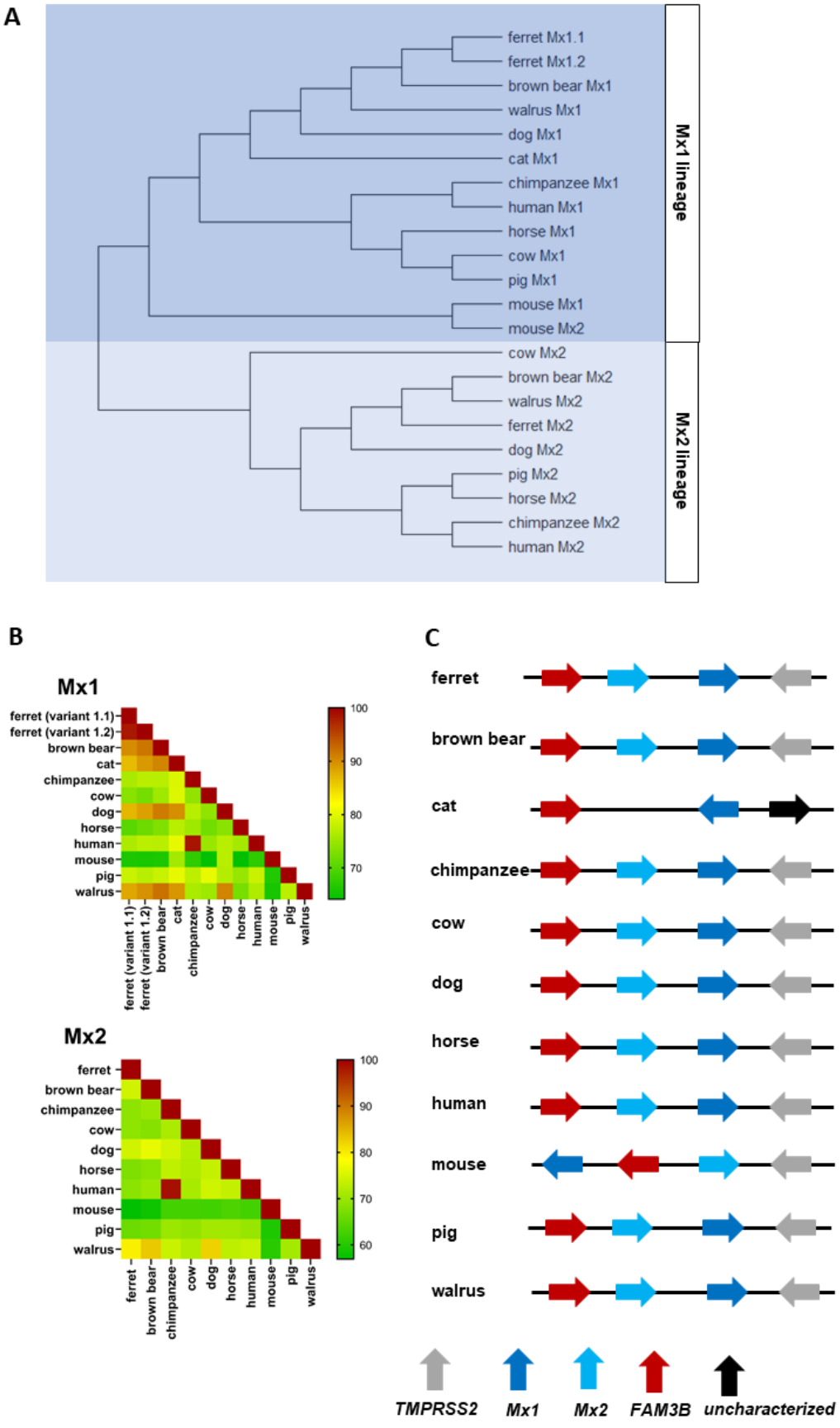
A
ferret Mx1.1
ferret Mx1.2
brown bear Mx1
walrus Mx1
dog Mx1
cat Mx1
chimpanzee Mx1
human Mx1
horse Mx1
cow Mx1
pig Mx1
mouse Mx1
mouse Mx2
cow Mx2
brown bear Mx2
walrus Mx2
ferret Mx2
dog Mx2
pig Mx2
horse Mx2
chimpanzee Mx2
human Mx2
Mx1 lineage
Mx2 lineage
B
Mx1
ferret (variant 1.1)
ferret (variant 1.2)
brown bear
cat
chimpanzee
cow
dog
horse
human
mouse
pig
walrus
100
90
80
70
Mx2
ferret
brown bear
chimpanzee
cow
dog
horse
human
mouse
pig
walrus
100
90
80
70
60
C
ferret
brown bear
cat
chimpanzee
cow
dog
horse
human
mouse
pig
walrus
TMPRSS2
Mx1
Mx2
FAM3B
uncharacterized

Figure 5.2: The ferret *Mx* locus shows similar architecture to the *Mx* loci from other species and ferret Mx1 and Mx2 show high levels of homology at the amino acid level. **A)** Phylogenetic trees generated by Maximum Likelihood methods show the relative evolutionary history of Mx proteins amongst different species. **B)** Heatmap showing the percent homology between Mx proteins from different species, include human, mouse and ferret. **C)** Representation of the *Mx* gene locus of ferrets and other mammalian species. Flanking genes are *TMPRSS2* and *FAM3B*. Arrow direction indicates the orientation of a particular gene.

5.2.2 3’-RNA sequencing of FRL cells reveals Mx1 and Mx2 induction upon 3pRNA or IFN-α stimulation

As a first step towards understanding cellular responses to RIG-I agonists and the induction of ferret Mx in FRL cells, we performed 3’-RNA sequencing on FRL cells to quantitatively measure the abundance of 3'-untranslated region (UTR) transcripts after treatment with 3pRNA, ctrl RNA or recombinant ferret IFN-α when compared to untreated control conditions. We performed pairwise comparisons, selected the 25 most differentially expressed genes from each comparison and combined them as shown in **Figure 5.3**.

In general, we found that 3pRNA or ferret IFN-α treatment resulted in upregulation of a number of known IFN-regulated genes, including both ferret Mx1 and Mx2. The results obtained using ctrl RNA and untreated cells were very similar, confirming that ctrl RNA (as well as the lipofectamine transfection reagent) did not activate IFN signaling pathways in FRL cells. Of note, as 3’-RNA sequencing only sequences approximately 100 bp from the 3’-UTR, we could not distinguish between Mx1.1 and Mx1.2 splice variants. In general terms, expression patterns after 3pRNA or IFN-α treatment were very similar, although the relative expression of transcripts was in general higher after IFN-α treatment.

We were most interested in genes differentially expressed after 3pRNA or IFN-α treatment compared to ctrl RNA treatment or untreated conditions. We used bioinformatic analyses to calculate the correlation distance between transcripts and identified several clusters of mRNA transcripts selectively upregulated following 3pRNA and IFN-α treatment, which were examined in more detail. The first cluster

(**cluster i) Figure 5.3**), consisted of a number of cellular proteins which have been implicated in antiviral immunity to one or more viruses. For example, sterile alpha motif domain containing 9 like (SAMD9L) has been reported to inhibit poxviruses in human cell lines (Meng et al., 2018) while galectin 3-binding protein LGALS3BP is a virus-induced protein which activates antiviral innate immune responses and induces IFN and pro-inflammatory production (Xu et al., 2019). Apolipoprotein L5 (APOL5) is an ISG reported to inhibit different murine viruses (Kreit et al., 2015), while zinc finger NFX1-type containing 1 (ZNFX1) localises to the mitochondria and acts as a dsRNA sensor to restrict replication of some RNA viruses (Wang, Yao et al., 2019). Finally, cytidine/uridine monophosphate kinase 2 (CMPK2) has been implicated in IFN-mediated restriction of HIV (El-Diwany et al., 2018) and E2 ubiquitin-conjugating enzyme UBE2L6 is involved in ISG15-dependent ISGylation pathways, which are relevant to inhibition of multiple viruses (Mathieu et al., 2021).

A second cluster (**cluster ii) Figure 5.3**) was characterised by a number of well-defined ISGs including MX2, ISG15, MX1, DDX60, USP18, DDX58 (coding gene for RIG-I) and OAS-1 that were upregulated by both RIG-I agonist and IFN-α treatment. A third cluster (**cluster iii) Figure 5.3**) also contained typical ISGs such as guanylate-binding protein (GBP)-1, GBP-6, IFIT2 and eukaryotic translation initiation factor 2 alpha kinase 2 (EIF2AK2), a protein which plays an important role in the innate immune response against multiple DNA and RNA viruses (Mao et al., 2020). Interestingly, RIG-I agonist treatment resulted in higher expression of GBP-6 and C-X3-C Motif Chemokine Ligand 1 (CX3CL1) compared to IFN-α treatment. It is well established that murine GBP proteins are important host effector molecules against intracellular pathogens, including some viruses (Degrandi et al., 2007) and human GBP-1 can inhibit VSV and HSV-1 (Zhang et al., 2021) while GBP-5 is active against IAV (Feng et al., 2017). CX3CL1 is a proinflammatory chemokine which can be membrane-anchored or expressed as a soluble, chemotactic cytokine. The soluble form interacts with CX3CR1 expressed on a variety of immune cells to induce monocyte infiltration (Rivas-Fuentes et al., 2021). Membrane-associated CX3CR1 is a co-receptor for HIV-1 as well as a receptor for RSV binding to human airway epithelial cells (Johnson et al., 2015) and CX3CL1

can block functional interactions between CX3CR1 with HIV-1 *in vitro*, therefore representing an attractive therapeutic target (Combadiere et al., 1998).

All in all, 3'-RNA sequencing confirmed that RIG-I agonist pre-treatment of FRL cells resulted in potent induction of a range of ferret ISGs, consistent with its ability to reduce IAV and RSV infection and growth in these cells in previous chapters. Amongst these ISGs, it was clear that RIG-I agonist treatment induced both ferret Mx1 and Mx2.

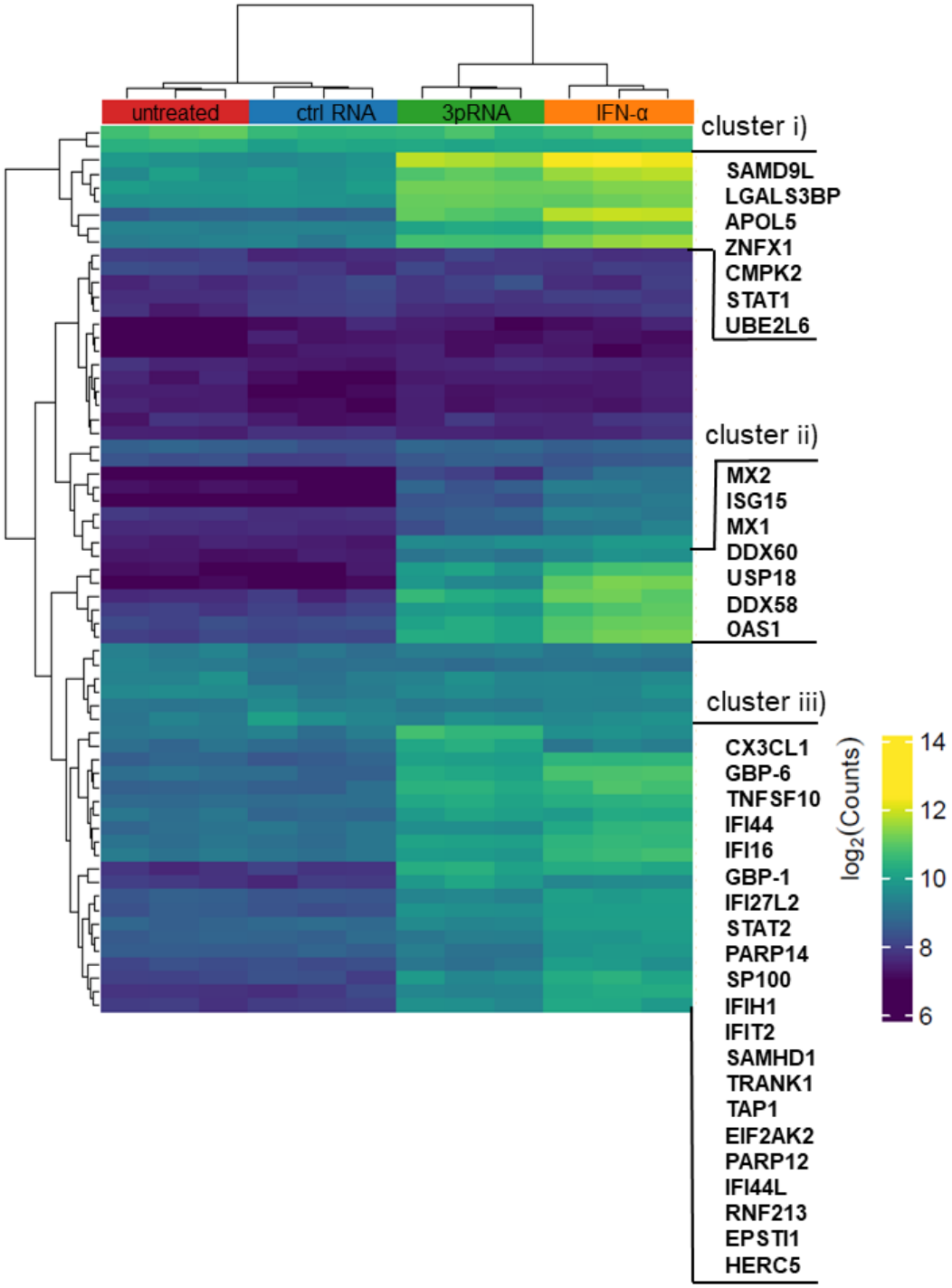

Figure 5.3: Clustered heat map of differentially expressed genes in FRL cells after 3pRNA, ctrl RNA or IFN-α treatment or in untreated control cells. FRL cells were transfected with RIG-I agonist (3pRNA, 200 ng/mL), control RNA (ctrl RNA, 200 ng/mL), or treated with ferret IFN-α (50 ng/mL) or left untreated. After 6 hrs, total RNA was isolated and sequenced with a 3' mRNA-Seq Kit on a NovaSeq 6000. Reads were trimmed and a STAR alignment was performed. Colours

indicate the prevalence of transcript expression from low (dark blue) to high (bright yellow). n=3 samples/group.

5.2.3 Sequencing of Mx1 in ferret airway cells

To determine if one or both splice variants of Mx1 were expressed in FRL cells we sequenced the Mx1 mRNA transcripts expressed in FRL cells. Mx1.1 and Mx1.2 show high sequence identity, however variants can be distinguished by a stretch of 36 bp of nucleotides which is specific for Mx1.1 and missing in variant Mx1.2. After stimulation of FRL cells with RIG-I agonists, total RNA was isolated and cDNA was generated. We then amplified the Mx1 region of interest by PCR using 'generic' Mx1 primers (i.e. directed to sequences common to both ferret Mx1.1 and Mx1.2) and sequenced the amplified product. Chromatograms from Sanger sequencing showed a region with single peaks (**Figure 5.4 B**) indicating that our PCR generated only one product consistent with amplification of a single splice variant of Mx1. When comparing the amplified sequence with annotated sequences of ferret Mx1.1 and Mx1.2, we found that only splice variant Mx1.2 (marked in yellow and green in **Figure 5.4 B and C**) was detected. The 36 bp sequence of nucleotides which is specific for Mx1.1 (red characters) was not detectable in the chromatogram. Note that due to the sequencing primer, which was in reverse orientation, the reverse complement sequences of Mx1.1 and Mx1.2 are shown in **Figure 5.4 C**.

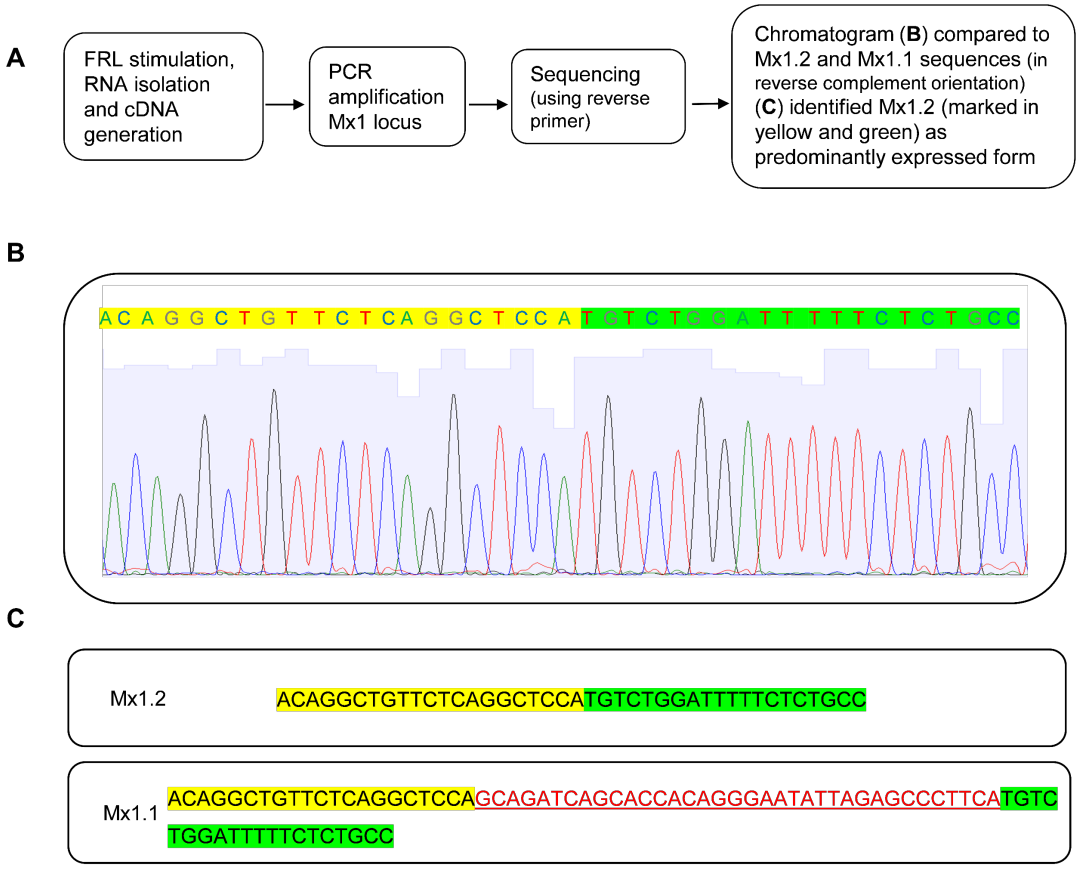

Figure 5.4: Identification of Mx1.2 as abundant splice variant in FRL cells. **A)** Flowchart of experimental design. **B)** FRL cells were stimulated with RIG-I agonist (200 ng/mL) and RNA was harvested after 24 hrs and cDNA was generated. Mx1 mRNA was amplified by PCR using 'generic Mx1 primers' that should detect both Mx1.1 and Mx1.2 splice variants and then sequenced with a ferret Mx1-primer (reverse orientation) that should also detect both variants. Sequencing chromatogram was generated using web-based PolyPeakParser tool (Hill et al., 2014). **C)** Reverse complement sequences from Mx1.1 and Mx1.2. Identical sequences are marked in yellow and green in B) and C). The 36 bp stretch of nucleotides unique to ferret Mx1.1 is shown in red.

5.2.4 Induction of different ferret Mx in ferret airway cells following RIG-I agonist treatment or respiratory virus infection

Next, we aimed to quantify the induction of different ferret Mx in FRL cells in response to 3pRNA stimulation or to respiratory virus infection via qRT-PCR. First, it was necessary to design primers to allow for detection of unique transcripts associated with expression of ferret Mx1.1, Mx1.2 and Mx2. Splice variants Mx1.1 and Mx1.2 could be distinguished by designing primers which specifically target the 36 bp stretch missing in Mx1.2 (resulting in a primer specific for Mx1.1) or to the adjacent sequences upstream and downstream of this 36 bp stretch (resulting in a primer specific for Mx1.2) (**Figure 5.5 B**). FRL cells with DOX-inducible overexpression of Mx1.1 or Mx1.2 generated and described later in this chapter (**section 5.2.6**) were used to confirm the specificity of Mx1.1 and Mx1.2 primers (**Figure 5.5 C**). We also designed 'generic' Mx1 primers to target sequences found in both transcripts of Mx1, as well as primers specific for ferret Mx2. Primers were then used to assess mRNA transcript levels of Mx in FRL cells after stimulation or infection via qRT-PCR.

We used specific primers for Mx1.1, Mx1.2 and Mx2 to examine their expression in response to RIG-I agonist treatment or to respiratory virus infection. For these studies, FRL cells were treated with 3pRNA, control (ctrl) RNA (each 200 ng/mL) or with ferret IFN-α and total RNA was isolated 24 hrs later. As seen in **Figure 5.5 D**, 3pRNA or IFN-α treatment induced potent upregulation of Mx1.1, Mx1.2 and Mx2, whereas ctrl RNA treatment did not and no major differences were noted between 3pRNA or IFN-α in their ability to induce ferret Mx expression. In terms of other ISGs, 3pRNA and ferret IFN-α also induced ISG15 and OAS1 expression in FRL cells, whereas only 3pRNA induced CCL5, consistent with results reported in section 4.2.5. Of interest, ferret Mx1.1 and Mx2 showed similar levels of upregulation at 24 hrs post-treatment (~100-fold compared to the unstimulated control), while generic Mx1 and ferret Mx1.2 were upregulated to much higher levels (~4000-fold compared to unstimulated). Ct levels for Mx1.1 detection were markedly higher than for Mx1.2 and, together with results

described in **Figure 5.4**, indicate that primarily Mx1.2 is expressed following IFN-α or RIG-I agonist stimulation in FRL cells.

To assess how ISGs are induced after IAV or RSV infection, FRL cells were infected for 1 hr at 37°C with IAV HKx31 (H3N2) or RSV Long (MOI = 1) and total RNA was isolated 24 hrs later. Infection of FRL cells with either IAV or RSV was associated with induction of each ferret Mx (**Figure 5.5 E**). While the fold induction was much lower for each ferret Mx compared to 3pRNA or IFN-α treatment (**Figure 5.5 D**), IAV and RSV infection still resulted in significant increases in Mx1.1, Mx1.2, Mx1 (generic) or Mx2 expression compared to uninfected cells. Of note, flow cytometry confirmed infection of cells by both IAV and RSV in these experiments (approximately 12 % and 40 % for IAV and RSV, respectively), indicating that the low ISG induction was not due to a lack of infection by these viruses (data not shown). When we performed an additional experiment including a mutant of IAV strain A/Puerto Rico/8/34 (PR8, H1N1) lacking a functional NS1 protein (PR8 ΔNS1) and assessed ISG induction after 24 hrs, we recorded a strong induction of ISG15, OAS and CCL5 (data not shown). It is well established that the IAV NS1 antagonises a number of steps in RIG-I mediated recognition and IFN induction and that NS1-deficient IAV induce strong activation of these innate antiviral pathways (Rosário-Ferreira et al., 2020), thus it is very likely that the minor expression of Mx transcripts recorded after IAV HKx31 infection is due to the IAV NS1-mediated suppression of endogenous IFN responses. It would be of interest to examine ferret Mx induction in future studies using this NS1-deficient IAV and to use a higher MOI to ensure a higher proportion of virus-infected cells.

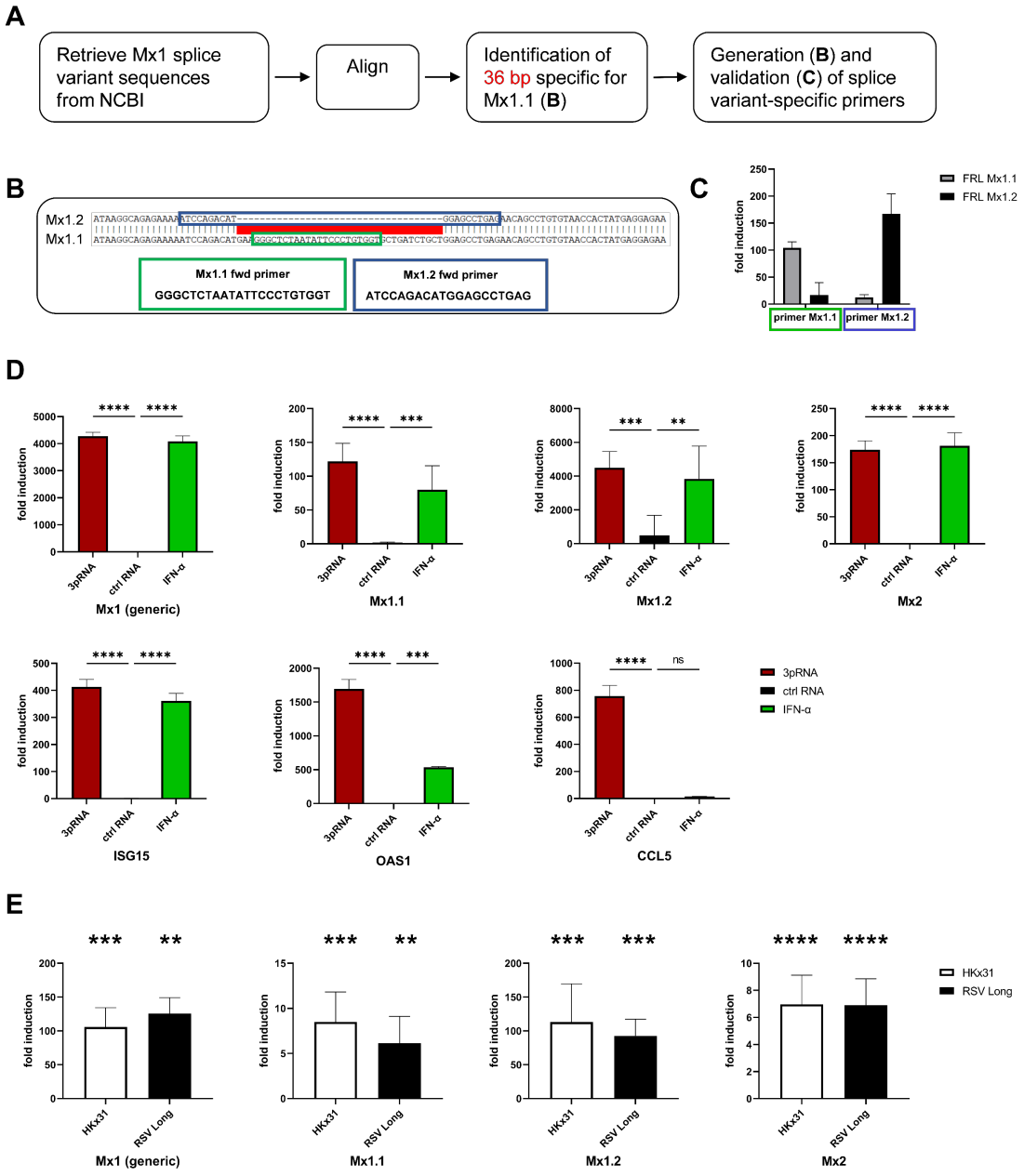

Figure 5.5: Induction of different ferret Mx in ferret airway cells in response to pre-treatment with 3pRNA or ferret IFN-α, or with infection with IAV or RSV. **A)** Flowchart of experimental design. **B)** qRT-PCR forward (fwd) primer with specific binding for splice variant Mx1.1 (green) or Mx1.2 (blue) were generated. **C)** qRT-PCR primers were evaluated in FRL cells with DOX-inducible overexpression of Mx1.1 (grey bars) or Mx1.2 (black bars). Cells were treated with 1 µg/mL DOX, incubated for 24 hrs and total RNA was harvested. qRT-PCR was performed, expression was normalised to GAPDH and expressed as fold induction relative to untreated cells. Data are from one experiment, n=3/group. **D)** FRL cells were transfected with RIG-I agonist (3pRNA, 200 ng/mL) or control RNA (ctrl RNA, 200 ng/mL), or treated with ferret IFN-α (50 ng/mL). Then, 24 hrs after treatment, total RNA was isolated and the expression of ISGs was assessed

by qRT-PCR. **E)** Cells were infected with HKx31 (H3N2) or RSV Long at MOI = 1, washed and cultured in serum-free media. Then, 24 hrs after infection, total RNA was isolated and the expression of ISGs was assessed by qRT-PCR. Expression is normalised to GAPDH and expressed as fold induction relative to untreated cells. D) and E) show the mean (± SD) from triplicate samples and are representative of 2 or more independent experiments. A one-way ANOVA with Bonferroni's correction was performed in D) to compare induction after 3pRNA or IFN-α treatment compared to ctrl RNA treatment. In E) expression of untreated cells was set to 1 and a one-way ANOVA with Bonferroni's correction was performed to compare fold-change in ISG expression after infection to untreated cells. ** = $p<0.01$; *** = $p<0.001$; **** = $p<0.0001$; ns = not significant.

5.2.5 Intracellular localisation of ferret Mx proteins

Analysis of amino acid sequences using the online tools cNLS mapper (Kosugi et al., 2009) and NLStradamus (Nguyen Ba et al., 2009) indicated that ferret Mx1.1, 1.2 and 2 did not contain a predicted nuclear localisation sequence (NLS). NLStradamus detected a putative NLS (RKFLKERLARLGQARRRLAKF) in Mx1.1 and Mx1.2, however, this sequence is also detected in dog Mx1 and mouse Mx2, which are both expressed in the cytoplasm (Verhelst et al., 2013). Each of the programs used detected the confirmed NLS in mouse Mx1 (REKKKFLKRRLLRLDEARQKLAKFS) and cNLS mapper detected a NLS in human MxB (ILQEKNRYSWLLQEQSETATKRRILK) and both of these proteins are known to localise to the nucleus. cNLS mapper predicts NLS-specific to the importin αβ pathway and NLStradamus can also identify additional known NLS (Nguyen Ba et al., 2009). However, as the power of such computational methods is limited, it was important to experimentally determine if different ferret Mx localised to the cytoplasm or to the nucleus.

For these studies, A549 cells were reverse transfected (i.e. plated and transfected at the same time, as per Materials and Methods) with pcDNA3.1 vectors expressing individual ferret Mx proteins (Mx1.1, 1.2 and 2), or with human MxA or human MxB pcDNA3.1 vectors were engineered to express each ferret Mx with a N-terminal FLAG tag to allow for immunohistochemical staining without the need of species-specific antibodies.

Therefore, at 30 hrs post transfection, cells were fixed, permeabilised and stained for intracellular expression of FLAG. The nuclear compartment was visualised by DAPI staining and pcDNA3.1 transfected cells could be identified by confocal microscopy due to constitutive expression of mCherry.

As seen in **Figure 5.6 (upper panels)**, human MxA expression was restricted to the cytoplasm, whereas human MxB localised to the nucleus, consistent with their reported cellular localisation (Aebi et al., 1989; Melén et al., 1996)**.** When examining ferret Mx proteins, we found that ferret Mx1.1, Mx1.2 and Mx2 were all expressed exclusively within the cytoplasmic compartment **Figure 5.6 (lower panels)**. When examining staining patterns in more detail, we noted that ferret Mx1.2 and Mx2 showed punctate staining in the cytoplasm, whereas ferret Mx1.1 showed a more diffuse staining pattern. Together, these studies confirm that all ferret Mx proteins localise exclusively to the cytoplasm when expressed in A549 cells. For future studies endolysosomal markers could be included to investigate if Mx proteins predominantly localise to vesicular compartments.

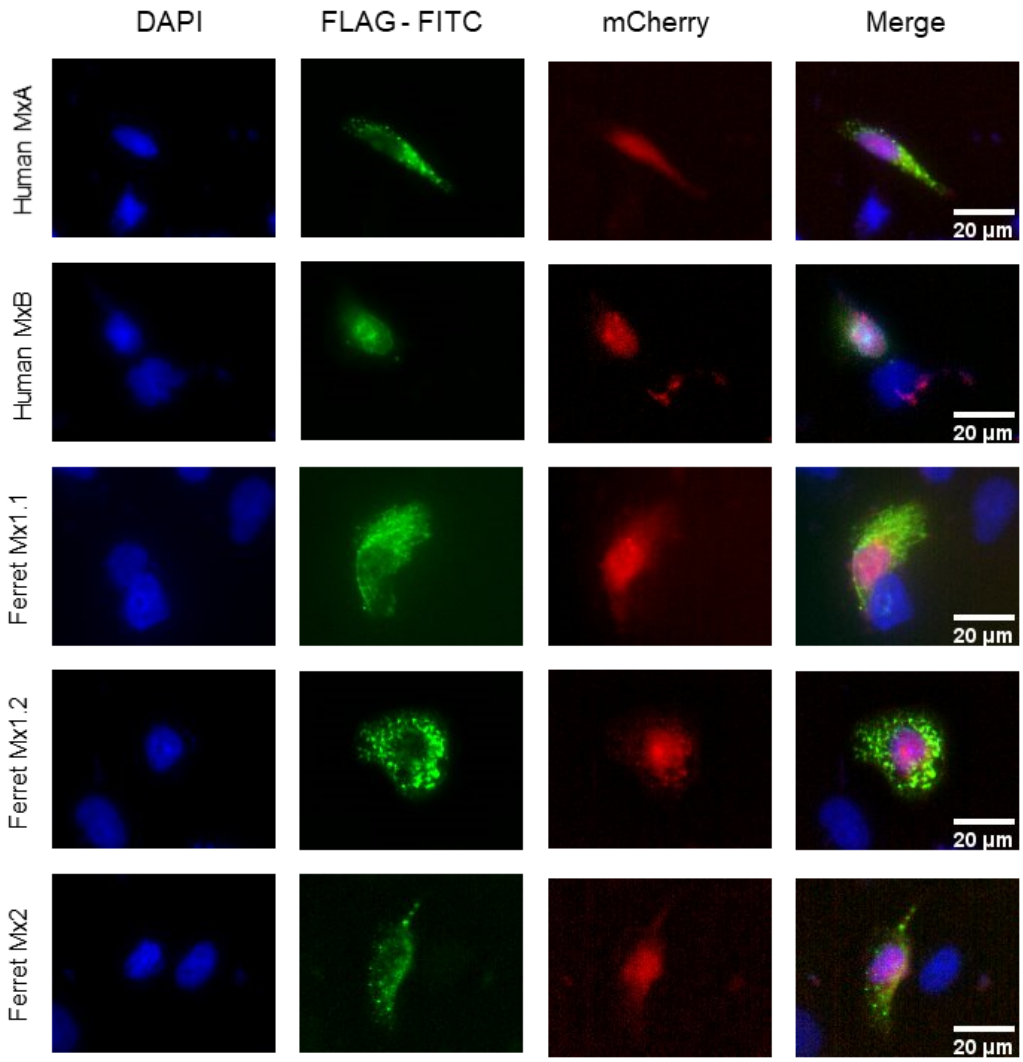

Figure 5.6: Subcellular localisation of ferret Mx1.1, Mx1.2 and Mx2 in A549 cells. A549 cells were reverse transfected with pcDNA3.1 plasmids expressing ferret Mx1.1, Mx1.2 or Mx2, or with human MxA or MxB, each with a N-terminal FLAG tag. Then, 30 hrs later, cells were fixed, permeabilised and stained for the intracellular expression of the FLAG-tagged proteins. Stained samples were analysed via immunofluorescence microscopy. Scale bar = 20 µm.

5.2.6 Investigating the utility of an inducible overexpression system to study the antiviral function of ferret Mx proteins

To assess the role of Mx proteins during RIG-I agonist-mediated protection from IAV and RSV infection, we aimed to generate human A549 and ferret FRL cells with DOX-inducible overexpression of species-specific Mx or with cytoplasmic ovalbumin (cOVA), as an irrelevant control protein. In initial experiments we assessed the utility of the DOX-inducible system using stable lines of mouse LA-4 cells with DOX-inducible overexpression of mouse Mx1 or cOVA (kindly provided by Melkamu Tessema, The University of Melbourne). LA-4 cells were transfected with 3pRNA or ctrl RNA (each 200 ng/mL). After transfection, cells were cultured for 24 hrs in media with or without 1 µg/mL DOX and then infected with RSV Long-GFP (MOI = 1) or IAV HKx31 (MOI = 10) and the percentage of RSV- or IAV-infected cells was determined by flow cytometry at 18 hpi or 8 hpi, respectively.

In untreated cells, inducible mouse Mx1, but not cOVA, reduced the percentage of IAV-infected cells (**Figure 5.7 A, middle and right panel**), confirming that DOX-inducible mouse Mx1 mediates anti-IAV activity. In all cell lines, 3pRNA treatment resulted in significant reduction in the proportion of IAV-infected cell. If cells were transfected with 3pRNA in addition to inducible mouse Mx1 expression, we detected further significant reductions in the percentage of infected cells, indicating additive antiviral effects (**Figure 5.7 A, right panel**). Importantly, these additive effects in inhibiting IAV infection were only observed in cells with inducible mouse Mx1 and not with cOVA.

3pRNA treatment also resulted in a significant reduction in the percentage of RSV-infected cells in all cell lines (**Figure 5.7 B**). Interestingly, mouse Mx1 induction alone did not reduce levels of RSV infection and 3pRNA stimulation of Mx1-induced cells did not result in further reduction in levels of RSV infection to significant levels (**Figure 5.7 B, right panel**). Together, these data confirm that

inducible mouse Mx1 is a potent antiviral protein against IAV HKx31, but not RSV Long, in LA-4 cells.

Given the success of the inducible system in studying mouse Mx1 in LA-4 cells, we attempted to generate A549 and FRL cell lines with DOX-inducible expression of human and ferret Mx proteins, respectively. However, following lentivirus transduction of A549 cells (with human MxA or cOVA) or FRL cells (with ferret Mx1.1, 1.2 or 2, or cOVA) we observed very low infection rates of untreated/uninduced cell lines by IAV and/or RSV. Moreover, following 3pRNA treatment ISG induction was greatly diminished and almost absent in some cell lines. Finally, DOX-inducible expression of human MxA, a known potent inhibitor of IAV infection (Xiao et al., 2013), in either A549 or FRL cells did not reduce the percentage of IAV-infected cells at 8 hrs post-infection (data not shown). The lack of anti-IAV activity using human MxA was particularly concerning. Overall, these studies suggested that the lentivirus transduction may have somehow altered the characteristics of the A549/FRL cells. Due to limited time towards the completion of the PhD, we considered alternative approaches to study the functionality of the ferret Mx proteins rather than repeat generation of these cell lines.

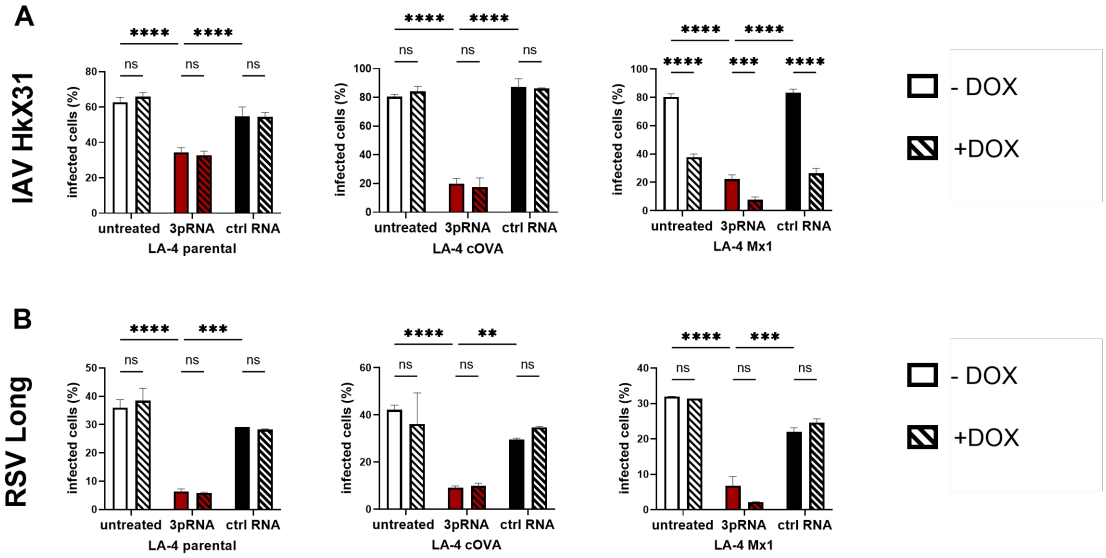

Figure 5.7: DOX-inducible overexpression of mouse Mx1 in LA-4 cells protects from IAV, but not RSV infection. LA-4 parental (i.e. not transduced) cells, or stable

LA-4 cells with DOX-inducible expression of cOVA or mouse Mx1 were transfected with 3pRNA (red bars) or ctrl RNA (black bars), each at 200 ng/mL, or untreated (white bars) 24 hrs prior to infection. After transfection, cells were cultured overnight with media with (striped) or without (solid) 1 µg/mL DOX. **A)** Cells were infected with IAV HKx31 (H3N2, MOI = 10) for 1 hr at 37°C, washed, and incubated an additional 7 hrs. Cells were fixed and stained for intracellular IAV NP and analysed by flow cytometry at 8 hpi. **B)** Cells were infected with RSV Long-GFP (MOI = 1) for 1 hr at 37°C, washed, and incubated an additional 17 hrs. Cells were fixed and analysed by flow cytometry at 18 hpi. Data shown are representative from at least 2 independent experiments. Data represent the mean ± SD (n=3). A two-way ANOVA with Bonferroni's correction was performed to compare 3pRNA treatment to ctrl RNA treatment or untreated conditions and to compare Doxycycline treatment to uninduced condition. ** = $p<0.01$; *** = $p<0.001$; **** = $p<0.0001$; ns = not significant.

5.2.7 Investigating the utility of a constitutive overexpression system to study the antiviral function of ferret Mx proteins in 293T cells

Given the utility of pcDNA3.1 vectors to generate high levels of protein expression in cells containing the SV40 T antigen (Takebe et al., 1988), we next cloned human MxA, mouse Mx1/2 and ferret Mx1.1, 1.2 and 2 into a pcDNA3.1 vector with constitutive expression of mCherry and a resistance marker for hygromycin selection. Note that all inserts contained a N-terminal FLAG tag to monitor protein expression. cOVA lacking a FLAG tag was included as a negative control. 293T cells were used for the following experiments as they exhibit high transfection efficiency and express exogenous proteins at high levels following transfection with pcDNA3.1 vectors.

Following transfection of 293T cells and culture in the presence of hygromycin, mCherry+ cells were enriched by two rounds of cell sorting before use in subsequent experiments. Stable expression of vectors encoding individual ferret, mouse or human proteins (or cOVA controls) was confirmed by monitoring mCherry expression over at least 8 passages (data not shown).

First, we performed flow cytometry to assess intracellular expression of FLAG-tagged proteins. We detected high mCherry expression in all cell lines generated, ranging from ~87 % in mouse (m)Mx2 to ~98 % in cOVA cells (**Figure 5.8**). With the exception of the cOVA cell line, the high mCherry expression correlated with high levels of intracellular FLAG staining with FLAG/mCherry double-positive cells ranging from ~86 % in mMx2 to ~98 % in mMx1 cells. Overall, these studies confirmed high levels of expression of FLAG-tagged ferret, mouse and human Mx proteins.

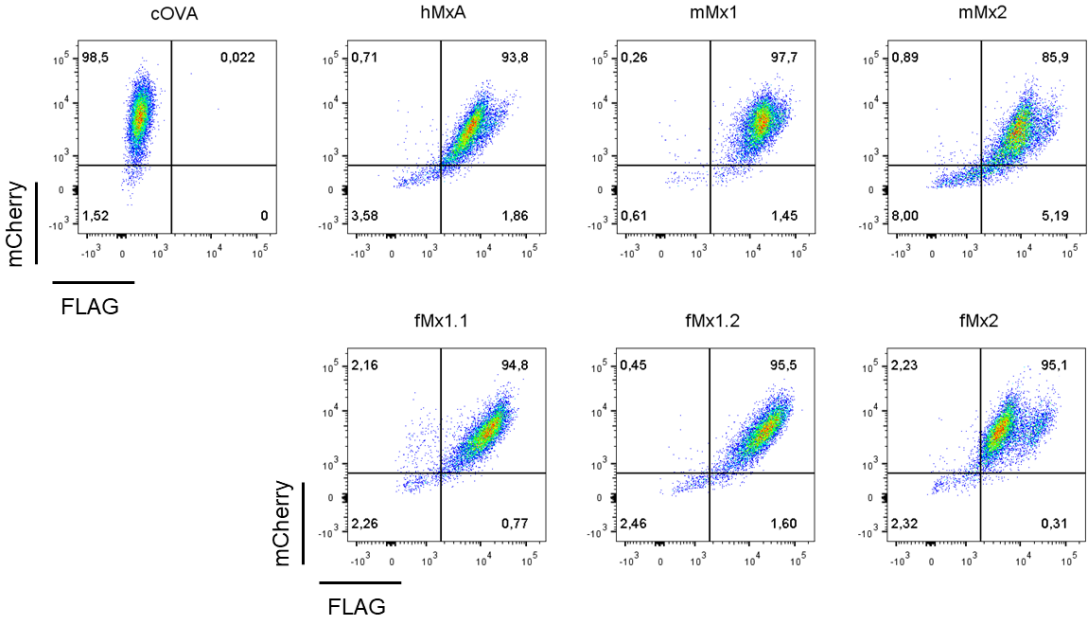

Figure 5.8: mCherry and FLAG-tagged protein expression in stably transfected 293T cells following selection in hygromycin and enrichment by cell sorting. 293T cells transfected with pcDNA3.1 plasmids expressing ferret (f)Mx1.1, (f)Mx1.2 or (f)Mx2, mouse (m)Mx1 or (m)Mx2, or human(h) MxA, each with a N-terminal FLAG tag were cultured in the presence of hygromycin and enriched for mCherry expression by two rounds of cell sorting, as described in Materials and Methods. Cells transfected with cOVA lacking a FLAG tag were included as a control. Cells were fixed, permeabilised and stained for intracellular expression of FLAG-tagged protein and analysed by flow cytometry. Representative dot plots of each cell line are shown.

5.2.8 Overexpression of mouse Mx1 and human MxA, but not ferret Mx proteins, in 293T cells inhibits IAV infection and growth

Next, we assessed IAV infection and growth in cell lines overexpressing individual Mx proteins. For these studies, cells were infected with IAV HKx31 (MOI = 2) for 1 hr at 37°C and the percentage of IAV-infected cells was determined by flow cytometry at 8 hpi. As seen in **Figure 5.9 A**, compared to cOVA control cells, IAV infection was potently and significantly inhibited by both human MxA and mouse Mx1, consistent with their known activity as potent inhibitors of IAV infection. Of note, the antiviral effect of human MxA and mouse Mx1 was also evident against a strain of H1N1pdm09 virus (data not shown). Mouse Mx2 did not inhibit IAV infection, also consistent with previous studies (Jin et al., 2001). These results were encouraging and provided confidence that our overexpression system represented a robust approach to study functional Mx1 proteins. However, we were surprised that none of the ferret Mx proteins inhibited IAV infection under experimental conditions where both mouse Mx1 and human MxA did (**Figure 5.9 A**).

To determine if Mx protein expression could affect virus growth, cells were infected with IAV HKx31 (MOI = 2.5) for 1 hr at 37°C and supernatants were harvested at 2 hpi (to determine residual virus) and at 24 hpi (to determine increase in virus titres). Of note, exogenous trypsin was not included in culture media allowing for the assessment of virus titres following a single cycle of infection. Consistent with infection data, human MxA and mouse Mx1 were potent inhibitors of IAV growth, whereas mouse Mx2 was not (**Figure 5.9 B**). Interestingly, none of the ferret Mx proteins had a major impact on IAV release at 24 hrs, indicating that ferret Mx proteins do not exhibit anti-IAV activity, at least when overexpressed in 293T cells. We also determined the fold change in viral titre by comparing titres at 2 hrs vs 24 hrs, confirming potent inhibition of IAV only by human MxA or mouse Mx1 (**Figure 5.9 B**).

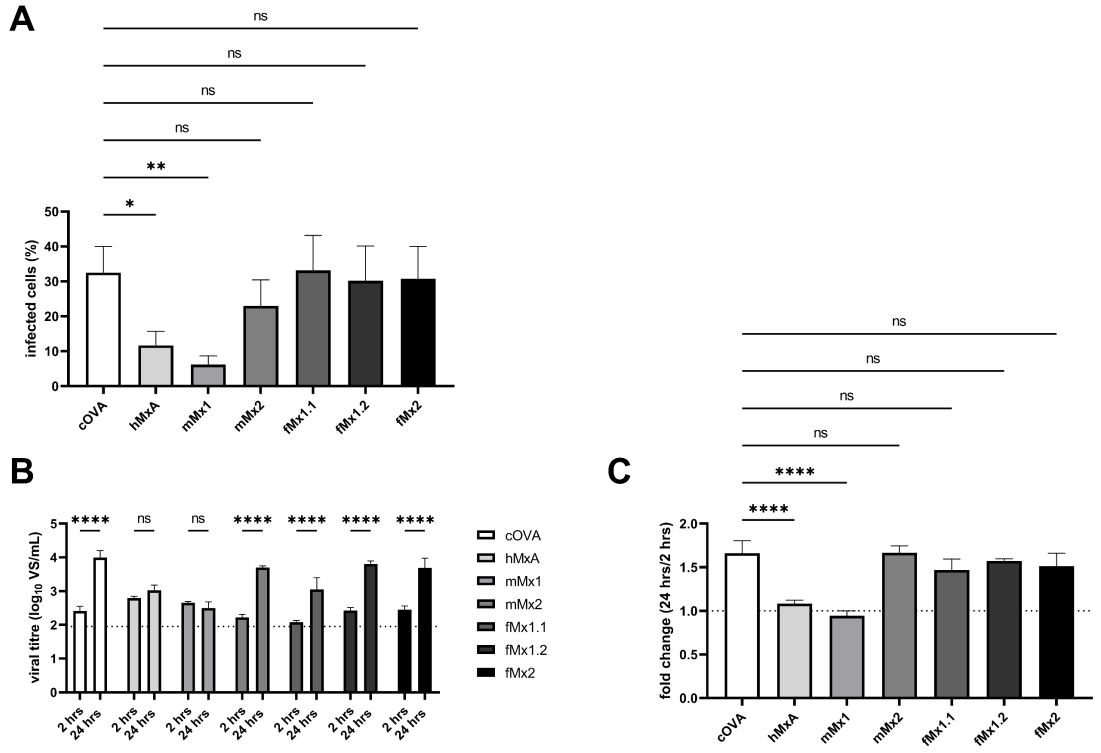

Figure 5.9: Expression of human MxA and mouse Mx1, but not ferret Mx proteins, in 293T cells results in inhibition of IAV infection and replication. 293T cells overexpressing cOVA, mouse Mx1 (mMx1), mouse Mx2 (mMx2), human MxA (hMxA), ferret Mx1.1 (fMx1.1), ferret Mx1.2 (fMx1.2) or ferret Mx2 (fMx2) protein were generated. **A)** Cells were inoculated for 1 hr at 37°C with IAV HKx31 (MOI = 2) and incubated an additional 7 hrs, fixed and the percentage of IAV-infected cells was determined by flow cytometry. **B)** Cells were inoculated for 1 hr at 37°C with IAV HKx31 (MOI = 2.5). Supernatants were harvested at 2 hpi and 24 hpi and titres of infectious virus were determined in clarified supernatants using a VS assay on MDCK cells. The dashed line represents the limit of detection. **C)** Fold change in virus growth from B) was determined by comparing titres after 24 hrs to residual virus after 2 hrs. Data show the mean (± SD) from triplicate samples and are representative of 2 or more independent experiments. A one-way ANOVA was used in A) and C) to assess viral infection or growth in all cell lines compared to cOVA and in B) a two-way ANOVA with Bonferroni's correction was used to compare viral titres after 2 hrs to 24 hrs. * = $p<0.05$; ** = $p<0.01$; **** = $p<0.0001$; ns = not significant.

5.2.9 Overexpression of different mammalian Mx proteins in 293T cells did not inhibit RSV growth

Having confirmed the utility of the 293T overexpression system using mouse Mx1 and human MxA to demonstrate inhibition of IAV, we next wanted to assess if Mx protein could affect RSV infection and virus growth. Cells were infected with RSV Long-GFP (MOI = 0.8) for 1 hr at 37°C and the percentage of RSV-infected cells was determined by flow cytometry at 18 hpi. As seen in **Figure 5.10 A**, RSV infection was not inhibited but was actually increased in cells expressing either human MxA or mouse Mx1 when compared to cOVA control cells. While increased infection was surprising (and could be investigated further in repeat experiments), our results are certainly consistent with others that indicate that neither human MxA nor mouse Mx1 display antiviral activity against RSV (Atreya et al., 1999). In these experiments, neither mouse Mx2, nor any of the ferret Mx proteins (Mx1.1, Mx1.2 or Mx2), inhibited RSV infection significantly compared to cOVA control cells.

To determine if Mx proteins inhibit RSV growth, cells were infected with RSV Long (MOI = 1) for 1 hr at 37°C and supernatants were harvested at 2 hpi and at 48 hpi. When examining virus growth, neither human MxA or mouse Mx1 inhibited RSV growth to a significant degree. Consistent with infection data, neither mouse Mx2 nor any of the ferret Mx proteins impacted RSV release at 48 hpi (**Figure 5.10 B**). Comparison of titres at 2 hpi vs 48 hpi to determine fold change in virus titre confirmed no significant inhibition of RSV growth by any of the Mx proteins studied (**Figure 5.10 C**).

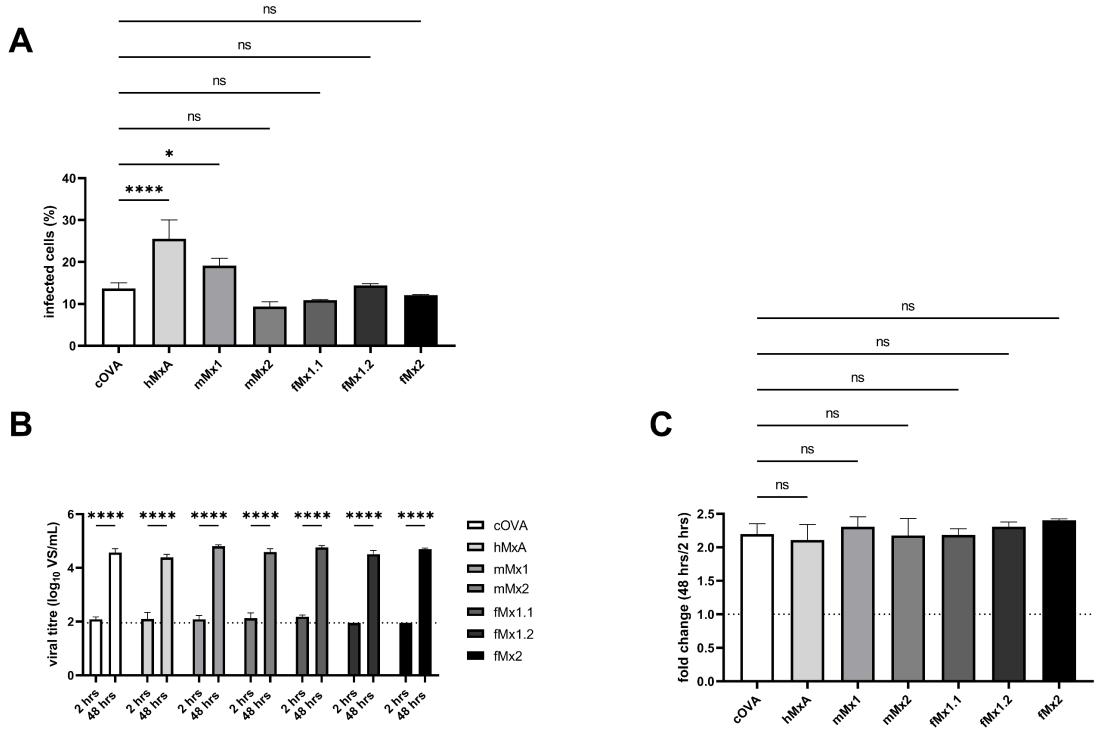

Figure 5.10: Expression of ferret Mx proteins does not inhibit RSV infection and replication in 293T cells. 293T cells overexpressing cOVA, mouse Mx1 (mMx1), mouse Mx2 (mMx2), human MxA (hMxA), ferret Mx1.1 (fMx1.1), ferret Mx1.2 (fMx1.2) or ferret Mx2 (fMx2) proteins were generated. **A)** Cells were inoculated for 1 hr at 37°C with RSV Long-GFP (MOI = 0.8) and incubated an additional 17 hrs, fixed and the percentage of RSV-infected cells was determined by flow cytometry. **B)** Cells were inoculated for 1 hr at 37°C with RSV Long (MOI = 1). Supernatants were harvested at 2 hpi and 48 hpi and titres of infectious virus were determined in clarified supernatants using a VS assay on HEp-2 cells. The dashed line represents the limit of detection. **C)** Fold change in virus growth from B) was determined by comparing titres after 48 hrs to residual virus after 2 hrs. Data show the mean (± SD) from triplicate samples and are representative of 2 or more independent experiments. A one-way ANOVA was used in A) and C) to assess viral infection or growth in all cell lines compared to cOVA and in B) a two-way ANOVA with Bonferroni's correction was used to compare viral titres after 2 hrs to 48 hrs. * = $p<0.05$; **** = $p<0.0001$; ns = not significant.

5.2.10 Preliminary characterisation of FRL cell lines that overexpress individual ferret Mx proteins

Evidence indicates that anti-IAV activity of MxA relies on additional cellular factors such as UAP 56, URH49 and/or the SMARCA2 chromatin remodelling factor (Wisskirchen et al., 2011a; Wisskirchen et al., 2011b; Dornfeld et al., 2018). We hypothesised that the lack of antiviral activity of overexpressed ferret Mx in 293T cells might result from incompatibility with particular human cellular proteins that are required to exert antiviral activity. Therefore, we generated ferret FRL cells with constitutive expression of ferret Mx1.1, Mx1.2 and Mx2, as well as human MxA and cOVA, using the pcDNA3.1 expression plasmid described above.

Following transfection of FRL cells and culture in the presence of hygromycin, mCherry+ cells were enriched by two rounds of cell sorting and expression of individual ferret or human proteins (or cOVA controls) was assessed by analysing mCherry expression. As seen in **Figure 5.11 A**, mCherry expression for all cell lines was >95 %. Due to time constraints, we only performed preliminary infection experiments and will use these cell lines in future studies to assess viral replication.

FRL cells overexpressing ferret or human Mx proteins, or cOVA, were infected with IAV HKx31 (MOI = 5) or RSV Long (MOI = 1) for 1 hr at 37°C and the percentage of infected cells was determined by flow cytometry at 8 hpi or 18 hpi, respectively. As seen in **Figure 5.11 B**, the percentage of IAV-infected cells was significantly reduced in FRL cells overexpressing ferret Mx1.2 and Mx2 when compared to cOVA expressing cells, while ferret Mx1.1 and human MxA did not reduce IAV infection. The result with human MxA was surprising, as this protein inhibited IAV when stably overexpressed in 293T cells (**Figure 5.9**). During RSV infection, ferret Mx1.1 expression resulted in a modest increase in the percentage of infected cells, while expression of ferret Mx2 and human MxA resulted in reductions, noting that the changes observed were more modest when compared to IAV (**Figure 5.11 C**). Unfortunately, these studies could not be pursued further due to lack of time, however they suggest that ferret Mx1.2 may exhibit some antiviral activity which could be explored further in subsequent studies. Of

interest, ferret Mx1.2 is also the predominant ferret Mx upregulated in response to RIG-I agonists (**Figure 5.5 D**).

Thus, these preliminary results suggest that one or more ferret Mx proteins may show some potential to mediate antiviral activity against IAV and RSV when overexpressed in ferret cells.

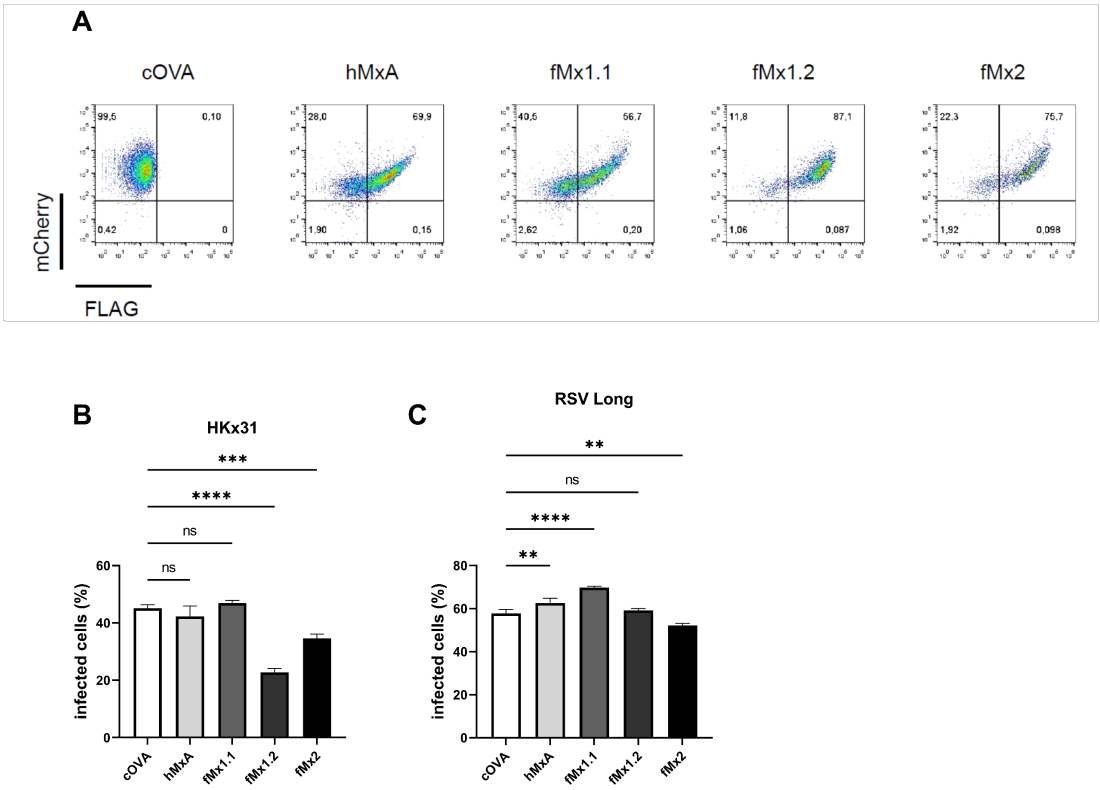

Figure 5.11: Expression of specific ferret Mx proteins can inhibit IAV and RSV infection of ferret FRL cells. FRL cells overexpressing cOVA, human MxA (hMxA), ferret Mx1.1 (fMx1.1), ferret Mx1.2 (fMx1.2) or ferret Mx2 (fMx2) protein were generated. **A)** Cells were stained for intracellular FLAG expression and analysed by flow cytometry. Dot plots show FLAG and mCherry expression for each cell line. **B)** FRL cells were inoculated for 1 hr at 37°C with IAV HKx31 (MOI = 5), incubated an additional 7 hrs, fixed and the percentage of IAV-infected cells was determined by flow cytometry. **C)** FRL cells were inoculated for 1 hr at 37°C with RSV Long (MOI = 1), incubated an additional 17 hrs, fixed and the percentage of RSV-infected cells was determined by flow cytometry. Data show the mean (± SD) from triplicate samples. A one-way ANOVA with Bonferroni's correction was used in B) and C) to assess viral infection in all cell lines compared to cOVA. ** = $p<0.01$; *** = $p<0.001$; **** = $p<0.0001$; ns = not significant.

5.3 Discussion

Mx proteins from different species have been shown to mediate antiviral activity against a range of viruses. In some cases, the antiviral functions of Mx proteins are conserved between species, however other studies suggest considerable inter-species variation. As (to our knowledge) ferret Mx proteins have not been investigated and reported, studies in this chapter aimed to characterise ferret Mx proteins by assessing their expression and induction, cellular localisation and antiviral function against IAV and RSV.

As for most mammals, ferrets express two variants of Mx, namely Mx1 and Mx2, with Mx1 expressed as two splice variants, Mx1.1 and Mx1.2. Phylogenetic analysis revealed that ferret Mx1 clusters to the Mx1 lineage whereas ferret Mx2 clustered to the Mx2 lineage (**Figure 5.2 A**). Within the Mx lineages, ferret Mx were most closely related to Mx from brown bear, walrus and dog and more distantly related to human Mx proteins, however this is not surprising because ferret, bear, walrus and dog all belong to the suborder of *caniformia* (Flynn et al., 2005). Mouse Mx proteins formed a distinct lineage in our analyses, as reported by others (Verhelst et al., 2013). While few other studies have assessed the phylogeny of ferret ISG proteins, a recent report indicated that ferret IFITM1, IFITM2 and IFITM3 showed greatest protein sequence homology to pig IFITMs, however, no member of *caniformia* such as bear, walrus or dog IFITMs were included in the study (Horman et al., 2021). In our analysis, sequence homology of ferret Mx1 to pig Mx1 is comparable to that of human Mx1 and similar is true for homologies in the Mx2 lineage. Our analyses of the predicted protein sequences of ferret Mx also confirmed specific signature sequences required for Mx activity were conserved (**Figure 5.1**), consistent with the potential for one or more ferret Mx to exhibit some form of antiviral function.

When analysing expression of splice variants Mx1.1 and Mx1.2, pre-treatment of FRL cells with RIG-I agonist induced splice variant Mx1.2 to much higher levels compared to Mx1.1. This was observed following sequencing of the Mx1 gene product amplified (using generic Mx1 primers) from the mRNA of 3pRNA-treated FRL cells as only nucleotides corresponding to the Mx1.2 variant were detected

in the amplified product (**Figure 5.4 B**). Moreover, qRT-PCR using specific primers to amplify either Mx1.1 or Mx1.2 indicated that Mx1.2 was induced to much higher levels following pre-treatment of cells with either IFN-α or RIG-I agonist (**Figure 5.5**). Further BLAST analyses indicate that the 36 bp sequence expressed in ferret Mx1.1, but not 1.2, has also been described in the Mx1 transcript variant X3 from sea otters (NCBI: XM_022516028.1) but not from any other species, indicating that this variant is not well conserved and therefore may not fulfil an essential function such as antiviral activity to promote its selection during evolution. A BLAST search for the 23 bp sequence in ferret Mx1.1, but not Mx 1.2, yielded ambiguous results perhaps due to the short nucleotide sequence. 3'-RNA sequencing confirmed upregulation of ferret Mx1 and Mx2 transcription levels in response to pre-treatment with IFN-α or RIG-I agonist, however it was not possible to distinguish Mx1.1 and Mx1.2 splice variants from this analysis (**Figure 5.3**).

We have shown that Mx1.2 appears to be preferably transcribed over Mx1.1 after RIG-I stimulation of FRL cells. However, it is well established that mRNA levels do not necessarily correlate to protein levels for a number of reasons including variation in the translational efficiency between different mRNA transcripts. It would be interesting to assess protein expression levels of ferret Mx1.1 and Mx1.2, which could be done in future studies if antibodies to other mammalian Mx proteins were suitably cross-reactive with the ferret Mx. Of interest, studies from van Riel *et al.* used a mouse monoclonal antibody (mAb) to detect cytoplasmic expression of MxA in lung tissue from IAV H5N1-infected human, macaque, cats and ferrets (van Riel et al., 2013). This confirms the utility of cross-reactive antibody reagents for such studies. To confirm the expression as well as molecular weight of individual overexpressed ferret Mx proteins in our system of FRL or 293T cells, it would also be of use to perform western blot using an anti-FLAG mAb.

An important caveat to our studies is that we performed relative qRT-PCR analysis and did not assess absolute expression of ferret Mx mRNA transcripts. Although our findings suggest that absolute expression of splice variant Mx1.2 is

higher than Mx1.1, it is important to consider that the efficiency of different qRT-PCR reactions will differ due to primer quality and other factors. Use of control plasmids to generate a standard curve for ferret Mx1.1, Mx1.2 and Mx2 represents an alternate approach to gain insights regarding the copy number of each ferret Mx transcript following treatment with IFN-α or RIG-I agonist or after virus infection. Another option to assess relative expression of different splice variants might be advanced qRT-PCR analysis using internal control primers present in both splice variants, as well as variant-specific primers in the one qRT-PCR reaction (Camacho Londoño et al., 2016).

Alternative splicing is a complicated but essential mechanism to increase complexity of gene expression and to regulate cellular processes (Wang et al., 2015). In humans, 95 % of multi-exon genes undergo alternative splicing although the significance of alternative splicing is still largely unknown (Skandalis et al., 2010). One study of particular interest showed that IFN-α treatment of human fibroblasts resulted in expression of a 76 kDa cytoplasmic MxA protein which mediated antiviral activity against HSV-1 (Ku et al., 2011). However, HSV-1 infection resulted in induction of an alternatively spliced variant of 56 kDa (with a deletion of exon 14-16 and a frameshift mutation) that was expressed in the nucleus and appeared to actually enhance HSV-1 replication. The authors proposed that expression of the alternatively spliced variant represents a mechanism to evade host-mediated immune responses (Ku et al., 2011). Based on our overexpression studies to date, the antiviral function of ferret Mx1.1 compared to Mx1.2 are not clear although our preliminary experiments suggest that they may differ in regards to their antiviral function at least against IAV and RSV (**Figure 5.11**). Refinement of our overexpression studies in FRL cells, combined with confirmation using the DOX-inducible system for each ferret Mx in FRL cells, represent approaches that could be used to confirm antiviral activity of ferret Mx proteins. Additionally, shRNA knockdown or CRISPR/Cas9 deletion methods could be used to confirm antiviral activity of endogenous ferret Mx1 and Mx2, but would not distinguish between the activity of the different Mx1 variants.

Transfection of A549 cells with pcDNA3.1 plasmids expressing ferret Mx proteins confirmed that Mx1.1, Mx1.2 and Mx2 were expressed exclusively in the cytoplasmic compartment (**Figure 5.6**). This is in line with a study from van Riel *et al.* who used a cross-reactive mouse mAb to detect MxA in the cytoplasm of lung cells from IAV H5N1-infected ferrets (van Riel et al., 2013). Nuclear transport is often dependent on the importin-protein family and we did not detect evidence of importin-specific NLS within ferret Mx1 and Mx2. However, future studies will confirm the localisation of each ferret Mx following ectopic expression in FRL cells to exclude any possibility of incompatibility between human cellular proteins and ferret Mx which might impact their localisation.

Studies in this chapter utilised a number of approaches to investigate if different ferret Mx could mediate antiviral activity against IAV or RSV. We validated a DOX-inducible Tet-On system for inducible expression of mouse Mx1 in mouse LA-4 cells however we were unable to generate stable FRL or A549 cell lines with DOX-inducible expression of ferret Mx proteins and speculate that the lentivirus transduction may have had unwanted effects on the cells in regard to ISG expression and susceptibility to virus infection.

Given that the same plasmids and experimental protocols were used to generate LA-4 cells with inducible mouse Mx1 expression we would suggest that rather than aberrant lentiviral integration into FRL and A549 cells or some form of underlying contamination might have led to these surprising results, although mycoplasma contamination was excluded by PCR analysis and culture of cells in antibiotic-free media did not result in amplification of bacterial contamination over time. While the usage of lentiviral vectors is a useful tool for stable integration and delivery of genes into host cells, this technique still bears obstacles as seen in our studies. Other groups such as Huang *et al.* have also reported that lentiviral transduction of shRNA non-specifically inhibited HCV infection in human hepatoma cells which was induced by a dysregulation of host miRNA (Huang et al., 2018). Although we lack experimental proof it is possible that similar effects resulted in significant alterations of the characteristics of A549 and FRL cells used in our studies.

We believe this approach will be an important one to confirm antiviral activity of ferret Mx in FRL cells in future studies and has recently been used by our group to investigate the antiviral activity of human IFITM proteins against IAV and parainfluenza viruses (Meischel et al., 2021).

Due to time limitations, we instead generated FRL and 293T cells with constitutive expression of Mx proteins. In contrast to DOX-inducible expression where protein expression is tightly regulated and for IFITM proteins has been shown to reach maximum levels comparable with those of the endogenous protein induced by type I IFNs (Meischel et al., 2021), constitutive expression can result in much higher levels of protein expression and continual protein expression might alter other cellular characteristics over time. Given that expression of ferret Mx proteins is regulated by type I and III IFNs an inducible-expression system would have been preferable however constitutive overexpression systems have been widely used to gain insights regarding Mx and other ISG proteins (Villalon-Letelier et al., 2017). A particularly elegant approach to study human MxA was described by Deeg *et al.* who generated a mouse strain with expression of human MxA under an interferon-stimulated response element (ISRE), allowing for expression of MxA after IFN treatment (Deeg et al., 2017). Use of an ISRE-inducible expression system could be an option for future studies to assess the antiviral activity of ferret Mx. In addition to overexpression studies and as mentioned above, shRNA knockdown or CRISPR/Cas9 knockout would be complementary approaches to confirm the antiviral activity of endogenous ferret Mx1 and Mx2 and would be particularly informative in FRL cells in the presence or absence of pre-treatment with ferret IFN or RIG-I agonist.

When constitutively overexpressed in 293T cells, none of the ferret Mx reduced infection or replication of IAV (**Figure 5.9**) or RSV (**Figure 5.10**), noting that human MxA and mouse Mx1 both restricted IAV infection, confirming the functionality of our system (**Figure 5.9**). Interestingly, following constitutive overexpression of the same constructs in FRL cells, ferret Mx1.2 and Mx2 did appear to inhibit IAV infection (**Figure 5.11**). These preliminary studies were

performed at the completion of the PhD and will require additional repeats. While it is concerning that human MxA did not inhibit IAV when expressed in FRL cells, it is intriguing to consider if ferret Mx might inhibit IAV when overexpressed in ferret cells and how this fits in with other results described in this chapter. First, antiviral activity of Mx1.2, but not Mx1.1, against IAV would correlate with preferred induction and expression of Mx1.2 in FRL cells and raises questions as to whether ferret Mx1.1 possesses antiviral function at all or if it is a poorly expressed splice variant with an alternate function. Additional experiments could assess the breadth of antiviral activity of the different ferret Mx against other viruses known to be inhibited by Mx from other species (e.g. VSV, HBV or herpesviruses, amongst others). Second, our results would suggest that ferret Mx proteins are only antiviral when expressed in ferret cells. Similarly, at face value human MxA exhibits anti-IAV activity following overexpression in human, but not ferret cells. Previous studies have indicated that some Mx proteins exhibit species-specific antiviral functions although this is determined more by features of the Mx proteins themselves rather than the cell species they are expressed in. For example, human MxB is antiviral against HIV-1 when expressed in the nucleus and a short isoform expressed in the cytoplasm does not inhibit HIV-1 while engineering the 91-residue N-terminal sequence of MxB onto human MxA targets expression to the nuclear envelope resulting in inhibition of HIV-1 (Goujon et al., 2014). However, human MxB has no activity against non-primate lentiviruses such as equine infectious anemia virus (EIAV) (Goujon et al., 2013; Kane et al., 2013; Goujon et al., 2014) whereas equine Mx2 restricts both HIV-1 and EIAV (Ji et al., 2018; Meier et al., 2018). Moreover, when the N-terminus of human MxB is substituted onto equine Mx2 its antiviral activity against EIAV is lost, confirming the requirement of the native N-terminus for the antiviral activity of equine Mx2 against this equine virus. Clearly, further controlled studies are required to confirm the antiviral activities of different ferret Mx and to resolve some of the confounding issues associated with our overexpression studies in human and ferret cell lines. Resolving the functionality of different ferret Mx in human and ferret cells is critical, as well as determining their spectrum of antiviral activity against human viruses used in the ferret model (e.g. IAV, RSV, HMPV),

but also viruses associated with natural infection of ferrets (e.g. canine distemper virus (Ludlow et al., 2014), ferret enteric coronavirus or ferret systemic coronavirus (Haake et al., 2020)).

Finally, after establishing a robust experimental system to study ferret Mx, it will be of interest to assess their antiviral activity against different IAV. Our preliminary studies have used HKx31, a reassortant of A/Aichi/2/68 (H3N2) with PR8, bearing the H3N2 surface glycoproteins, which is widely used for studies in mice by virtue of expressing the internal proteins of the mouse-adapted PR8 strain. However, the antiviral function of human MxA is more potent against non-human derived IAV and most human strains of IAV expressed 'MxA escape mutations' in the viral NP (Haller et al., 2020). Similarly, equine Mx1 restricts IAV of non-equine species whereas equine IAV, including certain H3N8 and H7N9 strains, also express mutations in the viral NP to escape restriction by equine Mx1 (Fatima et al., 2019). With a robust system in place to assess the anti-IAV activity of ferret Mx, it would be of interest to see if IAV strains with escape mutations against human MxA and/or equine Mx1 still remain sensitive to ferret Mx. Given the well-established role of human and mouse Mx proteins against IAV, understanding the antiviral activity of different Mx against human IAV is of particular importance, given the widespread use of this animal model to study human IAV infections.

6 Chapter: Overall Discussion

In late 2019, a novel severe acute respiratory syndrome coronavirus (SARS-CoV)-2 emerged from China and spread in the human population, resulting in a global pandemic of the disease known as COVID-19 (Felsenstein et al., 2020). As of July 20th 2021, more than 190 million cases and over 4 million fatalities have been associated with COVID-19. Although coronaviruses have previously crossed species barriers to infect humans, such as the SARS-CoV-1 outbreak in 2003/2004 and the Middle Eastern respiratory syndrome coronavirus (MERS-CoV) outbreak in 2012, treatment options against coronaviruses are currently limited and mainly consist of supportive care (Sanders et al., 2020). Moreover, historically IAVs have been responsible for the majority of pandemics in the human population and a range of additional viruses are also associated with respiratory disease and represent a significant burden to human health. Thus, there is the urgent need to develop new and broad-spectrum antiviral treatments, particularly against respiratory viruses.

In this thesis, we evaluated and characterised the antiviral effects of RIG-I agonists in mammalian cell culture, as well as in mouse and ferret models of IAV and RSV infection. Our studies demonstrate that prophylactic treatment of human, mouse and ferret airway cells with 3pRNAs *in vitro* resulted in protection from subsequent IAV and RSV infection. This protection was associated with induction of multiple ISGs in each cell type and with reduced levels of virus infection (determined by flow cytometry) and virus growth. We also translated our *in vitro* findings to different *in vivo* settings, demonstrating that a single prophylactic, i.v. injection of 3pRNA prior to IAV or RSV infection of mice or ferrets resulted in significant protection, particularly in regard to reduced virus growth in the lower respiratory tract of infected animals. In the mouse model, we confirmed that potent and long-lasting 3pRNA-mediated protection against IAV infection was dependent on the expression of a functional Mx1 protein. Additional studies have been described which investigate the induction and antiviral activity of ferret Mx proteins.

6.1 RIG-I agonists as antivirals against respiratory virus infections

Respiratory infections caused by IAV and RSV lead to a substantial global burden and are associated with high mortality and morbidity rates, especially among risk groups such as the elderly.

Therapeutic agents against IAV such as NAIs or polymerase inhibitors have been shown to efficiently reduce the duration of clinical symptoms however they have to be administered early after onset of symptoms and are limited in their effectiveness due to emerging viruses with reduced sensitivity to NAIs (Hurt et al., 2009; Davidson, 2018; Shirley, 2020). To date, vaccines represent the best prophylactic agent to prevent and ameliorate infection however vaccine effectiveness can be impacted by different factors such as age or previous influenza exposure (Radin et al., 2016). Moreover, vaccines have to be administered yearly due to the constant accumulation of mutation within HA and NA. Additionally, the generation of a new vaccine requires several months of preparation, which contradicts its usage against emerging pandemic IAVs.

In contrast, there are no licenced vaccines available for RSV although intense development of RSV vaccine candidates have recently shown promising results (Shan et al., 2021). There are two FDA-approved antiviral drugs, aerosolized ribavirin and pavilizumab, an guanosine-nucleoside analogue and monoclonal antibodies targeting RSV, respectively, however high costs associated with treatment and possible side effects have limited widespread use (Hu et al., 2010; Homaira et al., 2014; Olchanski et al., 2018).

While most of current drug discovery landscape aimed to design inhibitors specific to target IAV or RSV components itself, host-directed therapies such as RLR activation results in a stimulation of host immunity and an induction of an antiviral state independent on the specific virus. This makes it a promising treatment option especially against newly emerging viruses without pre-existing immunity in the population.

We used airway cells from humans, mice and ferrets to demonstrate conservation of the RIG-I signaling pathway across different species. It was evident that 3pRNA, but not ctrl RNA treatment, resulted in ISG induction in cells from each species, and this correlated with 3pRNA-mediated inhibition of virus infection and growth following subsequent challenge with IAV or RSV.

In silico analyses detected the DExD/H-containing RNA helicases RIG-I, MDA5 and LGP2 in the genome of different vertebrates and invertebrates and confirmed a high level of conservation (Zou et al., 2009). Of interest, RIG-I appears to be absent in chickens and Baber *et al*. suggested that this might provide a plausible explanation for the increased susceptibility of chickens to HPAI (Barber et al., 2010). However, subsequent studies showed that in chickens, IAV infection is sensed by MDA5 rather than by RIG-I and that this results in IFN-β induction (Karpala et al., 2011; Liniger et al., 2012), although knockdown of chicken MDA5 or induction of chicken IFN-β did not appear to affect HPAI replication (Karpala et al., 2011; Hayashi et al., 2014). Chicken MDA5 has been shown to preferentially sense short poly(I:C) instead of the longer RNA sequences typically detected by mammalian MDA5, providing another hint that the function of chicken MDA5 may have evolved to compensate for the loss of RIG-I (Hayashi et al., 2014).

In general terms, RLRs broadly function as an intracellular virus surveillance system although the function of RIG-I and MDA5 can show marked differences in different species. To further define specific roles of MDA5 and RIG-I, gene knockout approaches (e.g. CRISPR/Cas9) are preferable over gene knockdowns using RNAi because knockdowns can result in only a partial loss of gene expression, whereas knockouts generate a stable cell lines which do not express the gene of interest. However, in our studies the generation of CRISPR/Cas9 knockouts in mouse and ferret airway cells has been proven to be challenging largely due to characteristics of the particular cell lines. In the case of mouse LA-4 cells, the polyploid and unstable karyotype has been a major issue to generate stable knockout cell lines. Attempts to utilise CRISPR/Cas9 to delete RIG-I in

ferret FRL cells failed mainly due to high levels of cell death and poor cell recovery following electroporation. Given these issues, we generated RIG-I knockdown cells and were able to demonstrate that 3pRNA-mediated protection against IAV and RSV was significantly reduced in RIG-I knockdown cells (**Figure 4.4**). While CRISPR/Cas9 in FRL cells would seem an obvious approach to assess the role of endogenous ferret Mx1 and Mx2 against IAV and RSV infections in the future, our experience with attempting to knockout RIG-I from FRL cells suggests this should be approached with caution.

RIG-I agonist pre-treatment of human, mouse and ferret cells resulted in protection against subsequent infection by viruses from two distinct families, namely *Orthomyxoviridae* (IAV) or *Pneumoviridae* (RSV). These viruses were chosen for a number of reasons including (i) both represent a significant burden to human health (Ackerson et al., 2019), (ii) both can be studied in mouse and ferret models of infection (Taylor, 2017; Hemmink et al., 2018), and (iii) these viruses utilise very different strategies to replicate within host cells (Ascough et al., 2018). In terms of the latter point, IAV replicates within the nucleus, while RSV replicates exclusively within the cytoplasmic compartment, although RSV M protein has been reported to move between nuclear and cytoplasmic compartments at specific times during infection (Walker et al., 2017). IAV and RSV also show significant differences in terms of entry and exit pathways utilised in infected host cells (Dou et al., 2018; Hu et al., 2020). Despite these differences, our studies demonstrate that both infection (viral protein production following genomic replication, as detected by flow cytometry) and virus growth (release of infectious virus from infected cells) can be suppressed in human, mouse and ferret cells by pre-treatment with RIG-I agonists. These findings are consistent with other *in vitro* studies describing the ability of RIG-I agonists to inhibit VSV, vaccinia virus, HIV-1 and HCV (Goulet et al., 2013), CHIKV (Olagnier et al., 2014; Chiang et al., 2015), DENV (Goulet et al., 2013; Olagnier et al., 2014; Chiang et al., 2015) and IAV (Chakravarthy et al., 2010; Ranjan et al., 2010; Goulet et al., 2013; Chiang et al., 2015). Our studies are the first to demonstrate that RIG-I agonist treatment also reduces RSV infection and replication *in vitro*. Fewer studies have reported the effectiveness of RIG-I agonist treatment *in vivo*,

although mouse models have confirmed their protective role against IAV (Ranjan et al., 2010; Goulet et al., 2013; Chiang et al., 2015; Coch et al., 2017), SARS-CoV-2 (Mao et al., 2021; Marx et al., 2021) and CHIKV (Chiang et al., 2015). Our studies with IAV in mice have focused on determining the importance of a functional Mx1 in RIG-I agonist-mediated protection, moreover we are the first to report the effectiveness of this treatment against RSV in mice. In the ferret model of infection, our studies are the first to demonstrate the protective role of RIG-I agonists against both IAV and RSV.

Our *in vitro* and *in vivo* studies have focused on the effects of prophylactic RIG-I agonist treatment following transfection of mammalian cells or i.v. injection of mice and ferrets, prior to subsequent virus challenge. Preliminary *in vitro* studies examining the effectiveness of therapeutic RIG-I agonist treatment of A549 cells at various times after RSV infection did not yield evidence of significant protection (**Figure 4.1**). However, Chiang *et al.* showed that therapeutic administration of RIG-I agonists up to 4 hrs post-infection reduced levels of DENV and IAV infection in A549 cells and monocyte-derived dendritic cells, respectively, (Chiang et al., 2015). Olagnier *et al.* also described reduced replication of CHIKV if MRC-5 cells were treated with RIG-I agonists up to 5 hrs after infection (Olagnier et al., 2014) and Pattabhi *et al.* demonstrated that therapeutic treatment of RSV-infected HeLa cells with KIN1400, an activator for IRF3 signaling, also significantly reduced virus release (Pattabhi et al., 2015; Green et al., 2016). Thus, therapeutic effects of RIG-I agonists have been reported in several cell culture systems against different viruses. Clearly, further studies are required to assess the therapeutic effects of RIG-I agonist treatment against IAV and RSV in the *in vitro* models described in this thesis.

While we did not assess the utility of therapeutic RIG-I agonist treatment in mouse models of IAV or RSV, we did treat experimentally infected donor ferrets with RIG-I agonist at day 3 post-infection and found that this resulted in reduced viral titres in the lungs 2 days later (**Figure 3.9**). In mice, i.v. injection of B6.A2G-*Mx1* animals with RIG-I agonist 18 hrs after IAV infection protected them from the otherwise lethal virus challenge (Coch et al., 2017) and treatment of C57BL/6

mice lacking a functional Mx1 one day after IAV infection also provided some protection as reflected by reduced titres of infectious virus in the lung (Goulet et al., 2013). Recently, it was shown that therapeutic RIG-I agonist treatment in hACE2 *Rag*$^{-/-}$ mice deficient in T- and B-cell immunity reduced SARS-CoV-2 titres in lung tissue and resulted in complete clearance of infectious virus in 5/7 animals (Mao et al., 2021). When thinking about the most effective RIG-I agonist treatment regimen in mice and ferrets, a combination of prophylactic and therapeutic treatments may well prove optimal to reduce virus replication and virus-induced disease. Notably, Goulet *et al*. have already demonstrated that treatment of C57BL/6 mice one day prior to, as well as two days after IAV infection, resulted in reduced viral titres in the lung when compared to prophylactic treatment alone (Goulet et al., 2013). Thus, while studies described in this thesis have focused on prophylactic treatments to demonstrate the effectiveness of 3pRNA treatment against IAV and RSV, it is clearly of interest to explore its therapeutic potential in more detail in future studies.

6.2 The role of Mx proteins during RIG-I agonist-mediated protection

In the absence of 3pRNA treatment, we confirmed that mice expressing a functional Mx1 were much more resistant to IAV infection. This phenomenon is well established and has been widely reported (Haller et al., 1981; Arnheiter et al., 1990; Tumpey et al., 2007; Deeg et al., 2017). Expression of a functional Mx1 was critical for the potent and long-lasting effectiveness of RIG-I agonist treatment against IAV infection in mice. While Coch *et al*. used only B6.A2G-*Mx1* mice to demonstrate the prophylactic and therapeutic benefits of 3pRNA treatment against IAV infection (Coch et al., 2017), our studies focused on comparing 3pRNA treatment in mice which differed only in regard to expression of a functional Mx1.

Our *in vitro* studies demonstrated that in the absence of stimulation, primary fibroblasts from B6.A2G-*Mx1* mice expressed constitutively higher levels of ISGs such as IFIT1, ISG15 and Mx1 when compared to B6-WT mice (**Figure 3.2**).

In vivo, only Mx1 was expressed at higher levels in lung tissue from B6.A2G-*Mx1* mice and ISG15 levels were not significantly different between B6.A2G-*Mx1* and B6-WT mice (**Figure 3.4**). The reduced levels of Mx1 transcripts in B6-WT might relate to nonsense-mediated decay (NMD), a quality control mechanism in eukaryotic cells whereby mRNAs with premature termination codons are degraded (Chang et al., 2007). Mx1-deficient B6-WT mice have 424 nucleotides missing from the coding region of *Mx1*, resulting in a frame shift and premature termination of Mx transcripts (Staeheli et al., 1988). Aberrant mRNA transcripts with premature termination codons exhibit exon junction complexes (EJCs), protein complexes upstream of exon-exon junctions after RNA splicing, and these EJCs serve as signal to initiate NMD, resulting in reduced mRNA transcript levels (Matsuda et al., 2008). Thus, NMD is one possible explanation for the lower levels of endogenous Mx1 mRNA transcripts in B6-WT fibroblasts/mice when compared to B6.A2G-*Mx1* counterparts. *In vivo,* ISG15 mRNA levels were expressed to similar levels in B6-WT and B6.A2G-*Mx1* mice which would be consistent with NMD of aberrant Mx1 mRNA in B6-WT animals (**Figure 3.4**). However, *in vitro* we found that mRNA transcript levels of IFIT1 and ISG15 were also both enhanced in B6.A2G-*Mx1* fibroblasts and the reasons underlying these discrepancies are currently unclear.

It was surprising that RIG-I agonist treatment of B6.A2G-*Mx1* cells or mice did not enhance or prolong upregulation of ISGs, particularly Mx1, given their potent and long-lasting protection against IAV (**Figure 3.3 and Figure 3.4**). We hypothesise that rather than mRNA, it is Mx1 protein levels that might be critical for long-lasting protection against IAV. Unfortunately, we were unable to detect Mx1 by western blot in B6-WT or B6.A2G-*Mx1* fibroblasts using available antibodies, although different commercial antibodies could also be tested in future studies. The enhanced potency of RIG-I agonist treatment in B6.A2G-*Mx1* mice likely relates to upregulation of the potent antiviral Mx1 in these animals compared to upregulation of the non-functional protein in B6-WT mice, particularly likely given that we did not detect major differences in airway inflammation between the different mouse strains after RIG-I agonist treatment. As only a limited subset of ISGs were assessed in our studies, we cannot rule

out that the expression of functional Mx1 augments expression of other ISGs and other antiviral proteins and a broader ISG analysis would be beneficial in future studies.

Another interesting difference between the respiratory viruses used in our studies is that while it is well established that IAV is sensitive to both human MxA and mouse Mx1 (Tumpey et al., 2007; Deeg et al., 2017), there is no clear evidence that either protein mediates antiviral activity against RSV. This is of particular interest given the importance of Mx1 in the effectiveness of RIG-I agonist pre-treatment against IAV in the mouse model. To date, it has been reported that RSV is resistant to the antiviral effects of type I IFNs and human MxA *in vitro* (Atreya et al., 1999). These studies demonstrated that type I IFN pre-treatment of human A549 cells reduced growth of infectious RSV by only 5-10 % compared to untreated controls and this effect was lost if IFNs were applied to cells following infection. Moreover, Vero or human glioblastoma cells which were transfected to constitutively express human MxA remained equally susceptible to RSV infection. In our studies, we have used a number of approaches to investigate if mouse Mx1 can inhibit RSV, using IAV as a positive control with known sensitivity to this protein.

Using DOX-inducible overexpression of mouse Mx1 in LA-4 cells, we found that RSV infection was not restricted by Mx1, indicating that RSV is indeed resistant to Mx1 (**Figure 5.7**). Subsequent treatment with RIG-I agonists did not further reduce viral infection, indicating that RIG-I stimulation following DOX induction of Mx1 did not have additive effects in RSV restriction. Furthermore, following constitutive overexpression of mouse Mx1 and human MxA in 293T cells, both MxA and Mx1 potently inhibited IAV but had negligible effects on RSV infection and replication (**Figure 5.9 and Figure 5.10**). However, when assessing the effects of endogenous Mx1 using murine fibroblasts, cells from B6.A2G-*Mx1* cells (expressing functional Mx1) showed enhanced protection following RIG-I pre-treatment, although overall levels of RSV infection under ctrl conditions were higher in B6.A2G-*Mx1* fibroblasts compared to B6-WT cells (**Figure 4.2**). It is tempting to speculate that expression of a functional Mx1 in B6.A2G-*Mx1* mice

might contribute to the more potent RIG-I-mediated protection observed in these cells, however it is important to remember that DOX-inducible Mx1 did not mediate protection from RSV infection in LA-4 cells (**Figure 5.7**). In future studies, it would be interesting to assess if long-term RIG-I-mediated protection against RSV could be achieved in B6.A2G-*Mx1* fibroblasts or mice as was shown for IAV infection.

Expression of a functional Mx1 was critical for potent and long-lasting RIG-I agonist-mediated protection against IAV in the mouse model of infection. While i.v. RIG-I agonist pre-treatment of ferrets also reduced IAV replication in the lung, ferret Mx proteins have not been characterised to date, nor is it known if they mediate antiviral activity against IAV or other viruses. Phylogenetic analysis identified 3 potential ferret Mx proteins (Mx1.1, 1.2 and 2) which contained conserved Mx protein domains and showed similarity to other mammalian Mx proteins (**Figure 5.1 and Figure 5.2**). Moreover, we developed qRT-PCR to demonstrate that transcripts from each ferret Mx were induced following pre-treatment of FRL cells with ferret type I IFN or RIG-I agonist. Although we did not explicitly test induction in response to ferret IFN-λ, this is likely to occur given that both type I and type III IFNs are reported to induce Mx proteins from other species (**Figure 5.5**).

Initial studies using 3'-RNA sequencing in FRL cells indicated that ferret Mx1 and Mx2, amongst other ISGs, were potently induced following RIG-I agonist or IFN-α treatment. Further analysis of Mx expression following 3pRNA treatment indicated that the splice variant Mx1.2 was preferably expressed over Mx1.1 at least at the mRNA level as determined by variant-specific qRT-PCR assays, as well as by Sanger sequencing of amplified cDNA generated from cellular mRNA. Interestingly, HSV-1 infection appears to modulate alternative splicing of human MxA, promoting expression of a variant which lacks anti-HSV-1 activities, whereas the alternate variant induced by type I IFNs does mediate antiviral activity (Ku et al., 2011). Thus, there is a precedent for alternative splice variants of Mx in different species and it is interesting to note that such variants can differ in their antiviral activity. Toothed whales such as dolphins and orcas are reported

to express defunct copies of both *Mx1* and *Mx2* genes leading the authors to speculate that a viral outbreak ~33–37 million years ago might have exploited Mx function such that expression of functional *Mx* genes was sacrificed to ensure survival of the population (Braun et al., 2015). Thus, as for Mx1/Mx2 in most inbred strains of mice, expression of inactive forms of Mx which lack antiviral activity can also occur. In future studies, it will be important to determine if ferret Mx1 splice variants are expressed after infection with different viruses and if they exhibit distinct antiviral activities. Our preliminary studies suggest that ferret Mx1.2, but not Mx1.1, might mediate anti-IAV activity although this remains to be confirmed in future studies. Characterisation of different ferret Mx in lung tissues from multiple outbred ferrets in the presence or absence of infection will also address if prevalent expression of Mx1.2 is a specific feature of the FRL cell line or a broader characteristic among ferrets.

While it is well established that mouse Mx1 and human MxA are expressed in the nucleus and the cytoplasm, respectively, our studies confirmed that ferret Mx1.1, Mx1.2 and Mx2 proteins all localised to the cytoplasm, consistent with the lack of known nuclear localisation sequences detected in any of these proteins (**Figure 5.6**). While constitutive overexpression of human MxA and mouse Mx1 in human 293T cells resulted in potent inhibition of IAV infection and growth, none of the ferret Mx mediated antiviral activity against IAV or RSV in this system (**Figure 5.9 and Figure 5.10**). However, preliminary studies suggest that constitutive overexpression of ferret Mx1.2 and Mx2 in FRL cells did result in antiviral activity against IAV although human MxA did not inhibit IAV when expressed in ferret cells (**Figure 5.11**). Based on these findings, we propose that ferret-specific accessory proteins expressed in FRL, but not human 293T cells, are required for the antiviral function of Mx proteins. Clearly, there is a need to refine and extend these studies. CRISPR/Cas9 deletion of endogenous Mx1 or Mx2 from FRL cells represents one approach to assessing their antiviral activity, although as we were not successful in applying this technique to FRL cells to knockout ferret RIG-I we would be cautious in using this approach. Engineering the N-terminus of human MxB onto ferret Mx1 and Mx2 proteins to alter their cellular localisation to the nuclear envelope might also provide insight regarding their antiviral activities

against specific viruses, as has been performed for human MxA and MxB (Goujon et al., 2014; Steiner et al., 2020). Additionally, further studies are required to confirm if ferret Mx proteins are functional when expressed in cells of human origin or if antiviral functions are restricted to expression within ferret cells only.

6.3 Optimising delivery of RIG-I agonists for the treatment of respiratory virus infections

Our studies in mice and ferrets suggest that the effectiveness of 3pRNA-induced protection following i.v. administration may differ depending on the tissues examined. In general terms, systemic administration of 3pRNA reduced growth of IAV and RSV significantly in the lung but had little impact on virus titres in the upper airways. The only exception to this was the potent inhibition of IAV replication in both lung and nasal issues of B6.A2G-*Mx1* mice following pre-treatment with 3pRNA (**Figure 3.6 and Figure 3.7**). Expression of the well characterised Mx1 protein in mice was critical for this potent inhibition of IAV, which also occurred in the upper airways. In ferrets, it is currently unclear if any of the ferret Mx proteins mediate potent antiviral activity against IAV or RSV, although our preliminary *in vitro* studies suggest this might be possible. However, even if ferrets do express a Mx protein with antiviral activity against IAV and/or RSV, our studies indicate that i.v. 3pRNA treatment induced ISG expression in the lungs, but not in the nasal tissues of ferrets (**Figure 3.11**).

The upper respiratory tract consists of the nasal cavity, pharynx and larynx and connects to the lower respiratory tract, containing the conducting airways (trachea and bronchi), small airways (bronchioles) and the respiratory zone (the alveoli) (Invernizzi et al., 2020). In the upper respiratory tract, the epithelium contains pseudostratified epithelial cells, goblet cells and glands (Ramvikas et al., 2017) which cover bones and cartilage that form the structural basis of the nasal cavity. The conductive airways are lined by a pseudostratified epithelial cell layer, comprising multi-ciliated cells, mucus-secreting goblet cells and basal cells to promote clearance of inhaled pathogens by mucociliary transport (Invernizzi et

al., 2020). In contrast, over a dozen different cell types form the parenchyma of the lung, including type I and type II airway epithelial cells, fibroblasts, endothelial cells, dendritic cells and alveolar macrophages, amongst others (Rozycki, 2014). Thus, the lower respiratory tract displays a broader variety of cells than the upper respiratory tract. In addition to differences in overall structure and cellular composition, the lung is highly vascularised relative to the nasal cavity. This is likely to be a major factor relating to the effectiveness of i.v. RIG-I agonist treatment providing superior protection to the lung relative to the upper airways. While respiratory virus infection results in local inflammation as a result of chemokines and cytokines released from virus-infected cells (Vidaña et al., 2016), systemic RIG-I agonist pre-treatment delivers protection to the airways via distinct mechanisms. Following injection, we have shown that RIG-I agonist activates ISG induction in circulating leukocytes which could result in recruitment of these activated immune cells to the lung. Moreover, injection might result in direct delivery of soluble RIG-I to parenchymal cells in the lung, acting to induce ISG induction in the cells which represent the primary targets of virus infection and amplification.

In our studies, we used i.v. injection in an attempt to deliver RIG-I agonists to the respiratory tract, as this represents the primary site of IAV and RSV replication. Other studies have used RIG-I agonists formulated in nanoparticles for cancer immunotherapy, including for the treatment of pancreatic cancers (Ellermeier et al., 2013; Das et al., 2019). In a mouse model of pancreatic ductal adenocarcinoma, i.v. injection of RIG-I agonist encapsulated in anisamide-conjugated nanoparticles to target their delivery to cancer cells resulted in only 2-3 % of injected nanoparticles reaching the tumour tissue with the majority detected in the liver and lung (Das et al., 2019; Zillinger et al., 2019). Thus, it is likely that a substantial proportion of polyethylenimine (PEI)-formulated RIG-I agonist also reaches the lung of ferrets and mice following i.v. injection in our studies, which could offer a partial explanation for the enhanced protection observed in lung tissue compared to nasal tissues. Das *et al.* used Cy5-oligo fluorescent-labelled nanoparticles to determine cellular distribution and similar approaches could be used in our models to determine if RIG-I agonists are

delivered to lung endothelial and/or epithelial cells following i.v. injection (Das et al., 2019). Ultimately, our RIG-I agonists could be reformulated in nanoparticles and compared to PEI transfection reagent for their ability to protect against IAV and RSV challenge in ferrets and mice. Of interest, Das *et al.* used anisamide-conjugated nanoparticles to promote specific delivery to sigma-receptor-expressing tumour cells (Das et al., 2019) which highlights opportunities for promoting delivery of RIG-I agonists to airway epithelial cells in the upper and lower airways, such as the development of nanoparticles targeted to EpCam or other relevant cell-surface markers (Wang, L. et al., 2020).

A major limitation to the use of systemic 3pRNA treatment is its inability to provide protection in the upper airways and therefore its ability to impact virus shedding and transmission. As discussed, systemic delivery to limit virus growth in the lungs could be useful as a prophylactic in susceptible target groups and/or as a therapeutic in infected patients with severe lung disease and pneumonia, however systemic delivery is not ideal due to its invasive nature. Moreover, its inability to limit shedding and transmission limits its usefulness as a truly effective antiviral. In ferrets, systemic delivery of RIG-I agonists was clearly more effective than intranasal administration which, despite local delivery to the airways, also failed to effectively reduce virus shedding from the upper airways (**Figure 3.8 and Figure 3.12**). These findings imply that intranasal delivery of 3pRNA in liquid form failed to induce sufficient ISG induction in epithelial cells of the upper airways to significantly impact virus growth. As RIG-I is expressed in almost all nucleated cells (Loo et al., 2011), it is unlikely that deficiency in RIG-I signaling by cells of the upper airways is responsible for this although it would be of interest to test ISG induction in response to 3pRNA using nasal explants or nasal epithelial cells. More likely is that mucus and other secretions coating nasal and upper airway tissues might limit efficient drug delivery either by forming a physical barrier to prevent effective penetration to the underlying epithelium or due to degradation of RIG-I agonist due to its chemical composition. In our studies, RIG-I agonists are formulated in a PEI ‘in vivo’ transfection reagent and this, or the agonist itself, might be degraded in the upper airways although activity is obviously retained in other biological fluids such has the blood following i.v. injection.

Others have demonstrated effective intranasal delivery of certain siRNAs (Aguilera-Aguirre et al., 2014) and DNAs (Torrieri-Dramard et al., 2011) using the same PEI transfection reagent, although this may not necessarily be true for the 3pRNA used in our studies.

Our studies in mice and ferrets confirm that a single i.v. 3pRNA treatment induces potent protection against subsequent IAV challenge, particularly in terms of reducing virus replication in the lungs. Moreover, we demonstrate that a single i.v. treatment of 3pRNA to ferrets 3 days after experimental infection also reduced lung virus titres highlighting its potential utility in ameliorating disease associated with established virus infection in the lungs. These ferret studies highlight the potential for future studies examining different treatment regimens that include combinations of prophylactic and therapeutic treatments, as well as multiple treatments at different times relative to infection to determine the regimen for optimal effectiveness. RIG-I agonist-induced protection of the lower respiratory tract might be particularly useful in protecting patients at high risk of developing secondary bacterial infections (SBIs). For example, bacterial co-infections were confirmed in 75 % of IAV-infected patients with acquired pneumonia and this was associated with higher mortality and morbidity (Morris et al., 2017). In the context of RSV, SBIs caused by *S. pneumoniae* and *H. influenzae* have also been particularly linked to otitis media (Sande et al., 2019). Reducing virus replication and associated tissue damage in the lungs by 3pRNA treatment might represent an effective strategy to reduce predisposition to the subsequent establishment of SBIs.

6.4 Caveats of using RIG-I agonists

A major caveat when considering translating RIG-I agonists from pre-clinical to clinical studies, particularly in the context of respiratory virus infections, is the risk of excessive or uncontrolled immune activation. Exaggerated immune responses, broadly referred to as a “cytokine storm”, can be triggered by drug treatment, different pathogens, cancers or autoimmune conditions (Fajgenbaum et al.,

2020) and is implicated as a major factor contributing to the high fatality of the 1918 influenza pandemic (Kash et al., 2006). Of note, Coch *et al.* administered four doses of 3pRNA to mice on alternating days prior to lethal IAV infection and observed substantial protection from disease, indicating that repeated treatment did not result in desensitisation nor did it result in a cytokine storm or induction of other detrimental health effects in this model (Coch et al., 2017).

In humans, sustained or inappropriate RLR-mediated signaling can result in the onset of autoimmune diseases (Kato et al., 2014). Atypical activation of MDA5 signaling has been associated with increased susceptibility to the development of systemic lupus erythematosus (Robinson et al., 2011). Aicardi-Goutières syndrome represents another inflammatory disease associated with single nucleotide polymorphisms in genes of the RLR signaling pathways (Crow et al., 2009; Rice et al., 2014). Mutations in *DDX58*, the coding gene for RIG-I, are associated with atypical Singleton-Merten syndrome, a multi-system type I interferonopathy disorder characterised by dental dysplasia, aortic calcification, skeletal abnormalities, glaucoma or psoriasis (Jang et al., 2015). It is important to note that SB9200 (Inarigivir soproxil), a RIG-I and NOD2 agonist, is now being utilised in clinical studies for the treatment of HCV infection (Jones et al., 2017) and that the RIG-I agonist MK-4621 is used as treatment for solid tumors (NCT03065023), although it should be noted that oral or transdermal/transmucosal administration, respectively, have been used in these trials. Thus, it remains to be seen if systemic RIG-I agonist treatment would be tolerated in humans.

6.5 Outlook

Since the discovery of the RLR family and the description of their critical role in host defence against viral infections, much effort has been undertaken to understand RLR signaling and how these pathways might be exploited for possible clinical applications. Given their broad antiviral activity, an emerging area of investigation focuses on how RIG-I agonists might be developed most

effectively as a novel class of pan-antivirals. Studies described in this thesis broaden knowledge regarding RIG-I agonist-mediated protection in different models of IAV and RSV infection and has especially proven its practical use as prophylactic treatment against these viruses in ferret models of infection. Together, these studies provide a further important step towards the development of RIG-I agonists for clinical use. Moreover, we highlight the need for future studies focusing on defining the optimal treatment regimens for prophylactic and/or therapeutic use, the need to further investigate RIG-I agonist stability *in vivo* and determining if alternative (and preferably non-invasive) delivery approaches might retain protection of the lung but also effectively reduce virus shedding from the upper airways.

7 References

Ackerson, B.,Tseng, H. F.,Sy, L. S.,Solano, Z.,Slezak, J.,Luo, Y.,Fischetti, C. A. & Shinde, V. 2019. Severe Morbidity and Mortality Associated With Respiratory Syncytial Virus Versus Influenza Infection in Hospitalized Older Adults. *Clin Infect Dis,* 69**,** 197-203.

Acosta, P. L.,Caballero, M. T.,Polack, F. P. & Papasian, C. J. 2016. Brief History and Characterization of Enhanced Respiratory Syncytial Virus Disease. *Clinical and Vaccine Immunology,* 23**,** 189-195.

Aebi, M.,Fäh, J.,Hurt, N.,Samuel, C. E.,Thomis, D.,Bazzigher, L.,Pavlovic, J.,Haller, O. & Staeheli, P. 1989. cDNA structures and regulation of two interferon-induced human Mx proteins. *Mol Cell Biol,* 9**,** 5062-5072.

Aguilera-Aguirre, L.,Bacsi, A.,Radak, Z.,Hazra, T. K.,Mitra, S.,Sur, S.,Brasier, A. R.,Ba, X. & Boldogh, I. 2014. Innate Inflammation Induced by the 8-Oxoguanine DNA Glycosylase-1–KRAS–NF-κB Pathway. *The Journal of Immunology,* 193**,** 4643-4653.

Akira, S.,Uematsu, S. & Takeuchi, O. 2006. Pathogen recognition and innate immunity. *Cell,* 124**,** 783-801.

Alandijany, T. 2019. Host Intrinsic and Innate Intracellular Immunity During Herpes Simplex Virus Type 1 (HSV-1) Infection. *Front Microbiol,* 10.

Alison, B. & Peter, L. C. 1999. The M2-2 Protein of Human Respiratory Syncytial Virus Is a Regulatory Factor Involved in the Balance between RNA Replication and Transcription. *Proc Natl Acad Sci U S A,* 96**,** 11259-11264.

Allen, I. C.,Scull, M. A.,Moore, C. B.,Holl, E. K.,McElvania-TeKippe, E.,Taxman, D. J.,Guthrie, E. H.,Pickles, R. J. & Ting, J. P. 2009. The NLRP3 inflammasome mediates in vivo innate immunity to influenza A virus through recognition of viral RNA. *Immunity,* 30**,** 556-565.

Anhlan, D.,Grundmann, N.,Makalowski, W.,Ludwig, S. & Scholtissek, C. 2011. Origin of the 1918 pandemic H1N1 influenza A virus as studied by codon usage patterns and phylogenetic analysis. *RNA (New York, N.Y.),* 17**,** 64-73.

Apostolou, E.,Kapsogeorgou, E. K.,Konsta, O. D.,Giotakis, I.,Saridaki, M. I.,Andreakos, E. & Tzioufas, A. G. 2016. Expression of type III interferons (IFNλs) and their receptor in Sjögren's syndrome. *Clin Exp Immunol,* 186**,** 304-312.

Aristizábal, B., González Á. 2013. Autoimmunity: From Bench to Bedside. *Chapter 2.*

Arnheiter, H. & Haller, O. 1988. Antiviral state against influenza virus neutralized by microinjection of antibodies to interferon-induced Mx proteins. *The EMBO journal,* 7**,** 1315-1320.

Arnheiter, H.,Skuntz, S.,Noteborn, M.,Chang, S. & Meier, E. 1990. Transgenic mice with intracellular immunity to influenza virus. *Cell,* 62**,** 51-61.

Ascough, S.,Paterson, S. & Chiu, C. 2018. Induction and Subversion of Human Protective Immunity: Contrasting Influenza and Respiratory Syncytial Virus. *Front Immunol,* 9**,** 323.

ATCC. 2021. Available: https://www.atcc.org/products/ccl-196 [Accessed 18.06.2021 2021].

Atreya, P. L. & Kulkarni, S. 1999. Respiratory syncytial virus strain A2 is resistant to the antiviral effects of type I interferons and human MxA. *Virology,* 261**,** 227-241.

Bakker, S. E.,Duquerroy, S.,Galloux, M.,Loney, C.,Conner, E.,Eléouët, J.-F.,Rey, F. A. & Bhella, D. 2013. The respiratory syncytial virus nucleoprotein–RNA complex forms a left-handed helical nucleocapsid. *Journal of General Virology,* 94**,** 1734-1738.

Barber, M. R. W.,Aldridge, J. R.,Webster, R. G. & Magor, K. E. 2010. Association of RIG-I with innate immunity of ducks to influenza. *Proceedings of the National Academy of Sciences,* 107**,** 5913-5918.

Battles, M. B. & McLellan, J. S. 2019. Respiratory syncytial virus entry and how to block it. *Nat Rev Microbiol,* 17**,** 233-245.

Bazzigher, L.,Schwarz, A. & Staeheli, P. 1993. No enhanced influenza virus resistance of murine and avian cells expressing cloned duck Mx protein. *Virology,* 195**,** 100-112.

Bedard, K. M.,Wang, M. L.,Proll, S. C.,Loo, Y. M.,Katze, M. G.,Gale, M., Jr. & Iadonato, S. P. 2012. Isoflavone agonists of IRF-3 dependent signaling have antiviral activity against RNA viruses. *J Virol,* 86**,** 7334-7344.

Bedford, J. G.,Caminschi, I. & Wakim, L. M. 2020. Intranasal Delivery of a Chitosan-Hydrogel Vaccine Generates Nasal Tissue Resident Memory CD8(+) T Cells That Are Protective against Influenza Virus Infection. *Vaccines (Basel),* 8.

Behera, A. K.,Kumar, M.,Lockey, R. F. & Mohapatra, S. S. 2002. 2'-5' Oligoadenylate synthetase plays a critical role in interferon-gamma inhibition of respiratory syncytial virus infection of human epithelial cells. *J Biol Chem,* 277**,** 25601-25608.

Behzadi, M. A. & Leyva-Grado, V. H. 2019. Overview of Current Therapeutics and Novel Candidates Against Influenza, Respiratory Syncytial Virus, and Middle East Respiratory Syndrome Coronavirus Infections. *Front Microbiol,* 10**,** 1327.

Beigel, J. H.,Farrar, J.,Han, A. M.,Hayden, F. G.,Hyer, R.,de Jong, M. D.,Lochindarat, S.,Nguyen, T. K.,Nguyen, T. H.,Tran, T. H.,Nicoll, A.,Touch, S. & Yuen, K. Y. 2005. Avian influenza A (H5N1) infection in humans. *N Engl J Med,* 353**,** 1374-1385.

Belser, J. A.,Katz, J. M. & Tumpey, T. M. 2011. The ferret as a model organism to study influenza A virus infection. *Disease Models & Mechanisms,* 4**,** 575-579.

Belser, J. A.,Pulit-Penaloza, J. A. & Maines, T. R. 2020. Ferreting Out Influenza Virus Pathogenicity and Transmissibility: Past and Future Risk Assessments in the Ferret Model. *Cold Spring Harb Perspect Med,* 10.

Belshe, R. B. 2005. The Origins of Pandemic Influenza — Lessons from the 1918 Virus. *New England Journal of Medicine,* 353**,** 2209-2211.

Belshe, R. B. 2010. The need for quadrivalent vaccine against seasonal influenza. *Vaccine,* 28 Suppl 4**,** D45-53.

Benfield, C. T.,Lyall, J. W.,Kochs, G. & Tiley, L. S. 2008. Asparagine 631 variants of the chicken Mx protein do not inhibit influenza virus replication in primary chicken embryo fibroblasts or in vitro surrogate assays. *J Virol,* 82**,** 7533-7539.

Benitez, A. A.,Panis, M.,Xue, J.,Varble, A.,Shim, J. V.,Frick, A. L.,Lopez, C. B.,Sachs, D. & tenOever, B. R. 2015. In Vivo RNAi Screening Identifies

MDA5 as a Significant Contributor to the Cellular Defense against Influenza A Virus. *Cell Rep,* 11**,** 1714-1726.

Bernasconi, D.,Schultz, U. & Staeheli, P. 1995. The interferon-induced Mx protein of chickens lacks antiviral activity. *J Interferon Cytokine Res,* 15**,** 47-53.

Berry, K. N.,Kober, D. L.,Su, A. & Brett, T. J. 2018. Limiting Respiratory Viral Infection by Targeting Antiviral and Immunological Functions of BST-2/Tetherin: Knowledge and Gaps. *BioEssays : news and reviews in molecular, cellular and developmental biology,* 40**,** e1800086.

Bhoj, V. G.,Sun, Q.,Bhoj, E. J.,Somers, C.,Chen, X.,Torres, J. P.,Mejias, A.,Gomez, A. M.,Jafri, H.,Ramilo, O. & Chen, Z. J. 2008. MAVS and MyD88 are essential for innate immunity but not cytotoxic T lymphocyte response against respiratory syncytial virus. *Proc Natl Acad Sci U S A,* 105**,** 14046-14051.

Bitko, V.,Shulyayeva, O.,Mazumder, B.,Musiyenko, A.,Ramaswamy, M.,Look, D. C. & Barik, S. 2007. Nonstructural proteins of respiratory syncytial virus suppress premature apoptosis by an NF-kappaB-dependent, interferon-independent mechanism and facilitate virus growth. *J Virol,* 81**,** 1786-1795.

Boncristiani, H. F.,Criado, M. F. & Arruda, E. 2009. Respiratory Viruses. *In:* SCHAECHTER, M. (ed.) *Encyclopedia of Microbiology (Third Edition).* Oxford: Academic Press.

Bonilla, F. A. & Oettgen, H. C. 2010. Adaptive immunity. *J Allergy Clin Immunol,* 125**,** S33-40.

Boukhvalova, M. S.,Yim, K. C.,Prince, G. A. & Blanco, J. C. G. 2010. Methods for monitoring dynamics of pulmonary RSV replication by viral culture and by real-time reverse transcription-PCR in vivo: Detection of abortive viral replication. *Current protocols in cell biology,* Chapter 26**,** Unit26.26.

Boulo, S.,Akarsu, H.,Ruigrok, R. W. H. & Baudin, F. 2007. Nuclear traffic of influenza virus proteins and ribonucleoprotein complexes. *Virus Res,* 124**,** 12-21.

Bouvier, N. M. & Palese, P. 2008. The biology of influenza viruses. *Vaccine,* 26 Suppl 4**,** D49-53.

Boyapalle, S.,Wong, T.,Garay, J.,Teng, M.,San Juan-Vergara, H.,Mohapatra, S. & Mohapatra, S. 2012. Respiratory Syncytial Virus NS1 Protein Colocalizes with Mitochondrial Antiviral Signaling Protein MAVS following Infection. *PLoS One,* 7**,** e29386.

Boyle, J. S.,Koniaras, C. & Lew, A. M. 1997. Influence of cellular location of expressed antigen on the efficacy of DNA vaccination: cytotoxic T lymphocyte and antibody responses are suboptimal when antigen is cytoplasmic after intramuscular DNA immunization. *Int Immunol,* 9**,** 1897-1906.

Brass, A. L.,Huang, I. C.,Benita, Y.,John, S. P.,Krishnan, M. N.,Feeley, E. M.,Ryan, B. J.,Weyer, J. L.,van der Weyden, L.,Fikrig, E.,Adams, D. J.,Xavier, R. J.,Farzan, M. & Elledge, S. J. 2009. The IFITM proteins mediate cellular resistance to influenza A H1N1 virus, West Nile virus, and dengue virus. *Cell,* 139**,** 1243-1254.

Brauer, R. & Chen, P. 2015. Influenza virus propagation in embryonated chicken eggs. *J Vis Exp* [Online]. [Accessed 2015/03//].

Braun, B. A.,Marcovitz, A.,Camp, J. G.,Jia, R. & Bejerano, G. 2015. Mx1 and Mx2 key antiviral proteins are surprisingly lost in toothed whales. *Proceedings of the National Academy of Sciences,* 112**,** 8036-8040.

Brisse, M. & Ly, H. 2019. Comparative Structure and Function Analysis of the RIG-I-Like Receptors: RIG-I and MDA5. *Front Immunol,* 10**,** 1586.

Broad Institute. 2021. [Accessed 15.07.2021].

Brown, G. D.,Willment, J. A. & Whitehead, L. 2018. C-type lectins in immunity and homeostasis. *Nat Rev Immunol,* 18**,** 374-389.

Brubaker, Sky W.,Gauthier, Anna E.,Mills, Eric W.,Ingolia, Nicholas T. & Kagan, Jonathan C. 2014. A Bicistronic MAVS Transcript Highlights a Class of Truncated Variants in Antiviral Immunity. *Cell,* 156**,** 800-811.

Busnadiego, I.,Kane, M.,Rihn, S. J.,Preugschas, H. F.,Hughes, J.,Blanco-Melo, D.,Strouvelle, V. P.,Zang, T. M.,Willett, B. J.,Boutell, C.,Bieniasz, P. D. & Wilson, S. J. 2014. Host and viral determinants of Mx2 antiretroviral activity. *J Virol,* 88**,** 7738-7752.

Byrd-Leotis, L.,Cummings, R. D. & Steinhauer, D. A. 2017. The Interplay between the Host Receptor and Influenza Virus Hemagglutinin and Neuraminidase. *Int J Mol Sci,* 18.

Caini, S.,Kusznierz, G.,Garate, V. V.,Wangchuk, S.,Thapa, B.,de Paula Júnior, F. J.,Ferreira de Almeida, W. A.,Njouom, R.,Fasce, R. A.,Bustos, P.,Feng, L.,Peng, Z.,Araya, J. L.,Bruno, A.,de Mora, D.,Barahona de Gámez, M. J.,Pebody, R.,Zambon, M.,Higueros, R.,Rivera, R.,Kosasih, H.,Castrucci, M. R.,Bella, A.,Kadjo, H. A.,Daouda, C.,Makusheva, A.,Bessonova, O.,Chaves, S. S.,Emukule, G. O.,Heraud, J.-M.,Razanajatovo, N. H.,Barakat, A.,El Falaki, F.,Meijer, A.,Donker, G. A.,Huang, Q. S.,Wood, T.,Balmaseda, A.,Palekar, R.,Arévalo, B. M.,Rodrigues, A. P.,Guiomar, R.,Lee, V. J. M.,Ang, L. W.,Cohen, C.,Treurnicht, F.,Mironenko, A.,Holubka, O.,Bresee, J.,Brammer, L.,Le, M. T. Q.,Hoang, P. V. M.,El Guerche-Séblain, C.,Paget, J. & the Global Influenza, B. S. t. 2019. The epidemiological signature of influenza B virus and its B/Victoria and B/Yamagata lineages in the 21st century. *PLoS One,* 14**,** e0222381.

Camacho Londoño, J. & Philipp, S. E. 2016. A reliable method for quantification of splice variants using RT-qPCR. *BMC molecular biology* [Online], 17. [Accessed 2016/03//].

Carolan, L. A.,Butler, J.,Rockman, S.,Guarnaccia, T.,Hurt, A. C.,Reading, P.,Kelso, A.,Barr, I. & Laurie, K. L. 2014. TaqMan real time RT-PCR assays for detecting ferret innate and adaptive immune responses. *J Virol Methods,* 205**,** 38-52.

Carolan, L. A.,Rockman, S.,Borg, K.,Guarnaccia, T.,Reading, P.,Mosse, J.,Kelso, A.,Barr, I. & Laurie, K. L. 2015. Characterization of the Localized Immune Response in the Respiratory Tract of Ferrets following Infection with Influenza A and B Viruses. *J Virol,* 90**,** 2838-2848.

CDC. 2021. https://www.cdc.gov/flu/professionals/antivirals/summary-clinicians.htm. [Accessed 18.07.2021].

Céspedes, P. F.,Palavecino, C. E.,Kalergis, A. M. & Bueno, S. M. 2016. Modulation of Host Immunity by the Human Metapneumovirus. *Clin Microbiol Rev,* 29**,** 795-818.

Chakravarthy, K. V.,Bonoiu, A. C.,Davis, W. G.,Ranjan, P.,Ding, H.,Hu, R.,Bowzard, J. B.,Bergey, E. J.,Katz, J. M.,Knight, P. R.,Sambhara, S. & Prasad, P. N. 2010. Gold nanorod delivery of an ssRNA immune activator inhibits pandemic H1N1 influenza viral replication. *Proceedings of the National Academy of Sciences,* 107**,** 10172-10177.

Chan, K. F.,Carolan, L. A.,Druce, J.,Chappell, K.,Watterson, D.,Young, P.,Korenkov, D.,Subbarao, K.,Barr, I. G.,Laurie, K. L. & Reading, P. C. 2017. Pathogenesis, humoral immune responses and transmission between co-housed animals in a ferret model of human RSV infection. *J Virol*.

Chan, Y. K. & Gack, M. U. 2015. RIG-I-like receptor regulation in virus infection and immunity. *Curr Opin Virol,* 12**,** 7-14.

Chang, Y.-F.,Imam, J. S. & Wilkinson, M. F. 2007. The Nonsense-Mediated Decay RNA Surveillance Pathway. *Annual Review of Biochemistry,* 76**,** 51-74.

Chen, J.,Wu, Y.,Wu, X. D.,Zhou, J.,Liang, X. D.,Baloch, A. S.,Qiu, Y. F.,Gao, S. & Zhou, B. 2020. The R614E mutation of mouse Mx1 protein contributes to the novel antiviral activity against classical swine fever virus. *Vet Microbiol,* 243**,** 108621.

Chiang, C.,Beljanski, V.,Yin, K.,Olagnier, D.,Ben Yebdri, F.,Steel, C.,Goulet, M. L.,DeFilippis, V. R.,Streblow, D. N.,Haddad, E. K.,Trautmann, L.,Ross, T.,Lin, R. & Hiscott, J. 2015. Sequence-Specific Modifications Enhance the Broad-Spectrum Antiviral Response Activated by RIG-I Agonists. *J Virol,* 89**,** 8011-8025.

Choudhury, N. R.,Heikel, G.,Trus, I.,Dos Santos Pinto, R. M.,Trubitsyna, M.,Gaunt, E.,Digard, P. & Michlewski, G. 2021. TRIM25 inhibits Influenza A infection by destabilising its mRNA and is redundant for the RIG-I pathway. *bioRxiv***,** 2021.2009.2013.460052.

Cifuentes-Muñoz, N.,Dutch, R. E. & Cattaneo, R. 2018. Direct cell-to-cell transmission of respiratory viruses: The fast lanes. *PLoS Pathog,* 14**,** e1007015.

Cifuentes-Muñoz, N. & Ellis Dutch, R. 2019. To assemble or not to assemble: The changing rules of pneumovirus transmission. *Virus Res,* 265**,** 68-73.

Coates, H. V. & Chanock, R. M. 1962. Experimental infection with respiratory syncytial virus in several species of animals. *Am J Hyg,* 76**,** 302-312.

Coch, C.,Stumpel, J. P.,Lilien-Waldau, V.,Wohlleber, D.,Kummerer, B. M.,Bekeredjian-Ding, I.,Kochs, G.,Garbi, N.,Herberhold, S.,Schuberth-Wagner, C.,Ludwig, J.,Barchet, W.,Schlee, M.,Hoerauf, A.,Bootz, F.,Staeheli, P.,Hartmann, G. & Hartmann, E. 2017. RIG-I Activation Protects and Rescues from Lethal Influenza Virus Infection and Bacterial Superinfection. *Mol Ther,* 25**,** 2093-2103.

Collins, P. L. & Graham, B. S. 2008. Viral and host factors in human respiratory syncytial virus pathogenesis. *J Virol,* 82**,** 2040-2055.

Colomer-Lluch, M.,Ruiz, A.,Moris, A. & Prado, J. G. 2018. Restriction Factors: From Intrinsic Viral Restriction to Shaping Cellular Immunity Against HIV-1. *Front Immunol,* 9.

Combadiere, C.,Salzwedel, K.,Smith, E. D.,Tiffany, H. L.,Berger, E. A. & Murphy, P. M. 1998. Identification of CX3CR1. A chemotactic receptor for the

human CX3C chemokine fractalkine and a fusion coreceptor for HIV-1. *J Biol Chem,* 273**,** 23799-23804.

Connor, R. J.,Kawaoka, Y.,Webster, R. G. & Paulson, J. C. 1994. Receptor specificity in human, avian, and equine H2 and H3 influenza virus isolates. *Virology,* 205**,** 17-23.

Conrad, D. A.,Christenson, J. C.,Waner, J. L. & Marks, M. I. 1987. Aerosolized ribavirin treatment of respiratory syncytial virus infection in infants hospitalized during an epidemic. *Pediatr Infect Dis J,* 6**,** 152-158.

Crameri, M.,Bauer, M.,Caduff, N.,Walker, R.,Steiner, F.,Franzoso, F. D.,Gujer, C.,Boucke, K.,Kucera, T.,Zbinden, A.,Münz, C.,Fraefel, C.,Greber, U. F. & Pavlovic, J. 2018. MxB is an interferon-induced restriction factor of human herpesviruses. *Nat Commun,* 9**,** 1980.

Crow, Y. J. & Rehwinkel, J. 2009. Aicardi-Goutieres syndrome and related phenotypes: linking nucleic acid metabolism with autoimmunity. *Hum Mol Genet,* 18**,** R130-136.

Daikoku, T.,Mizuguchi, M.,Obita, T.,Yokoyama, T.,Yoshida, Y.,Takemoto, M. & Shiraki, K. 2018. Characterization of susceptibility variants of poliovirus grown in the presence of favipiravir. *Journal of Microbiology, Immunology and Infection,* 51**,** 581-586.

Das, M.,Shen, L.,Liu, Q.,Goodwin, T. J. & Huang, L. 2019. Nanoparticle Delivery of RIG-I Agonist Enables Effective and Safe Adjuvant Therapy in Pancreatic Cancer. *Molecular Therapy,* 27**,** 507-517.

Davidson, S. 2018. Treating Influenza Infection, From Now and Into the Future. *Front Immunol,* 9**,** 1946.

Dawood, F. S.,Jain, S.,Finelli, L.,Shaw, M. W.,Lindstrom, S.,Garten, R. J.,Gubareva, L. V.,Xu, X.,Bridges, C. B. & Uyeki, T. M. 2009. Emergence of a novel swine-origin influenza A (H1N1) virus in humans. *N Engl J Med,* 360**,** 2605-2615.

Deeg, C. M.,Hassan, E.,Mutz, P.,Rheinemann, L.,Götz, V.,Magar, L.,Schilling, M.,Kallfass, C.,Nürnberger, C.,Soubies, S.,Kochs, G.,Haller, O.,Schwemmle, M. & Staeheli, P. 2017. In vivo evasion of MxA by avian influenza viruses requires human signature in the viral nucleoprotein. *Journal of Experimental Medicine,* 214**,** 1239-1248.

Degrandi, D.,Konermann, C.,Beuter-Gunia, C.,Kresse, A.,Würthner, J.,Kurig, S.,Beer, S. & Pfeffer, K. 2007. Extensive characterization of IFN-induced GTPases mGBP1 to mGBP10 involved in host defense. *J Immunol,* 179**,** 7729-7740.

Dharan, N. J.,Gubareva, L. V.,Meyer, J. J.,Okomo-Adhiambo, M.,McClinton, R. C.,Marshall, S. A.,St George, K.,Epperson, S.,Brammer, L.,Klimov, A. I.,Bresee, J. S. & Fry, A. M. 2009. Infections with oseltamivir-resistant influenza A(H1N1) virus in the United States. *Jama,* 301**,** 1034-1041.

Diamond, M. S. & Farzan, M. 2013. The broad-spectrum antiviral functions of IFIT and IFITM proteins. *Nature Reviews Immunology,* 13**,** 46-57.

Dickens, L. E.,Collins, P. L. & Wertz, G. W. 1984. Transcriptional mapping of human respiratory syncytial virus. *J Virol,* 52**,** 364-369.

Dietzgen, R. G.,Kondo, H.,Goodin, M. M.,Kurath, G. & Vasilakis, N. 2017. The family Rhabdoviridae: mono- and bipartite negative-sense RNA viruses

with diverse genome organization and common evolutionary origins. *Virus Res,* 227**,** 158-170.

DiPiazza, A. T.,Richards, K. A.,Liu, W.-C.,Albrecht, R. A. & Sant, A. J. 2018. Analyses of Cellular Immune Responses in Ferrets Following Influenza Virus Infection. *In:* YAMAUCHI, Y. (ed.) *Influenza Virus: Methods and Protocols.* New York, NY: Springer New York.

Dittmann, J.,Stertz, S.,Grimm, D.,Steel, J.,García-Sastre, A.,Haller, O. & Kochs, G. 2008. Influenza A virus strains differ in sensitivity to the antiviral action of Mx-GTPase. *J Virol,* 82**,** 3624-3631.

Dornfeld, D.,Dudek, A. H.,Vausselin, T.,Günther, S. C.,Hultquist, J. F.,Giese, S.,Khokhlova-Cubberley, D.,Chew, Y. C.,Pache, L.,Krogan, N. J.,Garcia-Sastre, A.,Schwemmle, M. & Shaw, M. L. 2018. SMARCA2-regulated host cell factors are required for MxA restriction of influenza A viruses. *Sci Rep,* 8**,** 2092.

Dou, D.,Revol, R.,Ostbye, H.,Wang, H. & Daniels, R. 2018. Influenza A Virus Cell Entry, Replication, Virion Assembly and Movement. *Front Immunol,* 9**,** 1581.

Drori, Y.,Jacob-Hirsch, J.,Pando, R.,Glatman-Freedman, A.,Friedman, N.,Mendelson, E. & Mandelboim, M. 2020. Influenza A Virus Inhibits RSV Infection via a Two-Wave Expression of IFIT Proteins. *Viruses,* 12.

Du, Y.,Yang, F.,Wang, Q.,Xu, N.,Xie, Y.,Chen, S.,Qin, T. & Peng, D. 2020. Influenza a virus antagonizes type I and type II interferon responses via SOCS1-dependent ubiquitination and degradation of JAK1. *Virol J,* 17**,** 74.

Durbin, R. K.,Kotenko, S. V. & Durbin, J. E. 2013. Interferon induction and function at the mucosal surface. *Immunol Rev,* 255**,** 25-39.

Dutta, S.,Das, N. & Mukherjee, P. 2020. Picking up a Fight: Fine Tuning Mitochondrial Innate Immune Defenses Against RNA Viruses. *Front Microbiol,* 11**,** 1990.

Edelman, B. L. & Redente, E. F. 2018. Isolation and Characterization of Mouse Fibroblasts. *Methods Mol Biol,* 1809**,** 59-67.

Edenborough, K. M.,Lowther, S.,Laurie, K.,Yamada, M.,Long, F.,Bingham, J.,Payne, J.,Harper, J.,Haining, J.,Arkinstall, R.,Gilbertson, B.,Middleton, D. & Brown, L. E. 2016. Predicting Disease Severity and Viral Spread of H5N1 Influenza Virus in Ferrets in the Context of Natural Exposure Routes. *J Virol,* 90**,** 1888-1897.

El-Diwany, R.,Soliman, M.,Sugawara, S.,Breitwieser, F.,Skaist, A.,Coggiano, C.,Sangal, N.,Chattergoon, M.,Bailey, J. R.,Siliciano, R. F.,Blankson, J. N.,Ray, S. C.,Wheelan, S. J.,Thomas, D. L. & Balagopal, A. 2018. CMPK2 and BCL-G are associated with type 1 interferon-induced HIV restriction in humans. *Sci Adv,* 4**,** eaat0843.

Ellermeier, J.,Wei, J.,Duewell, P.,Hoves, S.,Stieg, M. R.,Adunka, T.,Noerenberg, D.,Anders, H.-J.,Mayr, D.,Poeck, H.,Hartmann, G.,Endres, S. & Schnurr, M. 2013. Therapeutic Efficacy of Bifunctional siRNA Combining TGF-β1 Silencing with RIG-I Activation in Pancreatic Cancer. *Cancer Research,* 73**,** 1709-1720.

Fajgenbaum, D. C. & June, C. H. 2020. Cytokine Storm. *New England Journal of Medicine,* 383**,** 2255-2273.

Farrukee, R.,Ait-Goughoulte, M.,Saunders, P. M.,Londrigan, S. L. & Reading, P. C. 2020. Host Cell Restriction Factors of Paramyxoviruses and Pneumoviruses. *Viruses,* 12.

Fasciano, S.,Hutchins, B.,Handy, I. & Patel, R. C. 2005. Identification of the heparin-binding domains of the interferon-induced protein kinase, PKR. *Febs j,* 272**,** 1425-1439.

Fatima, U.,Zhang, Z.,Zhang, H.,Wang, X.-F.,Xu, L.,Chu, X.,Ji, S. & Wang, X. 2019. Equine Mx1 Restricts Influenza A Virus Replication by Targeting at Distinct Site of its Nucleoprotein. *Viruses,* 11**,** 1114.

Fearns, R.,Collins, P. L. & Peeples, M. E. 2000. Functional analysis of the genomic and antigenomic promoters of human respiratory syncytial virus. *J Virol,* 74**,** 6006-6014.

Fearns, R. & Plemper, R. K. 2017. Polymerases of paramyxoviruses and pneumoviruses. *Virus Res,* 234**,** 87-102.

Feeley, E. M.,Sims, J. S.,John, S. P.,Chin, C. R.,Pertel, T.,Chen, L.-M.,Gaiha, G. D.,Ryan, B. J.,Donis, R. O.,Elledge, S. J. & Brass, A. L. 2011. IFITM3 Inhibits Influenza A Virus Infection by Preventing Cytosolic Entry. *PLoS Pathog,* 7**,** e1002337.

Felsenstein, S.,Herbert, J. A.,McNamara, P. S. & Hedrich, C. M. 2020. COVID-19: Immunology and treatment options. *Clinical Immunology,* 215**,** 108448.

Feng, J.,Cao, Z.,Wang, L.,Wan, Y.,Peng, N.,Wang, Q.,Chen, X.,Zhou, Y. & Zhu, Y. 2017. Inducible GBP5 Mediates the Antiviral Response via Interferon-Related Pathways during Influenza A Virus Infection. *J Innate Immun,* 9**,** 419-435.

Fernandez, H.,Banks, G. & Smith, R. 1986. Ribavirin: a clinical overview. *Eur J Epidemiol,* 2**,** 1-14.

Ferron, F.,Weber, F.,de la Torre, J. C. & Reguera, J. 2017. Transcription and replication mechanisms of Bunyaviridae and Arenaviridae L proteins. *Virus Res,* 234**,** 118-134.

Fielding, J. E.,Kelly, H. A.,Mercer, G. N. & Glass, K. 2014. Systematic review of influenza A(H1N1)pdm09 virus shedding: duration is affected by severity, but not age. *Influenza Other Respir Viruses,* 8**,** 142-150.

Fitzgerald, K. A. & Kagan, J. C. 2020. Toll-like Receptors and the Control of Immunity. *Cell,* 180**,** 1044-1066.

Flynn, J. J.,Finarelli, J. A.,Zehr, S.,Hsu, J. & Nedbal, M. A. 2005. Molecular Phylogeny of the Carnivora (Mammalia): Assessing the Impact of Increased Sampling on Resolving Enigmatic Relationships. *Systematic Biology,* 54**,** 317-337.

Fodor, E. 2013. The RNA polymerase of influenza a virus: mechanisms of viral transcription and replication. *Acta Virol,* 57**,** 113-122.

Fouchier, R. A. M.,Munster, V.,Wallensten, A.,Bestebroer, T. M.,Herfst, S.,Smith, D.,Rimmelzwaan, G. F.,Olsen, B. & Osterhaus, A. D. M. E. 2005. Characterization of a novel influenza A virus hemagglutinin subtype (H16) obtained from black-headed gulls. *J Virol,* 79**,** 2814-2822.

Frese, M.,Kochs, G.,Feldmann, H.,Hertkorn, C. & Haller, O. 1996. Inhibition of bunyaviruses, phleboviruses, and hantaviruses by human MxA protein. *J Virol,* 70**,** 915-923.

Frese, M.,Weeber, M.,Weber, F.,Speth, V. & Haller, O. 1997. Mx1 sensitivity: Batken virus is an orthomyxovirus closely related to Dhori virus. *J Gen Virol,* 78 (Pt 10)**,** 2453-2458.

Fritz, J. H. & Kufer, T. A. 2015. Editorial: NLR-Protein Functions in Immunity. *Front Immunol,* 6**,** 306.

Furuta, Y.,Takahashi, K.,Fukuda, Y.,Kuno, M.,Kamiyama, T.,Kozaki, K.,Nomura, N.,Egawa, H.,Minami, S.,Watanabe, Y.,Narita, H. & Shiraki, K. 2002. In Vitro and In Vivo Activities of Anti-Influenza Virus Compound T-705. *Antimicrobial agents and chemotherapy,* 46**,** 977-981.

Gack, M. U. 2014. Mechanisms of RIG-I-like receptor activation and manipulation by viral pathogens. *J Virol,* 88**,** 5213-5216.

Gack, M. U.,Albrecht, R. A.,Urano, T.,Inn, K. S.,Huang, I. C.,Carnero, E.,Farzan, M.,Inoue, S.,Jung, J. U. & Garcia-Sastre, A. 2009. Influenza A virus NS1 targets the ubiquitin ligase TRIM25 to evade recognition by the host viral RNA sensor RIG-I. *Cell Host Microbe,* 5**,** 439-449.

Gack, M. U.,Kirchhofer, A.,Shin, Y. C.,Inn, K. S.,Liang, C.,Cui, S.,Myong, S.,Ha, T.,Hopfner, K. P. & Jung, J. U. 2008. Roles of RIG-I N-terminal tandem CARD and splice variant in TRIM25-mediated antiviral signal transduction. *Proc Natl Acad Sci U S A,* 105**,** 16743-16748.

Gamblin, S. J. & Skehel, J. J. 2010. Influenza hemagglutinin and neuraminidase membrane glycoproteins. *J Biol Chem,* 285**,** 28403-28409.

Ganz, T. 2003. Defensins: antimicrobial peptides of innate immunity. *Nature Reviews Immunology,* 3**,** 710-720.

Gao, S.,von der Malsburg, A.,Dick, A.,Faelber, K.,Schröder, G. F.,Haller, O.,Kochs, G. & Daumke, O. 2011. Structure of myxovirus resistance protein a reveals intra- and intermolecular domain interactions required for the antiviral function. *Immunity,* 35**,** 514-525.

Garg, N. & Aggarwal, A. 2018. Advances Towards Painless Vaccination and Newer Modes of Vaccine Delivery. *Indian J Pediatr,* 85**,** 132-138.

Gitlin, L.,Benoit, L.,Song, C.,Cella, M.,Gilfillan, S.,Holtzman, M. J. & Colonna, M. 2010. Melanoma Differentiation-Associated Gene 5 (MDA5) Is Involved in the Innate Immune Response to Paramyxoviridae Infection In Vivo. *PLoS Pathog,* 6**,** e1000734.

Gnirß, K.,Zmora, P.,Blazejewska, P.,Winkler, M.,Lins, A.,Nehlmeier, I.,Gärtner, S.,Moldenhauer, A.-S.,Hofmann-Winkler, H.,Wolff, T.,Schindler, M. & Pöhlmann, S. 2015. Tetherin Sensitivity of Influenza A Viruses Is Strain Specific: Role of Hemagglutinin and Neuraminidase. *J Virol,* 89**,** 9178-9188.

Goldeck, M.,Schlee, M.,Hartmann, G. & Hornung, V. 2014. Enzymatic synthesis and purification of a defined RIG-I ligand. *Methods Mol Biol,* 1169**,** 15-25.

Gonzalez-Casas, R.,Jones, E. A. & Moreno-Otero, R. 2009. Spectrum of anemia associated with chronic liver disease. *World J Gastroenterol,* 15**,** 4653-4658.

González-Reyes, L.,Ruiz-Argüello, M. B.,García-Barreno, B.,Calder, L.,López, J. A.,Albar, J. P.,Skehel, J. J.,Wiley, D. C. & Melero, J. A. 2001. Cleavage of the human respiratory syncytial virus fusion protein at two distinct sites is required for activation of membrane fusion. *Proc Natl Acad Sci U S A,* 98**,** 9859-9864.

González-Sanz, R.,Mata, M.,Bermejo-Martín, J.,Álvarez, A.,Cortijo, J.,Melero, J. A. & Martínez, I. 2016. ISG15 Is Upregulated in Respiratory Syncytial Virus Infection and Reduces Virus Growth through Protein ISGylation. *J Virol,* 90**,** 3428-3438.

Götz, V.,Magar, L.,Dornfeld, D.,Giese, S.,Pohlmann, A.,Höper, D.,Kong, B. W.,Jans, D. A.,Beer, M.,Haller, O. & Schwemmle, M. 2016. Influenza A viruses escape from MxA restriction at the expense of efficient nuclear vRNP import. *Sci Rep,* 6**,** 23138.

Goubau, D.,Schlee, M.,Deddouche, S.,Pruijssers, A. J.,Zillinger, T.,Goldeck, M.,Schuberth, C.,Van der Veen, A. G.,Fujimura, T.,Rehwinkel, J.,Iskarpatyoti, J. A.,Barchet, W.,Ludwig, J.,Dermody, T. S.,Hartmann, G. & Reis e Sousa, C. 2014. Antiviral immunity via RIG-I-mediated recognition of RNA bearing 5'-diphosphates. *Nature,* 514**,** 372-375.

Goujon, C.,Moncorgé, O.,Bauby, H.,Doyle, T.,Barclay, W. S. & Malim, M. H. 2014. Transfer of the amino-terminal nuclear envelope targeting domain of human MX2 converts MX1 into an HIV-1 resistance factor. *J Virol,* 88**,** 9017-9026.

Goujon, C.,Moncorgé, O.,Bauby, H.,Doyle, T.,Ward, C. C.,Schaller, T.,Hué, S.,Barclay, W. S.,Schulz, R. & Malim, M. H. 2013. Human MX2 is an interferon-induced post-entry inhibitor of HIV-1 infection. *Nature,* 502**,** 559-562.

Goulet, M. L.,Olagnier, D.,Xu, Z.,Paz, S.,Belgnaoui, S. M.,Lafferty, E. I.,Janelle, V.,Arguello, M.,Paquet, M.,Ghneim, K.,Richards, S.,Smith, A.,Wilkinson, P.,Cameron, M.,Kalinke, U.,Qureshi, S.,Lamarre, A.,Haddad, E. K.,Sekaly, R. P.,Peri, S.,Balachandran, S.,Lin, R. & Hiscott, J. 2013. Systems analysis of a RIG-I agonist inducing broad spectrum inhibition of virus infectivity. *PLoS Pathog,* 9**,** e1003298.

Goutagny, N.,Jiang, Z.,Tian, J.,Parroche, P.,Schickli, J.,Monks, B. G.,Ulbrandt, N.,Ji, H.,Kiener, P. A.,Coyle, A. J. & Fitzgerald, K. A. 2010. Cell type-specific recognition of human metapneumoviruses (HMPVs) by retinoic acid-inducible gene I (RIG-I) and TLR7 and viral interference of RIG-I ligand recognition by HMPV-B1 phosphoprotein. *J Immunol,* 184**,** 1168-1179.

Grandvaux, N.,Guan, X.,Yoboua, F.,Zucchini, N.,Fink, K.,Doyon, P.,Martin, L.,Servant, M. J. & Chartier, S. 2014. Sustained activation of interferon regulatory factor 3 during infection by paramyxoviruses requires MDA5. *J Innate Immun,* 6**,** 650-662.

Green, R. R.,Wilkins, C.,Pattabhi, S.,Dong, R.,Loo, Y. & Gale, M., Jr. 2016. Transcriptional analysis of antiviral small molecule therapeutics as agonists of the RLR pathway. *Genom Data,* 7**,** 290-292.

Grove, J. & Marsh, M. 2011. The cell biology of receptor-mediated virus entry. *Journal of Cell Biology,* 195**,** 1071-1082.

Gubareva, L. V. & Fry, A. M. 2019. Baloxavir and Treatment-Emergent Resistance: Public Health Insights and Next Steps. *J Infect Dis,* 221**,** 337-339.

Guénet, J.-L. & Bonhomme, F. 2003. Wild mice: an ever-increasing contribution to a popular mammalian model. *Trends in Genetics,* 19**,** 24-31.

Guerrero-Plata, A.,Baron, S.,Poast, J. S.,Adegboyega, P. A.,Casola, A. & Garofalo, R. P. 2005. Activity and regulation of alpha interferon in respiratory syncytial virus and human metapneumovirus experimental infections. *J Virol,* 79**,** 10190-10199.

Guerrero-Plata, A.,Casola, A.,Suarez, G.,Yu, X.,Spetch, L.,Peeples, M. E. & Garofalo, R. P. 2006. Differential response of dendritic cells to human metapneumovirus and respiratory syncytial virus. *Am J Respir Cell Mol Biol,* 34**,** 320-329.

Guo, Z.,Chen, L.-m.,Zeng, H.,Gomez, J. A.,Plowden, J.,Fujita, T.,Katz, J. M.,Donis, R. O. & Sambhara, S. 2007. NS1 Protein of Influenza A Virus Inhibits the Function of Intracytoplasmic Pathogen Sensor, RIG-I. *Am J Respir Cell Mol Biol,* 36**,** 263-269.

Haake, C.,Cook, S.,Pusterla, N. & Murphy, B. 2020. Coronavirus Infections in Companion Animals: Virology, Epidemiology, Clinical and Pathologic Features. *Viruses,* 12**,** 1023.

Hale, B. G.,Randall, R. E.,Ortín, J. & Jackson, D. 2008. The multifunctional NS1 protein of influenza A viruses. *J Gen Virol,* 89**,** 2359-2376.

Haller, O.,Arnheiter, H.,Gresser, I. & Lindenmann, J. 1981. Virus-specific interferon action. Protection of newborn Mx carriers against lethal infection with influenza virus. *J Exp Med,* 154**,** 199-203.

Haller, O.,Frese, M.,Rost, D.,Nuttall, P. A. & Kochs, G. 1995. Tick-borne thogoto virus infection in mice is inhibited by the orthomyxovirus resistance gene product Mx1. *J Virol,* 69**,** 2596-2601.

Haller, O. & Kochs, G. 2020. Mx genes: host determinants controlling influenza virus infection and trans-species transmission. *Hum Genet,* 139**,** 695-705.

Haller, O.,Staeheli, P.,Schwemmle, M. & Kochs, G. 2015. Mx GTPases: dynamin-like antiviral machines of innate immunity. *Trends Microbiol,* 23**,** 154-163.

Hartmann, G. 2017. Chapter Four - Nucleic Acid Immunity. *In:* ALT, F. W. (ed.) *Advances in Immunology.* Academic Press.

Hayashi, T.,Watanabe, C.,Suzuki, Y.,Tanikawa, T.,Uchida, Y. & Saito, T. 2014. Chicken MDA5 Senses Short Double-Stranded RNA with Implications for Antiviral Response against Avian Influenza Viruses in Chicken. *J Innate Immun,* 6**,** 58-71.

Hayden, F. G.,Sugaya, N.,Hirotsu, N.,Lee, N.,de Jong, M. D.,Hurt, A. C.,Ishida, T.,Sekino, H.,Yamada, K.,Portsmouth, S.,Kawaguchi, K.,Shishido, T.,Arai, M.,Tsuchiya, K.,Uehara, T. & Watanabe, A. 2018. Baloxavir Marboxil for Uncomplicated Influenza in Adults and Adolescents. *N Engl J Med,* 379**,** 913-923.

Hemann, E. A.,Gale, M., Jr. & Savan, R. 2017. Interferon Lambda Genetics and Biology in Regulation of Viral Control. *Front Immunol,* 8**,** 1707.

Hemmink, J. D.,Whittaker, C. J. & Shelton, H. A. 2018. Animal Models in Influenza Research. *Methods Mol Biol,* 1836**,** 401-430.

Hernandez, D. & Fisher, E. M. C. 1999. Mouse autosomal trisomy: two's company, three's a crowd. *Trends in Genetics,* 15**,** 241-247.

Hill, J. T.,Demarest, B. L.,Bisgrove, B. W.,Su, Y. C.,Smith, M. & Yost, H. J. 2014. Poly peak parser: Method and software for identification of unknown indels using sanger sequencing of polymerase chain reaction products. *Dev Dyn,* 243**,** 1632-1636.

Holland, J.,Spindler, K.,Horodyski, F.,Grabau, E.,Nichol, S. & VandePol, S. 1982. Rapid evolution of RNA genomes. *Science,* 215**,** 1577-1585.

Holzinger, D.,Jorns, C.,Stertz, S.,Boisson-Dupuis, S.,Thimme, R.,Weidmann, M.,Casanova, J. L.,Haller, O. & Kochs, G. 2007. Induction of MxA gene expression by influenza A virus requires type I or type III interferon signaling. *J Virol,* 81**,** 7776-7785.

Homaira, N.,Rawlinson, W.,Snelling, T. L. & Jaffe, A. 2014. Effectiveness of Palivizumab in Preventing RSV Hospitalization in High Risk Children: A Real-World Perspective. *Int J Pediatr,* 2014**,** 571609.

Horman, W. S. J.,Kedzierska, K.,Rootes, C. L.,Bean, A. G. D.,Nguyen, T. H. O. & Layton, D. S. 2021. Ferret Interferon (IFN)-Inducible Transmembrane Proteins Are Upregulated by both IFN-α and Influenza Virus Infection. *J Virol,* 95**,** e0011121.

Hu, J.,Ma, C. & Liu, X. 2018. PA-X: a key regulator of influenza A virus pathogenicity and host immune responses. *Med Microbiol Immunol,* 207**,** 255-269.

Hu, J. & Robinson, J. L. 2010. Treatment of respiratory syncytial virus with palivizumab: a systematic review. *World J Pediatr,* 6**,** 296-300.

Hu, J. & Seeger, C. 2015. Hepadnavirus Genome Replication and Persistence. *Cold Spring Harb Perspect Med,* 5**,** a021386.

Hu, M.,Bogoyevitch, M. A. & Jans, D. A. 2020. Impact of Respiratory Syncytial Virus Infection on Host Functions: Implications for Antiviral Strategies. *Physiol Rev,* 100**,** 1527-1594.

Huang, H.,Zhang, C.,Wang, B.,Wang, F.,Pei, B.,Cheng, C.,Yang, W. & Zhao, Z. 2018. Transduction with Lentiviral Vectors Altered the Expression Profile of Host MicroRNAs. *J Virol,* 92.

Huang, T.,Pavlovic, J.,Staeheli, P. & Krystal, M. 1992. Overexpression of the influenza virus polymerase can titrate out inhibition by the murine Mx1 protein. *J Virol,* 66**,** 4154-4160.

Hurt, A. C. 2014. The epidemiology and spread of drug resistant human influenza viruses. *Curr Opin Virol,* 8**,** 22-29.

Hurt, A. C.,Holien, J. K.,Parker, M. W. & Barr, I. G. 2009. Oseltamivir Resistance and the H274Y Neuraminidase Mutation in Seasonal, Pandemic and Highly Pathogenic Influenza Viruses. *Drugs,* 69**,** 2523-2531.

Imaizumi, T.,Tanaka, H.,Matsumiya, T.,Yoshida, H.,Tanji, K.,Tsuruga, K.,Oki, E.,Aizawa-Yashiro, T.,Ito, E. & Satoh, K. 2010. Retinoic acid-inducible gene-I is induced by double-stranded RNA and regulates the expression of CC chemokine ligand (CCL) 5 in human mesangial cells. *Nephrol Dial Transplant,* 25**,** 3534-3539.

Invernizzi, R.,Lloyd, C. M. & Molyneaux, P. L. 2020. Respiratory microbiome and epithelial interactions shape immunity in the lungs. *Immunology,* 160**,** 171-182.

Iuliano, A. D.,Roguski, K. M.,Chang, H. H.,Muscatello, D. J.,Palekar, R.,Tempia, S.,Cohen, C.,Gran, J. M.,Schanzer, D.,Cowling, B. J.,Wu, P.,Kyncl, J.,Ang, L. W.,Park, M.,Redlberger-Fritz, M.,Yu, H.,Espenhain, L.,Krishnan, A.,Emukule, G.,van Asten, L.,Pereira da Silva, S.,Aungkulanon, S.,Buchholz, U.,Widdowson, M. A. & Bresee, J. S. 2018. Estimates of

global seasonal influenza-associated respiratory mortality: a modelling study. *Lancet,* 391**,** 1285-1300.

Jacobs, S. R. & Damania, B. 2012. NLRs, inflammasomes, and viral infection. *Journal of Leukocyte Biology,* 92**,** 469-477.

Jang, M.-A.,Kim, Eun K.,Now, H.,Nguyen, Nhung T. H.,Kim, W.-J.,Yoo, J.-Y.,Lee, J.,Jeong, Y.-M.,Kim, C.-H.,Kim, O.-H.,Sohn, S.,Nam, S.-H.,Hong, Y.,Lee, Yong S.,Chang, S.-A.,Jang, Shin Y.,Kim, J.-W.,Lee, M.-S.,Lim, So Y.,Sung, K.-S.,Park, K.-T.,Kim, Byoung J.,Lee, J.-H.,Kim, D.-K.,Kee, C. & Ki, C.-S. 2015. Mutations in DDX58, which Encodes RIG-I, Cause Atypical Singleton-Merten Syndrome. *The American Journal of Human Genetics,* 96**,** 266-274.

Jayaraman, A.,Chandrasekaran, A.,Viswanathan, K.,Raman, R.,Fox, J. G. & Sasisekharan, R. 2012. Decoding the Distribution of Glycan Receptors for Human-Adapted Influenza A Viruses in Ferret Respiratory Tract. *PLoS One,* 7**,** e27517.

Jefferson, T.,Jones, M. A.,Doshi, P.,Del Mar, C. B.,Hama, R.,Thompson, M. J.,Spencer, E. A.,Onakpoya, I.,Mahtani, K. R.,Nunan, D.,Howick, J. & Heneghan, C. J. 2014. Neuraminidase inhibitors for preventing and treating influenza in healthy adults and children. *Cochrane Database Syst Rev***,** Cd008965.

Ji, S.,Na, L.,Ren, H.,Wang, Y. & Wang, X. 2018. Equine Myxovirus Resistance Protein 2 Restricts Lentiviral Replication by Blocking Nuclear Uptake of Capsid Protein. *J Virol,* 92.

Ji, X.,Adams, S. T., Jr. & Miller, S. C. 2020. Bioluminescence imaging in mice with synthetic luciferin analogues. *Methods Enzymol,* 640**,** 165-183.

Jin, H. K.,Takada, A.,Kon, Y.,Haller, O. & Watanabe, T. 1999. Identification of the murine Mx2 gene: interferon-induced expression of the Mx2 protein from the feral mouse gene confers resistance to vesicular stomatitis virus. *J Virol,* 73**,** 4925-4930.

Jin, H. K.,Yoshimatsu, K.,Takada, A.,Ogino, M.,Asano, A.,Arikawa, J. & Watanabe, T. 2001. Mouse Mx2 protein inhibits hantavirus but not influenza virus replication. *Arch Virol,* 146**,** 41-49.

Johansson, C. & Kirsebom, F. C. M. 2021. Neutrophils in respiratory viral infections. *Mucosal Immunology,* 14**,** 815-827.

Johnson, S. M.,McNally, B. A.,Ioannidis, I.,Flano, E.,Teng, M. N.,Oomens, A. G.,Walsh, E. E. & Peeples, M. E. 2015. Respiratory Syncytial Virus Uses CX3CR1 as a Receptor on Primary Human Airway Epithelial Cultures. *PLoS Pathog,* 11**,** e1005318.

Johnson, T. R.,Johnson, C. N.,Corbett, K. S.,Edwards, G. C. & Graham, B. S. 2011. Primary Human mDC1, mDC2, and pDC Dendritic Cells Are Differentially Infected and Activated by Respiratory Syncytial Virus. *PLoS One,* 6**,** e16458.

Jones, D. T.,Taylor, W. R. & Thornton, J. M. 1992. The rapid generation of mutation data matrices from protein sequences. *Comput Appl Biosci,* 8**,** 275-282.

Jones, M.,Cunningham, M. E.,Wing, P.,DeSilva, S.,Challa, R.,Sheri, A.,Padmanabhan, S.,Iyer, R. P.,Korba, B. E.,Afdhal, N. & Foster, G. R.

2017. SB 9200, a novel agonist of innate immunity, shows potent antiviral activity against resistant HCV variants. *J Med Virol,* 89**,** 1620-1628.

Kane, M.,Yadav, S. S.,Bitzegeio, J.,Kutluay, S. B.,Zang, T.,Wilson, S. J.,Schoggins, J. W.,Rice, C. M.,Yamashita, M.,Hatziioannou, T. & Bieniasz, P. D. 2013. MX2 is an interferon-induced inhibitor of HIV-1 infection. *Nature,* 502**,** 563-566.

Kaneko, S.,Kurosaki, M.,Tamaki, N.,Itakura, J.,Hayashi, T.,Kirino, S.,Osawa, L.,Watakabe, K.,Okada, M.,Wang, W.,Shimizu, T.,Higuchi, M.,Takaura, K.,Yasui, Y.,Tsuchiya, K.,Nakanishi, H.,Takahashi, Y.,Watanabe, M. & Izumi, N. 2019. Tenofovir alafenamide for hepatitis B virus infection including switching therapy from tenofovir disoproxil fumarate. *J Gastroenterol Hepatol,* 34**,** 2004-2010.

Karpala, A. J.,Stewart, C.,McKay, J.,Lowenthal, J. W. & Bean, A. G. 2011. Characterization of chicken Mda5 activity: regulation of IFN-β in the absence of RIG-I functionality. *J Immunol,* 186**,** 5397-5405.

Karron, R. A. 2021. Preventing respiratory syncytial virus (RSV) disease in children. *Science,* 372**,** 686-687.

Kash, J. C.,Tumpey, T. M.,Proll, S. C.,Carter, V.,Perwitasari, O.,Thomas, M. J.,Basler, C. F.,Palese, P.,Taubenberger, J. K.,García-Sastre, A.,Swayne, D. E. & Katze, M. G. 2006. Genomic analysis of increased host immune and cell death responses induced by 1918 influenza virus. *Nature,* 443**,** 578-581.

Kasumba, D. M. & Grandvaux, N. 2019. Therapeutic Targeting of RIG-I and MDA5 Might Not Lead to the Same Rome. *Trends Pharmacol Sci,* 40**,** 116-127.

Kato, H. & Fujita, T. 2014. Autoimmunity caused by constitutive activation of cytoplasmic viral RNA sensors. *Cytokine Growth Factor Rev,* 25**,** 739-743.

Kato , H.,Takeuchi , O.,Mikamo-Satoh , E.,Hirai , R.,Kawai , T.,Matsushita , K.,Hiiragi , A.,Dermody , T. S.,Fujita , T. & Akira , S. 2008. Length-dependent recognition of double-stranded ribonucleic acids by retinoic acid–inducible gene-I and melanoma differentiation–associated gene 5. *Journal of Experimental Medicine,* 205**,** 1601-1610.

Kato, H.,Takeuchi, O.,Sato, S.,Yoneyama, M.,Yamamoto, M.,Matsui, K.,Uematsu, S.,Jung, A.,Kawai, T.,Ishii, K. J.,Yamaguchi, O.,Otsu, K.,Tsujimura, T.,Koh, C. S.,Reis e Sousa, C.,Matsuura, Y.,Fujita, T. & Akira, S. 2006. Differential roles of MDA5 and RIG-I helicases in the recognition of RNA viruses. *Nature,* 441**,** 101-105.

Kawai, T. & Akira, S. 2006. Innate immune recognition of viral infection. *Nat Immunol,* 7**,** 131-137.

Kawai, T.,Takahashi, K.,Sato, S.,Coban, C.,Kumar, H.,Kato, H.,Ishii, K. J.,Takeuchi, O. & Akira, S. 2005. IPS-1, an adaptor triggering RIG-I- and Mda5-mediated type I interferon induction. *Nat Immunol,* 6**,** 981-988.

Kawasaki, T. & Kawai, T. 2014. Toll-Like Receptor Signaling Pathways. *Front Immunol,* 5.

Kell, A. M. & Gale, M., Jr. 2015. RIG-I in RNA virus recognition. *Virology,* 479-480**,** 110-121.

Kilbourne, E. D. 2006. Influenza pandemics of the 20th century. *Emerg Infect Dis,* 12**,** 9-14.

Kim, H.,Webster, R. G. & Webby, R. J. 2018. Influenza Virus: Dealing with a Drifting and Shifting Pathogen. *Viral Immunol,* 31**,** 174-183.

Kim, H. W.,Canchola, J. G.,Brandt, C. D.,Pyles, G.,Chanock, R. M.,Jensen, K. & Parrott, R. H. 1969. Respiratory syncytial virus disease in infants despite prior administration of antigenic inactivated vaccine. *Am J Epidemiol,* 89**,** 422-434.

Kim, M.-J.,Hwang, S.-Y.,Imaizumi, T. & Yoo, J.-Y. 2008. Negative Feedback Regulation of RIG-I-Mediated Antiviral Signaling by Interferon-Induced ISG15 Conjugation. *J Virol,* 82**,** 1474-1483.

Klinkhammer, J.,Schnepf, D.,Ye, L.,Schwaderlapp, M.,Gad, H. H.,Hartmann, R.,Garcin, D.,Mahlakoiv, T. & Staeheli, P. 2018. IFN-lambda prevents influenza virus spread from the upper airways to the lungs and limits virus transmission. *Elife,* 7.

Ko, J.-H.,Jin, H.-K.,Asano, A.,Takada, A.,Ninomiya, A.,Kida, H.,Hokiyama, H.,Ohara, M.,Tsuzuki, M.,Nishibori, M.,Mizutani, M. & Watanabe, T. 2002. Polymorphisms and the differential antiviral activity of the chicken Mx gene. *Genome research,* 12**,** 595-601.

Kochs, G.,Haener, M.,Aebi, U. & Haller, O. 2002. Self-assembly of Human MxA GTPase into Highly Ordered Dynamin-like Oligomers*. *Journal of Biological Chemistry,* 277**,** 14172-14176.

Kolokoltsov, A. A.,Deniger, D.,Fleming, E. H.,Roberts, N. J., Jr.,Karpilow, J. M. & Davey, R. A. 2007. Small interfering RNA profiling reveals key role of clathrin-mediated endocytosis and early endosome formation for infection by respiratory syncytial virus. *J Virol,* 81**,** 7786-7800.

Korolowicz, K. E.,Iyer, R. P.,Czerwinski, S.,Suresh, M.,Yang, J.,Padmanabhan, S.,Sheri, A.,Pandey, R. K.,Skell, J.,Marquis, J. K.,Kallakury, B. V.,Tucker, R. D. & Menne, S. 2016. Antiviral Efficacy and Host Innate Immunity Associated with SB 9200 Treatment in the Woodchuck Model of Chronic Hepatitis B. *PLoS One,* 11**,** e0161313.

Kosugi, S.,Hasebe, M.,Tomita, M. & Yanagawa, H. 2009. Systematic identification of cell cycle-dependent yeast nucleocytoplasmic shuttling proteins by prediction of composite motifs. *Proc Natl Acad Sci U S A,* 106**,** 10171-10176.

Kotenko, S. V.,Gallagher, G.,Baurin, V. V.,Lewis-Antes, A.,Shen, M.,Shah, N. K.,Langer, J. A.,Sheikh, F.,Dickensheets, H. & Donnelly, R. P. 2003. IFN-lambdas mediate antiviral protection through a distinct class II cytokine receptor complex. *Nat Immunol,* 4**,** 69-77.

Kowalinski, E.,Lunardi, T.,McCarthy, A. A.,Louber, J.,Brunel, J.,Grigorov, B.,Gerlier, D. & Cusack, S. 2011. Structural basis for the activation of innate immune pattern-recognition receptor RIG-I by viral RNA. *Cell,* 147**,** 423-435.

Krammer, F.,Smith, G. J. D.,Fouchier, R. A. M.,Peiris, M.,Kedzierska, K.,Doherty, P. C.,Palese, P.,Shaw, M. L.,Treanor, J.,Webster, R. G. & García-Sastre, A. 2018. Influenza. *Nat Rev Dis Primers,* 4**,** 3.

Kreijtz, J. H. C. M.,Fouchier, R. A. M. & Rimmelzwaan, G. F. 2011. Immune responses to influenza virus infection. *Virus Res,* 162**,** 19-30.

Kreit, M.,Vertommen, D.,Gillet, L. & Michiels, T. 2015. The Interferon-Inducible Mouse Apolipoprotein L9 and Prohibitins Cooperate to Restrict Theiler's Virus Replication. *PLoS One,* 10**,** e0133190.

Krug, R. M.,Shaw, M.,Broni, B.,Shapiro, G. & Haller, O. 1985. Inhibition of influenza viral mRNA synthesis in cells expressing the interferon-induced Mx gene product. *J Virol,* 56**,** 201-206.

Krzyzaniak, M. A.,Zumstein, M. T.,Gerez, J. A.,Picotti, P. & Helenius, A. 2013. Host cell entry of respiratory syncytial virus involves macropinocytosis followed by proteolytic activation of the F protein. *PLoS Pathog,* 9**,** e1003309.

Ku, C.-C.,Che, X.-B.,Reichelt, M.,Rajamani, J.,Schaap-Nutt, A.,Huang, K.-J.,Sommer, M. H.,Chen, Y.-S.,Chen, Y.-Y. & Arvin, A. M. 2011. Herpes simplex virus-1 induces expression of a novel MxA isoform that enhances viral replication. *Immunology and cell biology,* 89**,** 173-182.

Kugel, D.,Kochs, G.,Obojes, K.,Roth, J.,Kobinger, G. P.,Kobasa, D.,Haller, O.,Staeheli, P. & von Messling, V. 2009. Intranasal administration of alpha interferon reduces seasonal influenza A virus morbidity in ferrets. *J Virol,* 83**,** 3843-3851.

Kumar, S.,Stecher, G.,Li, M.,Knyaz, C. & Tamura, K. 2018. MEGA X: Molecular Evolutionary Genetics Analysis across Computing Platforms. *Mol Biol Evol,* 35**,** 1547-1549.

Kummer, S.,Avinoam, O. & Kräusslich, H. G. 2019. IFITM3 Clusters on Virus Containing Endosomes and Lysosomes Early in the Influenza A Infection of Human Airway Epithelial Cells. *Viruses,* 11.

Lad, S. P.,Yang, G.,Scott, D. A.,Chao, T. H.,Correia Jda, S.,de la Torre, J. C. & Li, E. 2008. Identification of MAVS splicing variants that interfere with RIGI/MAVS pathway signaling. *Mol Immunol,* 45**,** 2277-2287.

Lee, N.,Le Sage, V.,Nanni, A. V.,Snyder, D. J.,Cooper, V. S. & Lakdawala, S. S. 2017. Genome-wide analysis of influenza viral RNA and nucleoprotein association. *Nucleic Acids Research,* 45**,** 8968-8977.

Lee, S. & Baldridge, M. T. 2017. Interferon-Lambda: A Potent Regulator of Intestinal Viral Infections. *Front Immunol,* 8**,** 749.

Lee, S.,Ishitsuka, A.,Noguchi, M.,Hirohama, M.,Fujiyasu, Y.,Petric, P. P.,Schwemmle, M.,Staeheli, P.,Nagata, K. & Kawaguchi, A. 2019. Influenza restriction factor MxA functions as inflammasome sensor in the respiratory epithelium. *Sci Immunol,* 4.

Lenschow, D. J.,Lai, C.,Frias-Staheli, N.,Giannakopoulos, N. V.,Lutz, A.,Wolff, T.,Osiak, A.,Levine, B.,Schmidt, R. E.,Garcia-Sastre, A.,Leib, D. A.,Pekosz, A.,Knobeloch, K. P.,Horak, I. & Virgin, H. W. t. 2007. IFN-stimulated gene 15 functions as a critical antiviral molecule against influenza, herpes, and Sindbis viruses. *Proc Natl Acad Sci U S A,* 104**,** 1371-1376.

Levy, D. E.,Marié, I. J. & Durbin, J. E. 2011. Induction and function of type I and III interferon in response to viral infection. *Curr Opin Virol,* 1**,** 476-486.

Li, N.,Zhang, L.,Chen, L.,Feng, W.,Xu, Y.,Chen, F.,Liu, X.,Chen, Z. & Liu, W. 2012. MxA inhibits hepatitis B virus replication by interaction with hepatitis B core antigen. *Hepatology,* 56**,** 803-811.

Li, X.,Gu, M.,Zheng, Q.,Gao, R. & Liu, X. 2021. Packaging signal of influenza A virus. *Virol J,* 18**,** 36.

Li, Y.,Banerjee, S.,Wang, Y.,Goldstein, S. A.,Dong, B.,Gaughan, C.,Silverman, R. H. & Weiss, S. R. 2016. Activation of RNase L is dependent on OAS3 expression during infection with diverse human viruses. *Proceedings of the National Academy of Sciences,* 113**,** 2241-2246.

Lin, L.,Liu, Q.,Berube, N.,Detmer, S. & Zhou, Y. 2012. 5'-Triphosphate-short interfering RNA: potent inhibition of influenza A virus infection by gene silencing and RIG-I activation. *J Virol,* 86**,** 10359-10369.

Lindenmann, J. 1962. Resistance of mice to mouse-adapted influenza A virus. *Virology,* 16**,** 203-204.

Lindenmann, J. 1964. Inheritance of Resistance to Influenza Virus in Mice. *Proceedings of the Society for Experimental Biology and Medicine,* 116**,** 506-509.

Lindenmann, J.,Lane, C. A. & Hobson, D. 1963. THE RESISTANCE OF A2G MICE TO MYXOVIRUSES. *J Immunol,* 90**,** 942-951.

Linehan, M. M.,Dickey, T. H.,Molinari, E. S.,Fitzgerald, M. E.,Potapova, O.,Iwasaki, A. & Pyle, A. M. 2018. A minimal RNA ligand for potent RIG-I activation in living mice. *Sci Adv,* 4**,** e1701854.

Ling, Z.,Tran, K. C. & Teng, M. N. 2009. Human respiratory syncytial virus nonstructural protein NS2 antagonizes the activation of beta interferon transcription by interacting with RIG-I. *J Virol,* 83**,** 3734-3742.

Liniger, M.,Summerfield, A.,Zimmer, G.,McCullough, K. C. & Ruggli, N. 2012. Chicken Cells Sense Influenza A Virus Infection through MDA5 and CARDIF Signaling Involving LGP2. *J Virol,* 86**,** 705-717.

Liu, G.,Lu, Y.,Liu, Q. & Zhou, Y. 2019. Inhibition of Ongoing Influenza A Virus Replication Reveals Different Mechanisms of RIG-I Activation. *J Virol,* 93.

Liu, G.,Lu, Y.,Thulasi Raman, S. N.,Xu, F.,Wu, Q.,Li, Z.,Brownlie, R.,Liu, Q. & Zhou, Y. 2018. Nuclear-resident RIG-I senses viral replication inducing antiviral immunity. *Nat Commun,* 9**,** 3199.

Liu, G.,Park, H. S.,Pyo, H. M.,Liu, Q. & Zhou, Y. 2015. Influenza A Virus Panhandle Structure Is Directly Involved in RIG-I Activation and Interferon Induction. *J Virol,* 89**,** 6067-6079.

Liu, P.,Jamaluddin, M.,Li, K.,Garofalo, R. P.,Casola, A. & Brasier, A. R. 2007. Retinoic acid-inducible gene I mediates early antiviral response and Toll-like receptor 3 expression in respiratory syncytial virus-infected airway epithelial cells. *J Virol,* 81**,** 1401-1411.

Liu, T.,Zhang, L.,Joo, D. & Sun, S.-C. 2017. NF-κB signaling in inflammation. *Signal Transduction and Targeted Therapy,* 2**,** 17023.

Liu, Y.,Olagnier, D. & Lin, R. 2017. Host and Viral Modulation of RIG-I-Mediated Antiviral Immunity. *Front Immunol,* 7.

Liu, Z.,Pan, Q.,Ding, S.,Qian, J.,Xu, F.,Zhou, J.,Cen, S.,Guo, F. & Liang, C. 2013. The interferon-inducible MxB protein inhibits HIV-1 infection. *Cell Host Microbe,* 14**,** 398-410.

Livak, K. J. & Schmittgen, T. D. 2001. Analysis of relative gene expression data using real-time quantitative PCR and the 2(-Delta Delta C(T)) Method. *Methods,* 25**,** 402-408.

Lo, M. S.,Brazas, R. M. & Holtzman, M. J. 2005. Respiratory syncytial virus nonstructural proteins NS1 and NS2 mediate inhibition of Stat2 expression and alpha/beta interferon responsiveness. *J Virol,* 79**,** 9315-9319.

Londrigan, S. L.,Tate, M. D.,Brooks, A. G. & Reading, P. C. 2012. Cell-surface receptors on macrophages and dendritic cells for attachment and entry of influenza virus. *J Leukoc Biol,* 92**,** 97-106.

Loo, Y. M.,Fornek, J.,Crochet, N.,Bajwa, G.,Perwitasari, O.,Martinez-Sobrido, L.,Akira, S.,Gill, M. A.,Garcia-Sastre, A.,Katze, M. G. & Gale, M., Jr. 2008. Distinct RIG-I and MDA5 signaling by RNA viruses in innate immunity. *J Virol,* 82**,** 335-345.

Loo, Y. M. & Gale, M., Jr. 2011. Immune signaling by RIG-I-like receptors. *Immunity,* 34**,** 680-692.

Lozano, R.,Naghavi, M.,Foreman, K.,Lim, S.,Shibuya, K.,Aboyans, V.,Abraham, J.,Adair, T.,Aggarwal, R.,Ahn, S. Y.,AlMazroa, M. A.,Alvarado, M.,Anderson, H. R.,Anderson, L. M.,Andrews, K. G.,Atkinson, C.,Baddour, L. M.,Barker-Collo, S.,Bartels, D. H.,Bell, M. L.,Benjamin, E. J.,Bennett, D.,Bhalla, K.,Bikbov, B.,Abdulhak, A. B.,Birbeck, G.,Blyth, F.,Bolliger, I.,Boufous, S.,Bucello, C.,Burch, M.,Burney, P.,Carapetis, J.,Chen, H.,Chou, D.,Chugh, S. S.,Coffeng, L. E.,Colan, S. D.,Colquhoun, S.,Colson, K. E.,Condon, J.,Connor, M. D.,Cooper, L. T.,Corriere, M.,Cortinovis, M.,de Vaccaro, K. C.,Couser, W.,Cowie, B. C.,Criqui, M. H.,Cross, M.,Dabhadkar, K. C.,Dahodwala, N.,De Leo, D.,Degenhardt, L.,Delossantos, A.,Denenberg, J.,Des Jarlais, D. C.,Dharmaratne, S. D.,Dorsey, E. R.,Driscoll, T.,Duber, H.,Ebel, B.,Erwin, P. J.,Espindola, P.,Ezzati, M.,Feigin, V.,Flaxman, A. D.,Forouzanfar, M. H.,Fowkes, F. G. R.,Franklin, R.,Fransen, M.,Freeman, M. K.,Gabriel, S. E.,Gakidou, E.,Gaspari, F.,Gillum, R. F.,Gonzalez-Medina, D.,Halasa, Y. A.,Haring, D.,Harrison, J. E.,Havmoeller, R.,Hay, R. J.,Hoen, B.,Hotez, P. J.,Hoy, D.,Jacobsen, K. H.,James, S. L.,Jasrasaria, R.,Jayaraman, S.,Johns, N.,Karthikeyan, G.,Kassebaum, N.,Keren, A.,Khoo, J.-P.,Knowlton, L. M.,Kobusingye, O.,Koranteng, A.,Krishnamurthi, R.,Lipnick, M.,Lipshultz, S. E., et al. 2012. Global and regional mortality from 235 causes of death for 20 age groups in 1990 and 2010: a systematic analysis for the Global Burden of Disease Study 2010. *The Lancet,* 380**,** 2095-2128.

Ludlow, M.,Rennick, L. J.,Nambulli, S.,de Swart, R. L. & Duprex, W. P. 2014. Using the ferret model to study morbillivirus entry, spread, transmission and cross-species infection. *Curr Opin Virol,* 4**,** 15-23.

Ma, W.,Kahn, R. E. & Richt, J. A. 2008. The pig as a mixing vessel for influenza viruses: Human and veterinary implications. *Journal of molecular and genetic medicine : an international journal of biomedical research,* 3**,** 158-166.

MacPhail, M.,Schickli, J. H.,Tang, R. S.,Kaur, J.,Robinson, C.,Fouchier, R. A.,Osterhaus, A. D.,Spaete, R. R. & Haller, A. A. 2004. Identification of small-animal and primate models for evaluation of vaccine candidates for human metapneumovirus (hMPV) and implications for hMPV vaccine design. *J Gen Virol,* 85**,** 1655-1663.

Maginnis, M. S. 2018. Virus-Receptor Interactions: The Key to Cellular Invasion. *J Mol Biol,* 430**,** 2590-2611.

Malik, G. & Zhou, Y. 2020. Innate Immune Sensing of Influenza A Virus. *Viruses,* 12.

Malur, M.,Gale, M., Jr. & Krug, R. M. 2012. LGP2 downregulates interferon production during infection with seasonal human influenza A viruses that activate interferon regulatory factor 3. *J Virol,* 86**,** 10733-10738.

Mänz, B.,Dornfeld, D.,Götz, V.,Zell, R.,Zimmermann, P.,Haller, O.,Kochs, G. & Schwemmle, M. 2013. Pandemic influenza A viruses escape from restriction by human MxA through adaptive mutations in the nucleoprotein. *PLoS Pathog,* 9**,** e1003279.

Manzoor, R.,Igarashi, M. & Takada, A. 2017. Influenza A Virus M2 Protein: Roles from Ingress to Egress. *Int J Mol Sci,* 18.

Mao, D.,Reuter, C. M.,Ruzhnikov, M. R. Z.,Beck, A. E.,Farrow, E. G.,Emrick, L. T.,Rosenfeld, J. A.,Mackenzie, K. M.,Robak, L.,Wheeler, M. T.,Burrage, L. C.,Jain, M.,Liu, P.,Calame, D.,Küry, S.,Sillesen, M.,Schmitz-Abe, K.,Tonduti, D.,Spaccini, L.,Iascone, M.,Genetti, C. A.,Koenig, M. K.,Graf, M.,Tran, A.,Alejandro, M.,Acosta, M. T.,Adam, M.,Adams, D. R.,Agrawal, P. B.,Alejandro, M. E.,Allard, P.,Alvey, J.,Amendola, L.,Andrews, A.,Ashley, E. A.,Azamian, M. S.,Bacino, C. A.,Bademci, G.,Baker, E.,Balasubramanyam, A.,Baldridge, D.,Bale, J.,Bamshad, M.,Barbouth, D.,Batzli, G. F.,Bayrak-Toydemir, P.,Beck, A.,Beggs, A. H.,Bejerano, G.,Bellen, H. J.,Bennet, J.,Berg-Rood, B.,Bernier, R.,Bernstein, J. A.,Berry, G. T.,Bican, A.,Bivona, S.,Blue, E.,Bohnsack, J.,Bonnenmann, C.,Bonner, D.,Botto, L.,Briere, L. C.,Brokamp, E.,Burke, E. A.,Burrage, L. C.,Butte, M. J.,Byers, P.,Carey, J.,Carrasquillo, O.,Chang, T. C. P.,Chanprasert, S.,Chao, H.-T.,Clark, G. D.,Coakley, T. R.,Cobban, L. A.,Cogan, J. D.,Cole, F. S.,Colley, H. A.,Cooper, C. M.,Cope, H.,Craigen, W. J.,Cunningham, M.,D'Souza, P.,Dai, H.,Dasari, S.,Davids, M.,Dayal, J. G.,Dell'Angelica, E. C.,Dhar, S. U.,Dipple, K.,Doherty, D.,Dorrani, N.,Douine, E. D.,Draper, D. D.,Duncan, L.,Earl, D.,Eckstein, D. J.,Emrick, L. T.,Eng, C. M., et al. 2020. De novo EIF2AK1 and EIF2AK2 Variants Are Associated with Developmental Delay, Leukoencephalopathy, and Neurologic Decompensation. *The American Journal of Human Genetics,* 106**,** 570-583.

Mao, T.,Israelow, B.,Lucas, C.,Vogels, C. B. F.,Fedorova, O.,Breban, M. I.,Menasche, B. L.,Dong, H.,Linehan, M.,Wilen, C. B.,Landry, M. L.,Grubaugh, N. D.,Pyle, A. M. & Iwasaki, A. 2021. A stem-loop RNA RIG-I agonist confers prophylactic and therapeutic protection against acute and chronic SARS-CoV-2 infection in mice. *bioRxiv***,** 2021.2006.2016.448754.

Marcelin, J. R.,Wilson, J. W. & Razonable, R. R. 2014. Oral ribavirin therapy for respiratory syncytial virus infections in moderately to severely immunocompromised patients. *Transpl Infect Dis,* 16**,** 242-250.

Margine, I. & Krammer, F. 2014. Animal models for influenza viruses: implications for universal vaccine development. *Pathogens (Basel, Switzerland),* 3**,** 845-874.

Marr, N.,Turvey, S. E. & Grandvaux, N. 2013. Pathogen recognition receptor crosstalk in respiratory syncytial virus sensing: a host and cell type perspective. *Trends Microbiol,* 21**,** 568-574.

Marriott, A. C.,Dove, B. K.,Whittaker, C. J.,Bruce, C.,Ryan, K. A.,Bean, T. J.,Rayner, E.,Pearson, G.,Taylor, I.,Dowall, S.,Plank, J.,Newman, E.,Barclay, W. S.,Dimmock, N. J.,Easton, A. J.,Hallis, B.,Silman, N. J. & Carroll, M. W. 2014. Low dose influenza virus challenge in the ferret leads to increased virus shedding and greater sensitivity to oseltamivir. *PLoS One,* 9**,** e94090.

Marx, S.,Kümmerer, B. M.,Grützner, C.,Kato, H.,Schlee, M.,Bartok, E.,Renn, M. & Hartmann, G. 2021. RIG-I-induced innate antiviral immunity protects mice from lethal SARS-CoV-2 infection. *bioRxiv***,** 2021.2008.2006.455405.

Mathieu, N. A.,Paparisto, E.,Barr, S. D. & Spratt, D. E. 2021. HERC5 and the ISGylation Pathway: Critical Modulators of the Antiviral Immune Response. *Viruses* [Online], 13. [Accessed 2021/06//].

Matsuda, D.,Sato, H. & Maquat, L. E. 2008. Chapter 9 - Studying Nonsense-Mediated mRNA Decay in Mammalian Cells. *In:* MAQUAT, L. E. & KILEDJIAN, M. (eds.) *Methods in Enzymology.* Academic Press.

Matsuzaki, Y.,Katsushima, N.,Nagai, Y.,Shoji, M.,Itagaki, T.,Sakamoto, M.,Kitaoka, S.,Mizuta, K. & Nishimura, H. 2006. Clinical Features of Influenza C Virus Infection in Children. *J Infect Dis,* 193**,** 1229-1235.

Mayor, J.,Engler, O. & Rothenberger, S. 2021. Antiviral Efficacy of Ribavirin and Favipiravir against Hantaan Virus. *Microorganisms,* 9**,** 1306.

Mazur, N. I.,Higgins, D.,Nunes, M. C.,Melero, J. A.,Langedijk, A. C.,Horsley, N.,Buchholz, U. J.,Openshaw, P. J.,McLellan, J. S.,Englund, J. A.,Mejias, A.,Karron, R. A.,Simões, E. A.,Knezevic, I.,Ramilo, O.,Piedra, P. A.,Chu, H. Y.,Falsey, A. R.,Nair, H.,Kragten-Tabatabaie, L.,Greenough, A.,Baraldi, E.,Papadopoulos, N. G.,Vekemans, J.,Polack, F. P.,Powell, M.,Satav, A.,Walsh, E. E.,Stein, R. T.,Graham, B. S. & Bont, L. J. 2018. The respiratory syncytial virus vaccine landscape: lessons from the graveyard and promising candidates. *Lancet Infect Dis,* 18**,** e295-e311.

McAuley, J. L.,Gilbertson, B. P.,Trifkovic, S.,Brown, L. E. & McKimm-Breschkin, J. L. 2019. Influenza Virus Neuraminidase Structure and Functions. *Front Microbiol,* 10.

McCormick, J. B.,King, I. J.,Webb, P. A.,Scribner, C. L.,Craven, R. B.,Johnson, K. M.,Elliott, L. H. & Belmont-Williams, R. 1986. Lassa fever. Effective therapy with ribavirin. *N Engl J Med,* 314**,** 20-26.

McKimm-Breschkin, J. L. 2013. Influenza neuraminidase inhibitors: antiviral action and mechanisms of resistance. *Influenza and Other Respiratory Viruses,* 7**,** 25-36.

Meier, K.,Jaguva Vasudevan, A. A.,Zhang, Z.,Bähr, A.,Kochs, G.,Häussinger, D. & Münk, C. 2018. Equine MX2 is a restriction factor of equine infectious anemia virus (EIAV). *Virology,* 523**,** 52-63.

Meijer, A.,Lackenby, A.,Hungnes, O.,Lina, B.,van-der-Werf, S.,Schweiger, B.,Opp, M.,Paget, J.,van-de-Kassteele, J.,Hay, A. & Zambon, M. 2009. Oseltamivir-resistant influenza virus A (H1N1), Europe, 2007-08 season. *Emerg Infect Dis,* 15**,** 552-560.

Meischel, T.,Fritzlar, S.,Villalon-Letelier, F.,Tessema, M. B.,Brooks, A. G.,Reading, P. C. & Londrigan, S. L. 2021. IFITM proteins that restrict the early stages of respiratory virus infection do not influence late-stage replication. *J Virol***,** Jvi0083721.

Mejias, A.,Garcia-Maurino, C.,Rodriguez-Fernandez, R.,Peeples, M. E. & Ramilo, O. 2017. Development and clinical applications of novel antibodies for prevention and treatment of respiratory syncytial virus infection. *Vaccine,* 35**,** 496-502.

Melén, K.,Keskinen, P.,Ronni, T.,Sareneva, T.,Lounatmaa, K. & Julkunen, I. 1996. Human MxB Protein, an Interferon-α-inducible GTPase, Contains a Nuclear Targeting Signal and Is Localized in the Heterochromatin Region beneath the Nuclear Envelope*. *Journal of Biological Chemistry,* 271**,** 23478-23486.

Meng, X.,Zhang, F.,Yan, B.,Si, C.,Honda, H.,Nagamachi, A.,Sun, L.-Z. & Xiang, Y. 2018. A paralogous pair of mammalian host restriction factors form a critical host barrier against poxvirus infection. *PLoS Pathog,* 14**,** e1006884.

Meyerson, N. R.,Zhou, L.,Guo, Y. R.,Zhao, C.,Tao, Y. J.,Krug, R. M. & Sawyer, S. L. 2017. Nuclear TRIM25 Specifically Targets Influenza Virus Ribonucleoproteins to Block the Onset of RNA Chain Elongation. *Cell Host Microbe,* 22**,** 627-638.e627.

Mifsud, E. J.,Tilmanis, D.,Oh, D. Y.,Ming-Kay Tai, C.,Rossignol, J. F. & Hurt, A. C. 2020. Prophylaxis of ferrets with nitazoxanide and oseltamivir combinations is more effective at reducing the impact of influenza a virus infection compared to oseltamivir monotherapy. *Antiviral Res,* 176**,** 104751.

Mitchell, Patrick S.,Patzina, C.,Emerman, M.,Haller, O.,Malik, Harmit S. & Kochs, G. 2012. Evolution-Guided Identification of Antiviral Specificity Determinants in the Broadly Acting Interferon-Induced Innate Immunity Factor MxA. *Cell Host Microbe,* 12**,** 598-604.

Moffat, J.,Grueneberg, D. A.,Yang, X.,Kim, S. Y.,Kloepfer, A. M.,Hinkle, G.,Piqani, B.,Eisenhaure, T. M.,Luo, B.,Grenier, J. K.,Carpenter, A. E.,Foo, S. Y.,Stewart, S. A.,Stockwell, B. R.,Hacohen, N.,Hahn, W. C.,Lander, E. S.,Sabatini, D. M. & Root, D. E. 2006. A lentiviral RNAi library for human and mouse genes applied to an arrayed viral high-content screen. *Cell,* 124**,** 1283-1298.

Morales, D. J.,Monte, K.,Sun, L.,Struckhoff, J. J.,Agapov, E.,Holtzman, M. J.,Stappenbeck, T. S. & Lenschow, D. J. 2015. Novel mode of ISG15-mediated protection against influenza A virus and Sendai virus in mice. *J Virol,* 89**,** 337-349.

Mordstein, M.,Kochs, G.,Dumoutier, L.,Renauld, J.-C.,Paludan, S. R.,Klucher, K. & Staeheli, P. 2008. Interferon-λ Contributes to Innate Immunity of Mice against Influenza A Virus but Not against Hepatotropic Viruses. *PLoS Pathog,* 4**,** e1000151.

Mordstein, M.,Neugebauer, E.,Ditt, V.,Jessen, B.,Rieger, T.,Falcone, V.,Sorgeloos, F.,Ehl, S.,Mayer, D.,Kochs, G.,Schwemmle, M.,Günther, S.,Drosten, C.,Michiels, T. & Staeheli, P. 2010. Lambda interferon renders epithelial cells of the respiratory and gastrointestinal tracts resistant to viral infections. *J Virol,* 84**,** 5670-5677.

Morens, D. M. & Taubenberger, J. K. 2018. The Mother of All Pandemics Is 100 Years Old (and Going Strong)! *Am J Public Health***,** e1-e6.

Moresco, E. M. Y. & Beutler, B. 2010. LGP2: Positive about viral sensing. *Proceedings of the National Academy of Sciences,* 107**,** 1261-1262.

Morris, D. E.,Cleary, D. W. & Clarke, S. C. 2017. Secondary Bacterial Infections Associated with Influenza Pandemics. *Front Microbiol,* 8.

Munday, D. C.,Wu, W.,Smith, N.,Fix, J.,Noton, S. L.,Galloux, M.,Touzelet, O.,Armstrong, S. D.,Dawson, J. M.,Aljabr, W.,Easton, A. J.,Rameix-Welti, M. A.,de Oliveira, A. P.,Simabuco, F. M.,Ventura, A. M.,Hughes, D. J.,Barr, J. N.,Fearns, R.,Digard, P.,Eléouët, J. F. & Hiscox, J. A. 2015. Interactome analysis of the human respiratory syncytial virus RNA polymerase complex identifies protein chaperones as important cofactors that promote L-protein stability and RNA synthesis. *J Virol,* 89**,** 917-930.

Nair, A. B. & Jacob, S. 2016. A simple practice guide for dose conversion between animals and human. *Journal of basic and clinical pharmacy,* 7**,** 27-31.

Nair, H.,Nokes, D. J.,Gessner, B. D.,Dherani, M.,Madhi, S. A.,Singleton, R. J.,O'Brien, K. L.,Roca, A.,Wright, P. F.,Bruce, N.,Chandran, A.,Theodoratou, E.,Sutanto, A.,Sedyaningsih, E. R.,Ngama, M.,Munywoki, P. K.,Kartasasmita, C.,Simões, E. A.,Rudan, I.,Weber, M. W. & Campbell, H. 2010. Global burden of acute lower respiratory infections due to respiratory syncytial virus in young children: a systematic review and meta-analysis. *Lancet,* 375**,** 1545-1555.

Nam, H. H. & Ison, M. G. 2019. Respiratory syncytial virus infection in adults. *Bmj,* 366**,** l5021.

Nayak, D. P.,Balogun, R. A.,Yamada, H.,Zhou, Z. H. & Barman, S. 2009. Influenza virus morphogenesis and budding. *Virus Res,* 143**,** 147-161.

Nguyen Ba, A. N.,Pogoutse, A.,Provart, N. & Moses, A. M. 2009. NLStradamus: a simple Hidden Markov Model for nuclear localization signal prediction. *BMC Bioinformatics,* 10**,** 202.

Nichol, S. T.,Arikawa, J. & Kawaoka, Y. 2000. Emerging viral diseases. *Proceedings of the National Academy of Sciences,* 97**,** 12411-12412.

Nie, L.,Cai, S.-Y.,Shao, J.-Z. & Chen, J. 2018. Toll-Like Receptors, Associated Biological Roles, and Signaling Networks in Non-Mammals. *Front Immunol,* 9.

Norrby, E.,Marusyk, H. & Orvell, C. 1970. Morphogenesis of respiratory syncytial virus in a green monkey kidney cell line (Vero). *J Virol,* 6**,** 237-242.

Noteborn, M.,Arnheiter, H.,Richter-Mann, L.,Browning, H. & Weissmann, C. 1987. Transport of the murine Mx protein into the nucleus is dependent on a basic carboxy-terminal sequence. *J Interferon Res,* 7**,** 657-669.

O'Brien, T. R.,Prokunina-Olsson, L. & Donnelly, R. P. 2014. IFN-λ4: the paradoxical new member of the interferon lambda family. *J Interferon Cytokine Res,* 34**,** 829-838.

Oestereich, L.,Lüdtke, A.,Wurr, S.,Rieger, T.,Muñoz-Fontela, C. & Günther, S. 2014. Successful treatment of advanced Ebola virus infection with T-705 (favipiravir) in a small animal model. *Antiviral Res,* 105**,** 17-21.

Oh, D. Y.,Barr, I. G. & Hurt, A. C. 2015. A novel video tracking method to evaluate the effect of influenza infection and antiviral treatment on ferret activity. *PLoS One,* 10**,** e0118780.

Oh, D. Y. & Hurt, A. C. 2016. Using the Ferret as an Animal Model for Investigating Influenza Antiviral Effectiveness. *Front Microbiol,* 7**,** 80.

Oh, D. Y.,Lowther, S.,McCaw, J. M.,Sullivan, S. G.,Leang, S.-K.,Haining, J.,Arkinstall, R.,Kelso, A.,Mcvernon, J.,Barr, I. G.,Middleton, D. & Hurt, A. C. 2014. Evaluation of oseltamivir prophylaxis regimens for reducing influenza virus infection, transmission and disease severity in a ferret model of household contact. *Journal of Antimicrobial Chemotherapy,* 69**,** 2458-2469.

Ohmori, Y.,Schreiber, R. D. & Hamilton, T. A. 1997. Synergy between interferon-gamma and tumor necrosis factor-alpha in transcriptional activation is mediated by cooperation between signal transducer and activator of transcription 1 and nuclear factor kappaB. *J Biol Chem,* 272**,** 14899-14907.

Okabayashi, T.,Kojima, T.,Masaki, T.,Yokota, S.,Imaizumi, T.,Tsutsumi, H.,Himi, T.,Fujii, N. & Sawada, N. 2011. Type-III interferon, not type-I, is the predominant interferon induced by respiratory viruses in nasal epithelial cells. *Virus Res,* 160**,** 360-366.

Okamoto, M.,Kouwaki, T.,Fukushima, Y. & Oshiumi, H. 2017. Regulation of RIG-I Activation by K63-Linked Polyubiquitination. *Front Immunol,* 8**,** 1942.

Okude, H.,Ori, D. & Kawai, T. 2020. Signaling Through Nucleic Acid Sensors and Their Roles in Inflammatory Diseases. *Front Immunol,* 11**,** 625833.

Olagnier, D.,Scholte, F. E.,Chiang, C.,Albulescu, I. C.,Nichols, C.,He, Z.,Lin, R.,Snijder, E. J.,van Hemert, M. J. & Hiscott, J. 2014. Inhibition of dengue and chikungunya virus infections by RIG-I-mediated type I interferon-independent stimulation of the innate antiviral response. *J Virol,* 88**,** 4180-4194.

Olchanski, N.,Hansen, R. N.,Pope, E.,D'Cruz, B.,Fergie, J.,Goldstein, M.,Krilov, L. R.,McLaurin, K. K.,Nabrit-Stephens, B.,Oster, G.,Schaecher, K.,Shaya, F. T.,Neumann, P. J. & Sullivan, S. D. 2018. Palivizumab Prophylaxis for Respiratory Syncytial Virus: Examining the Evidence Around Value. *Open Forum Infect Dis,* 5**,** ofy031.

Olsen, B.,Munster, V. J.,Wallensten, A.,Waldenström, J.,Osterhaus, A. D. M. E. & Fouchier, R. A. M. 2006. Global Patterns of Influenza A Virus in Wild Birds. *Science,* 312**,** 384-388.

Openshaw, P. J. 2013. The mouse model of respiratory syncytial virus disease. *Curr Top Microbiol Immunol,* 372**,** 359-369.

Osterholm, M. T.,Kelley, N. S.,Sommer, A. & Belongia, E. A. 2012. Efficacy and effectiveness of influenza vaccines: a systematic review and meta-analysis. *Lancet Infect Dis,* 12**,** 36-44.

Palm, M.,Garigliany, M.-M.,Cornet, F. & Desmecht, D. 2010. Interferon-induced Sus scrofa Mx1 blocks endocytic traffic of incoming influenza A virus particles. *Veterinary research,* 41**,** 29-29.

Pangesti, K. N. A.,Abd El Ghany, M.,Walsh, M. G.,Kesson, A. M. & Hill-Cawthorne, G. A. 2018. Molecular epidemiology of respiratory syncytial virus. *Reviews in Medical Virology,* 28**,** e1968.

Pastey, M. K.,Crowe, J. E., Jr. & Graham, B. S. 1999. RhoA interacts with the fusion glycoprotein of respiratory syncytial virus and facilitates virus-induced syncytium formation. *J Virol,* 73**,** 7262-7270.

Pattabhi, S.,Wilkins, C. R.,Dong, R.,Knoll, M. L.,Posakony, J.,Kaiser, S.,Mire, C. E.,Wang, M. L.,Ireton, R. C.,Geisbert, T. W.,Bedard, K. M.,Iadonato, S. P.,Loo, Y. M. & Gale, M., Jr. 2015. Targeting Innate Immunity for Antiviral Therapy through Small Molecule Agonists of the RLR Pathway. *J Virol,* 90**,** 2372-2387.

Paules, C. & Subbarao, K. 2017. Influenza. *Lancet,* 390**,** 697-708.

Pavlovic, J.,Haller, O. & Staeheli, P. 1992. Human and mouse Mx proteins inhibit different steps of the influenza virus multiplication cycle. *J Virol,* 66**,** 2564-2569.

Pavlovic, J.,Zürcher, T.,Haller, O. & Staeheli, P. 1990. Resistance to influenza virus and vesicular stomatitis virus conferred by expression of human MxA protein. *J Virol,* 64**,** 3370-3375.

Pei, J.,Wagner, N. D.,Zou, A. J.,Chatterjee, S.,Borek, D.,Cole, A. R.,Kim, P. J.,Basler, C. F.,Otwinowski, Z.,Gross, M. L.,Amarasinghe, G. K. & Leung, D. W. 2021. Structural basis for IFN antagonism by human respiratory syncytial virus nonstructural protein 2. *Proceedings of the National Academy of Sciences,* 118**,** e2020587118.

Peng, X.,Alföldi, J.,Gori, K.,Eisfeld, A. J.,Tyler, S. R.,Tisoncik-Go, J.,Brawand, D.,Law, G. L.,Skunca, N.,Hatta, M.,Gasper, D. J.,Kelly, S. M.,Chang, J.,Thomas, M. J.,Johnson, J.,Berlin, A. M.,Lara, M.,Russell, P.,Swofford, R.,Turner-Maier, J.,Young, S.,Hourlier, T.,Aken, B.,Searle, S.,Sun, X.,Yi, Y.,Suresh, M.,Tumpey, T. M.,Siepel, A.,Wisely, S. M.,Dessimoz, C.,Kawaoka, Y.,Birren, B. W.,Lindblad-Toh, K.,Di Palma, F.,Engelhardt, J. F.,Palermo, R. E. & Katze, M. G. 2014. The draft genome sequence of the ferret (Mustela putorius furo) facilitates study of human respiratory disease. *Nature Biotechnology,* 32**,** 1250-1255.

Perng, Y.-C. & Lenschow, D. J. 2018. ISG15 in antiviral immunity and beyond. *Nature Reviews Microbiology,* 16**,** 423-439.

Pichlmair, A.,Lassnig, C.,Eberle, C. A.,Górna, M. W.,Baumann, C. L.,Burkard, T. R.,Bürckstümmer, T.,Stefanovic, A.,Krieger, S.,Bennett, K. L.,Rülicke, T.,Weber, F.,Colinge, J.,Müller, M. & Superti-Furga, G. 2011. IFIT1 is an antiviral protein that recognizes 5'-triphosphate RNA. *Nat Immunol,* 12**,** 624-630.

Pichlmair, A.,Schulz, O.,Tan, C. P.,Naslund, T. I.,Liljestrom, P.,Weber, F. & Reis e Sousa, C. 2006. RIG-I-mediated antiviral responses to single-stranded RNA bearing 5'-phosphates. *Science,* 314**,** 997-1001.

Piedimonte, G. & Perez, M. K. 2014. Respiratory syncytial virus infection and bronchiolitis. *Pediatr Rev,* 35**,** 519-530.

Prince, G. A.,Horswood, R. L.,Berndt, J.,Suffin, S. C. & Chanock, R. M. 1979. Respiratory syncytial virus infection in inbred mice. *Infect Immun,* 26**,** 764-766.

Prince, G. A. & Porter, D. D. 1976. The pathogenesis of respiratory syncytial virus infection in infant ferrets. *Am J Pathol,* 82**,** 339-352.

Rabinovich, G. A. & Toscano, M. A. 2009. Turning 'sweet' on immunity: galectin–glycan interactions in immune tolerance and inflammation. *Nature Reviews Immunology,* 9**,** 338-352.

Radin, J. M.,Hawksworth, A. W.,Myers, C. A.,Ricketts, M. N.,Hansen, E. A. & Brice, G. T. 2016. Influenza vaccine effectiveness: Maintained protection

throughout the duration of influenza seasons 2010-2011 through 2013-2014. *Vaccine,* 34**,** 3907-3912.

Rajsbaum, R.,Albrecht, R. A.,Wang, M. K.,Maharaj, N. P.,Versteeg, G. A.,Nistal-Villan, E.,Garcia-Sastre, A. & Gack, M. U. 2012. Species-specific inhibition of RIG-I ubiquitination and IFN induction by the influenza A virus NS1 protein. *PLoS Pathog,* 8**,** e1003059.

Rameix-Welti, M. A.,Le Goffic, R.,Herve, P. L.,Sourimant, J.,Remot, A.,Riffault, S.,Yu, Q.,Galloux, M.,Gault, E. & Eleouet, J. F. 2014. Visualizing the replication of respiratory syncytial virus in cells and in living mice. *Nat Commun,* 5**,** 5104.

Ramvikas, M.,Arumugam, M.,Chakrabarti, S. R. & Jaganathan, K. S. 2017. Chapter Fifteen - Nasal Vaccine Delivery. *In:* SKWARCZYNSKI, M. & TOTH, I. (eds.) *Micro and Nanotechnology in Vaccine Development.* William Andrew Publishing.

Ranjan, P.,Jayashankar, L.,Deyde, V.,Zeng, H.,Davis, W. G.,Pearce, M. B.,Bowzard, J. B.,Hoelscher, M. A.,Jeisy-Scott, V.,Wiens, M. E.,Gangappa, S.,Gubareva, L.,García-Sastre, A.,Katz, J. M.,Tumpey, T. M.,Fujita, T. & Sambhara, S. 2010. 5'PPP-RNA induced RIG-I activation inhibits drug-resistant avian H5N1 as well as 1918 and 2009 pandemic influenza virus replication. *Virol J,* 7**,** 102.

Reed, L. J. & Muench, H. 1938. A SIMPLE METHOD OF ESTIMATING FIFTY PER CENT ENDPOINTS12. *Am J Epidemiol,* 27**,** 493-497.

Rehwinkel, J. & Gack, M. U. 2020. RIG-I-like receptors: their regulation and roles in RNA sensing. *Nat Rev Immunol,* 20**,** 537-551.

Rehwinkel, J.,Tan, C. P.,Goubau, D.,Schulz, O.,Pichlmair, A.,Bier, K.,Robb, N.,Vreede, F.,Barclay, W.,Fodor, E. & Reis e Sousa, C. 2010. RIG-I Detects Viral Genomic RNA during Negative-Strand RNA Virus Infection. *Cell,* 140**,** 397-408.

Rennie, Martin L.,McKelvie, Siri A.,Bulloch, Esther M. M. & Kingston, Richard L. 2014. Transient Dimerization of Human MxA Promotes GTP Hydrolysis, Resulting in a Mechanical Power Stroke. *Structure,* 22**,** 1433-1445.

Rice, G. I.,Del Toro Duany, Y.,Jenkinson, E. M.,Forte, G. M.,Anderson, B. H.,Ariaudo, G.,Bader-Meunier, B.,Baildam, E. M.,Battini, R.,Beresford, M. W.,Casarano, M.,Chouchane, M.,Cimaz, R.,Collins, A. E.,Cordeiro, N. J.,Dale, R. C.,Davidson, J. E.,De Waele, L.,Desguerre, I.,Faivre, L.,Fazzi, E.,Isidor, B.,Lagae, L.,Latchman, A. R.,Lebon, P.,Li, C.,Livingston, J. H.,Lourenço, C. M.,Mancardi, M. M.,Masurel-Paulet, A.,McInnes, I. B.,Menezes, M. P.,Mignot, C.,O'Sullivan, J.,Orcesi, S.,Picco, P. P.,Riva, E.,Robinson, R. A.,Rodriguez, D.,Salvatici, E.,Scott, C.,Szybowska, M.,Tolmie, J. L.,Vanderver, A.,Vanhulle, C.,Vieira, J. P.,Webb, K.,Whitney, R. N.,Williams, S. G.,Wolfe, L. A.,Zuberi, S. M.,Hur, S. & Crow, Y. J. 2014. Gain-of-function mutations in IFIH1 cause a spectrum of human disease phenotypes associated with upregulated type I interferon signaling. *Nat Genet,* 46**,** 503-509.

Richard, M.,van den Brand, J. M. A.,Bestebroer, T. M.,Lexmond, P.,de Meulder, D.,Fouchier, R. A. M.,Lowen, A. C. & Herfst, S. 2020. Influenza A viruses are transmitted via the air from the nasal respiratory epithelium of ferrets. *Nat Commun,* 11**,** 766.

Rivas-Fuentes, S.,Salgado-Aguayo, A.,Arratia-Quijada, J. & Gorocica-Rosete, P. 2021. Regulation and biological functions of the CX3CL1-CX3CR1 axis and its relevance in solid cancer: A mini-review. *Journal of Cancer,* 12**,** 571-583.

Robinson, T.,Kariuki, S. N.,Franek, B. S.,Kumabe, M.,Kumar, A. A.,Badaracco, M.,Mikolaitis, R. A.,Guerrero, G.,Utset, T. O.,Drevlow, B. E.,Zaacks, L. S.,Grober, J. S.,Cohen, L. M.,Kirou, K. A.,Crow, M. K.,Jolly, M. & Niewold, T. B. 2011. Autoimmune disease risk variant of IFIH1 is associated with increased sensitivity to IFN-α and serologic autoimmunity in lupus patients. *J Immunol,* 187**,** 1298-1303.

Rodriguez, K. R.,Bruns, A. M. & Horvath, C. M. 2014. MDA5 and LGP2: accomplices and antagonists of antiviral signal transduction. *J Virol,* 88**,** 8194-8200.

Rodriguez, L.,Nogales, A. & Martínez-Sobrido, L. 2017. Influenza A Virus Studies in a Mouse Model of Infection. *J Vis Exp***,** 55898.

Rosário-Ferreira, N.,Preto, A. J.,Melo, R.,Moreira, I. S. & Brito, R. M. M. 2020. The Central Role of Non-Structural Protein 1 (NS1) in Influenza Biology and Infection. *Int J Mol Sci,* 21.

Rossman, J. S. & Lamb, R. A. 2011. Influenza virus assembly and budding. *Virology,* 411**,** 229-236.

Rozycki, H. J. 2014. Potential Contribution of Type I Alveolar Epithelial Cells to Chronic Neonatal Lung Disease. *Frontiers in Pediatrics,* 2.

Sadler, A. J. & Williams, B. R. G. 2008. Interferon-inducible antiviral effectors. *Nature Reviews Immunology,* 8**,** 559-568.

Saito, T.,Hirai, R.,Loo, Y. M.,Owen, D.,Johnson, C. L.,Sinha, S. C.,Akira, S.,Fujita, T. & Gale, M., Jr. 2007. Regulation of innate antiviral defenses through a shared repressor domain in RIG-I and LGP2. *Proc Natl Acad Sci U S A,* 104**,** 582-587.

Salomon, R.,Staeheli, P.,Kochs, G.,Yen, H. L.,Franks, J.,Rehg, J. E.,Webster, R. G. & Hoffmann, E. 2007. Mx1 gene protects mice against the highly lethal human H5N1 influenza virus. *Cell Cycle,* 6**,** 2417-2421.

Samy, R. P. & Lim, L. H. K. 2015. DAMPs and influenza virus infection in ageing. *Ageing Research Reviews,* 24**,** 83-97.

Sande, C. J.,Njunge, J. M.,Mwongeli Ngoi, J.,Mutunga, M. N.,Chege, T.,Gicheru, E. T.,Gardiner, E. M.,Gwela, A.,Green, C. A.,Drysdale, S. B.,Berkley, J. A.,Nokes, D. J. & Pollard, A. J. 2019. Airway response to respiratory syncytial virus has incidental antibacterial effects. *Nat Commun,* 10**,** 2218.

Sanders, J. M.,Monogue, M. L.,Jodlowski, T. Z. & Cutrell, J. B. 2020. Pharmacologic Treatments for Coronavirus Disease 2019 (COVID-19): A Review. *Jama,* 323**,** 1824-1836.

Sarmiento, R. E.,Tirado, R. & Gómez, B. 2002. Characteristics of a respiratory syncytial virus persistently infected macrophage-like culture. *Virus Res,* 84**,** 45-58.

Saunders-Hastings, P. R. & Krewski, D. 2016. Reviewing the History of Pandemic Influenza: Understanding Patterns of Emergence and Transmission. *Pathogens (Basel, Switzerland),* 5**,** 66.

Schildgen, V.,van den Hoogen, B.,Fouchier, R.,Tripp, R. A.,Alvarez, R.,Manoha, C.,Williams, J. & Schildgen, O. 2011. Human Metapneumovirus: lessons learned over the first decade. *Clin Microbiol Rev,* 24**,** 734-754.

Schilling, M.,Bulli, L.,Weigang, S.,Graf, L.,Naumann, S.,Patzina, C.,Wagner, V.,Bauersfeld, L.,Goujon, C.,Hengel, H.,Halenius, A.,Ruzsics, Z.,Schaller, T.,Kochs, G. & Sandri-Goldin, R. M. 2018. Human MxB Protein Is a Pan-herpesvirus Restriction Factor. *J Virol,* 92**,** e01056-01018.

Schlee, M.,Roth, A.,Hornung, V.,Hagmann, C. A.,Wimmenauer, V.,Barchet, W.,Coch, C.,Janke, M.,Mihailovic, A.,Wardle, G.,Juranek, S.,Kato, H.,Kawai, T.,Poeck, H.,Fitzgerald, K. A.,Takeuchi, O.,Akira, S.,Tuschl, T.,Latz, E.,Ludwig, J. & Hartmann, G. 2009. Recognition of 5' triphosphate by RIG-I helicase requires short blunt double-stranded RNA as contained in panhandle of negative-strand virus. *Immunity,* 31**,** 25-34.

Schlender, J.,Hornung, V.,Finke, S.,Günthner-Biller, M.,Marozin, S.,Brzózka, K.,Moghim, S.,Endres, S.,Hartmann, G. & Conzelmann, K. K. 2005. Inhibition of toll-like receptor 7- and 9-mediated alpha/beta interferon production in human plasmacytoid dendritic cells by respiratory syncytial virus and measles virus. *J Virol,* 79**,** 5507-5515.

Schmidt, A.,Schwerd, T.,Hamm, W.,Hellmuth, J. C.,Cui, S.,Wenzel, M.,Hoffmann, F. S.,Michallet, M.-C.,Besch, R.,Hopfner, K.-P.,Endres, S. & Rothenfusser, S. 2009. 5′-triphosphate RNA requires base-paired structures to activate antiviral signaling via RIG-I. *Proceedings of the National Academy of Sciences,* 106**,** 12067-12072.

Schneider, C. A.,Rasband, W. S. & Eliceiri, K. W. 2012. NIH Image to ImageJ: 25 years of image analysis. *Nat Methods,* 9**,** 671-675.

Schnorr, J. J.,Schneider-Schaulies, S.,Simon-Jödicke, A.,Pavlovic, J.,Horisberger, M. A. & ter Meulen, V. 1993. MxA-dependent inhibition of measles virus glycoprotein synthesis in a stably transfected human monocytic cell line. *J Virol,* 67**,** 4760-4768.

Schoggins, J. W. & Rice, C. M. 2011a. Interferon-stimulated genes and their antiviral effector functions. *Curr Opin Virol,* 1**,** 519-525.

Schoggins, J. W.,Wilson, S. J.,Panis, M.,Murphy, M. Y.,Jones, C. T.,Bieniasz, P. & Rice, C. M. 2011b. A diverse range of gene products are effectors of the type I interferon antiviral response. *Nature,* 472**,** 481-485.

Schreiber, G. 2017. The molecular basis for differential type I interferon signaling. *Journal of Biological Chemistry,* 292**,** 7285-7294.

Schuberth-Wagner, C.,Ludwig, J.,Bruder, A. K.,Herzner, A. M.,Zillinger, T.,Goldeck, M.,Schmidt, T.,Schmid-Burgk, J. L.,Kerber, R.,Wolter, S.,Stumpel, J. P.,Roth, A.,Bartok, E.,Drosten, C.,Coch, C.,Hornung, V.,Barchet, W.,Kummerer, B. M.,Hartmann, G. & Schlee, M. 2015. A Conserved Histidine in the RNA Sensor RIG-I Controls Immune Tolerance to N1-2'O-Methylated Self RNA. *Immunity,* 43**,** 41-51.

Schwartz, S. L. & Conn, G. L. 2019. RNA regulation of the antiviral protein 2′-5′-oligoadenylate synthetase. *WIREs RNA,* 10**,** e1534.

Scott, L. J. & Lamb, H. M. 1999. Palivizumab. *Drugs,* 58**,** 305-311; discussion 312-303.

Segovia, J.,Sabbah, A.,Mgbemena, V.,Tsai, S.-Y.,Chang, T.-H.,Berton, M. T.,Morris, I. R.,Allen, I. C.,Ting, J. P. Y. & Bose, S. 2012. TLR2/MyD88/NF-

κB Pathway, Reactive Oxygen Species, Potassium Efflux Activates NLRP3/ASC Inflammasome during Respiratory Syncytial Virus Infection. *PLoS One,* 7**,** e29695.

Sehgal, P. B.,Yuan, H.,Scott, M. F.,Deng, Y.,Liang, F. X. & Mackiewicz, A. 2020. Murine GFP-Mx1 forms nuclear condensates and associates with cytoplasmic intermediate filaments: Novel antiviral activity against VSV. *J Biol Chem,* 295**,** 18023-18035.

Seth, R. B.,Sun, L.,Ea, C. K. & Chen, Z. J. 2005. Identification and characterization of MAVS, a mitochondrial antiviral signaling protein that activates NF-kappaB and IRF 3. *Cell,* 122**,** 669-682.

Shan, J.,Britton, P. N.,King, C. L. & Booy, R. 2021. The immunogenicity and safety of respiratory syncytial virus vaccines in development: A systematic review. *Influenza and Other Respiratory Viruses,* 15**,** 539-551.

Shi, T.,McAllister, D. A.,O'Brien, K. L.,Simoes, E. A. F.,Madhi, S. A.,Gessner, B. D.,Polack, F. P.,Balsells, E.,Acacio, S.,Aguayo, C.,Alassani, I.,Ali, A.,Antonio, M.,Awasthi, S.,Awori, J. O.,Azziz-Baumgartner, E.,Baggett, H. C.,Baillie, V. L.,Balmaseda, A.,Barahona, A.,Basnet, S.,Bassat, Q.,Basualdo, W.,Bigogo, G.,Bont, L.,Breiman, R. F.,Brooks, W. A.,Broor, S.,Bruce, N.,Bruden, D.,Buchy, P.,Campbell, S.,Carosone-Link, P.,Chadha, M.,Chipeta, J.,Chou, M.,Clara, W.,Cohen, C.,de Cuellar, E.,Dang, D. A.,Dash-Yandag, B.,Deloria-Knoll, M.,Dherani, M.,Eap, T.,Ebruke, B. E.,Echavarria, M.,de Freitas Lázaro Emediato, C. C.,Fasce, R. A.,Feikin, D. R.,Feng, L.,Gentile, A.,Gordon, A.,Goswami, D.,Goyet, S.,Groome, M.,Halasa, N.,Hirve, S.,Homaira, N.,Howie, S. R. C.,Jara, J.,Jroundi, I.,Kartasasmita, C. B.,Khuri-Bulos, N.,Kotloff, K. L.,Krishnan, A.,Libster, R.,Lopez, O.,Lucero, M. G.,Lucion, F.,Lupisan, S. P.,Marcone, D. N.,McCracken, J. P.,Mejia, M.,Moisi, J. C.,Montgomery, J. M.,Moore, D. P.,Moraleda, C.,Moyes, J.,Munywoki, P.,Mutyara, K.,Nicol, M. P.,Nokes, D. J.,Nymadawa, P.,da Costa Oliveira, M. T.,Oshitani, H.,Pandey, N.,Paranhos-Baccalà, G.,Phillips, L. N.,Picot, V. S.,Rahman, M.,Rakoto-Andrianarivelo, M.,Rasmussen, Z. A.,Rath, B. A.,Robinson, A.,Romero, C.,Russomando, G.,Salimi, V.,Sawatwong, P.,Scheltema, N.,Schweiger, B., et al. 2017. Global, regional, and national disease burden estimates of acute lower respiratory infections due to respiratory syncytial virus in young children in 2015: a systematic review and modelling study. *Lancet,* 390**,** 946-958.

Shigemoto, T.,Kageyama, M.,Hirai, R.,Zheng, J.,Yoneyama, M. & Fujita, T. 2009. Identification of loss of function mutations in human genes encoding RIG-I and MDA5: implications for resistance to type I diabetes. *J Biol Chem,* 284**,** 13348-13354.

Shirley, M. 2020. Baloxavir Marboxil: A Review in Acute Uncomplicated Influenza. *Drugs,* 80**,** 1109-1118.

Shope, R. E. 1934. THE INFECTION OF FERRETS WITH SWINE INFLUENZA VIRUS. *J Exp Med,* 60**,** 49-61.

Short, K. R.,Brooks, A. G.,Reading, P. C. & Londrigan, S. L. 2012. The fate of influenza A virus after infection of human macrophages and dendritic cells. *Journal of General Virology,* 93**,** 2315-2325.

Silva, M. T. 2010. When two is better than one: macrophages and neutrophils work in concert in innate immunity as complementary and cooperative partners of a myeloid phagocyte system. *J Leukoc Biol,* 87**,** 93-106.

Skandalis, A.,Frampton, M.,Seger, J. & Richards, M. H. 2010. The adaptive significance of unproductive alternative splicing in primates. *Rna,* 16**,** 2014-2022.

Skehel, J. J. & Wiley, D. C. 2000. Receptor binding and membrane fusion in virus entry: the influenza hemagglutinin. *Annu Rev Biochem,* 69**,** 531-569.

Smee, D. F.,von Itzstein, M.,Bhatt, B. & Tarbet, E. B. 2012. Exacerbation of influenza virus infections in mice by intranasal treatments and implications for evaluation of antiviral drugs. *Antimicrobial agents and chemotherapy,* 56**,** 6328-6333.

Smith, S. E.,Busse, D. C.,Binter, S.,Weston, S.,Soria, C. D.,Laksono, B. M.,Clare, S.,Nieuwkoop, S. V.,Hoogen, B. G. V. d.,Clement, M.,Marsden, M.,Humphreys, I. R.,Marsh, M.,Swart, R. L. d.,Wash, R. S.,Tregoning, J. S.,Kellam, P. & Dermody, T. S. 2019. Interferon-Induced Transmembrane Protein 1 Restricts Replication of Viruses That Enter Cells via the Plasma Membrane. *J Virol,* 93**,** e02003-02018.

Song, M. S.,Cho, Y. H.,Park, S. J.,Pascua, P. N.,Baek, Y. H.,Kwon, H. I.,Lee, O. J.,Kong, B. W.,Kim, H.,Shin, E. C.,Kim, C. J. & Choi, Y. K. 2013. Early regulation of viral infection reduces inflammation and rescues mx-positive mice from lethal avian influenza infection. *Am J Pathol,* 182**,** 1308-1321.

Spann, K. M.,Tran, K. C.,Chi, B.,Rabin, R. L. & Collins, P. L. 2004. Suppression of the induction of alpha, beta, and lambda interferons by the NS1 and NS2 proteins of human respiratory syncytial virus in human epithelial cells and macrophages [corrected]. *J Virol,* 78**,** 4363-4369.

Spann, K. M.,Tran, K. C. & Collins, P. L. 2005. Effects of nonstructural proteins NS1 and NS2 of human respiratory syncytial virus on interferon regulatory factor 3, NF-kappaB, and proinflammatory cytokines. *J Virol,* 79**,** 5353-5362.

Stabenow, D.,Frings, M.,Trück, C.,Gärtner, K.,Förster, I.,Kurts, C.,Tüting, T.,Odenthal, M.,Dienes, H. P.,Cederbrant, K.,Protzer, U. & Knolle, P. A. 2010. Bioluminescence imaging allows measuring CD8 T cell function in the liver. *Hepatology,* 51**,** 1430-1437.

Staeheli, P.,Grob, R.,Meier, E.,Sutcliffe, J. G. & Haller, O. 1988. Influenza virus-susceptible mice carry Mx genes with a large deletion or a nonsense mutation. *Molecular and cellular biology,* 8**,** 4518-4523.

Stark, G. R. & Darnell, J. E., Jr. 2012. The JAK-STAT pathway at twenty. *Immunity,* 36**,** 503-514.

Steiner, F. & Pavlovic, J. 2020. Subcellular Localization of MxB Determines Its Antiviral Potential against Influenza A Virus. *J Virol,* 94.

Steinhauer, D. A.,Domingo, E. & Holland, J. J. 1992. Lack of evidence for proofreading mechanisms associated with an RNA virus polymerase. *Gene,* 122**,** 281-288.

Stittelaar, K. J.,de Waal, L.,van Amerongen, G.,Veldhuis Kroeze, E. J.,Fraaij, P. L.,van Baalen, C. A.,van Kampen, J. J.,van der Vries, E.,Osterhaus, A. D. & de Swart, R. L. 2016. Ferrets as a Novel Animal Model for Studying

Human Respiratory Syncytial Virus Infections in Immunocompetent and Immunocompromised Hosts. *Viruses,* 8.

Stockman, L. J.,Curns, A. T.,Anderson, L. J. & Fischer-Langley, G. 2012. Respiratory syncytial virus-associated hospitalizations among infants and young children in the United States, 1997-2006. *Pediatr Infect Dis J,* 31**,** 5-9.

Sultan, H.,Salazar, A. M. & Celis, E. 2020. Poly-ICLC, a multi-functional immune modulator for treating cancer. *Semin Immunol,* 49**,** 101414.

Sun, Y. & López, C. B. 2017. The innate immune response to RSV: Advances in our understanding of critical viral and host factors. *Vaccine,* 35**,** 481-488.

Szretter, K. J.,Balish, A. L. & Katz, J. M. 2006. Influenza: propagation, quantification, and storage. *Curr Protoc Microbiol,* Chapter 15**,** Unit 15G.11.

Takashita, E. 2021. Influenza Polymerase Inhibitors: Mechanisms of Action and Resistance. *Cold Spring Harb Perspect Med,* 11.

Takebe, Y.,Seiki, M.,Fujisawa, J.,Hoy, P.,Yokota, K.,Arai, K.,Yoshida, M. & Arai, N. 1988. SR alpha promoter: an efficient and versatile mammalian cDNA expression system composed of the simian virus 40 early promoter and the R-U5 segment of human T-cell leukemia virus type 1 long terminal repeat. *Mol Cell Biol,* 8**,** 466-472.

Talon, J.,Horvath, C. M.,Polley, R.,Basler, C. F.,Muster, T.,Palese, P. & Garcia-Sastre, A. 2000. Activation of interferon regulatory factor 3 is inhibited by the influenza A virus NS1 protein. *J Virol,* 74**,** 7989-7996.

Tate, M. D.,Schilter, H. C.,Brooks, A. G. & Reading, P. C. 2011. Responses of mouse airway epithelial cells and alveolar macrophages to virulent and avirulent strains of influenza A virus. *Viral Immunol,* 24**,** 77-88.

Taylor, G. 2017. Animal models of respiratory syncytial virus infection. *Vaccine,* 35**,** 469-480.

Taylor, R. M. 1941. Experimental infection with influenza a virus in mice: the increase in intrapulmonary virus after inoculation and the influence of various factors thereon. *J Exp Med,* 73**,** 43-55.

Te Velthuis, A. J. W.,Long, J. C.,Bauer, D. L. V.,Fan, R. L. Y.,Yen, H. L.,Sharps, J.,Siegers, J. Y.,Killip, M. J.,French, H.,Oliva-Martin, M. J.,Randall, R. E.,de Wit, E.,van Riel, D.,Poon, L. L. M. & Fodor, E. 2018. Mini viral RNAs act as innate immune agonists during influenza virus infection. *Nat Microbiol,* 3**,** 1234-1242.

Techaarpornkul, S.,Barretto, N. & Peeples, M. E. 2001. Functional analysis of recombinant respiratory syncytial virus deletion mutants lacking the small hydrophobic and/or attachment glycoprotein gene. *J Virol,* 75**,** 6825-6834.

Thimme, R.,Frese, M.,Kochs, G. & Haller, O. 1995. Mx1 but not MxA confers resistance against tick-borne Dhori virus in mice. *Virology,* 211**,** 296-301.

Tong, S.,Zhu, X.,Li, Y.,Shi, M.,Zhang, J.,Bourgeois, M.,Yang, H.,Chen, X.,Recuenco, S.,Gomez, J.,Chen, L.-M.,Johnson, A.,Tao, Y.,Dreyfus, C.,Yu, W.,McBride, R.,Carney, P. J.,Gilbert, A. T.,Chang, J.,Guo, Z.,Davis, C. T.,Paulson, J. C.,Stevens, J.,Rupprecht, C. E.,Holmes, E. C.,Wilson, I. A. & Donis, R. O. 2013. New World Bats Harbor Diverse Influenza A Viruses. *PLoS Pathog,* 9**,** e1003657.

Toots, M.,Yoon, J. J.,Cox, R. M.,Hart, M.,Sticher, Z. M.,Makhsous, N.,Plesker, R.,Barrena, A. H.,Reddy, P. G.,Mitchell, D. G.,Shean, R. C.,Bluemling, G. R.,Kolykhalov, A. A.,Greninger, A. L.,Natchus, M. G.,Painter, G. R. & Plemper, R. K. 2019. Characterization of orally efficacious influenza drug with high resistance barrier in ferrets and human airway epithelia. *Sci Transl Med,* 11.

Torrieri-Dramard, L.,Lambrecht, B.,Ferreira, H. L.,Van den Berg, T.,Klatzmann, D. & Bellier, B. 2011. Intranasal DNA Vaccination Induces Potent Mucosal and Systemic Immune Responses and Cross-protective Immunity Against Influenza Viruses. *Molecular Therapy,* 19**,** 602-611.

Triantafilou, K.,Kar, S.,Vakakis, E.,Kotecha, S. & Triantafilou, M. 2013. Human respiratory syncytial virus viroporin SH: a viral recognition pathway used by the host to signal inflammasome activation. *Thorax,* 68**,** 66-75.

Tumpey, T. M.,Szretter, K. J.,Van Hoeven, N.,Katz, J. M.,Kochs, G.,Haller, O.,García-Sastre, A. & Staeheli, P. 2007. The Mx1 gene protects mice against the pandemic 1918 and highly lethal human H5N1 influenza viruses. *J Virol,* 81**,** 10818-10821.

Utley, T. J.,Ducharme, N. A.,Varthakavi, V.,Shepherd, B. E.,Santangelo, P. J.,Lindquist, M. E.,Goldenring, J. R. & Crowe, J. E. 2008. Respiratory syncytial virus uses a Vps4-independent budding mechanism controlled by Rab11-FIP2. *Proceedings of the National Academy of Sciences,* 105**,** 10209-10214.

van Baalen, C. A.,Jeeninga, R. E.,Penders, G. H.,van Gent, B.,van Beek, R.,Koopmans, M. P. & Rimmelzwaan, G. F. 2017. ViroSpot microneutralization assay for antigenic characterization of human influenza viruses. *Vaccine,* 35**,** 46-52.

van der Vries, E.,Schutten, M.,Fraaij, P.,Boucher, C. & Osterhaus, A. 2013. Chapter Six - Influenza Virus Resistance to Antiviral Therapy. *In:* DE CLERCQ, E. (ed.) *Advances in Pharmacology.* Academic Press.

van Riel, D.,Leijten, L. M.,Kochs, G.,Osterhaus, A. D. M. E. & Kuiken, T. 2013. Decrease of Virus Receptors during Highly Pathogenic H5N1 Virus Infection in Humans and Other Mammals. *The American Journal of Pathology,* 183**,** 1382-1389.

Vanderlinden, E.,Vrancken, B.,Van Houdt, J.,Rajwanshi, V. K.,Gillemot, S.,Andrei, G.,Lemey, P. & Naesens, L. 2016. Distinct Effects of T-705 (Favipiravir) and Ribavirin on Influenza Virus Replication and Viral RNA Synthesis. *Antimicrobial agents and chemotherapy,* 60**,** 6679-6691.

Varga, Z. T.,Ramos, I.,Hai, R.,Schmolke, M.,Garcia-Sastre, A.,Fernandez-Sesma, A. & Palese, P. 2011. The influenza virus protein PB1-F2 inhibits the induction of type I interferon at the level of the MAVS adaptor protein. *PLoS Pathog,* 7**,** e1002067.

Vasin, A. V.,Temkina, O. A.,Egorov, V. V.,Klotchenko, S. A.,Plotnikova, M. A. & Kiselev, O. I. 2014. Molecular mechanisms enhancing the proteome of influenza A viruses: an overview of recently discovered proteins. *Virus Res,* 185**,** 53-63.

Vekemans, J.,Moorthy, V.,Giersing, B.,Friede, M.,Hombach, J.,Arora, N.,Modjarrad, K.,Smith, P. G.,Karron, R.,Graham, B. & Kaslow, D. C. 2019. Respiratory syncytial virus vaccine research and development:

World Health Organization technological roadmap and preferred product characteristics. *Vaccine,* 37**,** 7394-7395.

Verhelst, J.,Hulpiau, P. & Saelens, X. 2013. Mx proteins: antiviral gatekeepers that restrain the uninvited. *Microbiol Mol Biol Rev,* 77**,** 551-566.

Verhelst, J.,Parthoens, E.,Schepens, B.,Fiers, W. & Saelens, X. 2012. Interferon-inducible protein Mx1 inhibits influenza virus by interfering with functional viral ribonucleoprotein complex assembly. *J Virol,* 86**,** 13445-13455.

Vidaña, B.,Martínez, J.,Martorell, J.,Montoya, M.,Córdoba, L.,Pérez, M. & Majó, N. 2016. Involvement of the different lung compartments in the pathogenesis of pH1N1 influenza virus infection in ferrets. *Vet Res,* 47**,** 113.

Vigant, F.,Santos, N. C. & Lee, B. 2015. Broad-spectrum antivirals against viral fusion. *Nature Reviews Microbiology,* 13**,** 426-437.

Villalon-Letelier, F.,Brooks, A. G.,Saunders, P. M.,Londrigan, S. L. & Reading, P. C. 2017. Host Cell Restriction Factors that Limit Influenza A Infection. *Viruses,* 9.

Villalón-Letelier, F.,Brooks, A. G.,Saunders, P. M.,Londrigan, S. L. & Reading, P. C. 2017. Host Cell Restriction Factors that Limit Influenza A Infection. *Viruses,* 9.

Vivier, E.,Tomasello, E.,Baratin, M.,Walzer, T. & Ugolini, S. 2008. Functions of natural killer cells. *Nat Immunol,* 9**,** 503-510.

Vladimer, G.,Górna, M. & Superti-Furga, G. 2014. IFITs: Emerging Roles as Key Anti-Viral Proteins. *Front Immunol,* 5.

von der Malsburg, A.,Abutbul-Ionita, I.,Haller, O.,Kochs, G. & Danino, D. 2011. Stalk Domain of the Dynamin-like MxA GTPase Protein Mediates Membrane Binding and Liposome Tubulation via the Unstructured L4 Loop *. *Journal of Biological Chemistry,* 286**,** 37858-37865.

Walker, E. J. & Ghildyal, R. 2017. Editorial: Viral Interactions with the Nucleus. *Front Microbiol,* 8.

Wang, H.,Dou, D.,Östbye, H.,Revol, R. & Daniels, R. 2019. Structural restrictions for influenza neuraminidase activity promote adaptation and diversification. *Nature Microbiology,* 4**,** 2565-2577.

Wang, H.,Xin, X.,Wang, M.,Han, L.,Li, J.,Hao, Y.,Zheng, C. & Shen, C. 2018. Myxovirus resistance protein A inhibits hepatitis C virus replication through JAK-STAT pathway activation. *Arch Virol,* 163**,** 1429-1438.

Wang, L.,Dorn, P.,Simillion, C.,Froment, L.,Berezowska, S.,Tschanz, S. A.,Haenni, B.,Blank, F.,Wotzkow, C.,Peng, R. W.,Marti, T. M.,Bode, P. K.,Moehrlen, U.,Schmid, R. A. & Hall, S. R. R. 2020. EpCAM(+)CD73(+) mark epithelial progenitor cells in postnatal human lung and are associated with pathogenesis of pulmonary disease including lung adenocarcinoma. *Am J Physiol Lung Cell Mol Physiol,* 319**,** L794-l809.

Wang, M.,Cao, R.,Zhang, L.,Yang, X.,Liu, J.,Xu, M.,Shi, Z.,Hu, Z.,Zhong, W. & Xiao, G. 2020. Remdesivir and chloroquine effectively inhibit the recently emerged novel coronavirus (2019-nCoV) in vitro. *Cell Res,* 30**,** 269-271.

Wang, X.,Li, M.,Zheng, H.,Muster, T.,Palese, P.,Beg, A. A. & Garcia-Sastre, A. 2000. Influenza A virus NS1 protein prevents activation of NF-kappaB and induction of alpha/beta interferon. *J Virol,* 74**,** 11566-11573.

Wang, Y.,Deng, L.,Kang, S. M. & Wang, B. Z. 2018. Universal influenza vaccines: from viruses to nanoparticles. *Expert Rev Vaccines,* 17**,** 967-976.

Wang, Y.,Liu, J.,Huang, B. O.,Xu, Y. M.,Li, J.,Huang, L. F.,Lin, J.,Zhang, J.,Min, Q. H.,Yang, W. M. & Wang, X. Z. 2015. Mechanism of alternative splicing and its regulation. *Biomed Rep,* 3**,** 152-158.

Wang, Y.,Yuan, S.,Jia, X.,Ge, Y.,Ling, T.,Nie, M.,Lan, X.,Chen, S. & Xu, A. 2019. Mitochondria-localised ZNFX1 functions as a dsRNA sensor to initiate antiviral responses through MAVS. *Nature Cell Biology,* 21**,** 1346-1356.

Weber-Gerlach, M. & Weber, F. 2016. Standing on three legs: antiviral activities of RIG-I against influenza viruses. *Curr Opin Immunol,* 42**,** 71-75.

Weber, M.,Sediri, H.,Felgenhauer, U.,Binzen, I.,Banfer, S.,Jacob, R.,Brunotte, L.,Garcia-Sastre, A.,Schmid-Burgk, J. L.,Schmidt, T.,Hornung, V.,Kochs, G.,Schwemmle, M.,Klenk, H. D. & Weber, F. 2015. Influenza virus adaptation PB2-627K modulates nucleocapsid inhibition by the pathogen sensor RIG-I. *Cell Host Microbe,* 17**,** 309-319.

Webster, R. G.,Bean, W. J.,Gorman, O. T.,Chambers, T. M. & Kawaoka, Y. 1992. Evolution and ecology of influenza A viruses. *Microbiol Rev,* 56**,** 152-179.

Weston, S. & Frieman, M. B. 2019. Respiratory Viruses. *In:* SCHMIDT, T. M. (ed.) *Encyclopedia of Microbiology (Fourth Edition).* Oxford: Academic Press.

Wies, E.,Wang, May K.,Maharaj, Natalya P.,Chen, K.,Zhou, S.,Finberg, Robert W. & Gack, Michaela U. 2013. Dephosphorylation of the RNA Sensors RIG-I and MDA5 by the Phosphatase PP1 Is Essential for Innate Immune Signaling. *Immunity,* 38**,** 437-449.

Wisskirchen, C.,Ludersdorfer, T. H.,Müller, D. A.,Moritz, E. & Pavlovic, J. 2011a. The cellular RNA helicase UAP56 is required for prevention of double-stranded RNA formation during influenza A virus infection. *J Virol,* 85**,** 8646-8655.

Wisskirchen, C.,Ludersdorfer, T. H.,Müller, D. A.,Moritz, E. & Pavlovic, J. 2011b. Interferon-induced antiviral protein MxA interacts with the cellular RNA helicases UAP56 and URH49. *J Biol Chem,* 286**,** 34743-34751.

Wong, J.,Layton, D.,Wheatley, A. K. & Kent, S. J. 2019. Improving immunological insights into the ferret model of human viral infectious disease. *Influenza Other Respir Viruses,* 13**,** 535-546.

Xia, C.,Vijayan, M.,Pritzl, C. J.,Fuchs, S. Y.,McDermott, A. B. & Hahm, B. 2015. Hemagglutinin of Influenza A Virus Antagonizes Type I Interferon (IFN) Responses by Inducing Degradation of Type I IFN Receptor 1. *J Virol,* 90**,** 2403-2417.

Xiao, H.,Killip, M. J.,Staeheli, P.,Randall, R. E. & Jackson, D. 2013. The human interferon-induced MxA protein inhibits early stages of influenza A virus infection by retaining the incoming viral genome in the cytoplasm. *J Virol,* 87**,** 13053-13058.

Xing, Z.,Harper, R.,Anunciacion, J.,Yang, Z.,Gao, W.,Qu, B.,Guan, Y. & Cardona, C. J. 2011. Host immune and apoptotic responses to avian influenza virus H9N2 in human tracheobronchial epithelial cells. *Am J Respir Cell Mol Biol,* 44**,** 24-33.

Xu, G.,Xia, Z.,Deng, F.,Liu, L.,Wang, Q.,Yu, Y.,Wang, F.,Zhu, C.,Liu, W.,Cheng, Z.,Zhu, Y.,Zhou, L.,Zhang, Y.,Lu, M. & Liu, S. 2019. Inducible

LGALS3BP/90K activates antiviral innate immune responses by targeting TRAF6 and TRAF3 complex. *PLoS Pathog,* 15**,** e1008002.

Xue, J.,Chambers, B. S.,Hensley, S. E. & López, C. B. 2016. Propagation and Characterization of Influenza Virus Stocks That Lack High Levels of Defective Viral Genomes and Hemagglutinin Mutations. *Front Microbiol,* 7.

Xue, J.,Chambers, B. S.,Hensley, S. E. & López, C. B. 2016. Propagation and Characterization of Influenza Virus Stocks That Lack High Levels of Defective Viral Genomes and Hemagglutinin Mutations. *Front Microbiol,* 7**,** 326.

Yamamoto, M.,Sato, S.,Hemmi, H.,Hoshino, K.,Kaisho, T.,Sanjo, H.,Takeuchi, O.,Sugiyama, M.,Okabe, M.,Takeda, K. & Akira, S. 2003. Role of Adaptor TRIF in the MyD88-Independent Toll-Like Receptor Signaling Pathway. *Science,* 301**,** 640-643.

Yoneyama, M. & Fujita, T. 2007. Function of RIG-I-like receptors in antiviral innate immunity. *J Biol Chem,* 282**,** 15315-15318.

Yoneyama, M.,Kikuchi, M.,Matsumoto, K.,Imaizumi, T.,Miyagishi, M.,Taira, K.,Foy, E.,Loo, Y. M.,Gale, M., Jr.,Akira, S.,Yonehara, S.,Kato, A. & Fujita, T. 2005. Shared and unique functions of the DExD/H-box helicases RIG-I, MDA5, and LGP2 in antiviral innate immunity. *J Immunol,* 175**,** 2851-2858.

Yoneyama, M.,Kikuchi, M.,Natsukawa, T.,Shinobu, N.,Imaizumi, T.,Miyagishi, M.,Taira, K.,Akira, S. & Fujita, T. 2004. The RNA helicase RIG-I has an essential function in double-stranded RNA-induced innate antiviral responses. *Nat Immunol,* 5**,** 730-737.

Yong, H. Y. & Luo, D. 2018. RIG-I-Like Receptors as Novel Targets for Pan-Antivirals and Vaccine Adjuvants Against Emerging and Re-Emerging Viral Infections. *Front Immunol,* 9**,** 1379.

Zaraket, H.,Hurt, A. C.,Clinch, B.,Barr, I. & Lee, N. 2021. Burden of influenza B virus infection and considerations for clinical management. *Antiviral Research,* 185**,** 104970.

Zhang, R.,Li, Z.,Tang, Y.-D.,Su, C. & Zheng, C. 2021. When human guanylate-binding proteins meet viral infections. *Journal of Biomedical Science,* 28**,** 17.

Zhang, W.,Zhang, L.,Zan, Y.,Du, N.,Yang, Y. & Tien, P. 2015a. Human respiratory syncytial virus infection is inhibited by IFN-induced transmembrane proteins. *J Gen Virol,* 96**,** 170-182.

Zhang, W.,Zhang, L.,Zan, Y.,Du, N.,Yang, Y. & Tien, P. 2015b. Human respiratory syncytial virus infection is inhibited by IFN-induced transmembrane proteins. *J Gen Virol,* 96 Pt 1**,** 170-182.

Zhang, Z.,Zou, T.,Hu, X. & Jin, H. 2015. Type III interferon gene expression in response to influenza virus infection in chicken and duck embryonic fibroblasts. *Mol Immunol,* 68**,** 657-662.

Zhao, M.,Wang, L. & Li, S. 2017. Influenza A Virus-Host Protein Interactions Control Viral Pathogenesis. *Int J Mol Sci,* 18.

Zillinger, T. & Hartmann, G. 2019. Targeted Nanoparticle Delivery of Bifunctional RIG-I Agonists to Pancreatic Cancer. *Molecular Therapy,* 27**,** 491-492.

Zimmermann, P.,Mänz, B.,Haller, O.,Schwemmle, M. & Kochs, G. 2011. The Viral Nucleoprotein Determines Mx Sensitivity of Influenza A Viruses. *J Virol,* 85**,** 8133-8140.

Zou, J.,Castro, R. & Tafalla, C. 2016. Chapter 7 - Antiviral Immunity: Origin and Evolution in Vertebrates. *In:* MALAGOLI, D. (ed.) *The Evolution of the Immune System.* Academic Press.

Zou, J.,Chang, M.,Nie, P. & Secombes, C. J. 2009. Origin and evolution of the RIG-I like RNA helicase gene family. *BMC evolutionary biology,* 9**,** 85-85.

Zürcher, T.,Pavlovic, J. & Staeheli, P. 1992a. Mechanism of human MxA protein action: variants with changed antiviral properties. *Embo j,* 11**,** 1657-1661.

Zürcher, T.,Pavlovic, J. & Staeheli, P. 1992b. Mouse Mx2 protein inhibits vesicular stomatitis virus but not influenza virus. *Virology,* 187**,** 796-800.

Zürcher, T.,Pavlovic, J. & Staeheli, P. 1992c. Nuclear localization of mouse Mx1 protein is necessary for inhibition of influenza virus. *J Virol,* 66**,** 5059-5066.